Gamma Decay of Virtual States in ^{20}Ne and ^{16}O Excited in Radiative Alpha-Particle Capture.

by

Michael John Hurst

The Queen's College

Oxford.

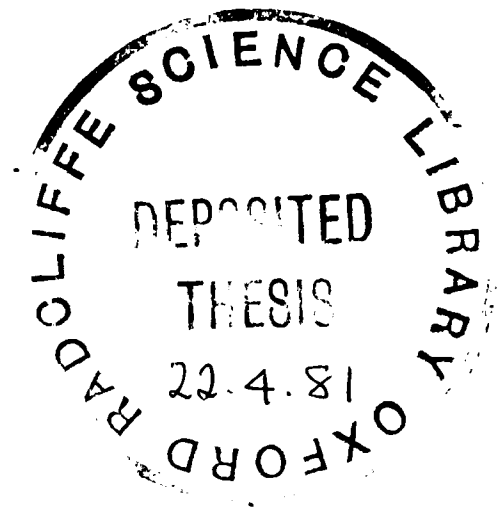

A thesis submitted in partial fulfilment of the requirements for the degree of Doctor of Philosophy in the University of Oxford.

October 1980

Gamma Decay of Virtual States in ^{20}Ne and ^{16}O Excited in Radiative Alpha-Particle Capture.

Michael John Hurst, The Queen's College, Oxford.

Abstract of thesis submitted for the degree of Doctor of Philosophy.

Michaelmas Term 1980.

ABSTRACT

A cryogenically pumped, windowless gas target has been used to study the radiative alpha-capture reaction on ^{16}O and ^{12}C targets, giving information on the electromagnetic decay properties of various unbound states in ^{20}Ne and ^{16}O. Several states in ^{20}Ne have been observed in this reaction for the first time.

The first five unit-isospin, natural parity states in ^{20}Ne have been observed. The isospin assignment of the 11.27 MeV (1^-) state has been made definite by the observation of a strong M1 decay to the 8.85 MeV (1^-) state, and the analogue of the 1.97 MeV state in ^{20}F has been identified with the ^{20}Ne state at 12.25 MeV. Angular distribution measurements have shown the spin of this state to be 3^-, and the total width has been shown to be less than 1 keV, contradicting previous reports. The 12.22 MeV (2^+) state has been resolved clearly as an individual resonance for the first time. The electromagnetic transition rates for the lower T=1 states in ^{20}Ne are compared with shell model calculations.

Five zero-isospin capture resonances in ^{20}Ne have been studied, the gamma-decay of the 8.70 MeV (1^-), 9.11 MeV (3^-) and 11.92 MeV (4^+) states being observed for the first time. A remeasurement has been made of the enhanced E2 decay strength of the 8^+ member of the ground state rotational band, giving $\omega\gamma = 131 \pm 18$ meV, in agreement with a previous less accurate value. This result is compared with shell model calculations.

A study of the capture reaction on ^{12}C has been performed in the beam energy range 5.22 MeV $< E\alpha <$ 9.53 MeV. No new capture resonances have been found but the known inelastic resonances have been seen. The 11.10 MeV (4^+) state has been studied and the strength for the decay to the 6.13 MeV (3^-) state has been shown to be only half of a previous result. The 12.05 MeV (0^+) state has not been observed, but a limit has been placed on its strength.

Table of Contents

Acknowledgements

The production of this thesis has taken a considerable time and I am indebted for its eventual completion to many people, both for their invaluable assistance and for persistent encouragement. Unfortunately not all can be mentioned individually.

Firstly I must thank Professor K.W.Allen, both as an understanding supervisor and as head of the department for much of my time in Oxford.

Particular thanks are due to Dr. Keith Fifield for advice and assistance both with experiments and during the writing up, but particularly for his (not always appreciated!) persistence in cajoling me into the eventual completion of this thesis - without him it would never have happened. I am also grateful to Dr. E.F.Garman for her encouragement and for easing the problems of completing a thesis when I was no longer resident in Oxford.

It has been a pleasure to work on the gas target, and briefly on the multi-gap, with Drs. F.Watt, T.J.M.Symons, C.H.Zimmerman, E.F.Garman, D.Roaf and H.M.Sen Gupta, and my thanks are also due to the present occupants of room 614 for their hospitality on my many weekend visits.

The gas target work would not have been posible without the efforts of Mr. H.R.McK.Hyder and the O.E.G. Machine Group, especially Messrs. A.Aitken, J.Early, R.Evans, R.Hole, R.Hopkins, N.Walters and the late S.Wybraniec who made night shifts and then weekend stays almost a pleasure.

I am also grateful to the members of the O.E.G. workshop and the Computer and Electronics groups for their willingness to lend assistance, and to Miss Daphne Pollard for agreeing to decipher my scrawl and type this thesis.

Lastly I should like to thank various members of The Queen's College for making my time in Oxford enjoyable, even though perhaps they were too successful.

CHAPTER 1

INTRODUCTION

1.1 Introduction

The independent particle shell model has had a great deal of success in describing various properties of light nuclei, particularly those which can be considered to consist of an ^{16}O core plus a few nucleons in the 2s1d shell. It is therefore of interest to measure such properties as energy, spin and parity, spectroscopic strength and electromagnetic decay probability for excited states in these nuclei to enable comparisons to be made with the predictions, not only of the shell model, but also of such alternative models as, for example, the collective model.

The electromagnetic decay probability of a state is a fairly sensitive test of a model's description of the state and can be predicted with an accuracy dependent only on the model wavefunctions for the two states involved in the transition, as the electromagnetic interaction is well known and does not introduce any further uncertainty. This differs from the case of particle transfer reactions where certain assumptions have to be made regarding the reaction mechanism, and this can reduce confidence in the significance of the agreement between measured and predicted values of particle and cluster widths.

Not only is the shell model successful in describing states bound against particle decay, but it also has considerable success for virtual states if their lifetimes are long compared with the time taken for a

nucleon to traverse the nuclear volume. This condition is satisfied for most states with energies of only a few MeV above the binding energy for particle decay because of the additional potential barrier due to Coulomb repulsion and angular momentum. An extended lifetime can also occur when decay is inhibited by the parity conservation rule or by a special configuration, when the wavefunction has little overlap with possible decay products.

1.2 Alpha Capture

The γ-decay of virtual states can be studied using the radiative α-capture reaction since for many light nuclei there is a useful range of excitation energy over which the virtual states are unbound only to emission of α-particles. This means that there are no competing α-induced reactions on the target nuclei except α-scattering, and so the radiative decay width can be easily extracted from the measured reaction yield as will be shown below.

The cross-section for a resonant reaction as a function of incident energy is given by the Breit-Wigner formula:-

$$\sigma_{\alpha\gamma}(E) = \pi\lambda^2 \frac{(2J+1)}{(2s+1)(2S+1)} \cdot \frac{\Gamma_\alpha \Gamma_\gamma}{[(E-E_o)^2 + \frac{1}{4}\Gamma^2]}$$

where Γ_α, Γ_γ are the partial widths for the entrance and exit channels

Γ is the total width

E_o, E are the resonance and incident energies (centre of mass)

J, s, S are the spins of the compound state and initial states

$\lambda\!\!\!^{-}$ is the centre of mass wavelength of the incident particle divided by 2π.

When this is integrated over a target of thickness such that the beam loses an energy ξ (ignoring straggling), the total yield per incident particle is obtained:-

$$Y = \int_{Eb-\xi}^{Eb} \frac{n\sigma}{\varepsilon}\, dE' = 2\pi n \frac{\lambda\!\!\!^{-2}}{\varepsilon} . \omega\gamma . \left[\tan^{-1} \frac{E_b - E_o}{\Gamma/2} - \tan^{-1} \frac{Eb - Eo - \xi}{\Gamma/2}\right]$$

This has a maximum value for a beam energy E_b of $E_o + \xi/2$ when:

$$Y_{max} = 4\pi n \frac{\lambda\!\!\!^{-2}}{\varepsilon} . \omega\gamma . \tan^{-1}\left(\frac{\xi}{\Gamma}\right)$$

where n is the number density of target nuclei

ε is the stopping power of the target (energy loss per unit distance)

$$\omega\gamma = \frac{2J+1}{(2s+1)(2S+1)} \cdot \frac{\Gamma_\alpha \Gamma_\gamma}{\Gamma}$$

For narrow resonances ($\Gamma << \xi$) the maximum yield approximates to $2n\pi^2\lambda\!\!\!^{-2}\omega\gamma/\varepsilon$ and if there are no competing reactions apart from elastic scattering and if $\Gamma_\gamma << \Gamma_\alpha$ (usually true) then $\Gamma_\alpha\Gamma_\gamma/\Gamma$ approximates to Γ_γ so that the only properties of the nuclear state affecting the yield are Γ_γ and the spin J. This means that a nuclear property easily linked to theoretical models can be measured without the need for simplifying assumptions about the reaction mechanism.

Since the α-particle has zero spin, angular momentum is only introduced to the compound state about an axis perpendicular to the beam, so the projection of angular momentum along the beam axis is unchanged in the reaction. If the target has zero spin (as is the case for ^{16}O and ^{12}C) then this projection must be zero and so the excited state is strongly aligned leading to a pronounced angular distribution of the decay γ-rays. The result of this is that the spin of the state can be deduced from measurements of the γ-ray intensity as a function of angle.

The fact that usually $\Gamma_\gamma << \Gamma_\alpha$ follows from the improbability of capture compared with elastic scattering. This is because γ-decay occurs through the electromagnetic interaction whereas scattering and particle decay proceed via the strong interaction, and are therefore far more probable. An unfortunate consequence of this is that capture γ-rays are easily masked by γ-rays from bound states populated by particle reactions of much larger cross-section. For this reason it is very important to minimise the presence of contaminant nuclei in the beam path.

The most troublesome contaminant has traditionally been ^{13}C (natural abundance 1.1%) in the backing of a solid target or from pump oil, owing to the prolific $^{13}C(\alpha,n_2)^{16}O^*$ reaction resulting in 6.13 MeV γ-rays, the Compton scattering of which provides a continuous distribution of γ-ray energies in a detector. The threshold for this reaction lies at a beam energy of 5.1 MeV and the first resonance is at 5.3 MeV [Sp63]. At higher energies, above about 7.6 MeV, the inelastic scattering of α-particles from ^{12}C leads to 4.44 MeV γ-rays, which can be a serious source of background.

Attempts have been made to avoid the problems of contaminated backings and uncertain target composition by using gas targets in which the gas is localised either by thin windows or by pumping restrictions. The development of gas targets will be discussed further in the next chapter.

1.3 Plan of Thesis

The bulk of the work reported in this thesis concerns the nucleus ^{20}Ne, and most of the data have been published in reference [Fi80]. Chapter two describes the gas target, and in chapter three, an introduction to the structure of this nucleus is given, the experimental work is summarised, and a list of the resonances observed is given. Chapter four discusses the T=1 states which were studied and chapter five discusses the T=0 states, including the 8^+ member of the ground state rotational band. The data on this last state have been published in reference [Hu80].

A survey of the $^{12}C(\alpha,\gamma)^{16}O$ reaction was also performed and one resonance was studied in detail. This work is described in chapter six.

CHAPTER 2

THE CRYOPUMPED GAS TARGET - DESCRIPTION AND PROCEDURES

2.1 The Development of Gas Targets

The design of a gas target cell is governed by the need to maintain a suitable pressure of target gas (typically 0.1→10 torr) in a well-localised region, requiring a rapid transition from the target pressure to the high vacuum needed for beam transport.

The simplest method for achieving this is to use thin metal foils to contain the gas without impeding the beam. Such gas cells have been in use for many years in a variety of applications. While this method does indeed avoid the difficulties of making solid targets, the background problems due to a solid target backing are to some extent transferred to the windows. In addition, the windows degrade the beam energy resolution and can be damaged by high beam currents. They are therefore of limited value, except for gases like neon which cannot readily be incorporated into solid targets, or for expensive gases available in limited quantities.

Various windowless targets have been developed during the last fifteen years, in which pumping restrictions replace the thin windows. In practice several restrictions in series are needed in order to provide the required pressure drop (a factor of 10^{-4}→10^{-6}) and very high pumping speeds are required. Most designs have used Roots blowers which are large, expensive and introduce hydrocarbon contamination. Cryopumping techniques were used by Parks et al[Pa64] in a target specifically designed to produce a monoenergetic beam of neutrons from

the strong reaction $^{3}H(p,n)^{3}He$. The large quantity of metal around the central target region and the very low target thickness ($\sim 3\times10^{16}$ atoms/cm^2) would have made it unsuitable for capture work.

The systems using Roots blowers fall into two groups, some (single ended) having the beam stop in the high pressure region [De71, Dw71] and the others (double ended) having another set of pumping restrictions to allow the beam to continue to a low pressure region and to be stopped at a distance from the target [Go66, Li67, Bu71, Ro78]. The disadvantages of a single ended arrangement are that the presence of ionised gas prevents accurate beam current measurement and, for γ-ray work, the proximity of the beam stop to the detectors introduces serious background radiation. The former problem was tackled by Dwarakanath and Winkler[Dw71] by using a calorimeter instead of conventional electrical measurements. A significant feature of the target described by Rolfs et al[Ro78] was that continuous recycling of the target gas enabled a very small charge of gas to be used (~25cc at S.T.P.).

All these systems suffer from the introduction of hydrocarbon contamination which, as shown in the previous chapter, is a serious problem for capture work.

2.2 The Cryopumped Gas Target - Design

The Oxford cryopumped transmission gas-target was designed to minimise contaminant reactions. The Mark II version has been described by Dolan [Do75] and by Allen et al [Al76]; this version was only used in this thesis for the work on the first T=1 resonance in Ne^{20}. The Mark III version, enabling angular distribution measurements to be made,

1.E.1:
3.A

Nuclear Physics **A334** (1980) 109–126; © *North-Holland Publishing Co., Amsterdam*

RADIATIVE DECAYS OF UNBOUND LEVELS IN ^{20}Ne

L. K. FIFIELD, M. J. HURST †, E. F GARMAN, T. J. M. SYMONS ††,
F WATT and K. W. ALLEN

Nuclear Physics Laboratory, University of Oxford, England

Received 27 August 1979

Abstract: Nine levels in the range 8.7 to 12.5 MeV in ^{20}Ne have been investigated with the ^{16}O(α, γ)^{20}Ne and ^{16}O(α, α')^{16}O*(6.13 MeV) reactions using a differentially pumped windowless gas target. Three of the levels have not been observed previously in these reactions, and new information has been obtained for most of the others. In particular, the 11.27 MeV 1^- level is shown to have $T = 1$, a result of relevance to a proposed parity violation experiment, and the analogue of the 1.97 MeV (3^- $T = 1$) level in ^{20}F is shown to lie at 12.25 MeV in ^{20}Ne rather than at 12.39 MeV as proposed previously. In addition, the 12.25 MeV level has a width $\Gamma < 1$ keV, in contrast to the value $\Gamma \sim 5$ keV reported in other work. The electromagnetic transition rates for positive parity $T = 1$ states in ^{20}Ne are compared with shell-model calculations.

E NUCLEAR REACTIONS ^{16}O(α, γ), (α, $\alpha'\gamma$), $E = 3.0$–9.5 MeV; measured $\sigma(E_\alpha, E_\gamma, \theta_\gamma)$. ^{20}Ne deduced levels, J, π, T, γ-ray branching ratios, Γ_γ. Windowless gas target.

1. Introduction

The ^{20}Ne nucleus has played a central role in the development and testing of theories of the structure of light nuclei, and in the exploration of the properties of the weak interaction as manifested in nuclear properties. In each of these areas, important information has been obtained from the radiative capture of α-particles by ^{16}O. The nuclear structure studies have concentrated on determining the electromagnetic properties of members of rotational bands [1–5]), and on the interpretation of these properties in terms of sophisticated shell-model calculations, while the weak interaction studies have been directed towards the search for a second-class nuclear weak current and a test of the conserved vector current (CVC) theory. In this latter case, information on the radiative decays of the 10.27 MeV 2^+ $T = 1$ state in ^{20}Ne [refs. [6,7])], which is the analogue of the ^{20}F and ^{20}Na ground states, is essential to the interpretation of measurements of recoil-order effects [8–11]) in the β-decays of ^{20}F and ^{20}Na in terms of second-class currents or CVC. Recently, it has also been proposed that parity violating effects due to the weak neutral current may be observable in a 1^- $T = 0$–1^+ $T = 1$–1^- $T = 1$ sequence of levels near 11.2 MeV in

† Present address: CEGB Computing Centre, 85 Park Street, London SE1.
†† Present address: Lawrence Berkeley Laboratory, Berkeley, California 94720, USA.

has been described by Watt et al [Wa78] and by Zimmerman [Zi77]. It was used for studying all the other states discussed in this thesis but, as it has been fully described elsewhere, only a brief outline will be given here.

The general layout is shown in figures 2.2.1 and 2.2.2 and the target flange with the main pumping nozzles is shown in more detail in figure 2.2.3. The actual target chamber is 5cm long with nozzles at each end which are 4cm long and have a diameter of 3.5mm.

An intense (5-20μA) beam of He^{+} ions from the RF source of the Oxford 10MV injector was momentum analysed and transported along a stainless steel beam line through the target chamber, where the remaining electron was stripped off by the gas, and on to a gold beam stop inside a concrete cave. The beam stop took the form of a Faraday cup, and a negative voltage was applied to a suppression ring to enable reliable current measurements of the He^{++} beam to be made. The vacuum in this region was sufficient to prevent ionisation from being a problem. Metal seals were used throughout, except for a limited number of viton O-rings, and mercury diffusion pumps backed by adsorption pumps were used to eliminate hydrocarbon vapour, thus preventing carbon build-up on collimators and pumping nozzles.

The target gas was localised by pumping nozzles which restricted the gas flow out of the target chamber to a rate which could be handled by cryopumps. About 99% of the gas accumulated on the Leybold pump, and the remaining fraction passed through the second differential pumping nozzles to the Oxford Instruments pump. This meant that only the Leybold pump needed to be warmed up for recycling the gas, the more

^{20}Ne, and some preliminary work to define the nuclear properties of this system has been carried out [12]).

As a consequence of these specific investigations, a number of selected levels in ^{20}Ne have been studied in considerable detail with the ^{16}O(α, γ)^{20}Ne reaction. However, prior to our undertaking the present work, the only systematic survey of the ^{16}O(α, γ)^{20}Ne reaction at beam energies between 5 and 10 MeV (8.7 to 12.7 MeV in ^{20}Ne) was the study of Pearson and Spear [13]) using solid targets and NaI(Tl) γ-ray detectors. Although they located a total of eight resonances, only two were studied in detail within the limitations imposed by the use of NaI detectors and thick targets. Subsequently, Steck [14]) has surveyed the region of α-particle energy from 6.9 to 10.0 MeV using Ge(Li) detectors and a gas target, but, as in the work of Pearson and Spear [13]), an intense 6.13 MeV γ-ray background from the ^{13}C(α, nγ)^{16}O reaction prevented the observation of γ-ray decays from a resonance to any but the lowest three levels in ^{20}Ne. Hence, only a limited amount of new information on the radiative decay properties of levels in ^{20}Ne is forthcoming from Steck's work [14]).

Since we have developed a differentially pumped gas target system [15]) which almost eliminates the 6.13 MeV γ-ray background and permits the use of thin targets, we have undertaken a new survey of the ^{16}O(α, γ)^{20}Ne reaction at beam energies up to 9.6 MeV. The aim of these measurements was to provide complete γ-ray decay schemes and resonance strengths for all narrow resonances ($\Gamma < 10$ keV) in the range of beam energies between 3.0 and 9.6 MeV for which such information was not already available. In the event we have obtained new information on a total of nine resonances. In particular, we have obtained a definitive $T = 1$ assignment to the 11.27 MeV 1^- level, and find an excitation energy which agrees with a recent measurement of Davidson and Lowry [12]), but not with the measurement of Steck [14]). The isospin and excitation energy of this level are relevant to the search for a possible parity-violating α-particle width of the 1^+ $T = 1$ state at 11.26 MeV [ref. [16])]. In addition, we have resolved the confused situation concerning the doublet of levels [17]) at 12.22 and 12.25 MeV, which is of some importance to the structure of the $A = 20$ nuclei since it is through the former level that γ-decay of the 2^+ $T = 2$ level proceeds [18]).

2. Experimental procedure

Details of the differentially cryopumped gas target employed in these measurements are presented in ref. [15]). Beams of α-particles at typical currents of 5–10 μA of ^{4}He$^+$ were obtained from the Oxford single-ended Van de Graaff accelerator and focussed through the differential pumping nozzles of the target. Typically, less than 0.2 % of the beam struck these nozzles, the remainder being transmitted to a Faraday cup located 3 m beyond the target. This ensured that the background of

6.13 MeV γ-rays from ^{13}C contamination was negligible. The target was gaseous oxygen, enriched to greater than 99.98 % in ^{16}O.

Gamma ray yield curves were measured using an automatic beam-energy modulation technique [19]), with γ-rays detected in a 7.6 × 7.6 cm NaI(Tl) detector. A target gas pressure of 200 μm, corresponding to a target thickness of 2 keV for 7 MeV α-particles, was usually employed when searching for resonances.

In order to cover the region of excitation energy between 7 and 12.5 MeV in ^{20}Ne as systematically as possible, the following procedure was adopted. For excitation energies between 7 and 11.1 MeV (beam energies between 2.8 and 8.0 MeV) a search was made for known natural parity levels with small total widths ($\Gamma < 10$ keV) which had either not been observed previously as resonances in the ^{16}O(α, γ)^{20}Ne reaction, or for which it was felt new information might be forthcoming. The γ-ray yield curves, therefore, covered only limited regions of excitation energy centred on the state of interest. Above 11.1 MeV in ^{20}Ne, however, a continuous survey of the region of excitation up to 12.5 MeV was carried out.

Once a resonance had been located, on- and off-resonance γ-ray spectra were measured with an 85 cm^3 Ge(Li) detector. In various runs, this was positioned at 125° or 135° to the beam direction with its front face either 9 cm or 11 cm from the centre of the target. The target pressure was maintained at 0.8 torr for beam energies below 9 MeV and at 1 torr above 9 MeV in order that the γ-ray yield from sharp resonances ($\Gamma < 1$ keV) be essentially that from a thick target. However, since the capture γ-rays did not all originate from the same point within the target, corrections to the observed γ-ray yields were necessary when extracting resonance strengths. A description of the correction procedure may be found in ref. [15]). Gamma-ray decay schemes were determined from the on-resonance spectra using the known efficiency of the Ge(Li) detector as a function of γ-ray energy. Values of the resonance strength, $\omega\gamma$ ($= (2J+1)\Gamma_\alpha\Gamma_\gamma/\Gamma$), were determined relative to the well known 6.93 MeV (2^+ $T = 1$) resonance for which $\omega\gamma$ was taken to be 19.7 ± 1.6 eV [refs. [6,7])].

A second detector, an intrinsic germanium detector with an active volume of 60 cm^3, could be used to measure γ-ray angular distributions over an angular range from 25° to 90°. This capability was used for the 11.09 and 12.25 MeV levels only. For the other resonances studied, which were all considerably weaker, the intrinsic detector was fixed at 30°, and the spectra from it served to complement the data from the larger Ge(Li) detector.

3. Results

A summary of excitation energies, widths and $\omega\gamma$ values for the resonances observed is presented in table 1, and the γ-ray decay schemes are shown in figs. 1 and 2. Electromagnetic transition rates for the levels studied are collected in table 2. Individual levels, or groups of levels, are discussed below in turn.

TABLE 1

Properties of resonances in the $^{16}O(\alpha, \gamma)^{20}Ne$ reaction as determined in the present work

E_x (keV)	E_α (keV)	J^π, T	$\Gamma_{c.m.}$ (keV)	$\omega\gamma$ [a] (eV)
8704.3±7	4969±9	$1^-, 0$	2.1±0.8	0.21±0.05
9110.6±3	5477±4	$3^-, 0$	< 4	0.18±0.02
11087 ±3	7948±4	$4^+, 1$	< 1	30.2±3.5
11273 ±4	8180±5	$1^-, 1$	< 1	2.06±0.25
11557 ±6	8535±6	$(0^+, 2^+), 0$	1.3±0.8	0.41±0.06
11924 ±6	8994±8	$4^+, 0$	< 1	0.23±0.05
12218 ±4	9362±5	$2^+, 1$	< 1	1.41±0.23
12253 ±3	9406±4	$3^-, 1$	< 1	6.6 ±0.8

[a]) $\omega\gamma = (2J+1)\Gamma_\alpha\Gamma_\gamma/\Gamma$ where Γ_γ is the total observed γ-ray width of the level.

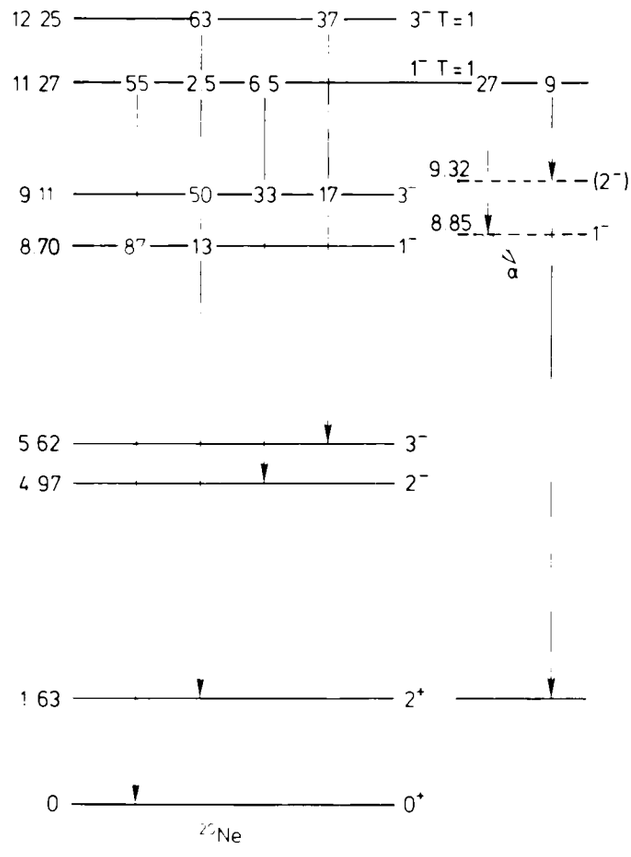

Fig. 1. Gamma-ray decay schemes for the negative parity levels studied as resonances in the present work.

3.1. LEVELS BETWEEN 7 AND 11 MeV

A search was made for resonances corresponding to the known [16]) negative parity levels at 7.17(3^-), 8.70(1^-) and 9.12(3^-) MeV in ^{20}Ne. We failed to observe the 7.17 MeV level, but the latter two levels were seen; information on them is

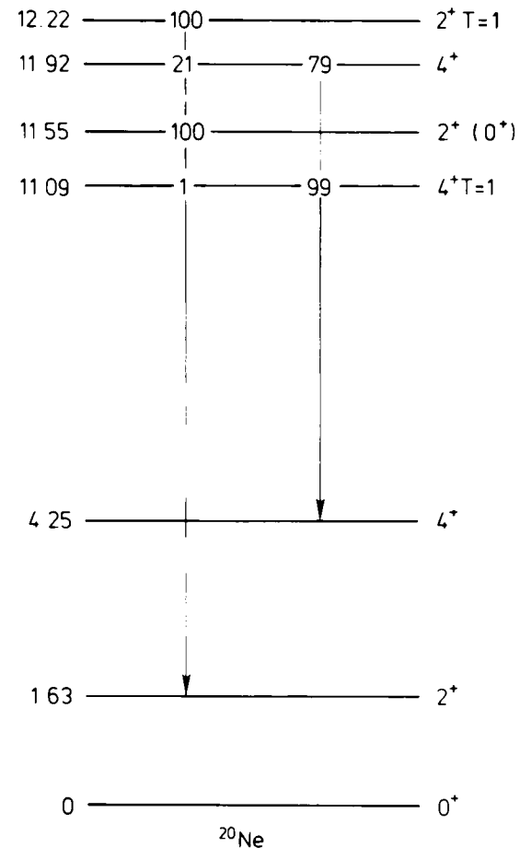

Fig. 2. Gamma-ray decay schemes for the positive parity levels studied as resonances in the present work.

included in table 1 and fig. 1. Since the target pressure was limited to less than about 1.5 torr, (corresponding to a target thickness of ~ 16 keV at a beam energy of 7 MeV) no attempt was made to study levels with widths greater than 10 keV. In addition, the 5^- level at 8.45 MeV has been the subject of a detailed study by Rogers *et al.* [5]) and was not studied further here.

A number of positive parity levels are also known in this region of excitation energy, but all the narrow ones have been comprehensively studied previously [2-4]) with the ^{16}O(α, γ)^{20}Ne reaction, and were not studied in the present work.

3.2. THE 11.09 MeV LEVEL

The 11.09 MeV level, observed as a strong capture resonance at 7.95 MeV, is believed to be the analogue of the 0.824 MeV 4^+ $T = 1$ level in ^{20}F, although, as we shall see below, this identification has not rested upon the firmest of evidence. In the present work, we have measured $\omega\gamma$ of the dominant $R \rightarrow$ 4.25 MeV transition and find a value in good agreement with those reported by Pearson and Spear [13]) and Steck [14]). In addition, we observe a weak branch to the 1.63 MeV (2^+) level.

The 4^+ assignment to this level rests largely upon the angular distribution of the $R \rightarrow$ 4.25 MeV γ-ray measured by Pearson and Spear [13]). However, their fit to this

TABLE 2

Electromagnetic transition rates for levels in ^{20}Ne

E_i	J_i^π	E_f	J_f^π	Branching ratio (%)	Mλ	B(Mλ) [a] (W.u.)
8.70	1	0.0	0^+	87 ±8	E1	$(1.9 \pm 0.4) \times 10^{-4}$
		1.63	2^+	13 ±8	E1	$(5.2 \pm 3.4) \times 10^{-5}$
9.11	3^-	1.63	2^+	50 ±5	E1	$(6.2 \pm 1.2) \times 10^{-5}$
		4.97	2^-	33 ±5	M1	$(5.8 \pm 1.1) \times 10^{-3}$
		5.62	3^-	17 ±4	M1	$(5.0 \pm 1.3) \times 10^{-3}$
11.09	4^+ $T = 1$	1.63	2^+	0.5±0.25	E2	0.09 ±0.04
		4.25	4^+	99.5±0.25	M1	0.50 ±0.06
11.27	1^- $T = 1$	0.0	0^+	55 ±2	E1	$(5.3 \pm 0.7) \times 10^{-4}$
		1.63	2^+	2.5±1	E1	$(3.9 \pm 1.6) \times 10^{-5}$
		4.97	2	6.5±1	M1	$(8.6 \pm 1.6) \times 10^{-3}$
		8.85	1	27 ±1.5	M1	0.63 ±0.08
		9.32	(2)	9 ±1	(M1)	0.40 ±0.07
11.56	$(0^+, 2^+)$	1.63	2^+	100	M1 ($J = 2$)	$(4.1 \pm 0.6) \times 10^{-3}$
					E2 ($J = 0$)	1.6 ±0.2
		[4.25	4^+	< 8	E2 ($J = 2$)	< 0.1]
11.92	4^+	1.63	2^+	21 ±11	E2	0.018±0.011
		4.25	4^+	79 ±11	M1	$(2.2 \pm 0.5) \times 10^{-3}$
12.22	2^+ $T = 1$	1.63	2^+	100	M1	> 0.013
12.25	3 $T = 1$	1.63	2^+	63 ±1.5	E1	$(1.0 \pm 0.1) \times 10^{-3}$
		5.62	3^-	37 ±1.5	M1	0.058±0.007

[a]) Assuming $\Gamma_\gamma \gg \Gamma_p$ except for the 12.22 MeV level, for which $\Gamma_\gamma/\Gamma > 0.25$ [ref. [17])].

angular distribution implied a mixing ratio δ(E2/M1) = 0.238±0.023 (using the phase convention of Rose and Brink), which in turn implies a reduced E2 transition probability of 4.4 Weisskopf units (W.u.). Since the M1 strength of this transition requires that the resonance state has $T = 1$, we have the unexpected [20]) phenomenon of an enhanced $\Delta T = 1$ E2 transition. Moreover, this transition is an order of magnitude larger than any known $\Delta T = 1$ E2 transition in this mass region. The same γ-ray angular distribution has been measured by Steck [14]), but his deduced mixing ratio, 0.3±0.3, is not sufficiently accurate to confirm or deny Pearson and Spear's value.

In view of the surprising apparent E2 strength of the $R \rightarrow 4.25$ MeV transition, we have undertaken a remeasurement of the angular distribution. The result is shown in fig. 3. As indicated by the χ^2 plot, the fit for $J = 4$ requires a mixing ratio, $\delta = 0.01 \pm 0.06$, which is consistent with zero but not with the value measured by Pearson and Spear. However, the measurement of Pearson and Spear was performed with NaI detectors positioned close to the target and was handicapped by a substantial background of 6.92 and 7.12 MeV γ-rays from the ^{13}C(α, nγ)^{16}O reaction,

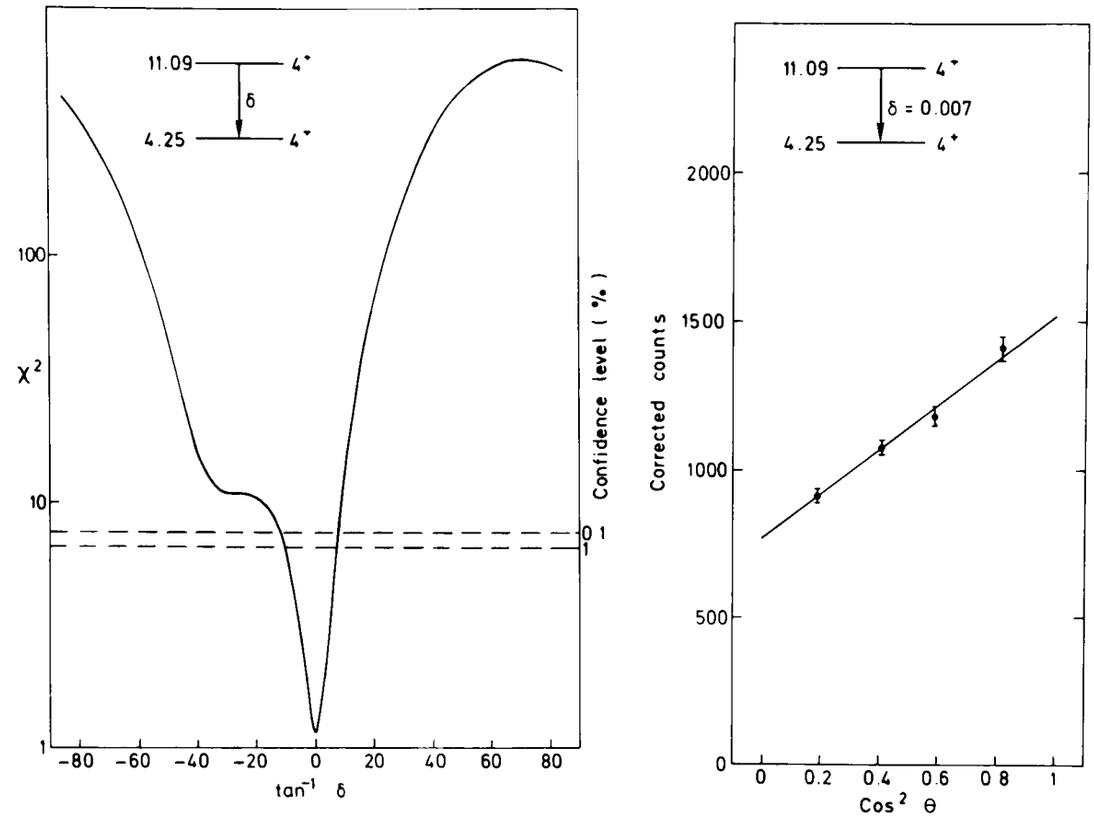

Fig. 3. χ^2 plot from the fit to the γ-ray angular distribution of the 11.09 → 4.25 MeV transition for a spin hypothesis of 4^+ for the 11.09 MeV level. The angular distribution is also shown, and the solid line is the best fit, obtained for $\delta = 0.007$.

whereas the angular distribution shown in fig. 3 was obtained from the full energy peak of the $R \rightarrow 4.25$ MeV γ-ray as measured in an intrinsic germanium detector, and the spectra were completely free of any background from 6.92 or 7.12 MeV γ-rays. We conclude, therefore, that if $J = 4$ for the resonance state, then the $R \rightarrow 4.25$ MeV transition is almost entirely M1, with only a very weak E2 component, as expected for a $\Delta T = 1$ transition.

Having shown that the angular distribution measured by Pearson and Spear is incorrect, we are obliged to re-evaluate their conclusions concerning other possible spin assignments to the resonance level. From fits to the angular distribution shown in fig. 3, spin-parity assignments of 3^- and 5^- can be rejected since they require unacceptably large M2 enhancements of > 350 and > 150 W.u. respectively, while a 2^+ assignment would require an M3 enhancement of $> 10^5$ W.u. and may also be rejected. On the other hand, an acceptable fit is obtained for a 6^+ assignment with $\delta(\mathrm{M3/E2}) \approx 0$. However, the 11.09 MeV has also been populated in the ^{21}Ne(d, t)^{20}Ne reaction via the pickup of an $l = 2$ neutron [21]). This observation is consistent with a 4^+ assignment but not with 6^+. The observation of the $R \rightarrow 1.63$ MeV (2^+) decay mode in the present work also favours the 4^+ assignment. Hence we may conclude that the 11.09 MeV level has spin and parity 4^+. A $T = 1$ assign-

ment to this level follows from the strength (0.5 W.u.) of the M1 transition to the 4.25 MeV level.

3.3. THE 11.27 MeV LEVEL

This resonance has been studied previously by Pearson and Spear [13]), by Steck [14]), and by Davidson and Lowry [12]). Its dominant γ-ray decay mode is to the ^{20}Ne ground state, and the angular distribution of this γ-ray provides [12,14]) an unambiguous spin and parity assignment of 1^-. In addition, Steck [14]) reports an upper limit of 0.3 keV for the total width of this level, and on the basis of this small α-particle width proposes that it is a $T = 1$ state which is the analogue of the 0.923 MeV 1^- state in ^{20}F. However, the strength of the $R \rightarrow$ g.s. E1 transition (5×10^{-4} W.u.) does not discriminate against a $T = 0$ assignment to the 11.27 MeV level.

We have also studied the 11.27 MeV level as a resonance in the ^{16}O(α, γ)^{20}Ne reaction; the on-resonance γ-ray spectrum is shown in fig. 4, and the γ-ray decay

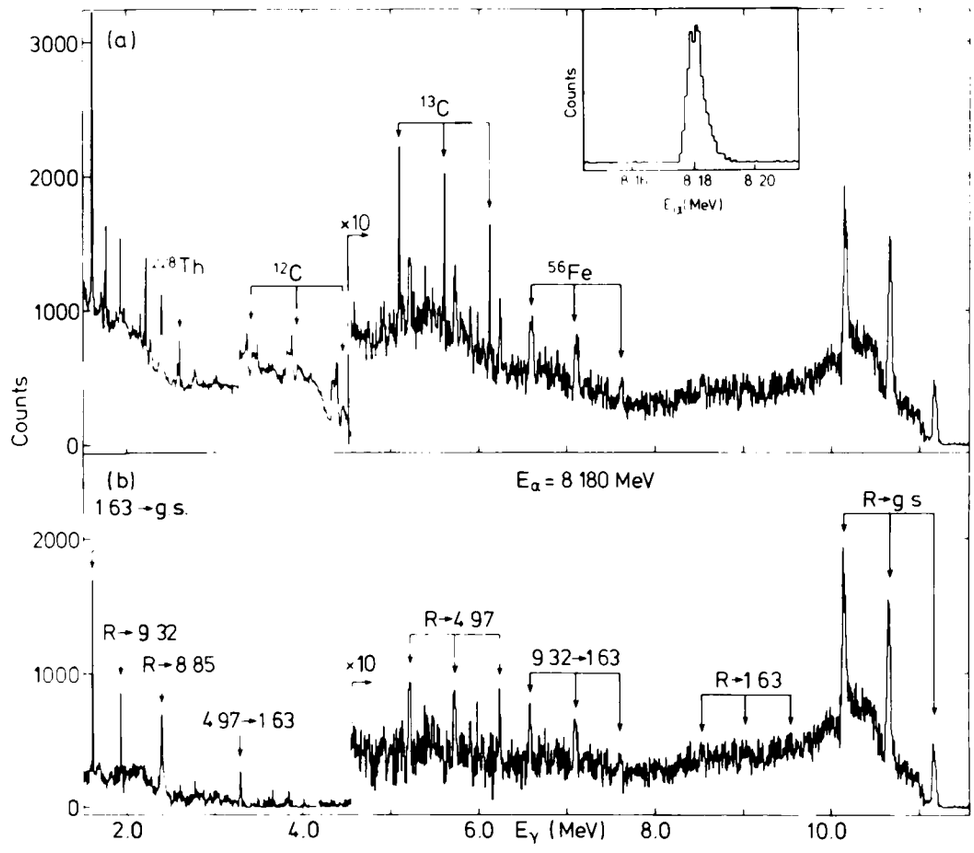

Fig. 4. (a) Spectrum of γ-rays at the 8.18 MeV resonance (E_x = 11.27 MeV) in the ^{16}O(α, γ)^{20}Ne reaction. (b) The same spectrum from which an off-resonance spectrum has been subtracted. The inset shows the γ-ray yield as a function of α-particle energy in the vicinity of the resonance. Gamma rays from the ^{16}O(α, γ)^{20}Ne reaction are labelled by the transition in ^{20}Ne in (b), and contaminant lines are labelled in (a). The lines labelled ^{56}Fe arise from the ^{56}Fe(n, γ)^{57}Fe reaction, while the other lines arise from α-induced reactions on the indicated nuclei. All energies are in MeV, and the on-resonance spectrum represents an accumulated charge of 0.15 C of ^{4}He^{++}

scheme derived from this spectrum is summarised in fig. 1. The advantages conferred by the use of a transmission gas target are immediately apparent. Our spectrum is almost free of 6.13 MeV γ-ray background from the $^{13}C(\alpha, n\gamma)^{16}O$ reaction, and as a consequence five γ-ray branches are observed, in contrast to the one or two branches observed in refs. [12,14]) respectively. One of the additional branches reported here, that to the 8.85 MeV (1^- $T = 0$) level has an important bearing on the properties of the resonance level in that it provides a definitive $T = 1$ assignment. The reduced M1 transition probability for this $R \rightarrow 8.85$ MeV transition, 0.63 ± 0.08 W.u., greatly exceeds the recommended upper limit [20]) for isoscalar M1 transitions, and therefore fixes the isospin of the 11.27 MeV level at $T = 1$.

Both the excitation energy and the resonance strength of the $11.27 \rightarrow$ g.s. transition measured here are in good agreement with those measured by Davidson and Lowry [12]), but are in conflict with the values reported by Steck [14]). His excitation energy differs by two standard deviations from ours, and his value of $\omega\gamma$ for the $R \rightarrow$ g.s. transition is only half that reported here. In addition, Steck reports a γ-ray branch to the 1.63 MeV level which is an order of magnitude greater than the branch shown in fig. 1, but given the very clean nature of our γ-ray spectrum it is difficult to see how his branching ratio could be correct.

These discrepancies are of some importance, since the 11.27 MeV level is perhaps the most topical of the levels studied in the present work. The current interest in this level arises from it being one of a triplet of $J = 1$ levels near this excitation energy. The other two levels, a 1^- $T = 0$ level at 11.23 MeV and a 1^+ $T = 1$ level at 11.26 MeV have been proposed [12,22]) as a favourable nuclear system in which to search for parity mixing produced by the weak neutral current. The significance of the 11.27 MeV 1^- $T = 1$ level to the interpretation of the result of any future experiment on parity mixing in this system has been discussed at some length by Davidson and Lowry [12]). Briefly, the effect of the 1^- $T = 1$ level on the parity-violating α-particle width of the 1^+ $T = 1$ state depends upon the separation of the 1^- $T = 1$ and 1^+ $T = 1$ levels, and upon the width of the 1^- $T = 1$ level. If the excitation energy of the 1^- level is taken from Steck [14]), then, using the best published value for the excitation energy of the 1^+ $T = 1$ level [23]), the separation of the levels is only 2 keV. In this case the parity mixing could be dominated by the $1^-T = 1$ level. If, on the other hand, the separation of the two $T = 1$ levels is obtained from the excitation energy given here or by Davidson and Lowry [12]), then the mixing will be due predominantly to the broad 1^- $T = 0$ level. Since the excitation energies measured by Davidson and Lowry and in the present work were derived from γ-ray spectra taken with Ge(Li) detectors, we feel that these energies are inherently more reliable than that quoted by Steck [14]) which was derived from a rather complicated excitation function. However, the excitation energy of the 1^+ $T = 1$ level is also the subject of some debate at present [12]), and there is a strong case for a direct measurement of the separation of this $1^+T = 1 - 1^-T = 1$ doublet, say by populating both levels in a charged particle reaction and measuring the separation of the two particle

groups. A measurement of the width of the 1^- $T = 1$ level will also be required in any analysis of parity mixing in this system.

There is also some nuclear structure information in the decays of the 11.27 MeV level. The observation of a decay to the 9.32 MeV level, and the subsequent decay of this level by γ-ray emission to the 1.63 MeV level, suggests strongly that the 9.32 MeV level has unnatural parity. The only spin-parity assignments consistent with the observed $11.27 \rightarrow 9.32$ decay strength are then 1^+ or 2^-, and the absence of a $9.32 \rightarrow$ g.s. decay would favour the 2^- assignment. If this assignment is correct, then the M1 transitions from the 11.27 MeV level to the $8.85(1^-)$ and $9.32(2^-)$ MeV levels have large and similar strengths (see table 2), suggesting similar intrinsic structures for the 8.85 and 9.32 MeV levels. This possibility has been noted previously by Millington *et al.* [21]), although their excitation energy of 9357 ± 17 keV for the possible 2^- state differs somewhat from our 9318 ± 2 keV.

3.4. LEVELS AT 11.56 AND 11.92 MeV

Of these two levels, that at 11.56 MeV was observed by Pearson and Spear [13]) as a weak radiative capture resonance, an observation confirmed by Steck [14]), who also observed the level as a narrow resonance ($\Gamma = 1.0 \pm 0.5$ keV) in the elastic scattering channel. The 11.92 MeV (4^+) level has been observed previously [24]) as a very narrow ($\Gamma = 0.44$ keV) elastic scattering resonance. Both levels have been observed here as weak capture resonances, and their properties are summarised in fig. 2 and table 1. We do not observe the branch from the 11.56 to the 4.25 MeV level reported by Steck [14]), although our value of $\omega\gamma$ for the $11.56 \rightarrow 1.63$ MeV transition is in excellent agreement with his $\omega\gamma$ value. The 11.92 MeV level was also observed as a resonance in the yield of 6.13 MeV γ-rays, with $(2J+1)\Gamma_{\alpha_0}\Gamma_{\alpha_2}/\Gamma = 5.2 \pm 0.9$ eV.

3.5. THE DOUBLET AT ~ 12.2 MeV

In their survey of the $^{16}O(\alpha, \gamma)^{20}Ne$ reaction, Pearson and Spear [13]) observed a resonance at a beam energy of 9.40 MeV which they ascribed to a single level with a width of 40 keV. This resonant structure has subsequently been shown by Marrs *et al.* [17]) to be a doublet of levels, with members at 12.216 and 12.254 MeV. Employing the $^{16}O(\alpha, \gamma)^{20}Ne$ reaction, they showed that the former level had spin and parity 2^+, and a total width $\Gamma < 2$ keV. To the latter level they ascribed a total width $\Gamma \sim 5$ keV, while the γ-ray angular distribution limited its spin and parity to 2^+ or 3^-. Further, using the $^{19}F(^3He, d)^{20}Ne$ reaction and looking at γ-rays in coincidence with deuterons, they showed that a level at 12.22 ± 0.03 MeV, which has an $l_p = 2$ stripping angular distribution [25]), has a γ-ray width which is an appreciable fraction of its total width ($\Gamma_\gamma/\Gamma > 0.25$). They concluded this level was therefore to be identified with the 12.216 MeV level ($\Gamma < 2$ keV) rather than the 12.254 MeV level ($\Gamma \sim 5$ keV).

With our facility to adjust the pressure within the gas target at will, we were able to explore this region of excitation energy in ^{20}Ne in finer detail than were Marrs *et al.* [17]) with their thicker solid targets. The relevant portion of the γ-ray yield curve taken at a target pressure of 100 μm (0.8 keV thick to 9.4 MeV α-particles) is shown in fig. 5. It is apparent at once that both resonances are very narrow, the upper resonance as well as the lower one having $\Gamma < 1$ keV, in marked contrast to

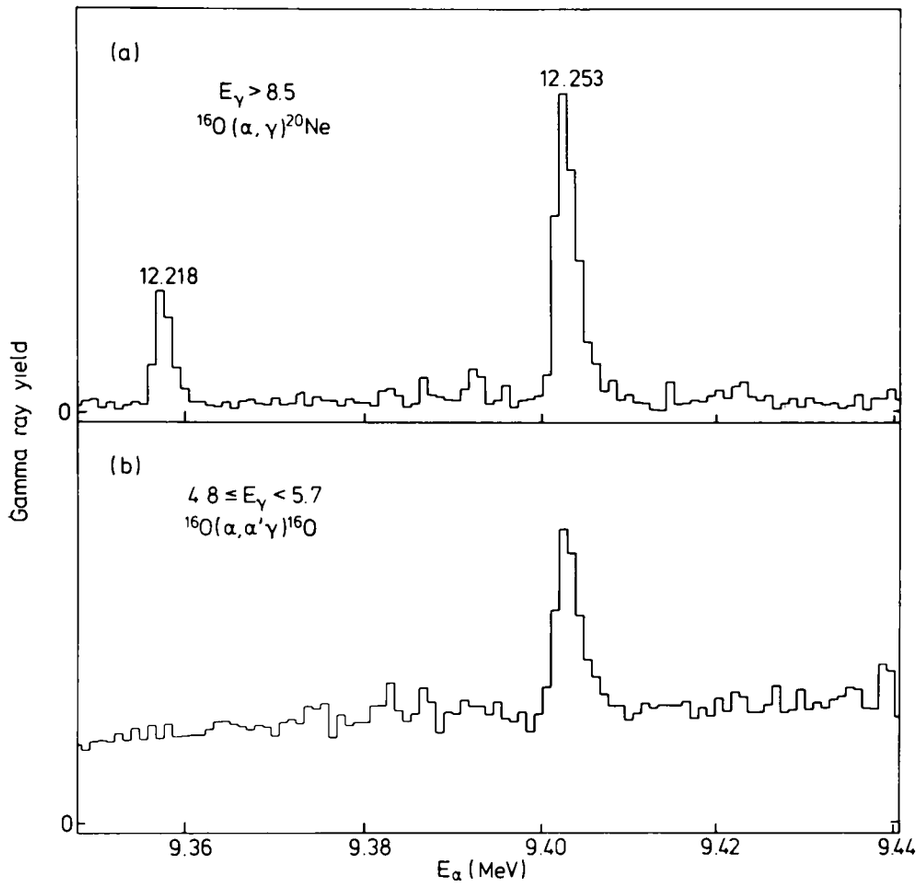

Fig. 5. Gamma-ray yield as a function of α-particle energy in the vicinity of the 12.22–12.25 MeV doublet in ^{20}Ne. The selected regions of the γ-ray spectrum are indicated, and correspond to the $^{16}O(\alpha, \gamma)^{20}Ne$ and $^{16}O(\alpha, \alpha'\gamma)^{16}O$ reactions for (a) and (b) respectively.

the 5 keV width measured by Marrs *et al.* [17]) at the upper resonance. Consequently, the identification of the 12.216 MeV 2^+ level observed in α-capture with the 12.22 MeV level observed in the $^{19}F(^3He, d)^{20}Ne$ reaction appears more tenuous than the data of Marrs *et al.* [17]) would suggest. However, there are other grounds discussed below for supposing that this identification is in fact correct. The origin of the discrepancy between the present work and that of Marrs *et al.* is to be found within the text of ref. [17]), for, having established their target thickness to be 85 keV at the well known 6.93 MeV 2^+ $T = 1$ resonance, they proceeded to use an incorrect value of 80 keV for the thickness of the same target at 9.4 MeV. Reference to the tables of Northcliffe and Schilling [26]) indicates that the target thickness

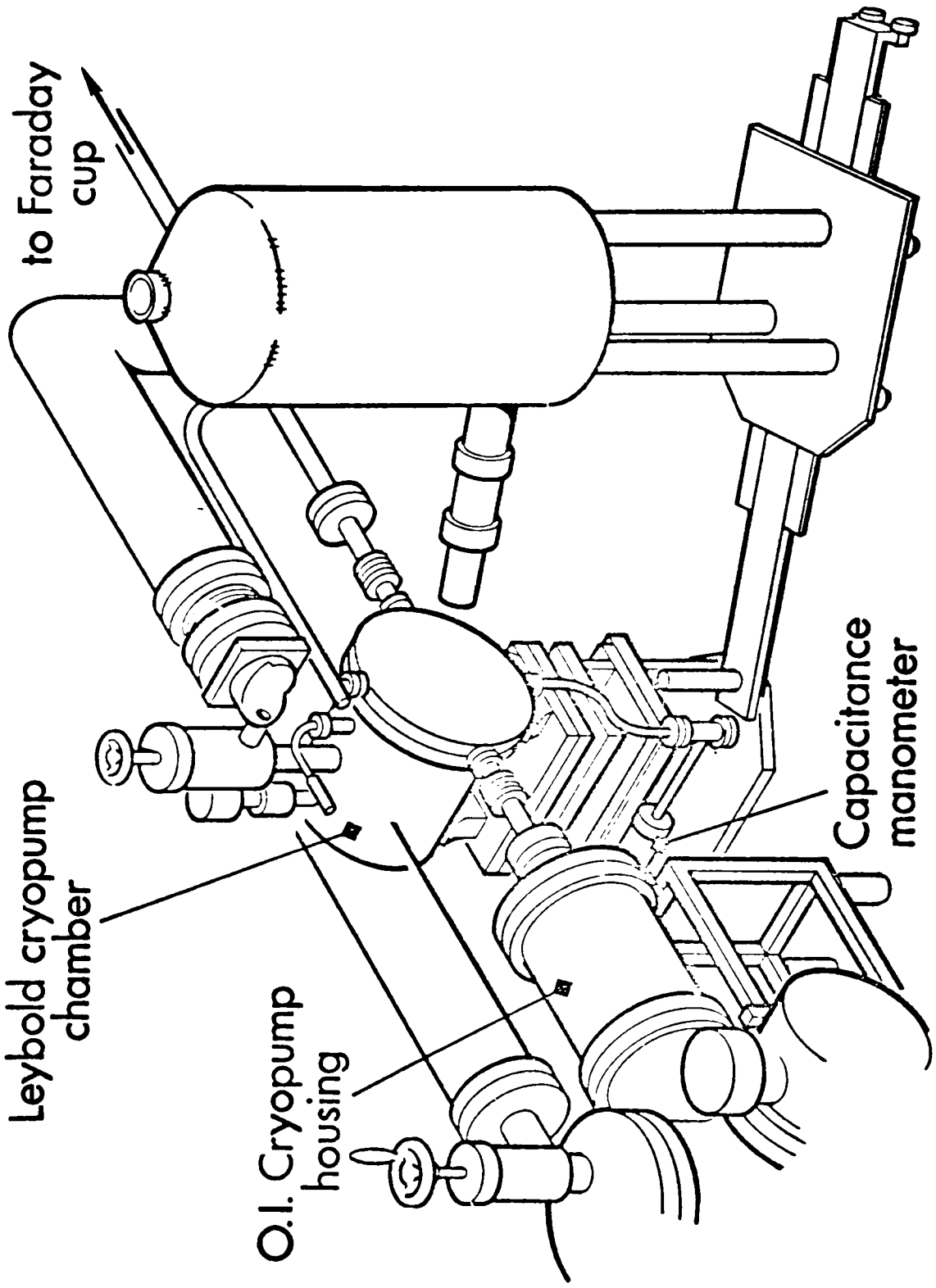

Fig.2.2.1 Layout of the MkIII cryogenically pumped gas target.

would in fact be 70 keV at the higher energy. The use of the incorrect target thickness in subtracting the resonance shape of the lower resonance from the composite yield curve has clearly led to an incorrect estimate of the width of the upper level. The possibility of an error in the width of this upper level has been noted also by Steck [14]) from an anlysis of the elastic scattering data.

In addition to measuring the γ-ray yield curve in this region, we have measured γ-ray decay schemes for both resonances, and have performed a γ-ray angular distribution measurement at the upper one. The decay schemes, values of $\omega\gamma$, and excitation energies are summarised in figs. 1 and 2 and table 1. For the 12.22 MeV level, and for $\omega\gamma$ of the $R \rightarrow 1.63$ MeV decay of the 12.25 MeV level, our results are in excellent agreement with those of Marrs *et al.* [17]). We also observe a branch from the 12.25 MeV level to the 5.62 MeV 3$^-$ level which was not observed by them. Further, the separation of the two members of the doublet is somewhat less in the present work than in ref. [17]), which may be a consequence of their incorrect subtraction procedure noted above. We note that, in common with Marrs *et al.* [17]), we see no evidence for the γ-ray decay from either member of the doublet to the ^{20}Ne ground state reported by Steck [14]) to have an $\omega\gamma$ of 2.7 eV.

The results of fits to both the 12.25 $\rightarrow$ 1.63 and 12.25 $\rightarrow$ 5.62 MeV γ-ray angular distributions are presented in fig. 6. An unambiguous spin and parity assignment of 3$^-$ to the 12.25 MeV level can be deduced from these fits. The angular distribution of the $R \rightarrow 1.63$ MeV transition rules out the 1$^-$ possibility since it requires an M2 strength of greater than 6 W.u. (two standard deviation limit) which exceeds the recommended upper limit of Endt and Van der Leun [20]). The alternative 2$^+$ assignment is ruled out, since the M2/E1 mixing ratio of the 12.25 $\rightarrow$ 5.62 MeV transition is constrained by the fit to be > 0.34 (at two standard deviations) if $J = 2$, which implies an unreasonably large M2 transition probability of > 36 W.u.

Having established a 3$^-$ assignment to the 12.25 MeV level, the transition to the 5.62 MeV level is an M1 transition with a strength (0.06 W.u.) which is characteristic of an isovector transition [21]). The 12.25 MeV level therefore has $T = 1$, and it, rather than the 12.39 MeV level as proposed by Steck [14]), must be the $T_z = 0$ analogue of the 1.97 MeV 3$^-$ level in ^{20}F.

An assignment of 3$^-$ to the 12.25 MeV level also implies that the level populated in the ^{19}F(^{3}He, d)^{20}Ne reaction via the transfer of an $l_p = 2$ proton is to be identified with the 12.216 MeV 2$^+$ level observed in α-capture, and not with the 12.25 MeV level.

One further piece of information forthcoming from the present work is the observation of the 12.25 MeV level as a resonance in the ^{16}O(α, α_2)^{16}O* (6.13 MeV) reaction (see fig. 5) with $(2J+1)\Gamma_{\alpha_0}\Gamma_{\alpha_2}/\Gamma = 14 \pm 2$ eV. This provides lower limits of 1.7 eV on both Γ_{α_0} and Γ_{α_2}, 6.8 eV on Γ, and an upper limit of 60 % on $\Gamma_\gamma/\Gamma_{\alpha_2}$, which translates into a conservative upper limit of 38 % on Γ_γ/Γ. If, as seems likely, Γ_{α_0} is comparable to or larger than Γ_{α_2}, then this upper limit would be reduced by at least a factor of two. Hence it is unlikely that the 12.25 MeV 3$^-$ $T = 1$ level has an appreci-

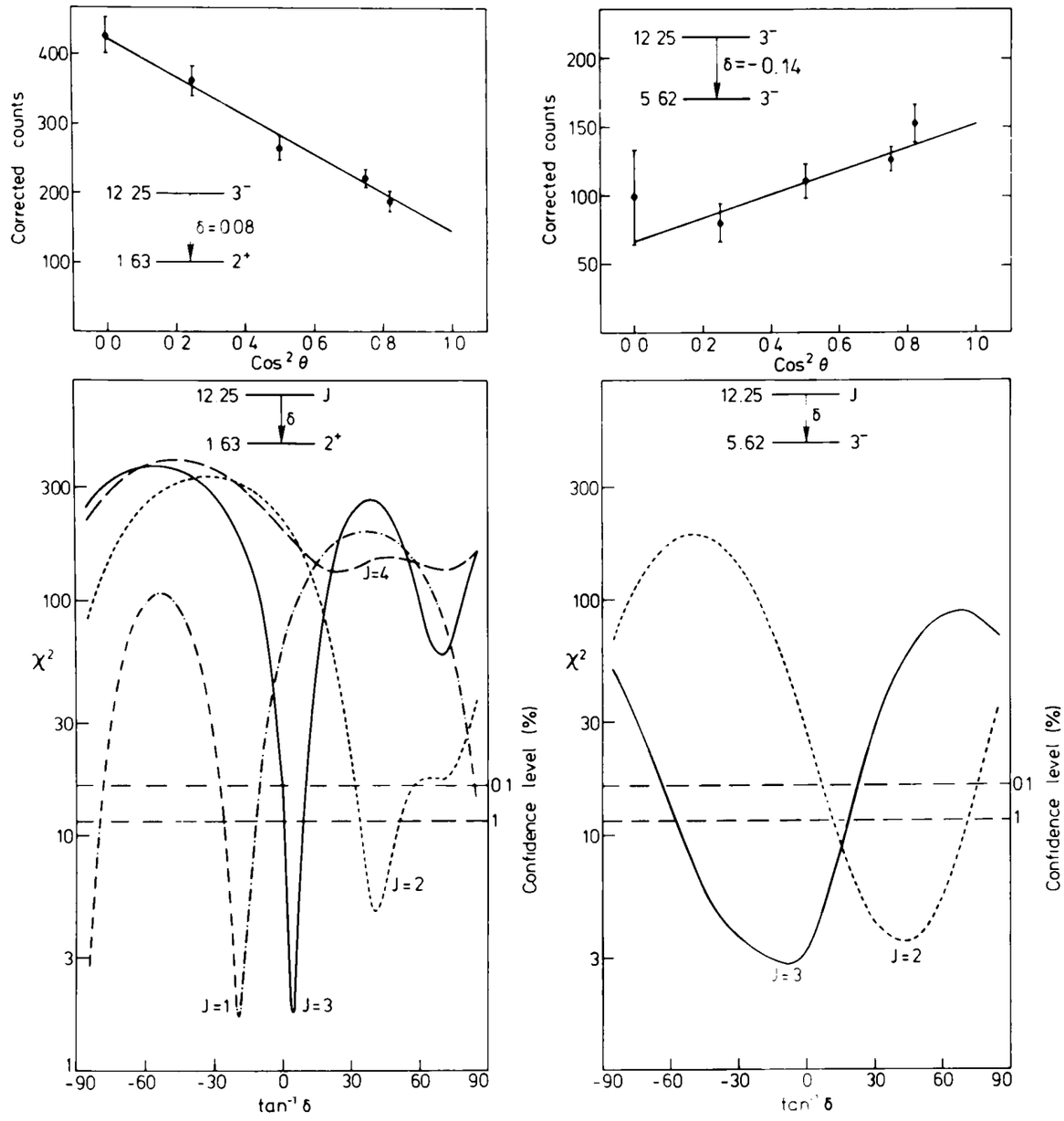

Fig. 6. χ^2 plots from fits to the γ-ray angular distributions of the 12.25 → 1.63 and 12.25 → 5.62 MeV transitions for various spin hypotheses for the 12.25 MeV level. The angular distributions are shown with the best fits for $J^\pi = 3$

able γ-ray branching ratio. This conclusion is of some importance to the interpretation of the properties of the 18.43 MeV 2^+ $T = 2$ state. This $T = 2$ level is populated as a resonance in the ^{19}F(p, γ)^{20}Ne reaction [18]), and its γ-ray decay proceeds through a level near 12.2 MeV in ^{20}Ne. However, since the primary 18.43 → 12.2 MeV decay is obscured by γ-rays from the prolific ^{19}F(p, α)^{16}O* reaction, only the secondary 12.2 → 1.63 MeV γ-ray is observed [18]). Clearly, this γ-ray will only be observed if the 12.2 MeV level has an appreciable γ-ray decay branch. The 12.22 MeV 2^+ level has this property ($\Gamma_\gamma/\Gamma > 0.25$) whereas the 12.25 MeV 3^- $T = 1$ level probably does not. It then follows that, since the 12.22 MeV 2^+ level is fed by a γ-ray decay

from a $T = 2$ level, it must have $T = 1$ and may be identified as the analogue of the 2.044 MeV 2^+ state in ^{20}F. The question of the 18.43 2^+ $T = 2$ and 12.22 2^+ $T = 1$ levels will be taken up again in the discussion section.

3.6. THE 12.14 MeV 6^+ LEVEL

This level has been observed previously in the ^{12}C(^{12}C, α)^{20}Ne reaction [27]), and is thought to be the 6^+ member of an 8p-4h band built upon the 7.19 MeV 0^+ level. A weak resonance in the ^{16}O(α, α_2)^{16}O* (6.13 MeV) reaction was observed at 9.25±0.04 MeV (E_x = 12.13±0.04 MeV) by Pearson and Spear [13]), and their value of $(2J+1)\Gamma_{\alpha_0}\Gamma_{\alpha_2}/\Gamma$ (with a 50 % error) was employed by Balamuth *et al.* [28]) in determining the partial α-decay widths of this level. However, neither Steck [14]) nor Marrs *et al.* [17]) observed this resonance, presumably due to the large background of 6.13 MeV γ-rays from the ^{13}C(α, nγ)^{16}O reaction.

The yield of 6.13 MeV γ-rays as a function of energy in the vicinity of the 12.14 MeV level as measured in the present work is shown in fig. 7. The resonance observed

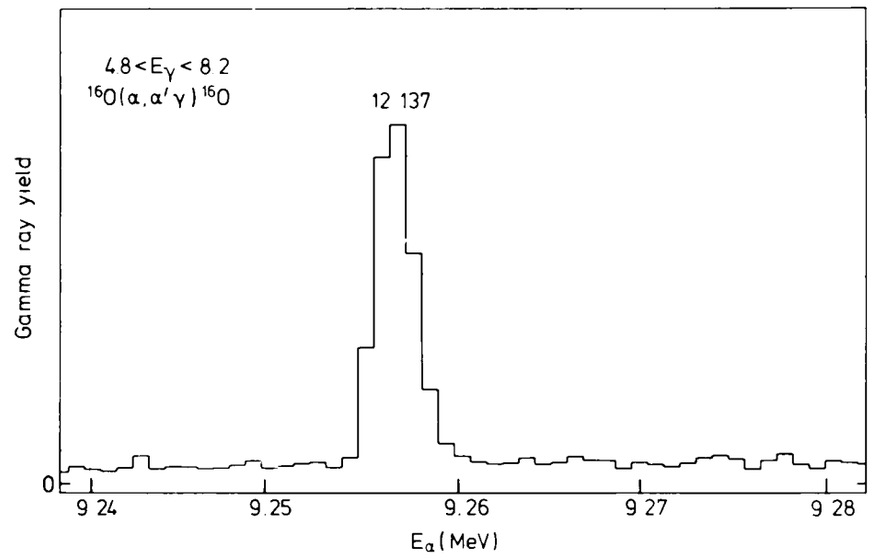

Fig. 7. Yield of 6.13 MeV γ-rays from the ^{16}O(α, $\alpha'\gamma$)^{16}O reaction as a function of α-particle energy in the vicinity of the 12.14 MeV (6^+) level in ^{20}Ne.

by Pearson and Spear [13]) just above background is now very clearly visible. On-resonance and off-resonance γ-ray spectra were measured with the Ge(Li) detector, both to determine an accurate value for $(2J+1)\Gamma_{\alpha_0}\Gamma_{\alpha_2}/\Gamma$ and to search for capture γ-rays from the 12.14 MeV level. No capture γ-rays were observed. Our value of the inelastic resonance strength, 81±12 eV is considerably more accurate than that of Pearson and Spear [13]), but is close to their value of 80±40 eV (after correcting it from the lab to the c.m. frame). Consequently, the conclusions of Balamuth *et al.* [28]) concerning the partial α-particle widths of this level are unaffected. A value of

12137±5 keV was deduced for its excitation energy from the relative α-particle energies at the resonances corresponding to this level and to the 12.253 MeV level. The excitation energy of the latter level was determined accurately from its on-resonance γ-ray spectrum.

4. Discussion and summary

Of the levels studied in the present work, four have been assigned $T = 1$ and may be unambiguously identified with levels in ^{20}F. Fig. 8 shows a comparison between the $T = 1$ spectrum of ^{20}Ne up to 12.3 MeV as far as it is currently known and the spectrum of ^{20}F. There is seen to be a one to one correspondence between the two sets of levels with the single exception of the 1.82 MeV 5^+ level in ^{20}F for which the counterpart in ^{20}Ne has not yet been observed. We observe that, as the excitation energy increases, the positive parity levels in ^{20}F are shifted by progressively larger amounts relative to their analogues in ^{20}Ne, whereas the negative parity levels in ^{20}F remain accurately aligned with their ^{20}Ne counterparts.

For the positive parity $T = 1$ levels in ^{20}Ne, it is possible to carry out shell-model calculations of the radiative decay rates within a complete $(sd)^4$ basis. Such calculations have been carried out using the effective interactions of Preedom and Wildenthal [29]) and Chung and Wildenthal [30]). The results for all the positive parity levels shown in fig. 8 are summarised in table 3, and compared with experimental results where these are available. The agreement between calculation and experi-

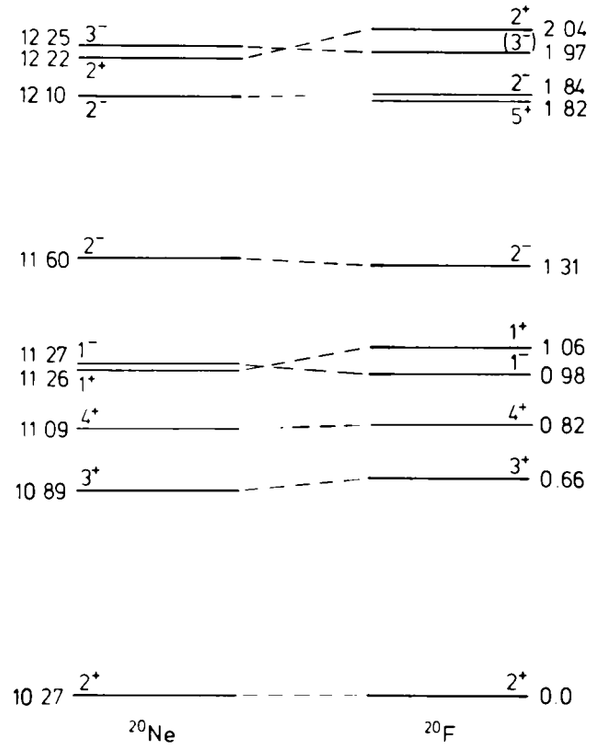

Fig. 8. Comparison of $T = 1$ energy spectra of ^{20}Ne and ^{20}F.

TABLE 3

Comparison of measured and calculated radiative transition rates for positive parity $T = 1$ and $T = 2$ levels in ^{20}Ne

E_i (MeV)	J_i^π, T_i	E_f (MeV)	J_f^π, T_f	Mλ	B(Mλ) (W.u.)		
					experiment	PW [a])	CW [a])
10.27	$2^+, 1$	0.0	$0^+, 0$	E2	0.10 ± 0.03 [b])	0.10	0.11
		1.63	$2^+, 0$	M1	0.31 ± 0.03 [b])	0.20	0.27
		7.42	$2^+, 0$	M1	0.65 ± 0.08 [b])	0.62	0.54
10.89	$3^+, 1$	1.63	$2^+, 0$	M1	$> 1 \times 10^{-3}$ [c])	0.13	0.14
		4.25	$4^+, 0$	M1	$> 8 \times 10^{-4}$ [c])	0.08	0.12
11.09	$4^+, 1$	1.63	$2^+, 0$	E2	0.09 ± 0.04	0.05	0.05
		4.25	$4^+, 0$	M1	0.50 ± 0.06	0.48	0.53
				E2	< 0.4	0.004	0.002
11.26	$1^+, 1$	0.0	$0^+, 0$	M1	0.38 ± 0.06 [d])	0.36	0.34
12.22	$2^+, 1$	1.63	$2^+, 0$	M1	> 0.013	0.29	0.25
18.42	$2^+, 2$	12.22	$2^+, 1$	M1	0.06 [e])	0.32	0.40

[a]) Shell-model calculations employing the Preedom-Wildenthal and Chung-Wildenthal effective interactions, effective charges $e_n = 0.5e$, $e_p = 1.5e$, and bare nucleon g-factors.

[b]) Ref. [7]).

[c]) Limit on lifetime from Ajzenberg-Selove, ref. [16]). Branching ratio from ref. [17]).

[d]) Bendel *et al.* [31]).

[e]) Ref. [18]); assumes $\Gamma_\gamma/\Gamma \simeq 1$ for 12.22 MeV level.

ment is generally very satisfactory. Of particular relevance to the present work are the levels at 11.09(4^+ $T = 1$) and 12.22(2^+ $T = 1$) MeV. For the 11.09 MeV level the calculated strengths of the decays to both the 4.25 and 1.63 MeV levels are in excellent accord with experiment for either interaction. For the 12.22 MeV level, a more accurate measurement of Γ_γ/Γ will be required before calculation and experiment can be compared. However, if we assume that the calculated value of Γ_γ for the 12.22 MeV level is approximately correct (the good agreement between calculation and experiment for the other $T = 1$ levels indicates that this is a reasonable thing to do), then, from the measured value of $\omega\gamma$ we would obtain $\Gamma_\alpha = 0.29$ eV and $\Gamma_\gamma/\Gamma \approx 0.96$. Such a tiny α-particle width, which is only 1/400 of the α-particle width of the lowest 2^+ $T = 1$ level at 10.27 MeV [ref. [6])], implies either a very high degree of isospin purity in the 12.22 MeV level, or a fortuitous cancellation of the α-particle amplitudes of the 2^+ $T = 0$ levels mixed into the 12.22 MeV level by the Coulomb interaction.

Although the agreement between calculation and experiment is very satisfactory for the positive parity $T = 1$ levels in ^{20}Ne, the status of the lowest 2^+ $T = 2$ level at 18.43 MeV is much less satisfactory. The shell-model calculations (table 3) predict an M1 strength around 0.36 W.u. for the 2_1^+ $T = 2 \rightarrow 2_2^+$ $T = 1$ transition, whereas the value measured by Kuan *et al.* [18]) was only 0.06 W.u., under the additional

assumption that Γ_γ/Γ of the 12.22 MeV (2_2^+ $T = 1$) level was approximately unity. As the discussion in the preceding paragraph indicates, there is a good chance that this assumption is correct, although a better measurement of Γ_γ/Γ is obviously needed. Hence, there appears to be a discrepancy of approximately a factor of 6 between the measured and calculated transition rate connecting the 2_1^+ $T = 2$ and 2_2^+ $T = 1$ levels in ^{20}Ne. Given the simple nature of the two levels involved this is a surprising result.

Recently, Millener [30]) has performed shell-model calculations for low-lying negative parity levels in ^{20}Ne. His basis included both $p^{-1}sd^5$ and sd^3pf configurations, and contained all states from the (82), (90), (71), (63) and (44) representations of SU(3). By including both hole and particle configurations, spurious components could be eliminated from the calculated wave functions. The calculated electromagnetic M1 transition rates for the lowest 1^- $T = 1$ and 3^- $T = 1$ levels are presented and compared with experiment in table 4. For the 1^- state, the calculations

TABLE 4

Comparison of calculated and measured M1 transition rates for negative parity $T = 1$ levels in ^{20}Ne

E_i (MeV)		J_i^π, T_i	E_f (MeV)		J_f^π, T_f	B(M1) (W.u.)	
expt	theory [a])		expt	theory		expt	theory [b])
11.27	10.67	$1^-, 1$	5.78	6.70	$1_1^-, 0$	$< 5\times10^{-3}$	3.7×10^{-3}
			8.72	8.75	$1_2^-, 0$	< 0.02	0.29
			8.85	9.56	$1_3^-, 0$	0.63 ± 0.08	1.00
			4.97	(4.97)	$2_1^-, 0$	0.009 ± 0.002	0.020
			(9.32)	9.12	$2_2^-, 0$	0.40 ± 0.07	0.49
12.25	10.99	$3^-, 1$	4.97	(4.97)	$2_1^-, 0$	$< 5\times10^{-3}$	1×10^{-3}
			5.62	5.30	$3_1^-, 0$	0.06 ± 0.01	0.26

[a]) Calculated excitation energies normalised to the 4.97 MeV 2^- level.
[b]) Calculations of Millener [30]). See text.

reproduce very nicely the strong M1 transitions to the 1_3^- $T = 0$ and 2_2^- $T = 0$ levels if the latter level is identified with the 9.32 MeV level observed experimentally. The only serious discrepancy lies in the transition to the 1_2^- $T = 0$ level which experimentally is substantially weaker than predicted. However, we feel these results are sufficiently encouraging to justify further refinement of these preliminary calculations, either by expanding the basis or by investigating the effect of using different effective interactions. For the 3^- $T = 1$ state the calculations correctly predict that the dominant transition should be to the lowest 3^- $T = 0$ level, although the predicted strength is too large.

To summarise, nine levels between 8.5 and 12.4 MeV in ^{20}Ne have been studied with the ^{16}O(α, γ)^{20}Ne reaction. Three of the levels have not been observed previously in this reaction, and a considerable amount of new information has been obtained for those resonances which had been observed in earlier work. In particular, definitive $T = 1$ assignments have been made to levels at 11.27(1^-), 12.22(2^+)

and 12.25(3^-) MeV in ^{20}Ne, and the rather confused situation concerning the 12.22/12.25 MeV doublet has been clarified. The properties of the 11.27 MeV (1^- $T = 1$) level are of considerable importance to the interpretation of a proposed parity mixing experiment, while the 12.22 MeV level is closely associated with the decay properties of the lowest 2^+ $T = 2$ level in ^{20}Ne.

We wish to thank N. S. Godwin and Dr. B. A. Brown for their advice on the shell-model calculations, and Dr. D. Kelvin of Glasgow University for several useful discussions.

References

1) T. K. Alexander, O. Häusser, A. B. McDonald, A. J. Ferguson, W. T. Diamond and A. E. Litherland, Nucl. Phys. **A179** (1972) 477
2) D. W. O. Rogers, J. H. Aitken, A. E. Litherland, W. R. Dixon and R. S. Storey, Can. J. Phys. **49** (1971) 1397
3) W. T. Diamond, T. K. Alexander and O. Häusser, Can. J. Phys. **49** (1971) 1589
4) T. K. Alexander, B. Y. Underwood, N. Anyas-Weiss, N. A. Jelley, J. Szucs, S. P. Dolan, M. R. Wormald and K. W. Allen, Nucl. Phys. **A197** (1972) 1
5) D. W. O. Rogers, K. W. Allen, H. C. Evans, N. A. Jelley, A. E. Litherland and B. Y. Underwood, Phys. Lett. **37B** (1971) 65
6) P. D. Ingalls, Nucl. Phys. **A265** (1976) 93
7) L. K. Fifield, F. P. Calaprice, C. H. Zimmerman, M. J. Hurst, A. Pakkanen, T. J. M. Symons, F. Watt and K. W. Allen, Nucl. Phys. **A288** (1977) 57
8) H. Genz, A. Richter and B. M. Schmitz, Nucl. Phys. **A267** (1976) 13
9) S. J. Freedman, R. D. Cousins, C. A. Gagliardi, G. T. Garvey and J. F. Greenhalgh, Phys. Lett. **67B** (1977) 165
10) N. Rolin, J. P. Deutsch, D. Favart, M. Lebrun and R. Prieels, Phys. Lett. **70B** (1977) 23
11) R. E. Tribble and D. P. May, Phys. Rev. **C18** (1978) 2704
12) J. M. Davidson and M. M. Lowry, Phys. Rev. **C18** (1978) 2276
13) J. D. Pearson and R. H. Spear, Nucl. Phys. **54** (1964) 434
14) D. J. Steck, Phys. Rev. **C17** (1978) 1034
15) F. Watt, L. K. Fifield, M. J. Hurst, T. J. M. Symons, C. H. Zimmerman and K. W. Allen, Nucl. Instr. **151** (1978) 163
16) F. Ajzenberg-Selove, Nucl. Phys. **A300** (1978) 1
17) R. E. Marrs, E. G. Adelberger and K. A. Snover, Nucl. Phys. **A277** (1977) 429
18) H. M. Kuan, G. L. Latshaw, W. J. O'Connell, D. W. Keikinen, E. G. Adelberger, A. V. Nero and S. S. Hanna, Nucl. Phys. **A193** (1972) 497
19) M. R. Wormald and J. Takacs, Nucl. Instr. **113** (1974) 263
20) P. M. Endt and C. van der Leun, Nucl. Data **13A** (1974) 67
21) G. F. Millington, J. R. Leslie, W. McLatchie, G. C. Ball, W. G. Davies and J. S. Forster, Nucl. Phys. **A228** (1974) 382
22) F. P. Calaprice, private communication
23) P. D. Ingalls, Phys. Rev. **C14** (1976) 254
24) O. Häusser, A. J. Ferguson, A. B. McDonald, I. M. Szöghy, T. K. Alexander and D. L. Disdier, Nucl. Phys. **A179** (1972) 465
25) R. R. Betts, H. T. Fortune and R. Middleton, Phys. Rev. **C11** (1975) 19
26) L. C. Northcliffe and R. F. Schilling, Nucl. Data **7A** (1970) 233
27) J. A. Kuehner and E. Almqvist, Can. J. Phys. **45** (1967) 1605
28) D. P. Balamuth, J. W. Noé, H. T. Fortune and R. W. Zurmühle, Phys. Rev. **C6** (1972) 1694
29) B. M. Preedom and B. H. Wildenthal, Phys. Rev. **C6** (1972) 1633
30) D. J. Millener, Brookhaven National Laboratory, private communication
31) W. L. Bendel, L. W. Fagg, S. K. Numrich, E. C. Jones and H. F. Kaiser, Phys. Rev. **C3** (1971) 1821

J. Phys. G: Nucl. Phys. 6 (1980) 891–899. Printed in Great Britain

An alpha-capture measurement of the radiative width of the first 8^+ state in ^{20}Ne

M J Hurst†, L K Fifield, E F Garman, T J M Symons‡, F Watt and K W Allen

Nuclear Physics Laboratory, Oxford University, Keble Road, Oxford OX1 3RH, UK

Received 31 December 1979, in final form 3 March 1980

Abstract. The radiative width of the 11·95 MeV 8^+ $K^\pi = 0^+$ level in ^{20}Ne has been remeasured using the ^{16}O$(\alpha, \gamma)^{20}$Ne reaction and a differentially cryopumped gas target. The resonance strength was measured to be $\omega\gamma = 131 \pm 18$ meV, which corresponds to a value of $9{\cdot}2 \pm 1{\cdot}3$ Weisskopf units for the $8^+ \rightarrow 6^+$ E2 in-band transition probability. This is somewhat weaker than shell-model predictions normalised to the transitions between the lower members of the $K^\pi = 0^+$ band.

NUCLEAR REACTIONS ^{16}O$(\alpha, \gamma)^{20}$Ne, $E = 9{\cdot}02$ MeV; measured $\sigma(E_\alpha, E_\gamma)$. ^{20}Ne, 11·95 MeV 8^+ level; deduced Γ_γ. Enriched gas target.

1. Introduction

The radiative width of the 8^+ member of the ground-state band in ^{20}Ne is a quantity of considerable interest and historical significance. Following the discovery of rotational band structure in light nuclei, the question arose as to whether the in-band E2 transition rates followed the rotational model prescription, or whether, as predicted by the shell model, there is a band cut-off which results in the transition between the highest spin members of a band falling substantially below the simple rotational value. The pioneering work of Alexander *et al* (1972) on the 8^+ level in ^{20}Ne demonstrated that the shell model gave qualitatively the correct description, and provided considerable impetus for shell-model calculations of the strongly deformed nuclei in the lower sd shell. A similar conclusion was reached from a consideration of the strength of the $\frac{13}{2}^+ \rightarrow \frac{9}{2}^+$ transition in ^{19}F (Jackson *et al* 1969).

However, the precision of the measurement of Alexander *et al* (1972) ($(2J + 1)\Gamma_\gamma\Gamma_\alpha/\Gamma = 104 \pm 35$ meV) was not very high. Given the accuracy of modern shell-model calculations, especially for simple states such as members of a GS rotational band, we felt that, if possible, a more accurate measurement of the $8^+ \rightarrow 6^+$ transition strength was called for. We report the result of such a measurement in this paper.

2. Experimental procedure

The present measurement employed a beam of 9 MeV α particles from the Oxford vertical accelerator incident on $^{16}O_2$ gas confined within a differentially pumped gas

† Present address: CEGB Computing Centre, 85 Park Street, London SE1.

‡ Present address: Lawrence Berkeley Laboratory, Berkeley, California 94720, USA.

0305-4616/80/070891+09$01.50

target (Watt 1978). In contrast, Alexander *et al* (1972) employed a differentially pumped helium target and an ^{16}O beam, and detected the 3·2 MeV capture γ rays in an annular NaI crystal surrounding the target. In this way they avoided the background problems outlined below, although at the expense of introducing a background of 6·13 MeV γ rays from inelastic scattering of their 36 MeV ^{16}O beam by target contaminants. However, provided that the background problems associated with a 9 MeV α-particle beam can be overcome, the use of a helium beam has the major advantage over an oxygen beam that its intensity can be at least an order of magnitude greater. This is because the helium beam may be produced directly using positive ions from a terminal ion source, whereas the production of an energetic oxygen beam involves negative-ion acceleration in a tandem generator.

The major source of background produced by a ^4He beam at 9 MeV arises from the $^{12}C(\alpha, \alpha'\gamma)^{12}C$ reaction on carbon contamination of the tantalum differential pumping nozzles, despite the very small fraction of beam ($\sim 0{\cdot}2\%$) striking them. This reaction has a strong, broad (70 keV) resonance at 8·98 MeV (Larson and Spear 1964) which overlaps the energy of 9·02 MeV (Häusser *et al* 1972) where the 8^+ resonance is expected. This radiation is particularly troublesome because the double escape peak of the 4·43 MeV γ ray falls at 3·41 MeV, which is close to the $8^+ \rightarrow 6^+$ transition in ^{20}Ne (the only possible γ-ray transition since the 6^+ level is α-unstable) expected at 3·17 MeV. The problem is exacerbated because of substantial Doppler shifts and Doppler broadening of the 4·43 MeV γ ray due to the different angles subtended by the nozzles at the detector and by the range of velocities of the γ-ray emitting $^{12}C^*$ nucleus. Consequently, it was not possible to locate the 8^+ resonance by our usual yield curve technique employing a NaI detector and automatic beam energy modulation, since tiny fluctuations in beam direction or focusing conditions would cause a substantial increase in count rate in a gate set about the 3·17 MeV γ ray from the $8^+ \rightarrow 6^+$ transition. Hence, instead of the usual NaI crystal, a 125 cm^3 (25%) Ge(Li) detector positioned 2 cm from the target and at 90° to the beam direction was used for the yield curves in order to set a much narrower energy gate around the expected $8^+ \rightarrow 6^+$ γ ray. The beam energy calibration was defined by a yield curve over the 4^+ resonance at $E_x = 11\,925$ keV, relative to which the energy of the 8^+ level was accurately known (Häusser *et al* 1972). After many modulations of the beam energy over a 40 keV scan centred on the expected position of the 8^+ resonance, the resonance became apparent as a small peak at the expected energy in the yield of γ rays in the 3·17 MeV gate.

When the 8^+ resonance had been located, the 25% Ge(Li) detector was moved to an angle of 127° at a distance of 11·5 cm from the target, and an 85 cm^3 (16·6%) Ge(Li) detector was positioned at 46° and 10 cm. The target pressure was maintained at 0·6 Torr, which corresponds to a target thickness of 6·7 keV, and spectra were accumulated on-resonance for an integrated beam charge ($^4He^{2+}$) of 0·151 C. This corresponds to $4{\cdot}7 \times 10^{17}$ incident particles and should be compared with the $7{\cdot}7 \times 10^{15}$ oxygen nuclei incident on a helium target in the measurement of Alexander *et al* (1972). The beam energy was then reduced by 12 keV and off-resonance spectra accumulated with the same detector geometry and gas pressure for a beam charge of 0·10 C. A week later, when the beam was again available, the yield curve over the 11·925 MeV 4^+ level was repeated to redefine the beam energy calibration, and the beam energy was then raised by the same amount as in the previous run. Spectra were accumulated with the larger Ge(Li) detector at 125° and 9·5 cm from the target, and with the 16·6% Ge(Li) in the same position as before. Three further pairs of spectra were taken with downwards adjustments of approximately 1 keV in the beam energy between each. The gas pressure

for this set of four runs was 0·8 Torr, which corresponds to a target thickness of 8·9 keV.

In all, ten spectra were taken on-resonance; a γ-ray peak was clearly visible at the expected energy of the $8^+ \rightarrow 6^+$ transition in ^{20}Ne in each of them, and it was absent from the two off-resonance spectra. The first of the five spectra taken with the larger Ge(Li) detector is shown in figure 1, together with the off-resonance spectrum taken with the same detector. Note that the spectra are dominated by the Doppler shifted and broadened peaks from the $^{12}C(\alpha, \alpha'\gamma)^{12}C$ reaction on carbon on the differential pumping nozzles, but are flat in the region of interest.

Spectra were also taken in each of the above geometries at the 6·92 MeV (2^+, $T = 1$) resonance in the $^{16}O(\alpha, \gamma)^{20}Ne$ reaction. The target pressures were chosen so that the beam energy losses in the target were the same as in the corresponding measurements on the 8^+ level. The strength $\omega\gamma$ ($=(2J + 1)\Gamma_\gamma\Gamma_\alpha/\Gamma$) of this resonance has been accurately measured recently by three groups (Ingalls 1976, Fifield *et al* 1977, Snover *et al* 1978), making it a convenient reference resonance. The value of $\omega\gamma$ for the 8^+ level was therefore determined by a comparison of γ-ray yields at the 2^+, $T = 1$ and 8^+ resonances, using the weighted average of the three accurate values of $\omega\gamma$ for the reference resonance, 19·5 ± 0·8 eV. The relative efficiency with γ-ray energy of the 16·6% detector was well known (Fifield *et al* 1977) and the relative efficiency of the 25% detector was measured with a ^{56}Co source.

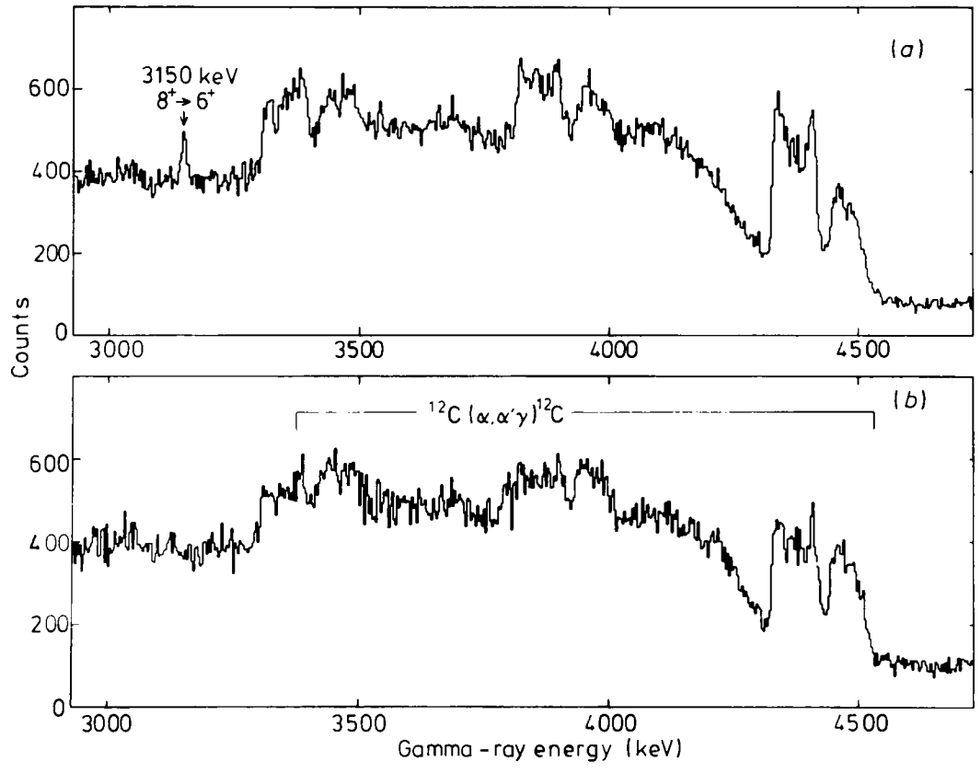

Figure 1. Spectra taken with the 25% Ge(Li) detector on- (*a*) and off-resonance (*b*) for the 11·95 MeV (8^+) state in ^{20}Ne. The position of the 3150 keV γ ray from the $8^+ \rightarrow 6^+$ transition is indicated in the on-resonance spectrum. The background of Doppler broadened and shifted 4·43 MeV γ rays from the $^{12}C(\alpha, \alpha'\gamma)^{12}C$ reaction is evident in both spectra. The off-resonance spectrum has been normalised to the same accumulated beam charge as the on-resonance spectrum.

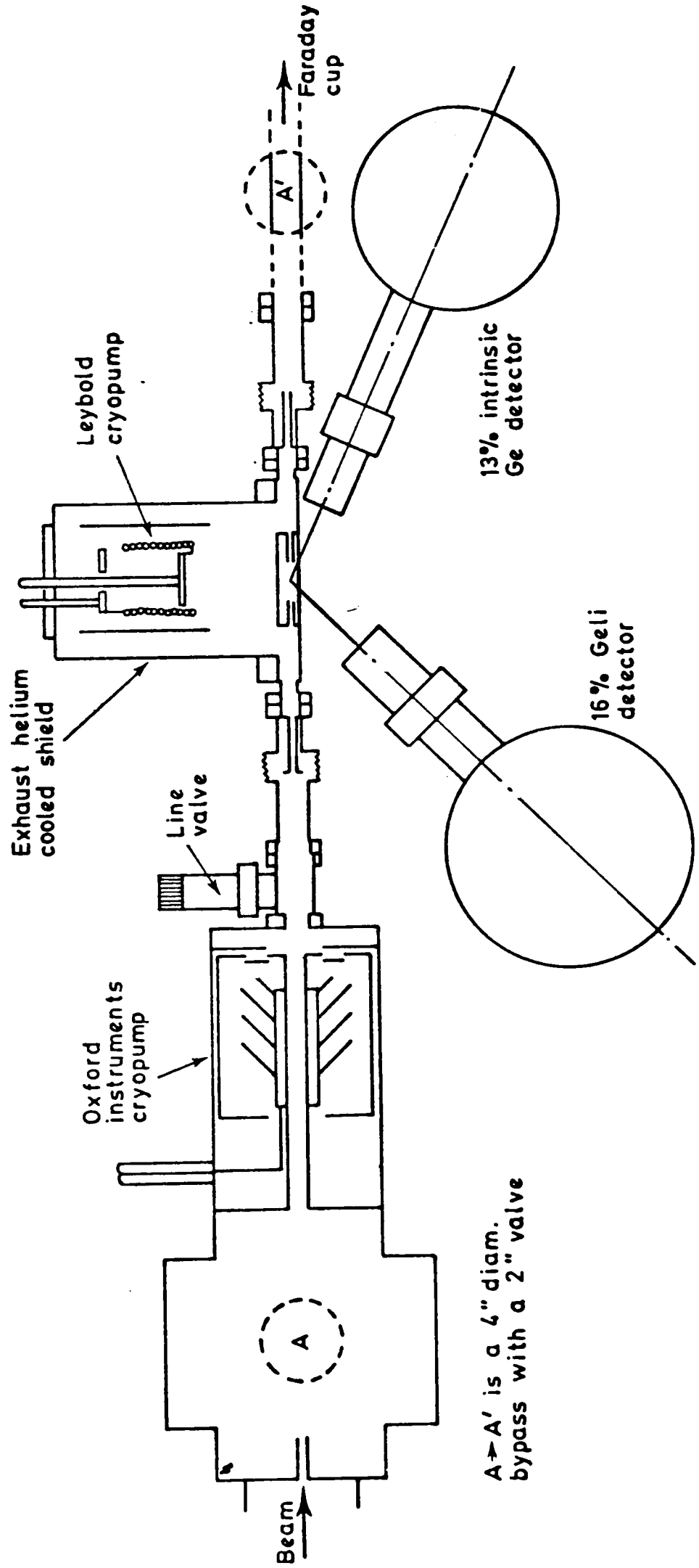

Fig.2.2.2 Plan of the gas target system and detectors.

3. Results

Since the γ rays from the resonance do not all emanate from the same point in the target, but rather are produced over a substantial fraction of the length of the target due to the spread in energies within the beam and to straggling in the target gas, it is necessary to correct the observed on-resonance γ-ray yield in order to arrive at a value for the resonance strength. This correction procedure has been described in detail by Watt *et al* (1978). Briefly, a computer program is used which, for a given value of the difference ΔE_x between beam energy and resonance energy, calculates the profile of the resonance along the target. This profile may be used to calculate the average Doppler shift of a γ ray of known unshifted energy observed at an angle θ. Hence, if the Doppler shift of a resonant γ ray is measured, ΔE_α may be adjusted to reproduce the observed shift. The resulting resonance profile may then be used to correct the observed number of counts in a given resonant γ-ray peak to that expected from a point target positioned at the centre of the gas target. Usually, the Doppler shift of the γ ray from a secondary transition is used in this correction procedure since the transition energy is generally known accurately. Unfortunately, in the decay of the 8^+ level in ^{20}Ne there is only one transition ($8^+ \rightarrow 6^+$) and its energy is known to only $\pm 5{\cdot}5$ keV, which is useless for our correction procedure. Hence a variant of the usual procedure was employed as outlined below.

The data consist of yields and energies of the $8^+ \rightarrow 6^+$ γ ray at two angles and at five slightly different beam energies; they are collected together in table 1. The procedure adopted in using these data to arrive at corrected yields and at the unshifted energy of the $8^+ \rightarrow 6^+$ transition was as follows. The γ-ray energy observed in the 46° detector was used to calculate resonance profiles for nine different assumed values of the unshifted γ-ray energy in the range 3169 to 3177 keV. For each of these profiles, we calculated the expected γ-ray energy in the 25% detector and the corrected yields in both detectors. The yields were derived by dividing the corrected counts by the detector efficiency and by a factor determined by the known γ-ray angular distribution at the angle of the detector. This procedure was followed for each of the five data sets. We then required consistency between the predicted and observed γ-ray energies in the 25% detector for each data set, and consistency in the corrected yields between the various data sets.

The results for the γ-ray energies are presented in figure 2 for three of the data sets. The uncertainty in the γ-ray energy measured in the 46° detector has been propagated through into an uncertainty in the predicted γ-ray energy in the 125° detector, whence the bands rather than lines of predicted energies in figure 2. It is apparent that for data set B, for which the beam energy was the lowest of the latter four data sets, consistency between calculated and observed γ-ray energies is only achieved for $E_\gamma^{(0)} \geqslant 3170$ keV. This is therefore a lower bound on the unshifted γ-ray energy. In the interests of clarity, data sets A and D are not shown in figure 2, but, like C and E, these exhibit consistency between observed and predicted γ-ray energies over the whole range of $E_\gamma^{(0)}$.

The behaviour of the derived value of $\omega\gamma$ as a function of $E_\gamma^{(0)}$ is portrayed in figure 3. Of the two bands shown, the narrower is the weighted average of the corrected yield for data sets A to D, and for both detectors. The wider band is the weighted average of the corrected yield for data set E, again for both detectors. We have chosen to present the data in this way because data set E was taken at the highest beam energy. For values of $E_\gamma^{(0)}$ greater than 3174 keV, the derived values of ΔE_α for the set E are such that more than 10% of the resonance yield is not observed because the resonance is not contained wholly within the target. The rise in corrected yield above 3174 keV for data set E is largely due to the correction for this unobserved yield. The derived values of ΔE_α for

Table 1. Data for the 9·02 MeV 8^+ resonance in the $^{16}O(\alpha, \gamma)^{20}Ne$ reaction.

			16·6% detector			25% detector		
Data set	Target pressure (Torr)	ΔE_α† (keV)	Angle (deg)	E_γ^{obs} (keV)	Counts/10 mC	Angle (deg)	E_γ^{obs} (keV)	Counts/10 mC
A	0·6	2·95 ± 0·44	46	3203·3 ± 1·7	25·0 ± 4·8	127	3150·2 ± 1·7	29·7 ± 4·3
B	0·8	4·06 ± 0·36	46	3203·8 ± 1·0	19·2 ± 3·5	125	3150·5 ± 1·0	41·6 ± 5·1
C	0·8	4·65 ± 0·32	46	3202·0 ± 1·0	28·1 ± 3·4	125	3148·4 ± 1·0	28·8 ± 4·8
D	0·8	4·97 ± 0·47	46	3201·0 ± 1·5	26·0 ± 6·0	125	3151·0 ± 3·0	24·0 ± 8·0
E	0·8	6·98 ± 0·76	46	3194·2 ± 2·0	26·7 ± 7·5	125	3144·1 ± 2·0	25·0 ± 10·0

† $\Delta E_\alpha = E_{beam} - E_{res}$, determined from the Doppler shift observed in the 16·6% detector assuming $E_\gamma^{(0)} = 3173$ keV.

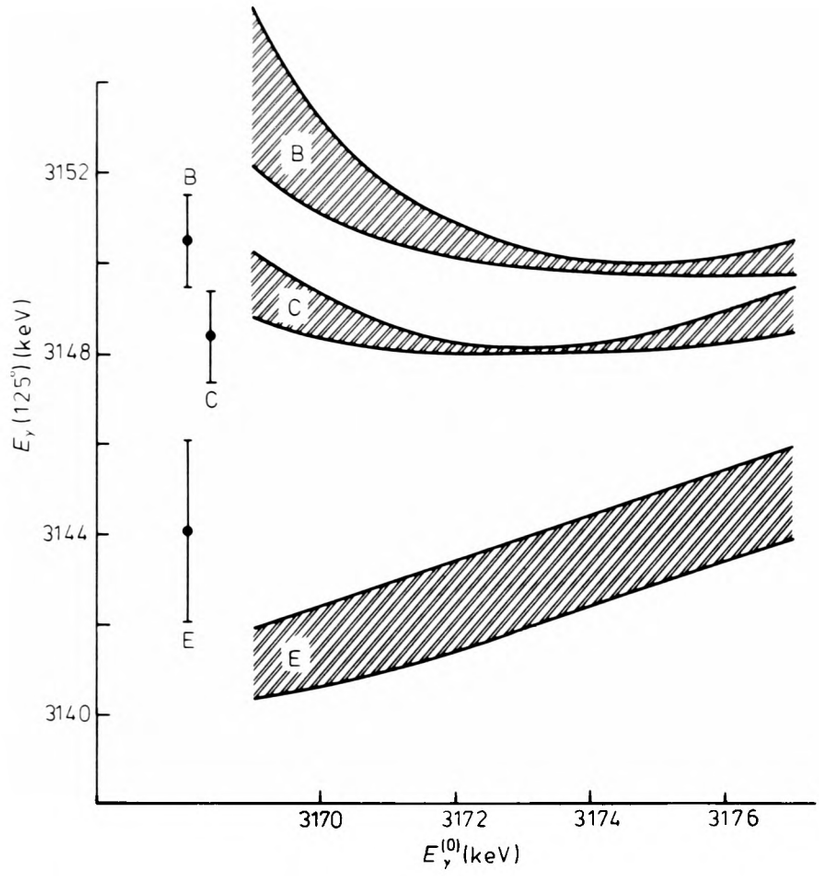

Figure 2. Plots of expected γ-ray energy in the 125° Ge(Li) detector as a function of the unshifted energy $E_\gamma^{(0)}$ of the $8^+ \rightarrow 6^+$ transition for data sets B, C and E. These energies were derived from the observed $8^+ \rightarrow 6^+$ γ-ray energies in the 46° detector (see text). The uncertainties in these 46° γ-ray energies give rise to the indicated uncertainties in the predicted energies at 125°. The data points to the left of the predictions are the observed γ-ray energies in the 125° detector.

the other four data sets, on the other hand, correspond to the resonance being contained almost completely within the target for the entire range of $E_\gamma^{(0)}$. From figure 3 we conclude, therefore, that the value of $\omega\gamma$ from data set E is not consistent with the remainder of the data unless $E_\gamma^{(0)} \leqslant 3176$ keV. Hence we adopt $E_\gamma^{(0)} = 3173 \pm 3$ keV, which corresponds to an excitation energy of 11 950 ± 4 keV, in excellent agreement with the value 11 948 ± 5 keV obtained by Häusser *et al* (1972).

Within the allowed range of $E_\gamma^{(0)}$ we can combine the value of $\omega\gamma$ from data set E with those from the other data sets, and hence derive a value of $\omega\gamma$ for the 8^+ resonance. From figure 3 it can be seen that the value $\omega\gamma$ does not depend strongly on $E_\gamma^{(0)}$. Our final value for $\omega\gamma$ is 131 ± 18 meV, where the quoted error includes the statistical error on the corrected yield, the variation of $\omega\gamma$ with $E_\gamma^{(0)}$, the uncertainties in the efficiency calibrations of the two detectors, and the error on the $\omega\gamma$ of the reference resonance. The α-particle width of the 8^+ level is 35 ± 10 eV (Häusser *et al* 1972), i.e. $\Gamma_\alpha \gg \Gamma_\gamma$, from which it follows that $\Gamma_\gamma = 7{\cdot}7 \pm 1{\cdot}1$ meV. This value corresponds to a reduced E2 transition probability of 9·2 ± 1·3 Weisskopf units (Wu) (Skorka *et al* 1966), which is in good agreement with the less precise value of 7·5 ± 2·5 Wu obtained by Alexander *et al* (1972).

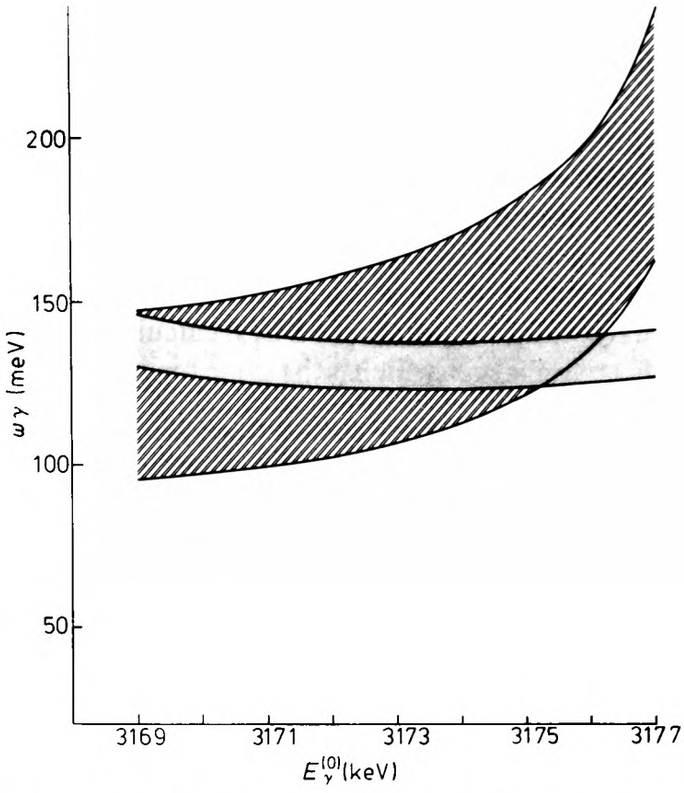

Figure 3. Plots of $\omega\gamma$ against the unshifted γ-ray energy $E_\gamma^{(0)}$ of the $8^+ \rightarrow 6^+$ transition. The narrower band is the weighted average of data sets A to D for both detectors, while the wider band is the average over the two detectors for data set E. For the purposes of this comparison the errors are statistical only.

4. Discussion

The original measurement of the B(E2) of the $8^+ \rightarrow 6^+$ transition in ^{20}Ne (Alexander *et al* 1972) was intended to test whether rotational bands in light nuclei followed the behaviour expected on the basis of the simple rotational model up to the highest spins possible with the limited number of valence particles available, or whether the shell model in fact gave a better account of the properties of these rotational levels. Their conclusion was very positively in favour of the latter alternative, and our more precise result does nothing to alter this conclusion. The shell-model calculations with which they compared their result were the SU(3) calculations of Harvey (1968), which assumed that the ground-state band in ^{20}Ne could be represented by the (80) representation only. More general calculations (Akiyama *et al* 1969) show that, although this is a good first approximation, other representations also contribute, the fraction of (80) varying from 91 % for the 2^+ level down to 81 % for the 8^+ level. This does not, however, alter the conclusion that the shell model gives the best fit, since full $(sd)^4$ basis calculations using the residual interaction of Preedom and Wildenthal (1972) show behaviour of the in-band B(E2)'s as a function of spin which is similar to the calculations of Harvey.

Since the measurement of Alexander *et al* (1972) was reported the precision of all the transition strengths within the ^{20}Ne ground-state band has been improved considerably. Hence, although there can be little doubt that the shell model gives a good qualitative description of the properties of the band whereas the rotational model does not, the experimental data are now sufficiently precise that one can ask whether the calculations are able to account quantitatively for the data. In particular, are the relative B(E2)'s well

reproduced, and what effective charges are required to reproduce the magnitude of these transition rates? In table 2 we bring together the transition rate data and compare with full $(sd)^4$ shell-model calculations using the residual interaction of Preedom and Wildenthal (1972). The residual interaction of Chung and Wildenthal (Chung 1976) gives nearly identical results. We observe that the relative transition rates as far as the 6^+ state are well reproduced by the calculations, but that the relative rate of the $8^+ \rightarrow 6^+$ transition is significantly weaker (i.e. more than two standard deviations) than the shell-model prediction. This conclusion is essentially independent of the effective interaction employed, being equally valid for the simple SU(3) calculations of Harvey (1968). If we define an additional effective charge ε which is the same for protons and neutrons, i.e.

$$e_p = (1 + \varepsilon)e \qquad e_n = \varepsilon e,$$

then a corollary of this conclusion is that the same value of ε will give quantitative agreement between the calculated and measured transition rates for transitions between the members of the band from the 6^+ level downwards, but that a smaller value of ε is required for the $8^+ \rightarrow 6^+$ transition. The magnitude of this additional effective charge will depend upon the choice of radial matrix elements $\langle r^2 \rangle$. Following Schwalm *et al* (1977), these were calculated using harmonic-oscillator wavefunctions with the oscillator nuclear size parameter

$$b = 1{\cdot}072\, A^{1/6}\ \text{fm}.$$

This expression for b was chosen to reproduce the root-mean-square charge radii of sd-shell nuclei as determined by electron scattering. The resulting values of ε for each of the transitions in the ^{20}Ne ground-state band are listed in table 2. The weighted average for the three lowest transitions is $\varepsilon = 0{\cdot}53 \pm 0{\cdot}02$. This differs appreciably from the value $0{\cdot}35 \pm 0{\cdot}02$ obtained by Schwalm *et al* (1977) from a fit to 26 B(E2) values distributed throughout the sd shell. This discrepancy was noted by Schwalm *et al* with reference to the inability of the model calculations to reproduce the accurately known ratio of the $2^+ \rightarrow 0^+$ B(E2) values for the ^{20}Ne–^{22}Ne pair. They suggested that the discrepancy might arise from additional core excitation in the ^{20}Ne states. If this is correct, then the additional core excitation is also present in the 4^+ and 6^+ levels of

Table 2. B(E2) values within the ^{20}Ne ground-state band.

Transition	B_{exp}(E2) (e^2 fm^4)	$B(E2)_{J\rightarrow J-2}/B(E2)_{2\rightarrow 0}$			Additional effective charge[g]
		Expt	SM[a]	SU(3)[b]	ε
$2^+ \rightarrow 0^+$	65·7 ± 3·4[c]				0·53 ± 0·03
$4^+ \rightarrow 2^+$	73·3 ± 7·0[d]	1·12 ± 0·13	1·19	1·27	0·49 ± 0·05
$6^+ \rightarrow 4^+$	68·0 ± 7·6[e]	1·04 ± 0·13	0·93	1·07	0·58 ± 0·06
$8^+ \rightarrow 6^+$	28·6 ± 3·7[f]	0·44 ± 0·06	0·58	0·64	0·39 ± 0·05

[a] Shell-model calculations within a complete $(sd)^4$ basis, using the effective interaction of Preedom and Wildenthal (1972).

[b] SU(3) calculations (Harvey 1968) assuming the states are described simply by the (80) representation.

[c] Weighted average of the values given by Olsen *et al* (1974) and Schwalm *et al* (1977).

[d] Häusser *et al* (1971).

[e] Weighted average of the results of Diamond *et al* (1971) and Rogers *et al* (1971).

[f] Weighted average of present work and result of Alexander *et al* (1972).

[g] See text.

^{20}Ne, but *not* in the 8^+ level, since the additional effective charge required to reproduce the $8^+ \rightarrow 6^+$ rate is in good agreement with the average sd-shell value of Schwalm *et al* (1977). This may be interpreted as evidence that the intrinsic structure of the 8^+ level is somewhat different from the first four members of the band. In particular, it may be that the 8^+ level is less affected by extra-sd-shell configurations than the lower members of the band.

References

Akiyama Y, Arima A and Sebe T 1969 *Nucl. Phys.* A **138** 273

Alexander T K, Häusser O, McDonald A B, Ferguson A J, Diamond W T and Litherland A E 1972 *Nucl. Phys.* A **179** 477

Chung W 1976 *PhD Thesis* Michigan State University

Diamond W T, Alexander T K and Häusser O 1971 *Can. J. Phys.* **49** 1589

Fifield L K, Calaprice F P, Zimmerman C H, Hurst M J, Pakkanen A, Symons T J M, Watt F and Allen K W 1977 *Nucl. Phys.* A **288** 57

Harvey M 1968 *Advances in Nuclear Physics* vol 1 (New York: Plenum) p67

Häusser O, Alexander T K, McDonald A B, Ewan G T and Litherland A E 1971 *Nucl. Phys.* A **168** 17

Häusser O, Ferguson A J, McDonald A B, Szöghy I M, Alexander T K and Disdier D L 1972 *Nucl. Phys.* A **179** 465

Ingalls P D 1976 *Nucl. Phys.* A **265** 93

Jackson K P, Bharuth-Ram K, Lawson P G, Chapman N G and Allen K W 1969 *Phys. Lett.* **30B** 162

Larson J D and Spear R H 1964 *Nucl. Phys.* **56** 497

Olsen D K, Barnett A R, Biagi S F, Merrill N H and Phillips W R 1974 *Nucl. Phys.* A **220** 541

Preedom B M and Wildenthal B H 1972 *Phys. Rev.* C **6** 1633

Rogers D W O, Aitken J K, Litherland A E, Dixon W R and Storey R S 1971 *Can. J. Phys.* **49** 1397

Schwalm D, Warburton E K and Olness J W 1977 *Nucl. Phys.* A **293** 425

Skorka S J, Hartel J and Retz-Schmidt T W 1966 *Nuclear Data* A **2** 347

Snover K A, Kim K and Dickey P A 1978 *Bull. Am. Phys. Soc.* **23** 501

Watt F, Fifield L K, Hurst M J, Symons T J M, Zimmerman C H and Allen K W 1978 *Nucl. Instrum. Meth.* **151** 163

NUCLEAR INSTRUMENTS AND METHODS 151 (1978) 163-173 ; © NORTH-HOLLAND PUBLISHING CO.

A CRYOGENICALLY PUMPED GAS TARGET FOR THE STUDY OF ANGULAR DISTRIBUTIONS OF GAMMA RAYS FOLLOWING RADIATIVE CAPTURE

F. WATT, L. K. FIFIELD, M. J. HURST, T. J. M. SYMONS, C. H. ZIMMERMAN and K. W. ALLEN

Nuclear Physics Laboratory, Keble Road, Oxford, U.K.

Received 19 September 1977

A cryogenically pumped gas target, suitable for the study of angular distributions of gamma rays following radiative capture, has been constructed. A correction procedure has been developed to take into account the finite extent of the gamma emitting region within the target. The system has been tested in a study of the angular distribution of gamma rays from the well known 2^+, $T=1$ state in ^{20}Ne at 10.27 MeV, excited as a resonance in the reaction $^{16}O(\alpha, \gamma)^{20}Ne$.

1. Introduction

The development in Oxford of a cryogenically pumped gas target[1]) has enabled the study of radiative alpha capture in light elements such as ^{15}N, ^{16}O and ^{20}Ne to be extended to much higher energies than is possible using solid targets on gold backings which inevitably give rise to background due to the impurity content of the gold. The gas target already described, which was of the transmission type, was designed mainly for the observation and precise location of resonances and for the study of the gamma decay of the resonant states. The length of the target tube and the geometrical layout did not allow the study of γ-ray angular distributions over a useful range of angles.

In this paper, a redesigned target chamber and cryopumping system are described which permit the study of angular distributions over the range 25° to 90°. These measurements, together with a knowledge of $\omega\gamma$ and branching ratios, usually enable the spin of the resonant state and gamma ray transition strengths to be determined. The attainable energy resolution is ≈ 1 to 2 keV up to excitation energies ≈ 8 MeV above the α-particle binding energy of the compound nucleus.

The use of gas targets does, however, introduce some special difficulties into the measurement of angular distributions. These difficulties arise as a result of the very low energy loss of the ion beam in the gas, which leads to the emission of gamma rays from an extended region of the target even for sharp resonances, and gives rise to problems in locating the centre of the resonance. Methods have been developed to overcome these problems;

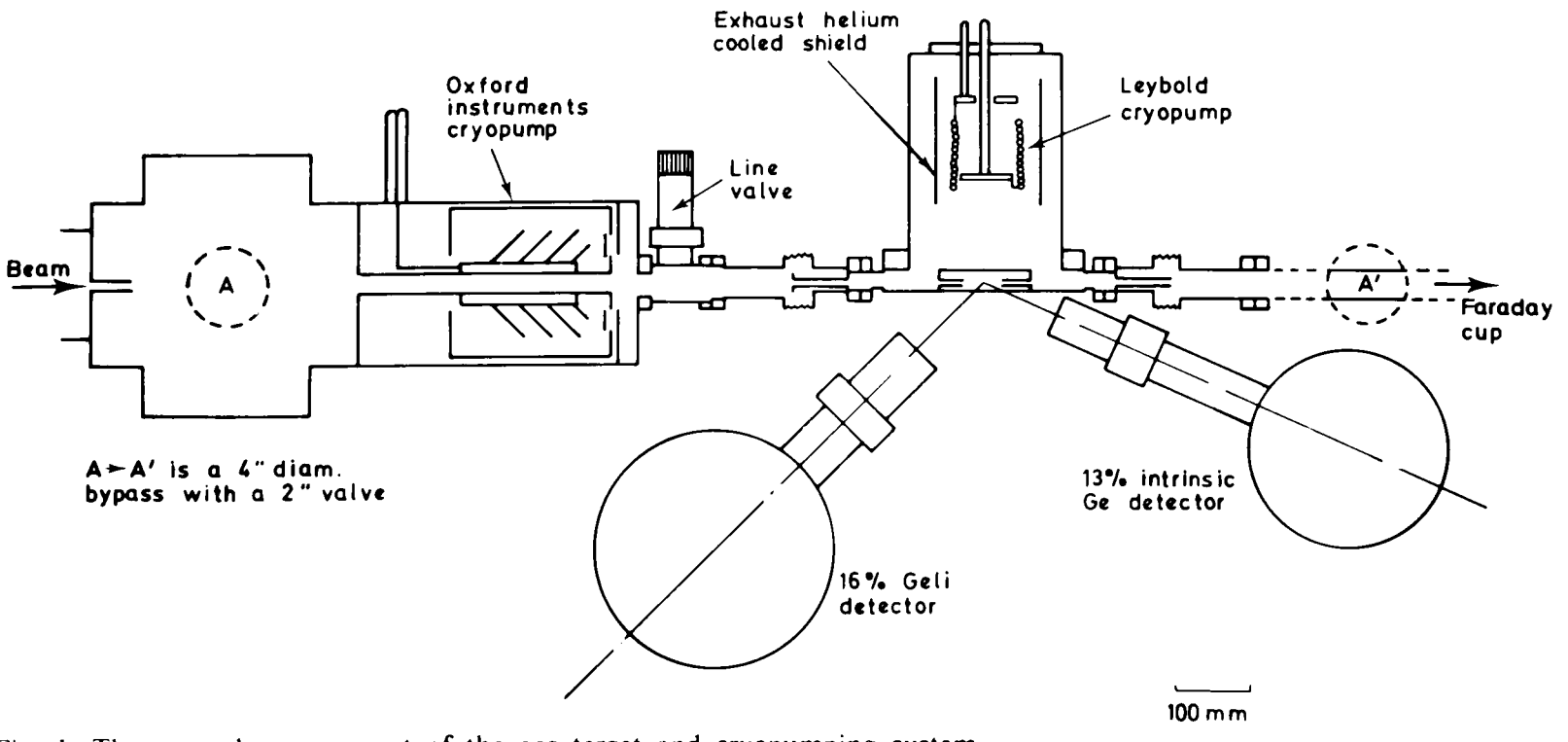

Fig. 1. The general arrangement of the gas target and cryopumping system.

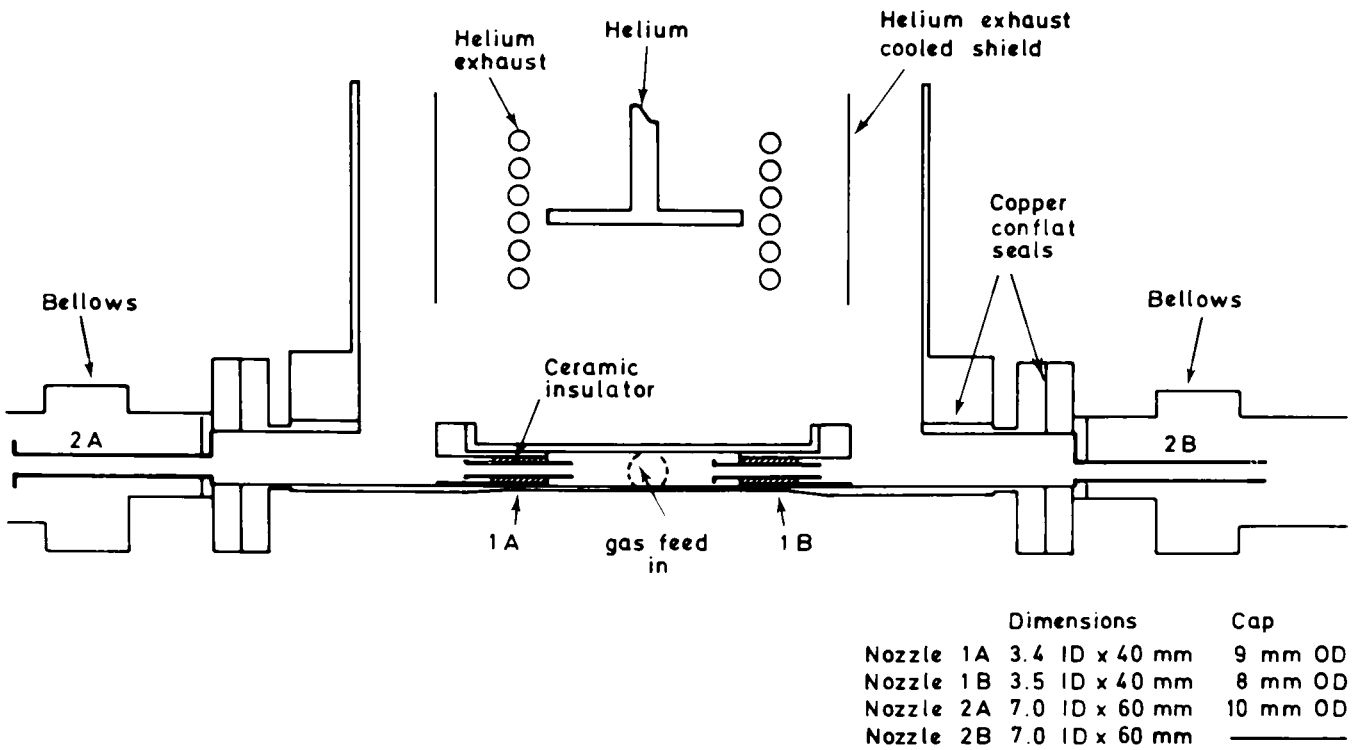

Fig. 2. Plan view of the gas target region showing nozzle dimensions.

they are illustrated by a study of the angular distribution of gamma rays from the well known 2^+, $T=1$ state in ^{20}Ne at 10.27 MeV, excited as a resonance in the reaction $^{16}O(\alpha, \gamma)Ne^{20}$.

2. Apparatus

The most important difference between the present target and the previous one is that the target length, taken as the distance between the midpoints of the entrance and exit nozzles, has been reduced from 190 mm to 90 mm. This has allowed several new design features to be incorporated.

A diagram showing the general arrangement of the gas target and cryopumping system is shown in fig. 1. The target assembly, which is shown in fig. 2, is built into a 10″ diameter, 1″ thick stainless steel flange. This has the advantage that the target nozzles 1A and 1B together with the differential pumping nozzles 2A and 2B, can be adjusted to be co-axial prior to installation in the beam line. The target assembly as a whole can then be aligned optically with the beam axis by means of vertical, horizontal and axial adjusters (not shown in the diagram) supporting the flange and Leybold pump housing. The gas inlet and pressure measuring lines enter the target chamber via holes bored vertically in the 10″ flange. The central region of the flange is machined to a thickness of 0.5 mm to minimise the attenuation of gamma rays from the gas target region. With the new arrangement, gas emerging from both ends of the target can be removed by a single cryopump. A diagram of the target assembly flange as viewed from the cryopump side of the beam axis is shown in fig. 3. The Leybold–Hereaus VPK 5000 cryopump was found to be capable of handling the increased gas flow due to the higher target pressure required to maintain a thick target yield in the shorter length. To avoid changes in the position of the resonance due to changes in target gas pressure, a servo-controlled needle valve (Granville Philips series 216), operated from the output of a capacitance manometer is used to regulate the gas flow.

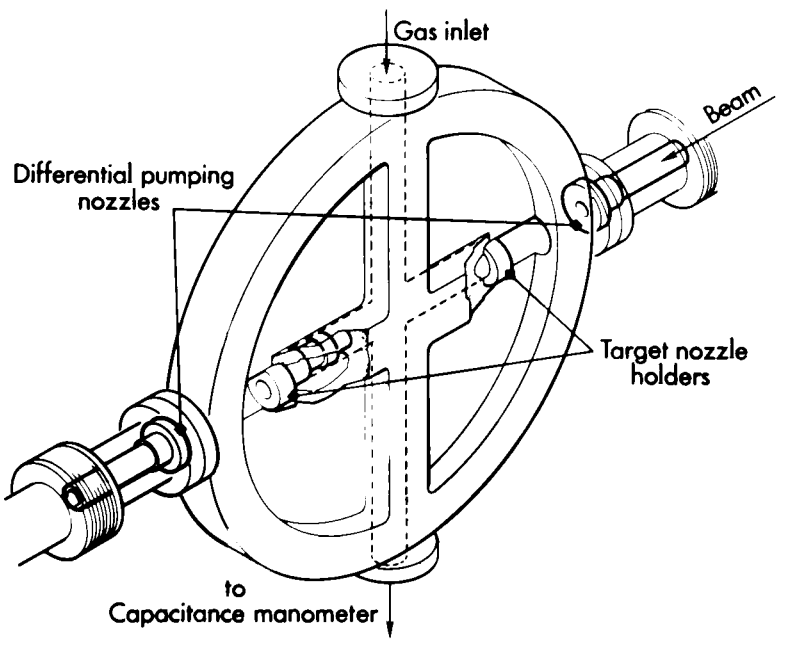

Fig. 3. Diagram of the target assembly flange as viewed from the cryopump side of the beam axis.

Gas emerging from apertures 2A and 2B is pumped by the Oxford Instruments annular cryopump. A 10 cm diameter valved bypass connects the region beyond aperture 2B to the Oxford Instruments pump, thereby ensuring low pressure in the Faraday cup region. As a result of the double differential cryogenic pumping, a negligible amount of gas reaches that part of the beam line pumped by the mercury diffusion pumps, even at high ($\approx$3 torr) target pressures. Table 1 shows measured gas pressures throughout the system for a selection of target pressures.

By including a valve between the Oxford Instruments and Leybold cryopumps, recycling can be achieved without warming up the annular cryopump (<1% of the target gas is condensed on its cryosurface), thus facilitating a faster turn round time. In the new system, recycling times of twenty minutes have been achieved, compared with an average of 45 min with the previous gas target. Recovery has also been greatly simplified by eliminating the diaphragm pump previously used to transfer gas into the storage reservoir at the end of an experiment. Each storage vessel (one per isotope) contains a liquid helium cooled cold finger, which condenses the gas evolved from the main cryopumps directly into the storage vessel. The advantages of this system lie in its cleanliness and in its ability to recover all the gas used. For condensation of the ^{15}N, ^{16}O, ^{36}Ar and ^{12}C (as CH_4) isotopes, a simple cryogenic system is used (fig. 4). A removable supply line feeds a He liquid/gas mixture into a cold finger terminated by a copper cup (one per storage vessel). For neon (boiling point 20 K) a more efficient cryogenic recovery system is required (fig. 5). This is achieved by surrounding the cryofinger with a vacuum isolated stainless steel shield. For both types of cryofinger, the condensation time for a ten atmospheric litre charge of isotopic gas is about 15 min. The liquid helium consumption is between one and two litres.

The 7 mm circular tantalum aperture situated just before the beam line quadrupoles in the original target has been replaced by four individually adjustable jaws which are insulated and water-cooled to permit measurement of stray beam. These serve not only to remove beam scattered by the energy analysing slits and to reduce uncertainty in the beam direction at the target chamber but also to provide an indication of the beam position relative to the central axis of the quadrupoles. A

TABLE 1

Measured gas pressures throughout the system for various target pressures. All pressures in torr unless otherwise stated. The gas used was oxygen and the temperatures of the Leybold and Oxford Instruments cryopumps were maintained at 6.5 K and 10 K respectively, corresponding to a total liquid helium consumption of about 2 l/h.

Target pressure (μm of Hg)	Leybold pump housing	Faraday cup region	Six-way cross	Mercury diffusion pump
0	$<10^{-6}$	$<10^{-7}$	$<10^{-7}$	6×10^{-7}
200	3×10^{-5}	2×10^{-5}	1×10^{-6}	6×10^{-7}
400	9×10^{-5}	4×10^{-5}	3×10^{-6}	6×10^{-7}
600	1×10^{-4}	6×10^{-5}	5×10^{-6}	6×10^{-7}
800	2×10^{-4}	8×10^{-5}	9×10^{-6}	6×10^{-7}
1 000	4×10^{-4}	1×10^{-4}	2×10^{-5}	7×10^{-7}
2 000	10^{-3}	5×10^{-4}	5×10^{-5}	8×10^{-7}
3 000	$10^{-2}\rightarrow10^{-3}$	1×10^{-3}	1×10^{-4}	9×10^{-7}

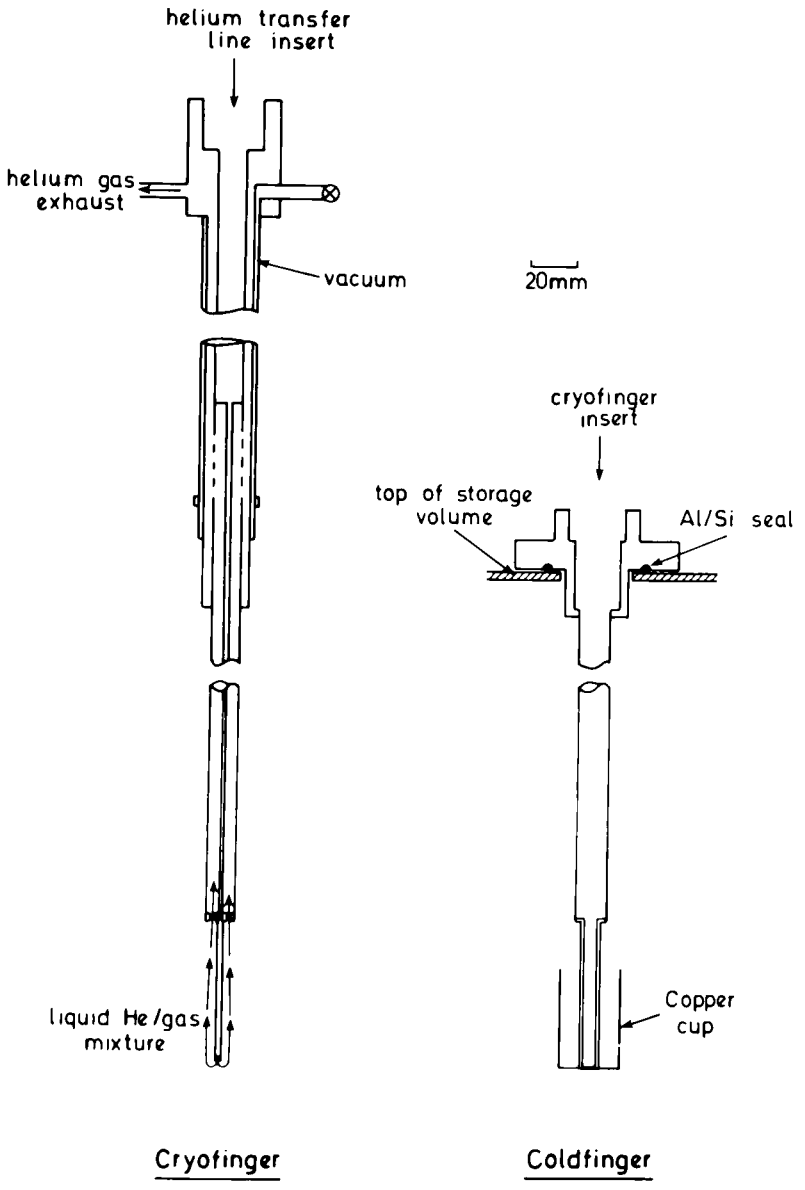

Fig. 4 Diagram showing the cryogenic system used in the recovery of the O_2, N_2, Ar and CH_4 isotopes. The cryofinger transfers the liquid helium from the transfer line into the cold finger

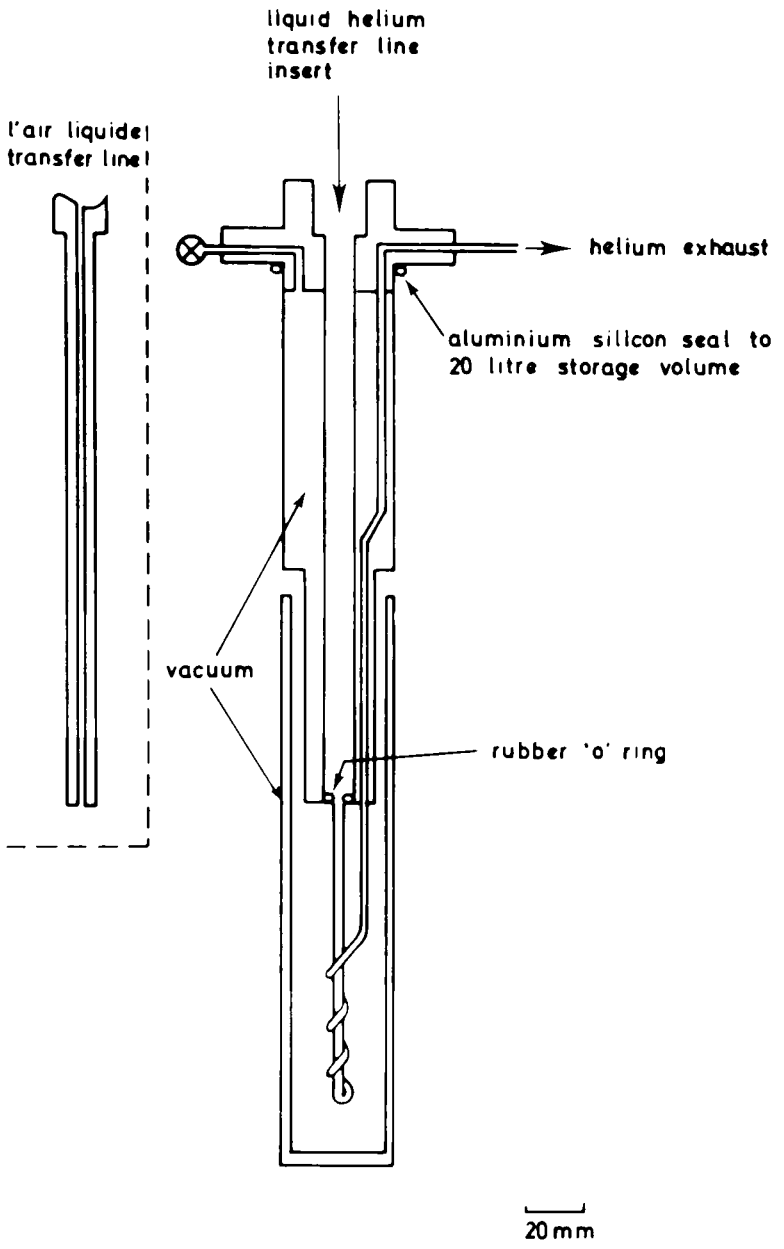

Fig. 5. Diagram showing the cryofinger used in the recovery of the Ne isotope.

second beam scanner has been added to check the profile of the beam as it enters the quadrupoles.

3. Experimental method

3.1. General features of angular distribution measurements employing an extended gas target

The general expression for the angular distribution of gamma rays from the radiative decay of an aligned state is:

$$W(\theta) = A_0[1 + A_2 P_2(\cos\theta) + A_4 P_4 \cos\theta) + \\ + \ldots A_{2L} P_{2L}(\cos\theta)], \qquad (1)$$

where L is the maximum gamma ray multipolarity and the coefficients A_k are defined by Rose and Brink[2]). This expression is valid for a point source only. In the present case, the resonant state under investigation may be formed at any point in the target at which an incident particle is sufficiently close to the resonance energy. Owing to finite beam energy resolution, energy straggling in the target gas, and the natural width of the resonance, this condition may be met over an extended region of the target along the beam direction. Hence it is necessary to correct the angular distribution data from such a target before fitting to the above expression (1). In order to make such corrections it is necessary to know the resonance profile, defined as the probability of forming the resonant state as a function of distance along the target.

The resonance profile depends on the following parameters:

1) the natural width, Γ, of the resonance,
2) the instrumental resolution of the system. This will contain contributions from the beam energy spread and the thermal motion of the molecules,
3) the probability $P(E_i, E, x)$ that an incident particle of energy E_i has lost an amount of energy $E_i - E$ after travelling a distance x through the target. This function expresses the straggling in the energy loss.

In a given experimental situation, (1) and (2) are usually known from prior measurements of the gamma-ray yield as a function of beam energy using low target pressures (see for example Symons et al.[3])). However, the effects of straggling are less easy to determine. Recently, a Monte Carlo technique has been developed (Symons et al.[3]), Cobb et al.[4])) for calculating the energy loss distribution

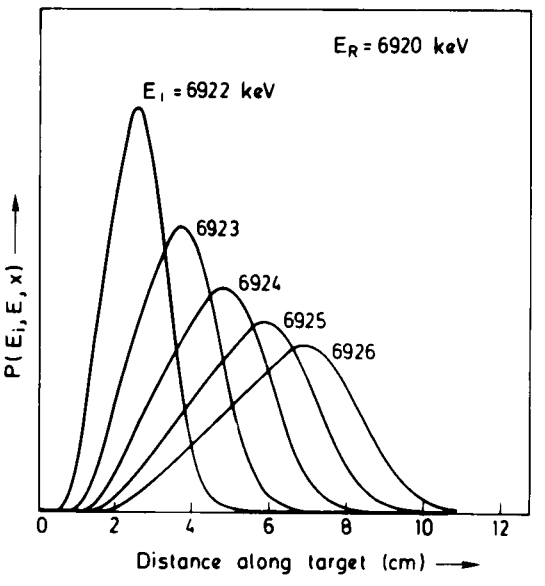

Fig. 6. Calculated energy loss profiles for alpha particles at selected values of $E_i - E_R$. The target gas is oxygen at 740 μm of Hg pressure.

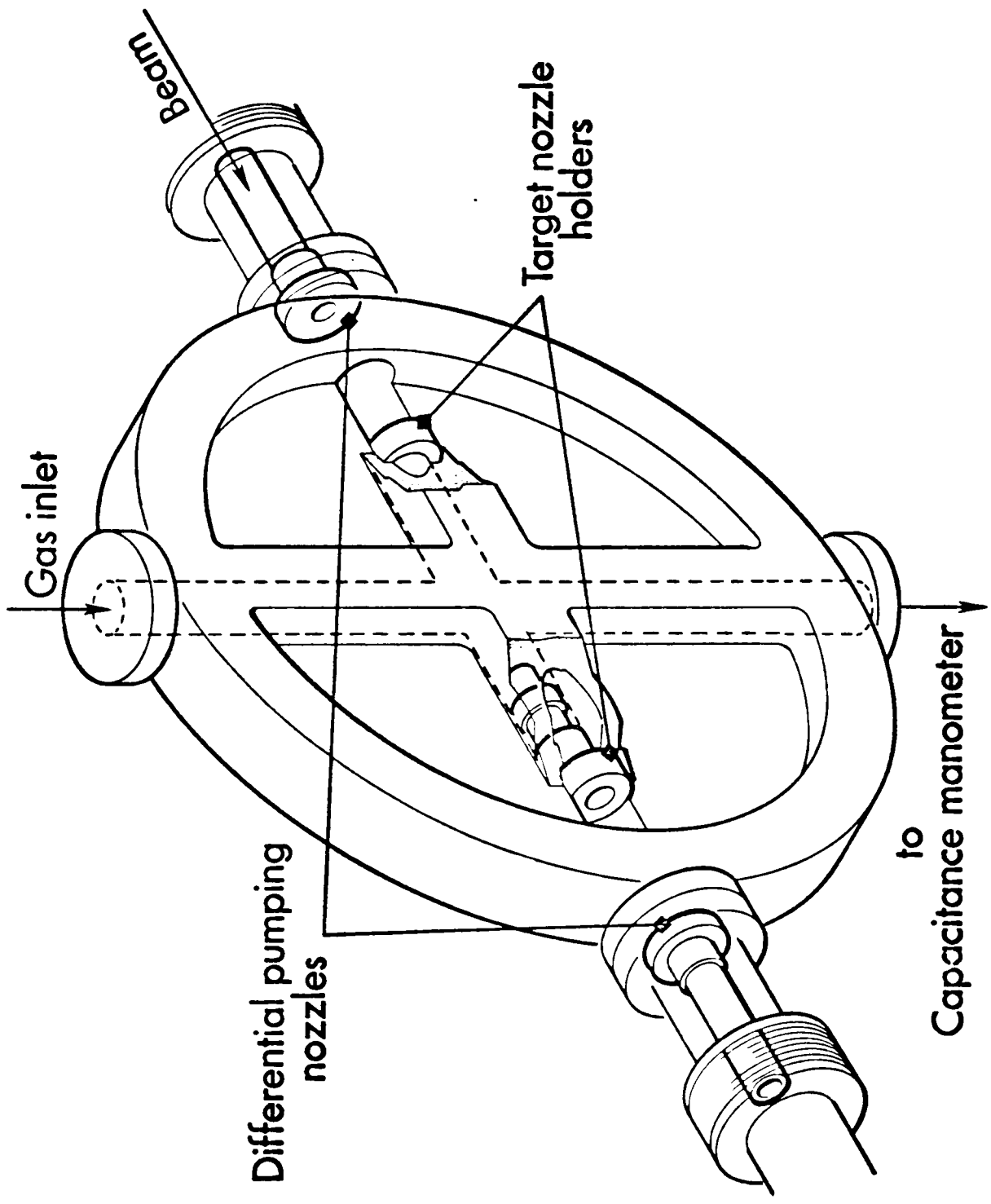

Fig.2.2.3 View of the target assembly flange from the Leybold pump side.

$P(E_i, E, x)$. Fig. 6 shows the calculated energy loss profiles for selected values of $E_i - E_R$, where E_R is the resonance energy. These curves represent the resonance profile in the limiting case of zero natural width and a monochromatic incident beam.

The value of $E_B - E_R$, which is used in calculating the resonance profile (E_B is the nominal or mean beam energy) is derived from the accurate measurement of the average Doppler shift of gamma rays from a particular decay mode of the resonance under investigation. These gamma rays, detected by a Ge(Li) detector placed at 125° or 135° to the beam direction, are averaged over a range of angles owing to the finite size of the detector and the length of the gamma emitting region. The peaks in the gamma-ray spectrum are

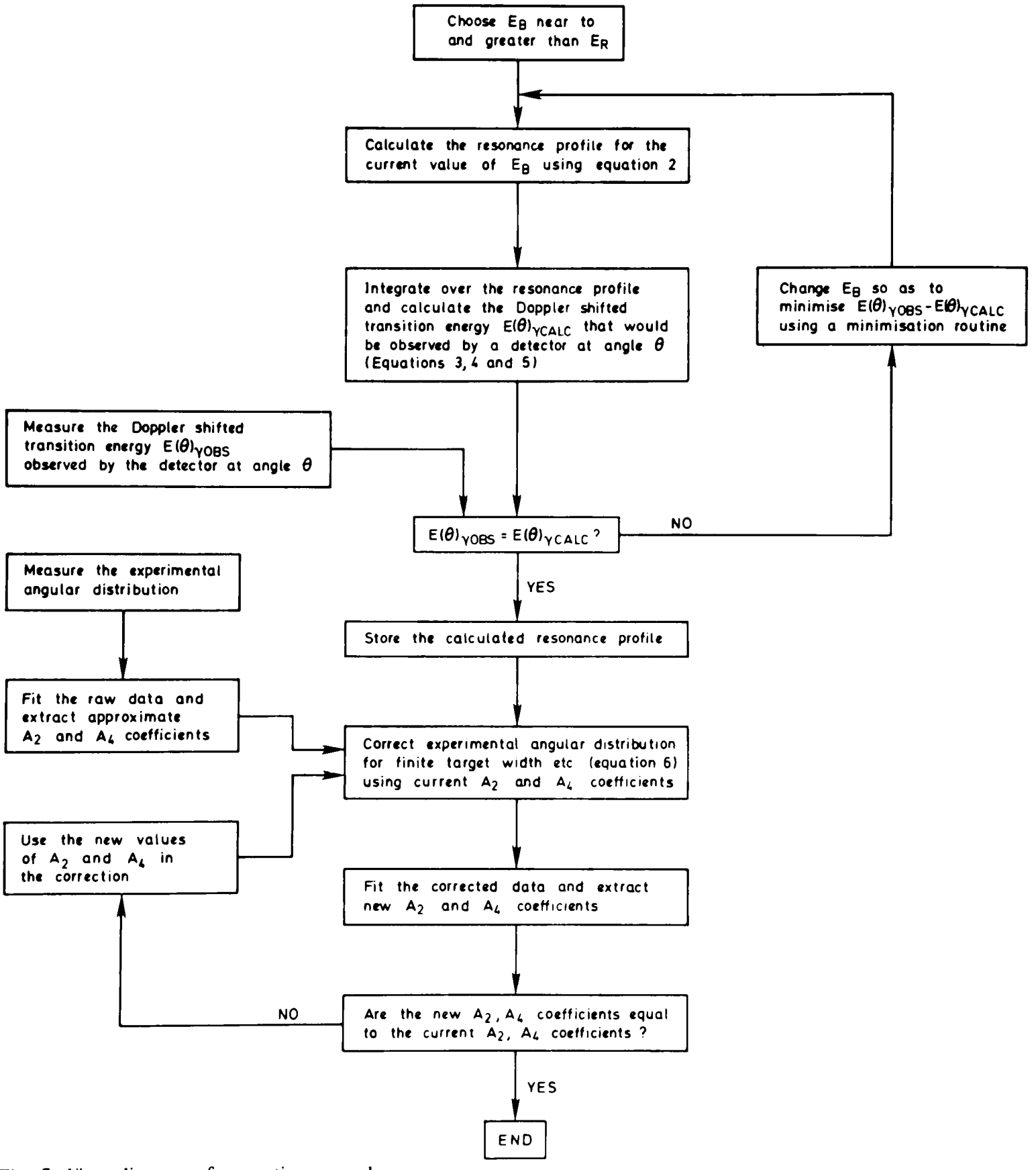

Fig. 7. Flow diagram of correction procedure.

both shifted and broadened as a consequence. Although the use of a Ge(Li) detector permits an accurate measurement of the average energy of a gamma ray, an accurate determination of the average Doppler shift also requires the choice of a transition between levels of accurately known excitation energies so that the unshifted gamma-ray energy is precisely known. For this reason, and for others outlined below, a secondary transition is usually employed to determine the Doppler shift. By comparing the experimentally measured average Doppler shift with theoretical values predicted from resonance profiles generated for different values of $E_B - E_R$ a resonance profile can be found which is consistent with the prevailing experimental conditions. In practice, the centre of the resonance can be located to an accuracy of typically ± 2 mm.

Angular distributions are measured with a second germanium detector which may be positioned at angles between 25° and 90° relative to the beam direction. At each angle of the distribution, the resonance profile is determined from the average Doppler shift observed in the fixed detector at the backward angle. Once the resonance profile has been determined in this way, it is a relatively straightforward matter to correct the observed yield in the moveable detector to that expected from a point target. Details of the correction procedure are given in the next section; the procedure is summarized in the flow diagram of fig. 7.

3.2. Details of the correction procedure

The resonance profile A for an average beam energy E_B and resonance energy E_R may be written:

$$A(E_B, E_R, x) = \int_0^x \int_0^x N(x)\, \beta(E_B, E_i) \times \times P(E_i, E, x)\, \sigma(E, E_R)\, dE dE_i, \quad (2)$$

where $N(x)$ is the density of target gas molecules as a function of target depth. The density profile used assumes a constant pressure inside the target chamber with a linear drop in pressure at the exit of the target. The beam energy distribution is represented by $\beta(E_B, E_i)$ assumed to be gaussian about E_B. Included in this function is the effective broadening of the beam energy spread in the centre of mass frame caused by the translational, vibrational and rotational motion of the target gas molecules. $P(E_i, E, x)$ is derived from the Monte–Carlo calculations. The cross-section for the radiative capture of α particles is given by the Breit–Wigner formula for an isolated resonance:

$$\sigma(E, E_R) = \pi \lambda^2 g \frac{\Gamma_\alpha \Gamma_\gamma}{(E - E_R)^2 + \frac{1}{4}\Gamma^2},$$

where λ is the CM wavelength of the α particle and g is a statistical factor.

The average Doppler shift of a γ ray is then

$$\bar{D}(E_B, E_R) = \frac{\int_0^L F(x)\, A(E_B, E_R, x)\, W(\theta)\, \{E_\gamma(\theta) - E_\gamma^{(0)}\}\, dx}{\int_0^L F(x)\, A(E_B, E_R, x)\, W(\theta)\, dx}, \quad (3)$$

where L is the length of the target. $F(x)$ is the efficiency function for detection of the γ rays. It includes any attenuation of the emitted γ rays in traversing the stainless steel target chamber wall and the tantalum target nozzles, as well as the energy dependence of γ-ray detection efficiency. Also, since points along the γ-emitting region are not equidistant from the detector, the efficiency function includes the change in effective solid angle of the detector as a function of x. $W(\theta)$ is the angular distribution of the γ rays emitted at angle θ. $E_\gamma(\theta)$ is the Doppler shifted energy of a γ ray emitted towards the detector at angle θ from a recoil nucleus with velocity v. The angle θ is a function of x.

$$E_\gamma(\theta) = \frac{E_\gamma^{(0)}\, (1 - v^2/c^2)^{1/2}}{1 - v \cos\theta / c}, \quad (4)$$

where $E_\gamma^{(0)}$ is the unshifted γ-ray energy:

$$E_\gamma^{(0)} = E_T - \frac{E_T}{2Mc^2}. \quad (5)$$

E_T is the transition energy and M is the nuclear mass. The second term accounts for the energy carried away by nuclear recoil.

For a given value of E_B, the expression for D can be evaluated by numerical integration and the result compared with the experimentally observed average shift. Using a standard minimisation procedure, the value of E_B can then be adjusted until the calculated value of $\bar{D}$ is consistent with the observed value. Once E_B is known, the resonance profile can be calculated from eq. (2).

It is then possible to correct the gamma-ray yield observed in the moveable detector for the transition of interest. The observed yield of gamma rays at a nominal detector angle θ_0 from a transition with a γ-ray angular distribution $W(\theta)$

is:

$$Y_{\mathrm{obs}}(\theta_0) = \frac{\int_0^L F(x)\, A(E_{\mathrm{B}}, E_{\mathrm{R}}, x)\, W(\theta)\, \mathrm{d}x}{\int_0^L A(E_{\mathrm{B}}, E_{\mathrm{R}}, x)\, \mathrm{d}x}, \qquad (6)$$

whereas the yield from a point target would be:

$$Y_{\mathrm{pt}}(\theta_0) = W(\theta_0). \qquad (7)$$

Hence, the correction factor by which the finite target yield must be multiplied to give the equivalent point target yield is:

$$C(\theta_0) = W(\theta_0) \int_0^L A(E_{\mathrm{B}}, E_{\mathrm{R}}, x)\, \mathrm{d}x \Big/ \int_0^L F(x) \times A(E_{\mathrm{B}}, E_{\mathrm{R}}, x)\, W(\theta)\, \mathrm{d}x. \qquad (8)$$

An iterative technique is required to extract $W(\theta)$ from the corrected results as the correction process is itself dependent on $W(\theta)$. Initially it is convenient to use in the correction process the A_k coefficients extracted from a fit to the raw angular distribution data. The A_k coefficients extracted from a fit to the corrected data may then in turn be used in the correction process until the A_k coefficients are unchanged from one step to the next. In practice, as the corrections are usually less than 10%, convergence is rapid and only two or three correction steps are needed.

For the target/detector distances involved in the present experiment, the effect of the finite size of the detector has to be taken into account, both when correcting the raw data and when fitting the corrected angular distribution. This effect is usually expressed in terms of Q_k coefficients which are included in the angular distribution expression:

$$W(\theta) = 1 + A_2 Q_2 P_2(\cos\theta) + A_4 Q_4 P_4(\cos\theta) + \ldots .$$

These Q_k coefficients are dependent on the geometry of the detector and on the distance of the detector from the target. Although the Q_k formalism is strictly valid only for a point source on the axis of a cylindrical detector, the effects of departures from cylindrical symmetry in the present case are assumed to be small and are neglected. However, as the source/detector distance varies along the resonance profile the Q_k coefficients are actually functions of distance along the target for a given detector position. Therefore, at each detector position, it is necessary to calculate average values $\bar{Q}_k$ by taking Q_k at each point along the target and weighting it by the value of the resonance profile at that point. These $\bar{Q}_k$ are used in the correction process in evaluating $W(\theta)$ in the denominator of eq. (8). The values of Q_k used in evaluating $W(\theta_0)$ in eq. (8), and in fitting the corrected angular distributions are, however, those applicable to a point target located at the centre of the target chamber.

3.3. Treatment of errors

Clearly, the correction process is a source of uncertainty in the data in addition to the statistical uncertainties on the raw data points. In general the main contribution to the uncertainty introduced by the correction process arises from the uncertainty in the average Doppler shift of the gamma ray which is used to define the resonance profile. This is due to:

1) statistical uncertainty in the observed average energy of the gamma ray. This gives rise to a statistical uncertainty in the resonance profile and hence in the corrections. This statistical uncertainty is added in quadrature to the errors on the raw data points before fitting the corrected angular distributions to eq. (1).
2) uncertainty in the unshifted gamma ray energy, and hence in the average Doppler shift $\bar{D}$. This leads to a systematic uncertainty in the resonance profile at each data point, the effect of which cannot be included directly in the statistical uncertainties on the points. Instead, three corrected angular distributions are obtained, using unshifted gamma-ray energies of $E_\gamma^{(0)}$ and $E_\gamma^{(0)} \pm \Delta E_\gamma^{(0)}$ respectively, where $\Delta E_\gamma^{(0)}$ is the uncertainty in $E_\gamma^{(0)}$ and is usually taken from a compilation. Assuming a particular value of the spin of the resonance level, the three corrected angular distributions are then fitted to eq. (1). Each fit will yield a value for the multipole mixing ratio δ of the transition together with an associated statistical uncertainty. In general, δ will be slightly different in the three cases, and the deviation from the main value obtained from the three fits is added in quadrature to the statistical uncertainty to give an estimate of the overall uncertainty in δ.

4. Tests of the angular distribution target

The angular distribution target has been tested by measuring the angular distributions of gamma rays from the 2^+, $T = 1$ resonance at 6.93 MeV in the $^{16}\mathrm{O}(\alpha, \gamma)^{20}\mathrm{Ne}$ reaction, using the α-particle

beam from the Oxford 10 MV Van de Graaff generator. This resonance was chosen for its large radiative width and small total width ($\Gamma = 120$ eV). The primary transition R→1.63 (2^+) is almost pure M1 radiation ($\Gamma_\gamma = 4.1$ eV) with only a small admixture of E2 radiation[5]) ($\delta = -0.02 \pm 0.013$, following the convention of Rose and Brink) and will therefore exhibit an angular distribution which is linear in $\cos^2\theta$. On the other hand, the secondary transition 1.63 (2^+)→g.s. (0^+) is pure E2 and its angular distribution has a strong quadratic dependence on $\cos^2\theta$.

An 85 cm^3 Ge(Li) detector and a 60 cm^3 intrinsic Ge detector were mounted on rotatable arms whose axes of rotation passed through the centre of the target chamber. The Ge(Li) detector was used as a monitor, and was fixed at an angle of 135° to the beam direction with its front face 13 cm from the centre of the target chamber. The intrinsic germanium detector was placed 11 cm from the centre of the target chamber, and at this distance had an angular range down to 24°.

In order to keep the corrections small, it is necessary in general to ensure that the resonance profile is as nearly central in the target chamber as possible. It is also very important that the resonance profile be completely localised within the target gas. If it is not, then the consequent loss of yield is extremely sensitive to small fluctuations in beam energy and target pressure so that any corrections become inaccurate. To avoid this situation, the target gas pressure was chosen such that the effective target thickness was considerably greater than both the natural width of the resonance and the spread of energies in the beam. Positioning the resonance centrally in the target chamber was accomplished by adjusting the beam energy until the average Doppler shift of the standard transition was consistent with that calculated for a centrally positioned resonance profile (see section 3.2).

For the 6.93 MeV 2^+, $T=1$ resonance in $^{16}O(\alpha, \gamma)^{20}Ne$, the transition used to define the resonance profile was the 1.63 (2^+)→g.s. transition for which the unshifted γ-ray energy is (1633.7 ± 0.4) keV [6]). With the pressure in the target chamber maintained at 740 μm of mercury, spectra of gamma rays were taken in both detectors with the moveable detector positioned at a number of angles between 24° and 90°. At this pressure the flow through the target nozzles is approximately laminar and hence the effective target length is 13 cm, corresponding to a target thickness of 12 keV for 6.93 MeV α particles. Gamma rays from sources of ^{60}Co and ^{228}Th were used to define the energy calibration of the fixed detector and it was found in practice that it was possible to determine the average energy of the 1.63 MeV gamma ray to an accuracy of 0.1 keV. For these measurements, the amplifier gain and effective

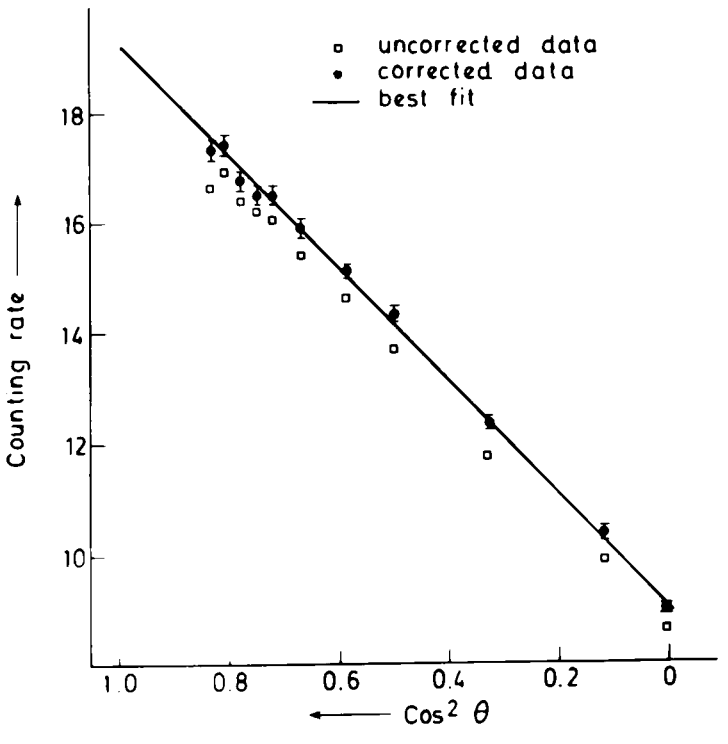

Fig. 8. Angular distribution of gamma rays from the primary 10.27 MeV (2^+)→1.63 MeV (2^+) transition in ^{20}Ne for the centrally positioned resonance profile.

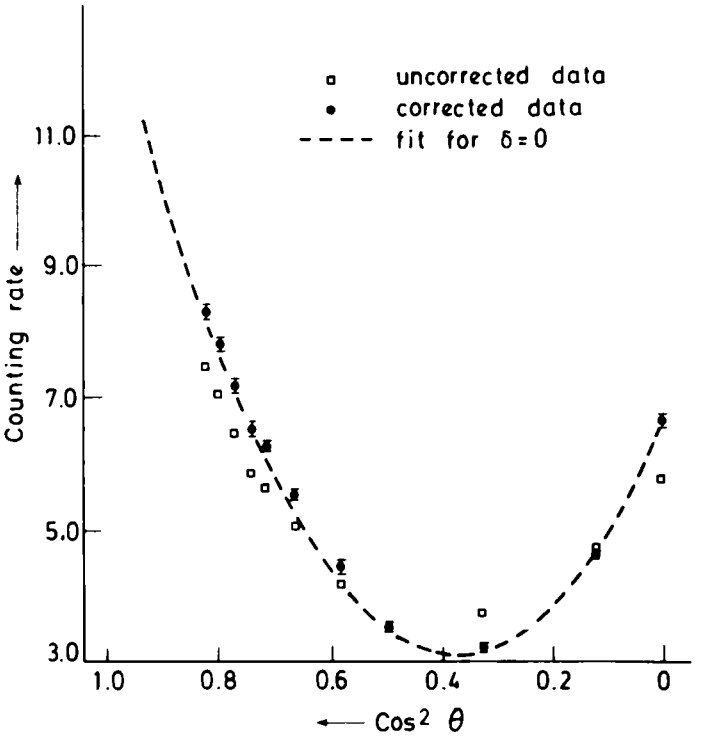

Fig. 9. Angular distribution of gamma rays from the secondary 1.63 (2^+)→0(0^+) transition in ^{20}Ne for the centrally positioned resonance profile.

threshold were digitally stabilized using a very stable precision pulse generator and the lower energy gamma ray from ^{60}Co, respectively.

As an additional more rigorous test of the correction procedure the angular distributions were remeasured with the resonance intentionally shifted about 2 cm upstream from its central position in the target chamber by reducing the beam energy by approximately 1.5 keV.

5. Results of tests

Corrected and uncorrected angular distributions for the primary and secondary transitions from the 10.27 MeV 2^+, $T=1$ state in ^{20}Ne are shown in figs. 8, 9, 10 and 11 for the central and non-central positions of the resonance profile respectively. The resulting resonance profiles for the two beam energies are shown in fig. 12. The corrections take into account the following (see section 3.4):

1) the extended nature of the gamma emitting region along the beam direction,
2) attenuation of gamma rays in the stainless steel target chamber wall and in the tantalum target nozzles,
3) the small change in gamma ray detection efficiency caused by the change in Doppler shifted energy of the gamma radiation with angle,
4) variation in the attenuation coefficients (Q_k) with nominal detector angle.

The errors shown for each point of the corrected angular distribution data include a contribution arising from the statistical uncertainty in measuring the Doppler shifted energy of the 1.63 MeV ray in the monitor detector spectra, in addition to the statistical uncertainty of the raw data.

A simple but effective test was carried out to give an indication of the accuracy with which the correction procedure can be applied. The accurate

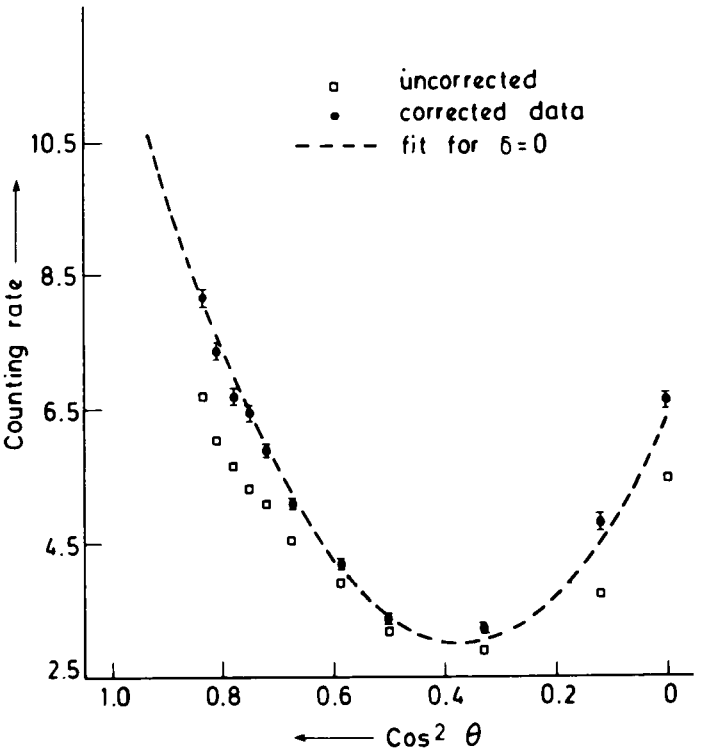

Fig. 11. Angular distribution of gamma rays from the secondary 1.63 (2^+)→0 (0^+) transition in ^{20}Ne for the non centrally positioned resonance profile.

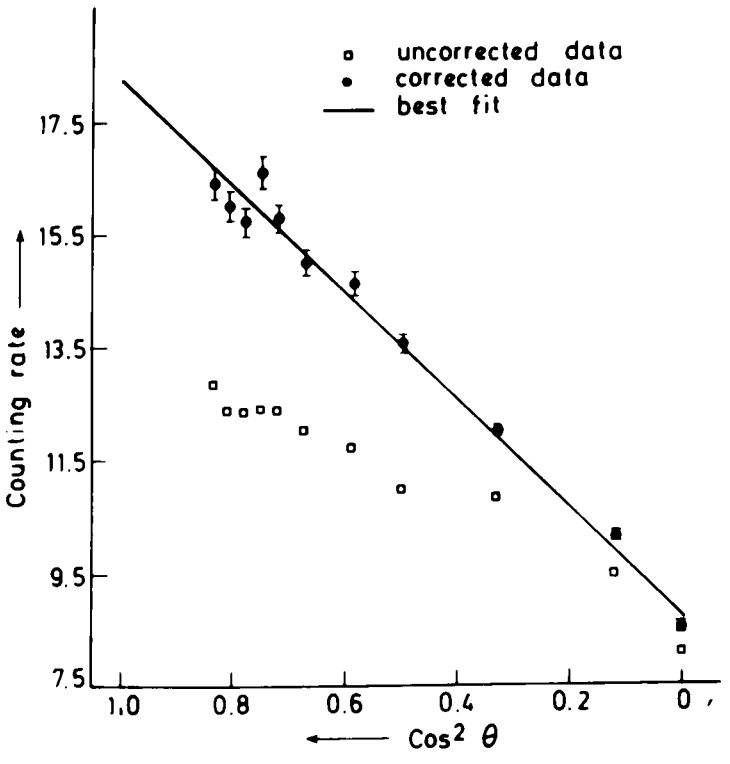

Fig. 10. Angular distribution of gamma rays from the primary 10.27 (2^+)→1.63 (0^+) transition in ^{20}Ne for the non centrally positioned resonance profile.

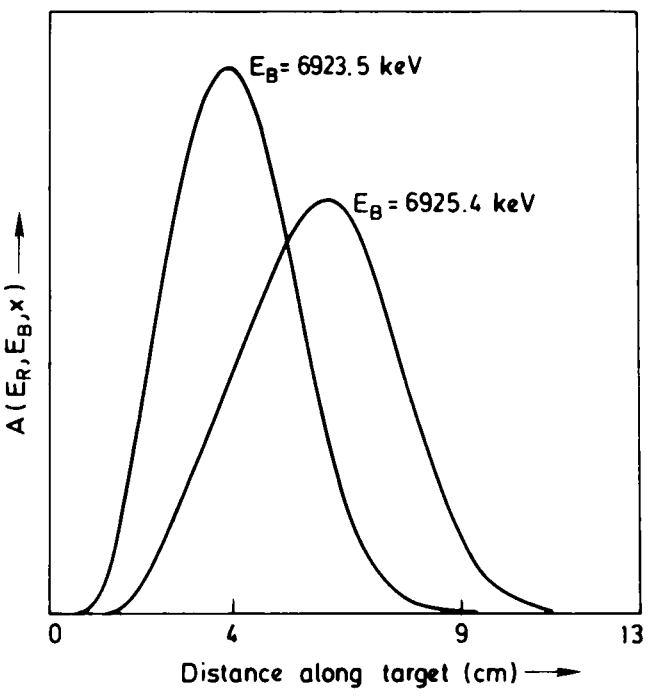

Fig. 12. The calculated resonance profiles for the centrally positioned resonance ($E_B = 6925.4$ keV) and the off centre resonance ($E_B = 6923.5$ keV). The resonance energy is taken as 6920 keV. The effective beam spread is assumed to be 1.5 keV fwhm and the natural width of the resonance taken to be zero.

determination of the profile of the resonance in the target chamber, from the Doppler shifted secondary transition gamma ray as measured by the monitor detector, is crucial to the correction process. A good test therefore is to estimate how accurately the Doppler shifted secondary transition gamma ray energy, as measured by the moveable detector, can be predicted from the calculated profile. In the central resonance case, the energy of the 1.63 MeV secondary gamma ray was measured from the spectra taken from the moveable detector and compared at each angle to the value predicted by the correction process. It was found that in every case the predicted energy was within 0.2 keV of the observed energy, a value consistent with the error in the measurement of the 1.63 MeV gamma ray energy.

In the fits to the angular distributions of the $R \rightarrow 1.63$ transition, the mixing ratio δ_1 was allowed to vary freely. In the fits to the $1.63 \rightarrow 0$ angular distributions, the mixing ratio δ_2 was fixed at zero while δ_1 was fixed at the value obtained by Pearson and Spear ($\delta_1 = -0.02$)[5]. The data were also corrected and fitted using the limiting values of 1633.3 and 1634.1 keV for the unshifted γ-ray energy of the $1.63 \rightarrow 0$ transition. Table 2 summarises the values of normalised χ^2 and δ_1 obtained from the fits.

We see at once that in the central resonance case the quality of the fit to the primary transition is good ($\chi^2/N = 1.16$). Furthermore the value of the mixing ratio $\delta_1 = -0.038^{+0.035}_{-0.028}$ is in good agreement with the value of Pearson and Spear ($\delta_1 = -0.02 \pm 0.013$). As might be expected due to the large corrections involved, for the off central resonance case the quality of the fit is not quite as good ($\chi^2/N = 3.58$). Nevertheless, in spite of the large correction factors involved, the value of the mixing ratio $\delta_1 = -0.028^{+0.031}_{-0.035}$ is in good agreement with the value obtained with the resonance in the centre of the target. The quality of the fit to the secondary transition (central case), $\chi^2/N = 2.2$, is not as good as for the primary transition, although the quality of the fits in the off central resonance cases is comparable. However, there are possible sources of systematic error in the extraction and analysis of the secondary angular distributions which are absent for the fits to the primary angular distributions. These are listed below:

1) the 1.63 MeV gamma ray lies in a region of the gamma-ray spectrum in which there are a large number of background lines, both from natural radioactivity and from reactions induced by the small fraction of beam that strikes the target nozzles and differential pumping apertures. Since the statistical accuracy of the data points is very high, a small ($< 1\%$) contribution from a background line to the number of counts extracted from the data could produce a significant systematic error,
2) off-resonance spectra also show a weak 1.63 MeV gamma ray, which arises from contaminant reactions. This constitutes a background contribution to the yield of 1.63 MeV gamma rays which does not have either the same angular distribution or the same resonance profile as the contribution from the 6.93 MeV, 2^+, $T = 1$ resonance,
3) the angular distribution of the $1.63 \rightarrow 0$ transition has a large P_4 component ($A_4 = 1.109$) and is therefore sensitive to the value of Q_4 used in the analysis. But because $P_4(\cos\theta)$ varies more rapidly with angle than $P_2(\cos\theta)$, the value of Q_4 is considerably more sensitive to the experimental geometry than Q_2. Hence the uncertainties in the evaluation of Q_4 are considerably larger than for Q_2, and are a source of systematic uncertainty in the correction and analysis of the secondary transition.
4) The uncertainty in the angle between the detectors and the beam axis measured at the centre of the target chamber was estimated to be less than 1° at a detector/target distance of 10 cm. The systematic error introduced in the fit due to this uncertainty is negligible in the case of the primary transition, but may be significant in the case of a highly structured dis-

TABLE 2

Summary of the normalised χ^2 and δ_1 obtained from the fits to the primary and secondary angular distributions.

E_γ^0	$\delta_{\text{free fit}}$	χ^2/N	E_γ^0	χ^2/N ($\delta = 0$ fit)
Primary (central case)			Secondary (central case)	
1633.7	−0.038	1.16	1633.7	2.22
1633.3	−0.066	0.87	1633.3	4.58
1634.1	−0.003	2.93	1634.1	7.31
Primary (off centre case)			Secondary (off centre case)	
1633.7	−0.028	3.58	1633.7	3.17
1633.3	−0.063	2.68	1633.3	4.26
1634.1	+0.003	4.83	1634.1	3.11

tribution such as that of the 1.63→g.s. secondary transition.

In view of these difficulties, it is perhaps not surprising that the quality of the fits to the secondary transition is not as good as for those to the primary transition. However it is worth noting that if, in the central case, the errors on the data are arbitrarily increased to 2%, then the normalised χ^2 falls to unity. Hence, for the majority of cases either carried out or in prospect, the fits to the angular distributions measured using this target can be considered extremely reliable down to counting statistics as small as 3%.

We may conclude, then, that the gas target described here can be used with confidence for the measurement of γ-ray angular distributions. In general, corrections to the raw data are necessary to take into account the extended nature of the γ-emitting region, but provided that the resonance is located centrally in the target chamber these corrections are small. The accuracy with which these corrections can be made has been tested using the 6.93 MeV, 2^+, $T=1$ resonance in the $^{16}O(\alpha, \gamma)^{20}Ne$ reaction which has well known radiative decay properties. The corrected angular distributions were found to be in very good agreement with the theoretical predictions. Furthermore, this agreement was maintained for angular distributions measured with the resonance located substantially off-centre in the target chamber, indicating that the correction process is reliable even when the corrections are quite large.

A program of angular distribution measurements using the reactions $^{15}N(\alpha, \gamma)^{19}F$, $^{16}O(\alpha, \gamma)^{20}Ne$ and $^{20}Ne(\alpha, \gamma)^{24}Mg$ is now in hand using this target.

The authors wish to thank Mr. A. R. Holmes for his technical advice and help with the angular distribution gas target design and the members of the Oxford electrostatic generator workshop under Mr. J. C. Graham involved in the construction of the gas target.

M. J. Hurst, T. J. M. Symons and C. H. Zimmerman wish to acknowledge financial support from the Science Research Council.

References

1) K. W. Allen, S. P. Dolan, A. R. Holmes, T. J. M. Symons, F Watt, C. H. Zimmerman, A. E. Litherland and A. M. J. Sandorfi, Nucl. Instr. and Meth. **134** (1976) 1.
2) H. J. Rose and D. M. Brink, Rev. Mod. Phys. **39** (1967) 306.
3) T. J. M. Symons, L. K. Fifield, M. J. Hurst, F. Watt, C. H. Zimmerman and K. W. Allen, to be published.
4) J. H. Cobb, W W. M. Allison and J. N. Bunch, Nucl. Instr. and Meth. **133** (1976) 315.
5) J. D. Pearson and R. H. Spear, Nucl. Phys. **54** (1964) 434.
6) F. Ajzenberg-Selove, Nucl. Phys. **A190** (1972) 1.

1.E.4:
2.B

Nuclear Physics A288 (1977) 57–81: © *North-Holland Publishing Co., Amsterdam*

MEASUREMENTS OF THE RADIATIVE WIDTHS OF THE FIRST $T = 1, 2^+$ STATE OF ^{20}Ne AND THEIR RELATIONSHIP TO ANALOG β-DECAYS

L. K. FIFIELD, F P. CALAPRICE †, C. H. ZIMMERMAN, M. J. HURST, A. PAKKANEN ††, T. J. M. SYMONS, F. WATT and K. W. ALLEN

Nuclear Physics Laboratory, Oxford, England

Received 18 February 1977

Abstract: The radiative widths for decays of the ^{20}Ne $T = 1$, 2^+ (10.27 MeV) state were measured by resonance α-capture in the reaction $^{16}O(\alpha, \gamma)^{20}Ne$. A special windowless gas-cell target yielded a low-background spectrum enabling six γ-branches to be observed with a Ge(Li) detector. The six branches correspond to decays from the 10.27 MeV level to the following levels: 2^+(7.83 MeV), 2^+(7.42 MeV), 3^-(5.62 MeV), 2^-(4.97 MeV), 2^+(1.63 MeV) and 0^+(g.s.). The branching ratios and radiative widths Γ_γ to these levels are: 7.83 MeV [$(0.22 \pm 0.06)\%$, 0.008 ± 0.002 eV], 7.42 MeV [$(6.9 \pm 0.4)\%$, 0.31 ± 0.04 eV], 5.62 MeV [$(2.1 \pm 0.2)\%$, 0.097 ± 0.014 eV], 4.97 MeV [$(1.3 \pm 0.1)\%$, 0.060 ± 0.008 eV], 1.63 MeV [$(88.9 \pm 0.5)\%$, 4.08 ± 0.43 eV] and 0.0 MeV [$(0.64 \pm 0.14)\%$, 0.029 ± 0.008 eV]. The radiative widths to the 1.63 MeV and 7.42 MeV levels are used to determine the CVC predictions of the weak magnetism form factors and their effects on certain β-decay observables are evaluated.

E NUCLEAR REACTIONS $^{16}O(\alpha, \gamma)$, $E = 6.93$ MeV; measured $\sigma(E_\gamma, E_\gamma)$. ^{20}Ne 10.27 MeV, 2^+ $T = 1$ level deduced branching ratios, Γ_γ, weak magnetism form factors. Enriched gas target.

1. Introduction

The γ-decay of the $T = 1$, 2^+ state of ^{20}Ne has an important relationship to the analog β-decays of ^{20}F and ^{20}Na. This relationship is the result of the conserved vector current theory [1]) which asserts that there is a general isovector conserved vector current whose isospin components are the isovector electromagnetic current and the vector current of the weak interaction. As a result of this relationship all vector form factors, or matrix elements, which characterize analog β- and γ-transitions are related by isospin Clebsch-Gordan coefficients. In particular, the isovector M1 matrix element for the γ-decay of the $T = 1$ state of ^{20}Ne is related to a "weak magnetism" counterpart in the analog β-decays of ^{20}F and ^{20}Na.

Measurements of the analog magnetic form factors for the decays of the ^{12}B-^{12}C-^{12}N triad have been made and the data generally support the validity of the

† Alfred P. Sloan Fellow. Permanent address: Department of Physics, Princeton University, Princeton, New Jersey 08540, USA.

†† Permanent address: Physics Department, University of Jväskylä, Finland.

CVC theory [2,3]). However, because the evidence for the weak magnetism aspect of CVC is not extensive [3]) we have carried out a study of the analog γ-decay in the mass-20 system in the hope that this system might provide a new test of the CVC theory. In the following we present the results of measurements of the radiative decays of the first $T = 1$, 2^+ state of ^{20}Ne. From these data we evaluate the weak magnetism form factor by CVC theory, and calculate its expected effect on the shape of the β-spectrum for the analog decays of ^{20}F and ^{20}Na.

As an additional motivation for these measurements, we note that the question of the possible existence of second-class currents is still undecided and measurements of the β-γ correlations for the ^{20}F-^{20}Na mirror β-decays would help to settle the issue. At the present time there appears to be positive evidence for the existence of second-class currents from angular correlation data on the $A = 12$ [ref. [4])] and $A = 19$ [ref. [5])] systems, while related experiments on the $A = 8$ [ref. [6])] decays and *ft* asymmetry systematics [7]) detect no such effects. In the angular correlation experiments, the measured effect depends on a linear combination of the weak magnetism and second-class tensor form factors. Thus to determine the second-class

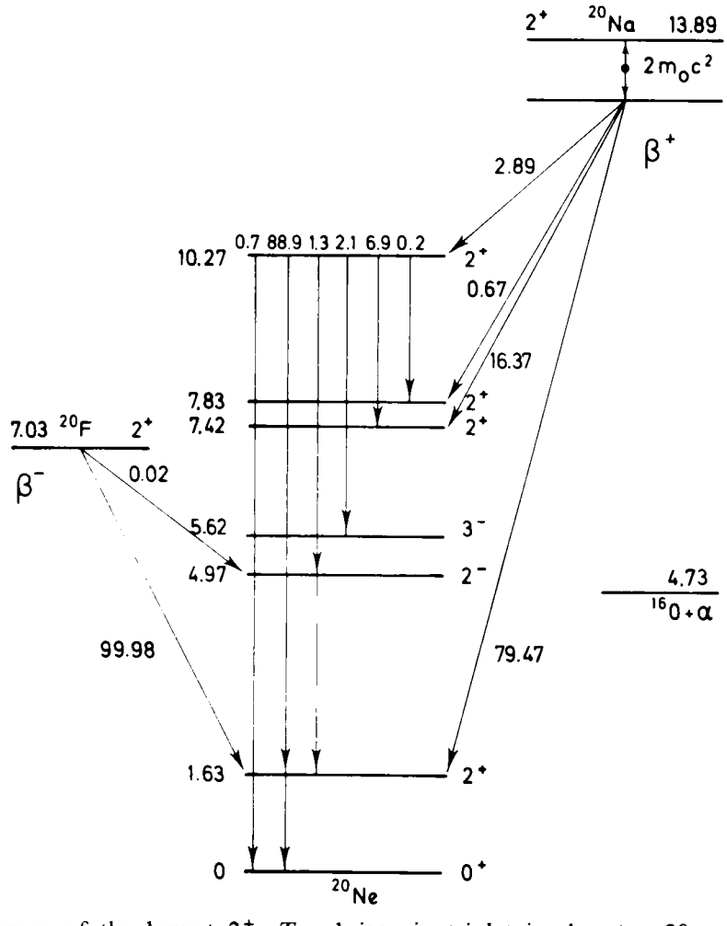

Fig. 1. Decay schemes of the lowest 2^+, $T = 1$ isospin triplet in the $A = 20$ system. The β-decay branching ratios for ^{20}Na and ^{20}F were taken, respectively, from ref. [22]) and ref. [23]) while the γ-ray branching ratios in ^{20}Ne are from the present work.

term one must first specify the weak magnetism form factor and this is usually done by invoking the CVC theory to relate the weak magnetism form factor to the measured analog electromagnetic term. The $A = 20$ β-γ correlations can be studied in this way and in the following we evaluate the correlation expected from the weak magnetism form factor. Higher-order form factors are calculated within a $(2s\text{-}1d)^4$ shell-model basis and their effects on the angular correlation parameters are also evaluated.

The analog decays of the mass-20 $T = 1$ states are illustrated in fig. 1. The principal decays of the ^{20}F and ^{20}Na states are to the $T = 0$, 2^+ level of ^{20}Ne (1634 keV). The $T = 1$ ^{20}Ne analog state is at an excitation of 10.27 MeV and, in addition to its radiative decay, it is unstable to α-particle decay to ^{16}O. This is an isospin forbidden transition, and it occurs because the ^{20}Ne state is probably not a pure $T = 1$ analog but instead contains admixtures of $T = 0$ states. It is the isovector radiative width that is needed for the CVC determination of the weak magnetism form factor and therefore isospin non-conservation, if it is a large effect, makes the interpretation of the experimental width complicated. This issue is discussed further in subsect. 3.7 but for the present we note that the α-decay width of the 10.27 MeV level has been measured recently by Ingalls [8]), with the result $\Gamma_\alpha = 0.116 \pm 0.020$ keV. From the α-widths of isospin allowed decays of nearby $T = 0$, 2^+ levels, Ingalls estimates a 1 % limit in intensity for the isospin impurity in the 10.27 MeV level, due to these nearby levels.

The log ft values for the ^{20}F and ^{20}Na β-decays to the 1634 keV level are 4.97 and 4.99, respectively. These are slightly slow transitions which may be due to the fact that in LS coupling the dominant parts of the initial and final states are characterized by $L = 1$ and $L = 2$, respectively, and the Gamow-Teller operator $\boldsymbol{\sigma}$ is unable to change L.

The radiative width of the ^{20}Ne $T = 1$ analog state was previously measured by Pearson and Spear [9]) using the resonance radiative capture reaction ^{16}O$(\alpha, \gamma)^{20}$Ne. The radiative width Γ_γ was obtained from the absolute yield of the 8635 keV γ-ray corresponding to the $2^+ \rightarrow 2^+$ transition from the $T = 1$ level at 10271 keV to the 1634 keV level. The γ-ray spectra were obtained with a NaI detector and the targets were solid compounds of oxygen. The radiative width quoted by Pearson and Spear was given without a lab to c.m. correction as 5.6 ± 0.6 eV. After multiplying by the mass ratio 16:20 and using Ingalls value [8]) for Γ_α/Γ we obtain the c.m. value $\Gamma_\gamma = 4.65 \pm 0.51$ eV. In a recent measurement with a Ge(Li) detector Ingalls [8]) obtained $\Gamma_\gamma = 4.08 \pm 0.33$ eV, in reasonable agreement with the corrected value of Pearson and Spear.

In the present work, the radiative width is again measured by the resonance yield of 8635 keV γ-rays in the reaction ^{16}O$(\alpha, \gamma)^{20}$Ne. In this case, however, the value of $\omega\gamma = (2J+1)\Gamma_\gamma\Gamma_\alpha/\Gamma$ is deduced by comparing the yield with the resonance yield from the 6^+ level at 8775 keV, for which $\omega\gamma$ is known from previous work. In addition to this difference in procedures, we note that for the present work we employed a gas target of enriched $^{16}O_2$. This yielded a very low background γ-ray spectrum which is significantly better than those of previous experiments.

massive Oxford Instruments pump only being warmed up for final recovery. The clean nature of these pumps ensured that the gas could be re-used many times without being contaminated by hydrocarbons. This facility was important as an initial charge of ten litres of gas would only last for half a day of running.

With this arrangement contaminant reactions could only occur with impurities in the target gas (eg ^{14}N, ^{17}O) or in the tantalum pumping nozzles which were only struck by a small fraction of the beam (usually ~0.1-0.2%). To summarise, the advantages of the gas target were:-

a) The target composition was known and reproducible

b) Very thin targets were possible, enabling the study of sharp resonances

c) No non-target materials were present in the path of the bulk of the beam

d) High beam currents could be sustained without target deterioration.

e) Expensive isotopically pure gases could be re-used many times without significant contamination.

2.3 The Cryopumped Gas Target - Operation

An indication of the success of the design is that the troublesome contaminant ^{13}C was hardly ever observed. However, γ-rays were observed whose origin was the reaction $^{27}Al(\alpha,p\gamma)^{30}Si$ and, at higher beam energies, $^{12}C(\alpha,\alpha_2\gamma)^{12}C$. In addition, the weak capture reaction $^{56}Fe(n,\gamma)^{57}Fe$ was usually observed, the 7.6 MeV γ-rays then providing useful γ-ray energy calibration lines. The neutrons were primarily produced by beam striking collimators and slits at a distance from the

2. The experiment

2.1 THE GAS TARGET

Beams of α-particles from the Oxford 10 MV single-ended Van de Graaff accelerator were employed in measurements on the $^{16}O(\alpha, \gamma)^{20}Ne$ resonance at 6.93 MeV. A windowless gas cell and a hydrocarbon-free beam line were used in order to eliminate the strong background of 6.13 MeV γ-rays arising from the $^{13}C(\alpha, n\gamma)^{16}O$ reaction. This background constitutes the main drawback in the use of solid targets at α-energies above 5.12 MeV. The gas-target system has been described in detail elsewhere [10], so only a brief description will be given here. The flow of target gas out of the 15.6 cm long target tube was restricted by nozzles at each end, with a length of 3 cm and a bore of 3.3 mm as illustrated in fig. 2. Gas escaping from these nozzles

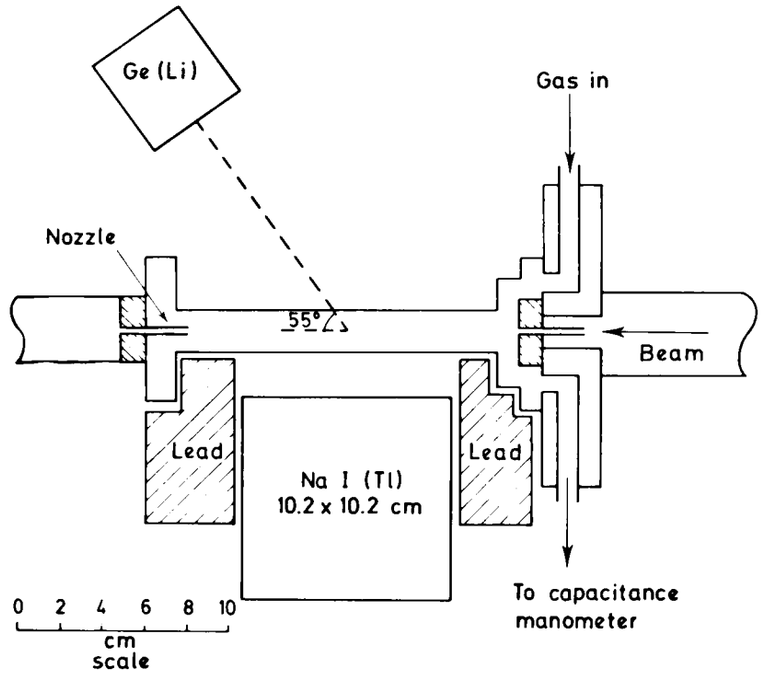

Fig. 2. Schematic representation of the gas target and γ-ray detectors. Yield curves were taken with the NaI(Tl) detector, while the Ge(Li) detector was employed in obtaining on-resonance γ-ray spectra.

was pumped by two cryopumps cooled to approximately 10 K by cold helium gas. The gas pressure within the target tube was monitored by a capacitance manometer, the output of which was fed back to a servo-driven needle valve which controlled the flow of gas into the target tube. In this way the target pressure was maintained constant to better than 5 %. Retrieval of the target gas was accomplished with the aid of a cryofinger within the target gas reservoir; the operation consisted of cooling the cryofinger and allowing the cryopumps to warm up above the boiling point of the target gas.

The target gas used in the present work was enriched to 99.98 % in ^{16}O in order to

eliminate background from the prolific $^{18}O(\alpha, n\gamma)^{21}Ne$ reaction. Gas pressures employed in the various runs ranged from 0.015 to 0.8 Torr, which corresponded to target thicknesses of 0.3 to 16 keV for 6.9 MeV α-particles. Beam currents varied between 10 and 20 μA of $^4He^+$, and the ratio of beam current to current on the target nozzles was typically better than 500:1. After passing through the target, the beam travelled a further 3.7 m to a water-cooled Faraday cup, with an electron suppression ring near the entrance aperture, which provided accurate values of relative collected charge between different runs.

2.2. LOCATING RESONANCES

Resonances were located with the aid of a beam-energy modulator [11]) which

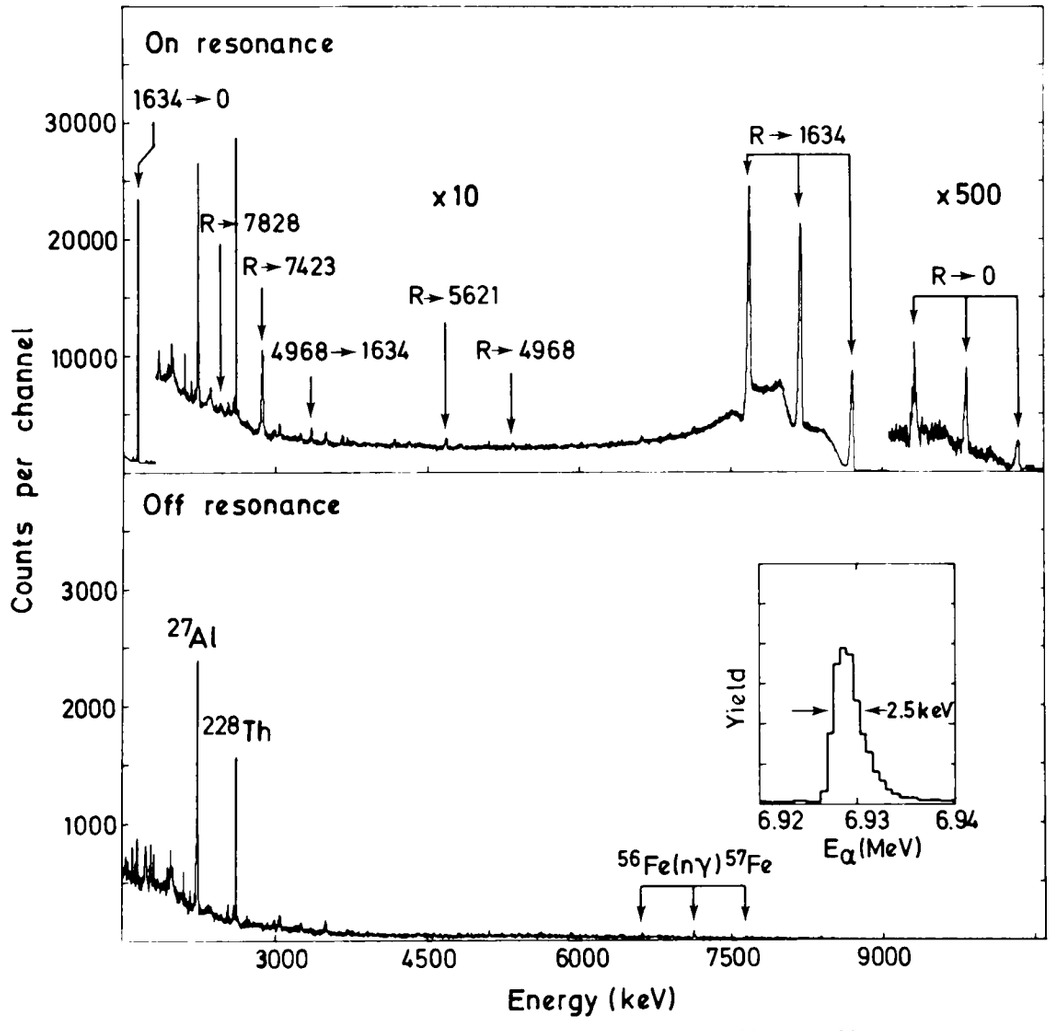

Fig. 3. Spectra of γ-rays taken on and off the 6.93 MeV resonance in the $^{16}O(\alpha, \gamma)^{20}Ne$ reaction. The target pressure was 0.8 torr and the two spectra are normalized to the same collected charge. Peaks arising from the decay of the 2^+, $T = 1$ level at 10.27 MeV in ^{20}Ne are labelled by the corresponding transition. The peak labelled ^{27}Al was due to the $^{27}Al(\alpha, p\gamma)^{30}Si$ reaction on a small Al contaminant in the target nozzles, and the ^{228}Th line was due to a source placed 50 cm from the Ge(Li) detector. The inset shows a yield curve over the 6.93 MeV resonance, taken at a target pressure of 0.04 Torr.

allowed the beam energy to be varied continuously over a typical range of 60 keV in 200 sec. Gamma rays were detected in a 10.2 × 10.2 cm NaI crystal positioned at 90 to the beam direction with its front face 3.2 cm from the centre of the target. Lead collimators provided shielding from γ-rays from the target nozzles. The target and detectors are depicted schematically in fig. 2.

Yield curves were obtained with the aid of an interface between the modulator and a Laben multichannel analyzer. This interface scaled the number of logic pulses at each of eight inputs as a function of the NMR frequency derived from the NMR probe in the accelerator analyzing magnet. Seven of the logic pulses were derived from single channel analyzers with windows set about selected portions of the γ-ray spectrum, while the eighth input scaled the digitized beam current. At the end of a run, which would usually involve a number of sweeps over the selected energy region, the resulting yield curves were transferred to the computer and normalized to a fixed amount of collected charge in each frequency interval. Separate yield curves were obtained for increasing and decreasing beam energy. The yield curves shown in figs. 3 and 4 were obtained in this way.

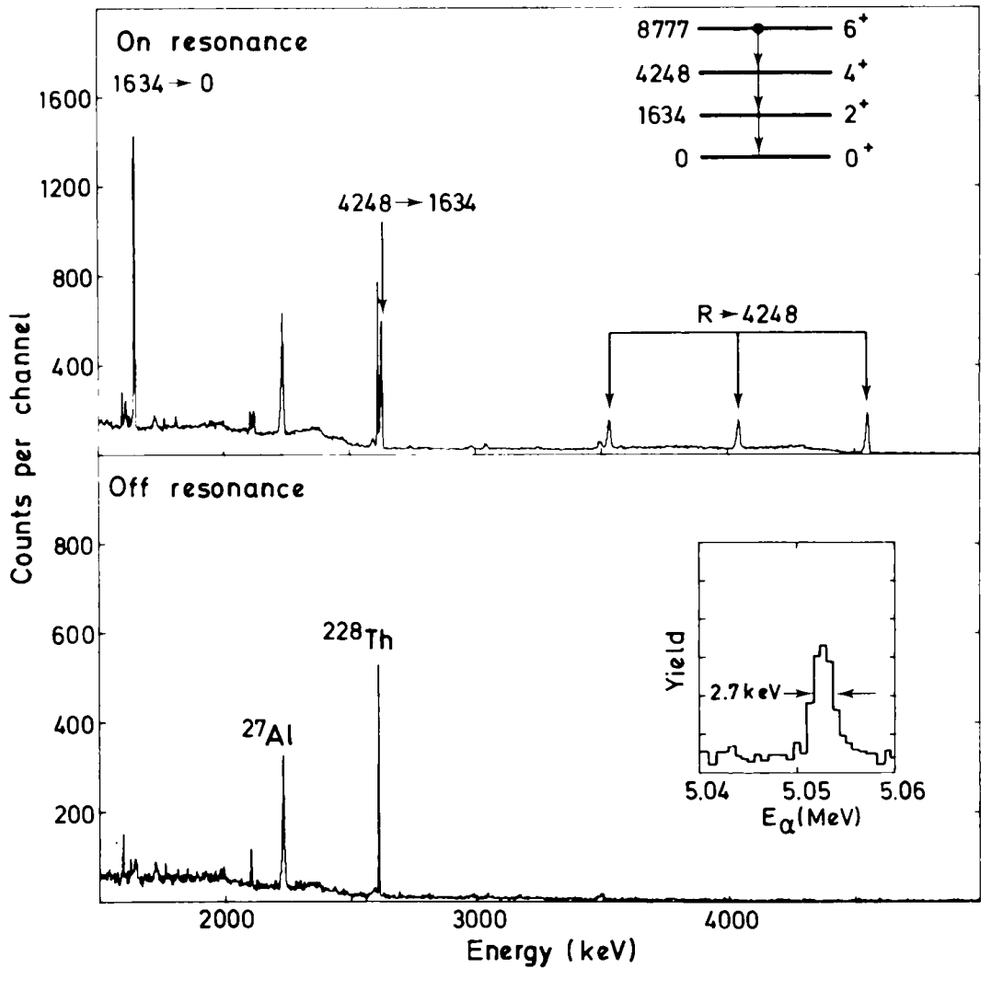

Fig. 4. Spectra of γ-rays taken on and off the 5.05 MeV resonance in the $^{16}O(\alpha, \gamma)^{20}Ne$ reaction.

2.3. GAMMA-RAY SPECTRA

Once the 6.93 MeV resonance had been located, γ-ray spectra both on and off resonance were taken with an 85 cm^3 Ge(Li) detector positioned at a nominal angle of 55 to the beam with its front face 12.5 cm from the centre of the target. The target gas pressure was 0.8 Torr and the resonance was positioned in the target tube with the aid of a yield curve taken immediately prior to the on-resonance spectrum and at the same target pressure. For this yield curve the NaI(Tl) crystal was positioned at 90° and at a distance of 10 cm from the target, and was collimated so that only those γ-rays from a 5 cm section in the middle of the target could reach the detector. The on-resonance spectrum was then taken at the beam energy corresponding to the peak of this yield curve. During the acquisition of the on-resonance spectrum in the Ge(Li) detector, the yield of γ-rays from the NaI detector was monitored continuously as a check on the stability of the resonance position. In addition, the on-resonance spectrum was transferred to the computer at one hour intervals where the Doppler shift of the γ-ray from the 1634 $\rightarrow$ 0 keV transition in ^{20}Ne could be determined as a further check on the resonance position. With the exception of one interval, which was discarded, the energies of this γ-ray derived from peak centroids agreed to within $\pm$ 0.5 keV, which corresponded to a variation in the nominal angle of the Ge(Li) detector of $\pm 1.7°$. The on-resonance spectrum presented in fig. 3 is the sum of this sequence of hourly spectra. A similar procedure was followed in obtaining the on-resonance spectrum at the 5.05 MeV (6^+) resonance shown in fig. 4. The off-resonance spectra were taken at α-particle energies 15 keV below those employed in the on-resonance measurements. It is worth noting that the 6129 keV γ-ray from the $^{13}C(\alpha, n\gamma)^{16}O$ reaction is barely visible in fig. 3, even though the beam energy is 1.81 MeV above threshold.

Yield curves taken with the NaI detector over the 6.93 and 5.05 MeV resonances at a target gas pressure of 0.04 Torr are shown as inserts in figs. 3 and 4. Single-channel analyzer windows were set to accept γ-rays with energies $E_\gamma > 5$ MeV and $4.4 \leqq E_\gamma \leqq 4.6$ MeV, respectively. The spread in beam energy was estimated from the leading edges of these yield curves to have a FWHM of approximately 2 keV.

Gamma-ray branches from the 6.93 MeV (2^+ $T = 1$) resonance to levels in ^{20}Ne at 0, 1.63(2^+), 4.97(2^-), 5.62(3^-), 7.42(2^+) and 7.83(2^+) MeV are indicated in fig. 3. In contrast, only the branch to the 1.63 MeV level was observed in the earlier studies [8, 9]) of this resonance. The higher sensitivity of the present measurement, particularly for transitions to states above the 1.63 MeV level, was due to the use of a Ge(Li) detector and to the absence of a strong background of 6.13 MeV γ-rays from the $^{13}C(\alpha, n\gamma)^{16}O$ reaction.

2.4. EFFECTS DUE TO FINITE LENGTH OF TARGET

Before going on to present results for branching ratios, excitation energies and $\omega\gamma$

measurements, it is necessary to consider the special difficulties introduced by the finite extension of the source of γ-rays along the beam axis.

Gamma rays were emitted towards the detector over a range of angles determined by the distribution of the resonance along the target tube. Consequently, the observed γ-ray intensities and centroid energies were not those from a point target, but rather were averages of the γ-ray yield and Doppler-shifted energies over the range of angles subtended by the target at the detector. In order to derive values of $\omega\gamma$ and excitation energies from the data, it was therefore necessary to calculate the *average* values of the γ-ray angular distributions and Doppler shifts at the position of the detector. These average values were determined by weighting the number and energy of γ-rays emitted from each point along the target by the value of the resonance profile at that point, and by the value of the γ-ray angular distribution at the angle of emission towards the detector. Account was also taken of the variation in target-detector distance along the target tube, and of the small change in the efficiency of the Ge(Li) detector over the range of Doppler-shifted energies of a given transition.

At the target pressures and beam energies chosen for the $\omega\gamma$ measurements, an α-particle with the average beam energy lost 8.4 and 10.6 keV respectively in attaining the resonance energies of the 6.93 and 5.05 MeV resonances. As these energy losses were considerably greater than the maximum energy lost by an α-particle in a single collision with an electron (3.8 and 2.7 keV respectively), the distribution through the target of α-particles with the resonance energy was expected to be approximately Gaussian. This expectation was verified by Monte Carlo calculations [12]) of $P(E_\alpha, \Delta E, x)$, the probability that an α-particle with energy E_α loses an amount of energy ΔE in traversing a length x of the target. By fixing E_α and ΔE at the above values of the average beam energy and energy loss, and varying x, a picture of the contribution to the resonance profile from energy straggling was built up. The resulting curves were skewed slightly towards small values of x, but could be represented to sufficient accuracy by a Gaussian function, and the resonance profile was taken to have a Gaussian functional form. Contributions to the resonance profile arose from both the spread and fluctuations in the beam energy, in addition to energy straggling in the target gas. The position and width of the resonance profile at the 6.93 MeV resonance were then determined empirically by a fit to the line shape of the full-energy peak of the 8.64 MeV γ-ray in the on-resonance spectrum. The fit was restricted to the set of values of the parameters which reproduced the observed average Doppler shift of the γ-ray from the 1.63 $\rightarrow$ 0 transition. In addition, the unshifted energy of the 8.64 MeV γ-ray was treated as a free parameter in the fit. The angular distributions of the 8.64 and 1.63 MeV γ-rays were calculated using the mixing ratio of the $R \rightarrow$ 1.63 transition from ref. [9]). Fig. 5 shows the experimental line shape of the 8.64 MeV γ-ray together with the fit obtained, and the parameters determined from the fit are listed in table 1. The quality of the fit bears out the choice of the Gaussian form of the resonance profile.

A similar procedure was followed for the 6^+ reference resonance at $E_\alpha = 5.05$ MeV,

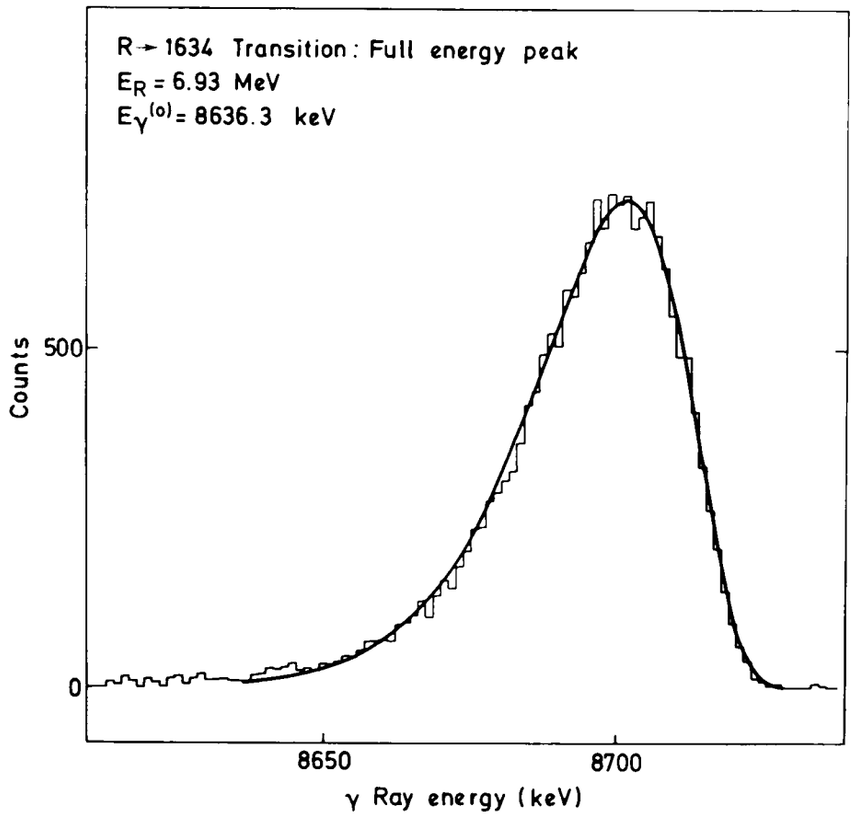

Fig. 5. Detail of the on-resonance γ-ray spectrum of fig. 3 showing the full energy peak of the $R \rightarrow 1634$ transition. The solid line represents the fit to the peak shape obtained under the assumption that the resonance profile could be represented by a Gaussian function. The parameters of this Gaussian profile extracted from the fit are listed in table 1.

TABLE 1

Parameters of the resonance profiles

Resonance energy (MeV)	Peak position [a]) θ_0 (deg)	Width [b]) (cm)	Beam spread [c]) (cm)	Straggling width [d]) (cm)
6.93	54.0 ± 1.4	6.1 ± 0.4	2.1	5.5
5.05	56.0 ± 1.9	5.6 ± 0.3	1.8	5.3

[a]) Here θ_0 is the angle between the Ge(Li) detector and the peak of the resonance profile.
[b]) All widths are FWHM.
[c]) Estimated from the yield curves shown in figs. 3 and 4.
[d]) Estimated from Monte Carlo calculations (see text).

in which case the parameters of the Gaussian resonance profile were determined from a fit to the lineshape of the $R \rightarrow 4.25$ γ-ray. These are also listed in table 1, along with estimates of the contributions to the widths of the resonance profiles from straggling and from the intrinsic beam spread. It can be seen that the dominant contribution arises from straggling in the energy loss of the α-particles in the target gas.

2.5. BRANCHING RATIO AND EXCITATION ENERGIES

Relative branches of the various decay modes of the 2^+ $T = 1$ level at 10271 keV are presented in table 2, and are summarized in the decay scheme of fig. 1. Corrections have been made for the effect of the γ-ray angular distributions. With the exception of the $R \rightarrow 0.0$ and $1.63 \rightarrow 0.0$ transitions the corrections were small, as the measurement was made near a zero of $P_2(\cos\theta)$ and the transitions were either known to be, or could be assumed to be of predominantly dipole character. In particular, an upper limit of 3 W.u. for isospin changing E2 transitions has been proposed by Endt and Van der Leun [13]) and consequently the mixing ratios of the transitions to the 7.42 and 7.83 MeV levels were not expected to be significantly non-zero. In the case of the $R \rightarrow 0.0$ transition, a correction was made for summing of the $R \rightarrow 1.63$ and $1.63 \rightarrow 0.0$ γ-rays in the Ge(Li) detector. The relative efficiency of the Ge(Li) detector as a function of γ-ray energy was determined up to 3.85 MeV using sources of ^{22}Na, ^{60}Co, ^{228}Th and ^{56}Co. Higher-energy points up to 11.5 MeV were obtained from known cascades [14, 15]) at the 1318, 1394 and 1417 keV resonances in the ^{23}Na(p, γ)^{24}Mg reaction, and at the 5413 and 8105 keV resonances in the ^{15}N(α, γ)^{19}F reaction [16]). The errors on the branching ratios include uncertainties in the angular distribution and summing corrections, in the relative efficiency of the Ge(Li) detector, and in the extraction of the number of counts in the peaks in the on-resonance γ-ray spectrum.

TABLE 2

Branching ratios and transition energies for the 6.93 MeV resonance

Transition	$E_\gamma^{(0)}$ (keV)	Branch (%)
$R \rightarrow 0$	10266.1 ± 5.0	0.65 ± 0.14
$R \rightarrow 1.63$	8636.3 ± 3.2	88.9 ± 0.5
$R \rightarrow 4.97$	5305.2 ± 3.8	1.3 ± 0.1
$R \rightarrow 5.62$	4649.6 ± 2.2	2.1 ± 0.2
$R \rightarrow 7.42$	2847.9 ± 1.2	6.9 ± 0.4
$R \rightarrow 7.83$	2442.9 ± 2.6	0.22 ± 0.06
$4.97 \rightarrow 1.63$	3332.0 ± 1.9	

The energy calibration employed in obtaining the average γ-ray energies from peak centroids was defined by *in situ* lines from ^{60}Co and ^{228}Th sources at 511.0, 1173.2, 1332.5 and 2614.5 keV, a line at 3854 ± 1 keV from an Am-^{10}B source [17]) and lines at 6129.2 ± 0.4 [ref. [18])], 7645.7 ± 0.5 and 7631.3 ± 0.5 keV [ref. [19])]. The latter three lines arise respectively from the ^{13}C(α, nγ)^{16}O reaction and from γ-decay to the ground and first excited states of ^{57}Fe following thermal neutron capture in ^{56}Fe. They were obtained by taking a spectrum with the target gas out and with a fraction of the beam diverted on to the target nozzles.

Unshifted γ-ray energies were evaluated using the calculated average Doppler

TABLE 3

Excitation energies in ^{20}Ne

State	J^π	E_x (present) [a] (keV)	E_x (previous) (keV)
10.27	2^+, $T = 1$	10271.2 ± 2.7	10271 ± 3 [b]
7.83	2^+	7828.1 ± 3.8	7826 ± 3 [b]
7.42	2^+	7423.1 ± 3.0	7420 ± 1 [b]
5.62	3^-	5621.0 ± 3.5	5621.7 ± 2 [c]
4.97	2^-	4966.0 ± 1.9	4968.2 ± 0.8 [c]
8.78	6^+	8776.7 ± 2.3	8775.0 ± 2.2 [c]
4.25	4^+	4247.9 ± 1.3	4247.3 ± 1.8 [c]

[a]) Corrected for γ-ray recoil.
[b]) Ref. [25]).
[c]) F Ajzenberg-Selove, Nucl. Phys. **A190** (1972) 1.

shifts (correct to second order), and the excitation energies derived from them and presented in table 3 have been corrected for γ-ray recoil. The errors arise from uncertainties in the average Doppler shift of the 1.63 → 0.0 transition, in the energy calibration, and in the determination of peak centroids.

It can be seen from table 3 that rather good agreement is obtained between the excitation energies measured in the present work and those from earlier measurements.

2.6. RADIATIVE-WIDTH MEASUREMENTS

The radiative width of the decay branch from the 2^+ $T = 1$ resonance to the 1.63 MeV level was determined by comparison of its thick target yield with that of the 6^+, 5052 keV resonance, using the relation

$$\omega\gamma(2^+\ T = 1) = \frac{\varepsilon(6.93)}{\varepsilon(5.05)} \frac{6.93}{5.05} \frac{Y(2^+\ T = 1)}{Y(6^+)} \omega\gamma(6^+),$$

where the stopping powers ε were taken from the tables of Northcliffe and Schilling [20]), and the yields Y have been corrected for angular distribution effects. On-resonance and off-resonance γ-ray spectra were taken for the two resonances in turn under identical conditions of target pressure and detector/target geometry. The value of 1.37 ± 0.13 eV for $\omega\gamma$ of the 6^+ reference resonance was taken from ref. [21]). Two independent estimates of $\omega\gamma$ of the $R_{6.93} \rightarrow 1.63$ transition were obtained from the data, the first by comparison of the intensities of the $R_{6.93} \rightarrow 1.63$ and $R_{5.05} \rightarrow 4.25$ transitions, the second by comparison of the yields of the 1.63 → 0.0 transition at the two resonances. In the latter case, a small correction to the observed yield of 1.63 MeV γ-rays from the 6.93 MeV resonance was made for feeding from the 4.97 MeV level. Values of 14.9 ± 1.3 and 14.1 ± 1.0, respectively,

TABLE 4

Transition strengths for the 6.93 MeV resonance

Transition	Type	$\omega\gamma$ (eV)	Γ_γ (eV)	$\lvert M\rvert^2$	$\lvert M\rvert^2$ (W.u.)
$R \rightarrow 0.0$	E2	0.14 ± 0.04	0.029 ± 0.008	$0.32 \pm 0.09\ e^2 \cdot \mathrm{fm}^4$	0.10 ± 0.03
$R \rightarrow 1.63$	M1	19.7 ± 2.1	4.08 ± 0.44	$0.55 \pm 0.06\ \mu_N^2$	0.31 ± 0.03
$R \rightarrow 4.97$	E1	0.29 ± 0.04	0.060 ± 0.008	$(3.8 \pm 0.5) \times 10^{-4} e^2\ \mathrm{fm}^2$	$(8.3 \pm 1.0) \times 10^{-4}$
$R \rightarrow 5.62$	E1	0.47 ± 0.07	0.097 ± 0.014	$(9.2 \pm 1.3) \times 10^{-4} e^2\ \mathrm{fm}^2$	$(2.0 \pm 0.3) \times 10^{-3}$
$R \rightarrow 7.42$	M1	1.5 ± 0.2	0.31 ± 0.04	$1.16 \pm 0.15\ \mu_N^2$	0.65 ± 0.08
$R \rightarrow 7.83$	M1	0.04 ± 0.01	0.008 ± 0.002	$0.050 \pm 0.012\ \mu_N^2$	0.027 ± 0.006

were obtained for the ratio $\omega\gamma(R \rightarrow 1.63)/\omega\gamma(6^+)$, and the weighted average was used in deriving the adopted value of $\omega\gamma(R \rightarrow 1.63) = 19.7 \pm 2.1$ eV. The error includes an uncertainty of 5 % in the relative stopping power. This adopted value was used to evaluate the resonance strengths of the other branches from the branching ratios given in table 2; the results are collected in table 4.

3. Discussion

3.1. SUMMARY OF MEASUREMENTS OF $\Gamma_\gamma(10.27 \rightarrow 1.63)$

In table 5 we summarize all measurements of the radiative width for the decay of the $T = 1$, 2^+ (10.27 MeV) level to the 1.63 MeV level of ^{20}Ne. The published $\omega\gamma$ of Pearson and Spear [9]) is not corrected for the lab to c.m. transformation and, as indicated, we have made the correction by multiplying by the mass ratio $M(^{16}\mathrm{O})/M(^{20}\mathrm{Ne}) = 16/20$. The second entry of the table was obtained by combining the inelastic electron scattering data of Mitsunobu and Torizuka [24]) with the resonance α-capture data of Alexander *et al.* [25]). The former determine $\omega\gamma$ for the transition between the ground state and the $T = 0$, 2^+ state at 7.826 MeV while the latter measure the ratio of $\omega\gamma$ for the decay of the $T = 1$, 2^+ (10.27 MeV) state to the 1.63

TABLE 5

Summary of measurements of $\Gamma_\gamma(10.27 \rightarrow 1.63)$

Experiment	Ref.	$\omega\gamma$ (eV)	Γ_γ (eV) [a])
Pearson and Spear	[9])	27.8 ± 3.0	
corrected (16/20)		22.2 ± 2.4	4.65 ± 0.51
Mitsunobu and Torizuka	[24])		
Alexander *et al.*	[25])	25 ± 5	5.2 ± 1.0
Ingalls	[8])	19.7 ± 1.6	4.08 ± 0.33
This work		19.7 ± 2.1	4.08 ± 0.46
Weighted average			4.26 ± 0.23

[a]) Calculated from $\omega\gamma = (2J+1)\Gamma_\gamma\Gamma_\alpha/(\Gamma_\gamma+\Gamma_\alpha)$ with $\Gamma_\alpha = 116 \pm 20$ eV [ref. [8])].

MeV level to that for the decay of the $T = 0, 2^+$ level (7.826 MeV) to the ground state. The third and fourth entries are those of Ingalls [8]) and the present work.

All of the measurements are consistent and since there is no legitimate reason to reject any one, we judge the best value to be the weighted average of all four values, which gives $\Gamma_\gamma = 4.26 \pm 0.23$ eV. The total radiative width is thus known to within an error of 5.5 %. Note, however, that Pearson and Spear have the only measurement of the multipole character of the decay, which indicates that the decay is almost entirely M1.

3.2. VECTOR FORM FACTORS AND CVC

In the "elementary particle" treatment of the β-decay process one characterizes the decay in terms of nuclear form factors, as defined in terms of a special multipole expansion of the interaction. For the weak vector current, the leading form factors are denoted by Holstein and Treiman [26, 27]) as $a(q^2)$, $b(q^2)$ and $e(q^2)$, corresponding to the Fermi matrix element, the weak magnetism form factor, and the scalar form factor, respectively. These are functions of the momentum transfer q and, in general, all details of the nuclear structure which affect the vector decay process to first order in recoil are contained in these form factors. In the next order of recoil, two other form factors arise from the vector current, $f(q^2)$ and $g(q^2)$. These correspond to rank-two operators and under certain conditions they are related to the electric quadrupole moment.

According to the CVC theory we expect the weak vector current to be related to the isovector electromagnetic current. One consequence of this relationship, in its strongest sense, is that the weak vector current must be first class with respect to the G-parity classification of Weinberg [28]). For a $\Delta T = 0$ analog decay this implies that $e(q^2) = f(q^2) = 0$, as these are manifestly second-class form factors for such decays [27]). To the extent that isospin is a good quantum number, the decays we consider in the mass-twenty system are $\Delta T = 1$ transitions and therefore the requirement that e and f are zero is no longer true. These may have first-class components which, in principle, could be non-zero. However, in the impulse approximation e is zero even for $\Delta T = 1$ decays, since the strong form of CVC rules out second-class vector currents, and in the following we use this result.

For our purposes, the main prediction of the CVC theory is the specification of the leading form factors by the following

$$a(0) = g_V \langle \beta | T\pm | \alpha \rangle, \tag{1}$$

$$b(0) = b_\gamma. \tag{2}$$

Here b_γ is the magnetic form factor for the analog γ-decay, which is related to the isovector M1 radiative width by

$$\Gamma_{M1}^{T=1} = \tfrac{1}{6}\alpha E_\gamma^3 b_\gamma^2 / M^2, \tag{3}$$

target chamber, being subsequently thermalised by scattering in the target room. Another γ-ray which would often be observed arises from the 2.6 MeV transition in ^{208}Pb fed by the decay, via ^{208}Tl, of the ^{232}Th in concrete. In practice a thorium (^{228}Th) source was used to enhance this γ-ray as it was useful for calibration.

The electronics and experimental procedure were as described by Zimmerman [Zi77]. Two γ-ray detectors were used, a 16% (85cc) lithium drifted germanium detector and a 13% (59cc) intrinsic germanium detector. The latter was only used in angular distribution measurements. In addition, a 25% (126cc) Ge(Li) detector was used in the study of the 8^+ resonance in Ne^{20}. In each case, pulses were amplified by a linear amplifier and analysed by a multichannel analyser which was periodically read out to the department's PDP10 computer for subsequent analysis.

For yield curve measurements a 3"x3" NaI crystal was used, the pulses being sorted into several gates defined by single channel analysers, and stored against the NMR frequency from the beam analysing magnet, using the multichannel analyser in a multiscaler mode. The digitised beam current was stored in the eighth gate to enable subsequent normalisation to current, thus avoiding spurious peaks due to current fluctuations. An automatic beam energy modulation technique was used and has been described by Wormald and Takacs[Wo74]. This enabled yield curves covering large energy ranges to be made in 1 keV steps without repetitive operator action.

where $\alpha = 1/137.04$ is the fine structure constant, E_γ is the γ-ray energy and M is the nuclear mass. As may be noted from eq. (1), the Fermi form factor $a(0)$ is zero for $\Delta T = 1$ decays. Thus the main vector term is just b.

By CVC and for $\Delta T = 1$ decays, Holstein [27]) shows that the form factors f and g are related to each other and to the isovector radiative E2 width by

$$g(0) = -\sqrt{\tfrac{2}{3}}(2M\Delta)f(0), \tag{4}$$

$$\Gamma_{E2} = \tfrac{1}{20}\alpha E_\gamma^3 f_\gamma^2(0)/M^2, \tag{5}$$

where $\Delta = M_i - M_f$ is the difference of nuclear masses. If Δ were the same for the analog β- and γ-transitions we would have $f(0) = f_\gamma(0)$. However, because of the Coulomb displacement energy, Δ is not the same for analog decays so the determination of f and g for the e^+ and e^- decays from Γ_{E2} is not straightforward. To overcome this difficulty we use the impulse approximation which relates g to the matrix element of the quadrupole operator M_Q as follows [27])

$$g(0) = -\tfrac{4}{3}g_V M^2 M_Q, \tag{6}$$

$$M_Q = \sqrt{\tfrac{4}{5}\pi}\langle\beta\|\sum_{i=1}^{A}\tau_i^{\pm} r_i^2 Y_2(\hat{r}_i)\|\alpha\rangle. \tag{7}$$

Then by eq. (4) we have

$$f(0) = (\tfrac{2}{3})^{\frac{1}{2}} g_V M\Delta M_Q, \tag{8}$$

$$\Gamma_{E2}^{T=1} = \tfrac{1}{30}\alpha E_\gamma^5 M_Q^2, \tag{9}$$

where in the last equation we have used $\Delta = E_\gamma$. Thus, in practice, to determine f and g for e^+ and e^- decays we first calculate M_Q from the experimental radiative width Γ_{E2} [eq. (9)]. Then on the assumption that M_Q is the same for all analog decays, we calculate g and f for the $e^\pm$ decays, using eq. (6) and (8) and the appropriate experimental value of Δ.

In summary, we observe that for the $\Delta T = 1$ decays there are just three form factors arising from the vector current, b, f and g. The b-term is the weak analog of the isovector magnetic moment and can be determined, according to CVC, from the radiative M1 decay width Γ_{M1} by eq. (3). The remaining two form factors f and g are related to each other at zero momentum transfer [eq. (4)] and to the quadrupole radiative width Γ_{E2}, but because Δ is not the same for the analog decays an additional condition is needed from the impulse approximation. Thus all weak vector form factors are determined in terms of the radiative widths. To test the CVC prediction these can be determined directly from measurements on the γ-decay processes and the results compared with the radiative values. In practice, for the $\Delta T = 1$ decays only b is amenable to direct measurement as, for example, by measuring the shape of the beta spectrum.

3.3. AXIAL-VECTOR FORM FACTORS

For the purpose of calculating spectral shapes and angular correlations we summarize the axial-vector form factors in this section.

The leading form factor corresponds to the Gamow-Teller matrix element and is denoted as "c"; the higher-order terms are denoted as $d, j_k (k = 2, 3)$ and h. None of these are related to the EM moments by CVC and in general each may be a linear combination of first-class and second-class components. In the following we will assume that they are first class and will proceed to calculate their effects on certain β-decay phenomena. The experimental determination of the second-class components of these form factors is discussed in subsect. 3.4; the most sensitive test for second-class currents usually involves the tensor form factor d.

The Gamow-Teller form factor is the predominant term in the total decay rate and thus it may be determined from the experimental rate. In terms of the ft value we have

$$c^2 = 2ft_F/ft, \tag{10}$$

where $ft_F = 3086$ sec [ref. [29])] is the $0^+ \rightarrow 0^+$ pure Fermi ft value. For the ^{20}Na-^{20}F decays to the 1634 keV level we have log $ft = 4.97$ and therefore $c_{exp} = 0.256$. The first-class contributions to the form factors d, j_k and h can be estimated from nuclear wave functions. The one-body matrix elements which contribute to the axial-vector form factors in the impulse approximation are specified in eq. (67) of ref. [27]).

3.4. COMPARISON OF ANALOG β- AND γ-TRANSITIONS

In this section we compare the ratio of the experimental M1 and Gamow-Teller matrix elements to that expected by the impulse approximation. According to the expression given in ref. [27]) one expects

$$b_\gamma/Ac \approx (4.7 + M_L/M_{GT}) g_V/g_A. \tag{11}$$

Thus the value of b_γ/Ac is a measure of the relative strengths of M_L and M_{GT}. For example, with $M_L \ll M_{GT}$ and $g_A/g_V = 1.23$ one obtains the ratio $b_\gamma/Ac = 3.83$

TABLE 6

Comparison of β- and γ-transitions

Transition	Γ_{M1} (eV) [a])	b_γ	log ft [b])	c	$(b/Ac)_{exp}$	M_L/M_{GT}
$T = 1, 2^+ \rightarrow T = 0, 2_1^+(1.63)$	4.08 ± 0.43	42.5 ± 2.2	4.97 ± 0.01	0.256	8.3 ± 0.4	5.5 ± 0.5
$T = 1, 2^+ \rightarrow T = 0, 2_2^+(7.42)$	0.31 ± 0.04	61.9 ± 4.1	4.19 ± 0.05	0.632	4.9 ± 0.4	1.3 ± 0.5
$T = 1, 2^+ \rightarrow T = 0, 2_3^+(7.83)$	0.008 ± 0.002	13 ± 3	5.42 ± 0.03	0.154	4.1 ± 0.5	0.3 ± 0.5

[a]) Based on the assumption $\Gamma_{M1} = \Gamma_\gamma$.
[b]) Ref. [22]).

for all transitions. Equivalent comparisons of analog β- and γ-transitions of this type have been made by others in a different context [30]). We emphasize that this comparison is not related to CVC predictions but is merely a result of the impulse approximation.

A summary of the form factors for the three $2^+ \rightarrow 2^+$ transitions is given in table 6. The M1 radiative widths are taken from this work assuming that the transitions are pure M1, i.e. $\Gamma_{M1} \approx \Gamma_\gamma$. The magnetic form factor b_γ was calculated from Γ_{M1} using eq. (3) and the Gamow-Teller form factor c was obtained from the experimental ft value by eq. (10). Note that for the transition to the 1.63 MeV level the value of b/Ac is about twice the value expected from a pure-spin transition. Indeed, the orbital and spin contributions to b are comparable despite the larger spin g-factor. The other two transitions do not exhibit an enhancement of b/Ac, however.

3.5. SHELL-MODEL CALCULATIONS OF THE MATRIX ELEMENTS

In the following paragraphs we present the results of calculations of the nuclear matrix elements required in evaluating the first-class contributions to the form factors defined in eq. (67) of ref. [27]). Our motivation for these calculations was to provide a comparison between the observed decay rates and the theoretical predictions and to evaluate, using the same wave functions, the higher-order matrix elements which affect β-decay observables but which are not amenable to direct experimental verification. The calculations were made with the shell-model wave functions of Millener [31]). The states of the $A = 20$ system were assumed to be described by an inert ^{16}O core with four valence nucleons in the sd shell, and the wave functions are built up from a complete $(sd)^4$ basis of SU(3) states. The $T = 1$, 2^+ level and the $T = 0$ levels at 7.42, 1.63 and 0.0 MeV are well described in such a basis. However, the 7.83 MeV level is believed to be predominantly an 8p-4h state and the negative-parity levels at 4.97 and 5.62 MeV require p-shell and fp shell configurations and therefore these three states were not considered in the following.

TABLE 7

Comparison of theoretical matrix elements for $T = 1, 2^+ \rightarrow T = 0, 2^+$ transitions

	$T = 1, 2^+ \rightarrow T = 0, 2_1^+(1.63)$			$T = 1, 2^+ \rightarrow T = 0, 2_2^+(7.42)$		
	PW	Kuo	CCW	PW	Kuo	CCW
M_{GT}	−0.208	−0.148	−0.237	−0.553	−0.482	−0.495
M_L	−0.759	−0.629	−0.842	−0.450	−0.360	−0.416
$M_{\sigma L}$	−0.818	−0.792	−0.835	−0.801	−0.796	−0.902
$M_Q(F^2)$	−0.277	−0.263	−0.203	+0.212	+0.109	+0.163
$M_{k\gamma}(F^2)$ $k = 1$	−2.32	−2.22	−2.92	−0.006	+0.143	−0.084
$k = 2$	+4.56	+4.91	+5.32	−1.76	−1.45	−1.99
$k = 3$	−8.50	−8.31	−10.6	−3.66	−2.80	−4.01

In table 7 we present the calculated matrix elements for the transitions from the $T = 1, 2^+$ level to the $T = 0, 2^+$ levels at 1.63 and 7.42 MeV. In the present work, we have calculated the matrix elements with wave functions generated with the two-body matrix elements of Preedom and Wildenthal (PW)[32]) as well as those of Kuo [33]). For comparison we also give the matrix elements calculated in ref. [34]), which utilized the new two-body matrix elements of Chung and Wildenthal [35]). The variations of the three calculations are not very large. This indicates that the calculated matrix elements are not terribly sensitive to the choice of two-body matrix elements within the assumed $(sd)^4$ basis.

TABLE 8

Comparison of predicted and measured transition strengths

Transition / Parameter	$T = 1, 2^+ \rightarrow T = 0, 2_1^+(1.63)$				$T = 1, 2^+ \rightarrow T = 0, 2_2^+(7.42)$			
	PW	Kuo	CCW	exp. [a])	PW	Kuo	CCW	exp. [a])
B(M1) (W.u.)	0.20	0.12	0.26	0.31 ±0.03	0.62	0.46	0.50	0.63 ±0.08
b	34.7	26.5	39.1	42.5 ±2.2	61.0	52.5	54.9	61.9 ±4.1
log ft	4.97	5.27	4.87	4.97 ±0.01	4.13	4.25	4.22	4.19 ±0.05
c	0.256	0.182	0.291	0.256±0.006	0.680	0.583	0.609	0.632±0.077
b/Ac	6.68	7.16	6.70	8.3 ±0.4	4.41	4.36	4.51	4.9 ±0.4

[a]) This work and refs. [22, 23]).

A more meaningful test of the calculations is given in table 8 where we compare the predicted and observed β- and γ-transition rates to the levels at 1.63 and 7.42 MeV. Here it may be noted that the Kuo matrix elements give a B(M1) for the decay to the 1.63 MeV level which is significantly smaller than the experimental value but generally the agreement with experiment is within about 25 % (for matrix elements). The calculations predict an enhancement of b/Ac for the transition to the 1.63 MeV level, although not quite as large as the observed ratio.

The data on the E2 transition strengths are less complete but what is known is summarized in table 9. The E2 radiative width for the transition to the 1.63 MeV level was derived from the mixing ratio of Pearson and Spear [9]), $\delta = -0.020 \pm 0.013$,

TABLE 9

Comparison of predicted and measured E2 decays

Transition / Parameter	$T = 1, 2^+ \rightarrow T = 0, 2_1^+(1.63)$				$T = 1, 2^+ \rightarrow T = 0, 0^+$(g.s.)			
	PW	Kuo	CCW	exp. [a])	PW	Kuo	CCW	exp. [b])
$\Gamma_{\gamma 2}$ (eV)	0.00061	0.00054	0.00033	$0.0016^{+0.0028}_{-0.0014}$	0.028	0.018	0.046	0.029±0.008
B(E2) (W.u.)	0.0048	0.0043	0.0026	$0.013^{+0.022}_{-0.011}$	0.097	0.062	0.16	0.10 ±0.03

[a]) Ref. [9]). [b]) This work.

using the total γ-ray width from the present work. From table 9 it can be seen that all three wave functions predict a very weak E2 transition, and this is confirmed by experiment, although the large errors prevent a more quantitative comparison. The decay to the ground state, which is considerably stronger, has been measured more accurately and in this case the agreement between theory and experiment is good.

3.6. WEAK MAGNETISM AND β-DECAY OBSERVABLES

We now consider the effect of the weak magnetism form factor on the shapes of the β-spectra and the effect on β-γ angular correlations for the $e^{\pm}$ decays to the 1.63 MeV level of ^{20}Ne. The value of the weak magnetism form factor predicted by CVC from the weighted average of all measurements of Γ_{M1} for the analog γ-decay is

$$b = 43.4 \pm 1.2. \tag{12}$$

This value will be used in the following two subsections for estimates of phenomena for decays to the 1.63 MeV level. In the third subsection we consider the β-α correlation for the ^{20}Na decay to the 7.42 MeV level of ^{20}Ne.

Spectrum shape factor for transitions to the 1.63 MeV level. The shape of the energy spectrum for the decay of unpolarized nuclei has been calculated by Holstein and Treiman [26]. The decay rate is given by the following

$$\mathrm{d}\lambda = 4\frac{G_V^2 \cos^2\theta_C}{(2\pi)^3} F_0(Z, E) pE(E_0 - E)^2 f_1(E)\mathrm{d}E. \tag{13}$$

Here g_V and θ_C are the vector coupling constant and Cabibbo angle respectively, p and E are the momentum and total energy of the β-particle, and $F_0(Z, E)$ is the point charge Fermi function. The spectral function $f_1(E)$ for $\Delta T = 1$ decays is given in terms of the form factors by the following

$$f_1(E) = c^2 - \frac{2}{3}\frac{E_0}{M} c(c + d' \pm b \pm d'') + \frac{2}{3}\frac{E}{M} c(5c \pm 2b) - \frac{1}{3}\frac{m_e^2}{ME}[2c^2 + c(d' \pm 2b \pm d'')]. \tag{14}$$

The quantity M is the nuclear mass and the upper (lower) sign refers to electron (positron) decay.

If we define a spectrum shape factor by normalizing $f_1(E)$ at an energy E_n, and keep only the large linear term, we see that $f_1(E_n) \approx c^2$ and the slope of the shape factor is given by

$$\mathrm{d}S/\mathrm{d}E = \frac{2}{3M}\left(5 \pm \frac{2b}{c}\right) = \begin{cases} +1.23\,\% \text{ MeV}^{-1} & (e^-) \\ -1.19\,\% \text{ MeV}^{-1} & (e^+). \end{cases} \tag{15}$$

We have used the experimental values for b and c given in eq. (12) and table 6, respectively. The slopes of the shape factors given by eq. (15) should be compared to those for the $A = 12$ decays which are $\approx \pm 0.5\,\%$ MeV^{-1}. The larger slopes for the $A = 20$ decays are due to the relative enhancement of the orbital matrix element over the spin matrix element (see subsect. 3.4). More correctly, it is due to the fact that M_{GT} is hindered but M_L is not.

The main cause for the energy dependence of the shape factor is due to the weak magnetism factor. However, for more precise calculations it is necessary to consider effects which are not described by eqs. (13) and (14). The necessary corrections are due to bremsstrahlung radiation, finite size nuclear charge distribution, and the dependence of the Gamow-Teller form factor c on the momentum transfer. These corrections are discussed in ref. [3]) and are evaluated for the $A = 20$ decays in ref. [34]). Using $b = 43.4$ and $c = 0.256$ (same as above) and normalizing to $E_n = m_e^2$, Calaprice, Chung and Wildenthal [34]) obtain

$$S(e^-) = 0.9980 + 0.0117E - 0.00034E^2 - 0.0020/E, \tag{16}$$

$$S(e^+) = 1.0007 - 0.00506E - 0.00032E^2 - 0.00102/E. \tag{17}$$

For the ^{20}F decay ($E_0 = 5.9$ MeV) the result is that the average slope of the complete shape factor is only slightly smaller than the approximate value of eq. (15). However, for the ^{20}Na decay ($E_0 = 11.74$ MeV) the slope of the more precise shape factor is significantly different from the approximate value. Thus, although the weak magnetism form factor is the dominant feature of the shape factor, other contributions are important and a careful comparison of the shapes of the ^{20}F and ^{20}Na spectra will be necessary for a good test of CVC.

Recent measurements of the spectrum shape for the ^{20}F decay have been made by Genz *et al.* [36]) and by Calaprice and Alburger [37]). The average slopes are as follows:

$$\mathrm{d}S/\mathrm{d}E = \begin{cases} +0.78 \pm 0.4\,\% \text{ MeV}^{-1} \text{ [ref. [36])]} & (18) \\ +0.4 \pm 0.5\,\% \text{ MeV}^{-1} \text{ [ref. [37])]}. & (19) \end{cases}$$

The weighted average, $\mathrm{d}S/\mathrm{d}E = 0.62 \pm 0.33\,\%$ MeV^{-1}, is lower than the average slope of the predicted shape factor of eq. (16), $\mathrm{d}S/\mathrm{d}E = 1.10\,\%$ MeV^{-1}, but not inconsistent with it. Thus these data generally support the CVC prediction. Improvements of the ^{20}F measurements and a measurement of the ^{20}Na spectrum would be very desirable, however. We note that the error in the predicted slope due to the uncertainty in Γ_{M1} is only $0.03\,\%$ MeV^{-1}.

Beta-gamma correlations for transitions to the 1.63 MeV level. For a process in which the β-decay is followed by the emission of a γ-ray, there is a β-γ angular correlation of the form

$$d\lambda \approx 1 + A_{e\pm\gamma}\frac{p}{E}\cos\theta + B_{e\pm\gamma}\left(\frac{p}{E}\right)^2\cos^2\theta. \tag{20}$$

Here θ is the angle between the directions of $e^{\pm}$ and γ and the correlation parameters are defined in terms of the form factors by eq. (61) of ref. [27]).

It is useful to consider the main terms which affect the correlation parameter B. These involve the b and d form factors and are linear in the β-energy E, and for a $2^+(T=1) \rightarrow 2^+(T=0) \rightarrow 0^+(T=0)$ spin sequence are given by

$$B_{e\mp\gamma} = \pm \frac{E}{4M}\left(\frac{b}{c} - \frac{d^{II}}{c} \mp \frac{d^{I}}{c} \pm 1\right). \tag{21}$$

We can eliminate the first-class tensor form factor (d^I) by subtracting the correlation parameters to obtain

$$\delta = B_{e^-\gamma} - B_{e^+\gamma} = \frac{E}{2M}\left(\frac{b}{c} - \frac{d^{II}}{c}\right). \tag{22}$$

Eq. (22) illustrates the essential fact that the weak magnetism form factor b must be known before the correlation parameters can be used to detect a possible second-class tensor form factor (d^{II}). Using the value $b = 43.4 \pm 1.2$, $c = 0.256$ and $d^{II} = 0$ we have from eq. (22)

$$\delta(d^{II} = 0) = 0.00455E. \tag{23}$$

To calculate the individual correlation parameters we use the CCW shell-model calculation of $d^I = 20.5$ and obtain (for $d^{II} = 0$)

$$B_{e^-\gamma} \approx +0.00121E, \tag{24}$$

$$B_{e^+\gamma} \approx -0.00334E. \tag{25}$$

Eq. (23) is based on the approximate form of the correlation parameter given in eq. (21). The complete expression given in ref. [27]) leads to a correlation parameter with modifications to the term linear in energy and an additional quadratic energy dependence. Using the above experimental values and the calculated values of the (CCW) form factors given by table 7 yields (with $d^{II} = 0$)

$$B_{e^-\gamma} = 0.00128E + 0.00014E^2, \tag{26}$$

$$B_{e^+\gamma} = -0.00310E + 0.00015E^2, \tag{27}$$

$$\delta = 0.00438E - 0.00002E^2. \tag{28}$$

Thus we observe that the full calculation of the correlation parameters does not give a drastic change in the linear energy dependence of B. More importantly, the term in δ which is linear in energy is only 2 % smaller for the complete expression [eq. (28)] compared to that for the approximate expression [eq. (23)] and therefore its interpretation vis-à-vis d^{II} is only weakly affected by uncertainties in the calculations of the form factors f, g and j_k.

It should be noted that the quadratic energy dependence of B is a sizeable effect, particularly for the more energetic ^{20}Na decay ($E_0 = 11.75$ MeV). The main cause of the quadratic dependence is the j_3 form factor and since this is an axial-vector term it would have, in addition to the calculated first-class part, a second-class component, if second-class currents exist. If this were the case one would expect $j_3 = j_3^{\mathrm{I}} \pm j_3^{\mathrm{II}}$ for mirror $e^{\mp}$ decays which implies that the quadratic term would be different for the two decays. Thus it is important to separate the linear and quadratic terms for each decay if a reliable limit for d^{II} is to be obtained. If this is not done there could be an accidental cancellation between d^{II} and j_3^{II} for *both* decays.

Beta-alpha correlation for ^{20}Na decay to the 7.42 MeV level. Oakey and Macfarlane [38]) have measured the β-α angular correlation for the e^+ decay of ^{20}Na to the ^{20}Ne level at 7.42 MeV. If we express the correlation in the form

$$d\lambda = 1 + A_{e^+\alpha}\frac{p}{E}\cos\theta + B_{e^+\alpha}\left(\frac{p}{E}\right)^2\cos^2\theta, \tag{29}$$

their results can be stated as follows:

$$\langle A_{e^+\alpha} p/E\rangle_{\mathrm{exp}} = -0.026 \pm 0.001, \tag{30}$$

$$\langle B_{e^+\alpha} p^2/E^2\rangle_{\mathrm{exp}} = -0.083 \pm 0.013. \tag{31}$$

The averages are over the complete β-spectrum ($E_0 = 5.96$ MeV). This correlation [27]) has a dependence on the form factors which is quite similar to the β-γ correlation discussed above, the main difference being a factor of 2 in the $\cos^2\theta$ term.

To calculate the parameter $B_{e^+\alpha}$ we use our measurement of Γ_γ for the analog γ-decay to determine b, assuming that the transition is a pure M1 decay. This yields the value given in table 6, $b = 61.9 \pm 4.1$. We also use the experimental value for the Gamow-Teller form factor, $c = 0.632 \pm 0.077$, which gives $(b/c)_{\mathrm{exp}} = 96.4 \pm 13.4$. Then with the remaining form factors determined from the CCW theoretical matrix elements of table 7 we calculate

$$B_{e^+\alpha} = -(0.00302 \pm 0.00036)E + 0.00006E^2, \tag{32}$$

where the error is due to the uncertainty in $(b/c)_{\mathrm{exp}}$. For comparison with the experimental results we average $B_{e^+\alpha} p^2/E^2$ over the full-energy spectrum to obtain

$$\langle B_{e^+\alpha} p^2/E^2\rangle = -0.0094 \pm 0.0010. \tag{33}$$

The CVC prediction is clearly inconsistent with the experiment and the cause of the discrepancy does not appear to be explained by the higher-order matrix elements, contrary to the speculation of Oakey and Macfarlane. In addition, the kinematic correlation coefficient which is calculated to be $\langle A_{e^+\alpha} p/E\rangle \approx -0.009$ is also inconsistent with the experiment. In a recent measurement of $B_{e^+\alpha}$, Freedman and Gagliardi [39]) obtain a value which is consistent with the prediction of eq. (32), thus

indicating that the Oakey-Macfarlane anomaly may be associated with experimental difficulties.

We emphasize that the prediction given by eq. (32) is made on the assumption that the γ-decay is a pure M1 transition. The calculated radiative E2 width is only 8×10^{-7} eV and since this is much smaller than the observed width ($\Gamma_\gamma = 0.31 \pm 0.04$ eV), the assumption is probably justified. Careful measurements of the γ-ray angular distributions would confirm this assertion.

3.7. ISOSPIN PURITY OF THE $T = 1$, 2^+ STATE OF ^{20}Ne

We have already commented that the α-decay of the $T = 1$, 2^+ state of ^{20}Ne (10.27 MeV) is isospin forbidden and that from the α-particle decay width ($\Gamma_\alpha = 0.116 \pm 0.020$ keV) Ingalls estimates a 1 % upper limit in intensity (10 % in amplitude) for a $T = 0$ impurity. The isospin purity of the $T = 1$ state bears on the CVC issues discussed above because it is only the isovector M1 radiative width which relates to the weak magnetism form factor. If there is a $T = 0$ impurity in the analog state, its radiative decay width must be taken into account when determining the isovector M1 decay width from Γ_{M1}.

In the following, we comment on another approach to the question of the purity of the analog state. This method utilizes the superallowed β-decay of ^{20}Na to the analog state of ^{20}Ne and, in principle, it is capable of a more direct and more general test of the quality of the analog state, both with regard to isospin impurities as well as dynamic distortions, the latter of which could spoil analog symmetry without introducing $T = 0$ impurities.

The shape of the energy spectrum of the delayed α-particles which are emitted after ^{20}Na decays to the analog state depends on the $e^+\alpha$, $\nu\alpha$ and, most importantly, the $e^+\nu$ angular correlations in the β-decay process. These correlations depend on the β-decay form factors and thus the delayed α-spectra can reveal something about the β-decay interaction and/or the states.

There are four form factors which contribute to the ^{20}Na decay to the analog state of ^{20}Ne: a, b, c and d. If the states are perfect analogs, the Fermi form factor should have the value $a = \sqrt{2}$. A measurement of "a" therefore provides a test of the analog state. To see how this is accomplished we observe that the energy average $e^+\nu$ correlation parameter $\langle A \rangle$ and the ft value are specified in terms of the form factors as follows:

$$\langle A \rangle \approx \frac{a^2 - \frac{1}{3}c^2}{a^2 + c^2} - \frac{2}{3}\frac{E_0}{M}\frac{cd^{11}}{a^2 + c^2}, \tag{34}$$

$$(ft)^{-1} \sim a^2 + c^2 - \frac{2}{3}\frac{E_0}{M}cd^{11}. \tag{35}$$

To the extent that we can ignore the d-term (which is necessarily second class for

an analog decay) we note that both a and c are determined from measurements of $\langle A\rangle$ and ft. Let us examine the present measurements. For the $e^+\nu$ correlation, Macfarlane, Oakey and Nickles [40]) measured

$$\langle A\rangle = 0.80\pm0.08, \tag{36}$$

and for the ft value, Torgerson *et al.* [23]) obtain

$$ft = 2992\pm233 \text{ sec}. \tag{37}$$

Ignoring the d-term, we calculate from $\langle A\rangle$ the result $(c/a)^2 = 0.18\pm0.09$ and from ft we get $a^2+c^2 = 2.06\pm0.16$. Combining these yields $a = 1.32\pm0.07$ and $c = 0.56\pm0.14$. Compared to the prediction $a = \sqrt{2}$ we have

$$\frac{\sqrt{2}-a}{\sqrt{2}} = +(6.7\pm4.9)\%. \tag{38}$$

Thus, there is an indication that "a" is lower than expected for a pure $T = 1$ state.

To illustrate the purity of the ^{20}Ne state in a more meaningful way, we calculate the amplitude ε of the $T = 0$ impurity which would give the experimental a. In an obvious notation, describe the states by their isospin quantum numbers $|T, T_3\rangle$ and suppose

$$|^{20}\text{Na}\rangle = |1, 1\rangle, \tag{39}$$

$$|^{20}\text{Ne}\rangle = \sqrt{1-\varepsilon^2}\,|1, 0\rangle+\varepsilon|0, 0\rangle. \tag{40}$$

Then $a = \langle\beta|T_-|\alpha\rangle = \sqrt{1-\varepsilon^2}\sqrt{2}$ and using $a_{\text{exp}} = 1.32\pm0.07$, we obtain $|\varepsilon| = 0.36\pm0.13$, which is a rather large impurity compared to the Ingalls estimate ($|\varepsilon| < 0.1$).

Macfarlane, Oakey and Nickles [40]) have discussed the ^{20}Na $e^+\nu$ correlation along similar lines. In addition to suggesting that the analog state is not very pure, they also indicate that the $T = 0$ states near the analog state show evidence for mixing of the $T = 1$ state into them.

If the isospin impurity is as large as the delayed α-particle spectrum suggests, it will be important to correct the observed magnetic form factor (b_γ^{obs}) for the isoscalar component. With a spin-dominated transition moment, the isoscalar form factor ($b_\gamma^{T=0}$) would be smaller than the isovector form factor by the ratio of the spin g-factors ($g_s^{T=0}/g_s^{T=1} = 1/5.3$). Note that from eqs. (39) and (40) we can write

$$b_\gamma^{\text{obs}} = \varepsilon b_\gamma^{T=0}+\sqrt{1-\varepsilon^2}\,b_\gamma^{T=1}, \tag{41}$$

$$b_\gamma^{T=1} = \frac{b_\gamma^{\text{obs}}}{\sqrt{1-\varepsilon^2}+\varepsilon(b_\gamma^{T=0}/b_\gamma^{T=1})}. \tag{42}$$

Thus, with $b_\gamma^{T=0}/b_\gamma^{T=1} \approx g_s^{T=0}/g_s^{T=1} = 1/5.3$ and $\varepsilon = \pm0.36$ we obtain $b_\gamma^{T=1} = (^{1.00}_{1.16})b_\gamma^{\text{obs}}$ where the upper (lower) value corresponds to the positive (negative) sign

Gas handling proved to be straightforward. Each isotopic gas was kept in its individual storage volume, fitted with its own cryopump, and recovery of the gas from the Leybold cryopump in the beam line to the storage volume could be accomplished in under 30 minutes. A failsafe system incorporating a fast shut-off valve triggered from a Penning gauge was used to prevent loss of gas to the accelerator in the event of cryopump failure.

2.4 Correction Procedure

Although a gas target removes uncertainties about the target composition, this advantage is to some extent offset by the extended nature of the active region of the target. This arises because straggling and beam energy spread, together with the natural width of the resonance, cause resonant reactions throughout most of the target chamber instead of at an ideal point. Since the detectors were at distances comparable to the target length, it is important to correct for the fact that photons entering the detector could come from a range of angles and distances.

The correction procedure has been described by Watt et al. [Wa78] and uses a parameterisation [Sy76] of the results of Monte Carlo energy loss calculations performed by Cobb et al. [Co76]. This gives the beam energy distribution as a function of position in the target and, together with the Breit-Wigner cross-section formula, the relative reaction rate as a function of position in the target chamber can be determined (fig.2.4.1). This is then integrated along the target chamber, weighting the value at each point by the gas density profile, the angular distribution factor and the inverse square distance of the

of ε. However, as discussed in subsect. 3.4 the M1 decay of the analog state is not a spin-dominated transition, being roughly an equal mixture of spin and orbital components. A more realistic estimate of $b_\gamma^{T=0}/b_\gamma^{T=1}$ can be obtained from the measured radiative width of the $2^+ T = 0$ level at 9.49 MeV in ^{20}Ne which is a likely candidate for an isospin impurity in the analog state. Using the values $\Gamma_{M1}(2^+ T = 0) = 0.21$ eV from ref. [9]) (corrected to the c.m. system) and $\Gamma_{M1}(2^+ T = 1) = 4.08$ eV from the present work, we obtain $b_\gamma^{T=0}/b_\gamma^{T=1} = 1/3.8$. By eq. (50) this gives $b_\gamma^{T=1} = (^{0.97}_{1.19})b_\gamma^{obs}$.

We conclude by observing that the breakdown of analog symmetry which is suggested by the delayed α-spectrum leads to a 3–20 % uncertainty in the determination of the isovector magnetic form factor. The estimate of 1 % for the intensity of isospin impurities made by Ingalls implies an amplitude of 10 %, and while this is smaller than implied by the α-spectrum, it is not necessarily inconsistent because there could be interference effects which cancel in the α-decay but not in the β-decay.

To further our understanding of isospin mixing in the ^{20}Ne analog state and particularly how it relates to the test of CVC vis-à-vis the M1 decay, it is important to improve the experimental value of a. The uncertainties in $\langle A \rangle$ and ft contribute comparable errors to a so both measurements must be improved for a significant gain. In addition, the effects of higher-order matrix elements on the shape of the delayed α-spectrum should be investigated.

References

1) R. P. Feynman and M. Gell-Mann, Phys. Rev. **109** (1958) 193;
S. S. Gerschtein and J. G. Zeldovich, ZhETF (USSR) **29** (1955) 698 [JETP (Sov. Phys.) **2** (1957) 76];
M. Gell-Mann, Phys. Rev. **111** (1958) 362
2) T. Mayer-Kukuk and F. C. Michel, Phys. Rev. **127** (1962) 545;
N. W. Glass and R. W. Peterson, Phys. Rev. **130** (1963) 299;
Y. K. Lee, L. W. Mo and C. S. Wu, Phys. Rev. Lett. **10** (1963) 253;
C. S. Wu, Rev. Mod. Phys. **36** (1964) 618
3) F. P. Calaprice and B. R. Holstein, Nucl. Phys. **A273** (1977) 301
4) K. Sugimoto, I. Tanihata and J. Göring, Phys. Rev. Lett. **34** (1975) 1533
5) F. P. Calaprice, S. J. Freedman, W. C. Mead and H. C. Vantine, Phys. Rev. Lett. **35** (1975) 1566
6) A. M. Nathan, G. T. Garvey, P. Paul and E. K. Warburton, Phys. Rev. Lett. **35** (1975) 1137
7) D. H. Wilkinson, Phys. Lett. **48B** (1974) 169
8) P. Ingalls, Nucl. Phys. **A265** (1976) 93
9) J. D. Pearson and R. H. Spear, Nucl. Phys. **54** (1964) 434
10) K. W. Allen, S. P. Dolan, A. R. Holmes, T. J. M. Symons, F. Watt, C. H. Zimmerman, A. E. Litherland and A. M. J. Sandorfi, Nucl. Instr. **134** (1976) 1
11) M. R. Wormald and J. Takacs, Nucl. Instr. **113** (1974) 263
12) J. H. Cobb, W. W. M. Allison and J. N. Bunch, Nucl. Inst. **133** (1976) 315;
T. J. M. Symons, D. Phil. thesis, Oxford University, unpublished;
T. J. M. Symons *et al.*, to be published
13) P. M. Endt and C. van der Leun, Nucl. Data **13A** (1974) 67
14) B. P. Singh and H. C. Evans, Nucl. Instr. **97** (1971) 475
15) M. A. Meyer, J. P. L. Reinecke and D. Reitmann, Nucl. Phys. **A185** (1972) 625
16) B. Y. Underwood, M. R. Wormald, N. Anyas-Weiss, N. A. Jelley and K. W. Allen, Nucl. Phys. **A225** (1974) 253;
T. J. M. Symons *et al.*, to be published

17) A. E. Litherland, T. K. Alexander and A. T. Jeffs, Can. J. Phys. **47** (1969) 1961
18) E. B. Shera, Phys. Rev. **C12** (1975) 1003
19) J. Rapaport, Nucl. Data Sheets **B3-3** (1970) 4-103
20) L. C. Northcliffe and R. F Schilling, Nucl. Data **A7** (1970) 233
21) D. W. O. Rogers, J. K. Aitken, A. E. Litherland, W. R. Dixon and R. S. Storey, Can. J. Phys. **49** (1971) 1397
22) D. F. Torgerson, K. Wien, Y. Fares, N. S. Oakey, R. D. Macfarlane and W. A. Lanford, Phys. Rev. **C8** (1973) 161
23) A. Gallmann, F. Jundt, E. Aslanides and D. E. Alburger, Phys. Rev. **179** (1969) 921
24) S. Mitsunobu and Y. Torizuka, Phys. Rev. Lett. **28** (1972) 920
25) T. K. Alexander, B. Y. Underwood, N. Anyas-Weiss, N. A. Jelley, J. Szücs, S. P. Dolan, M. R. Wormald and K. W. Allen, Nucl. Phys. **A197** (1972) 1
26) B. R. Holstein and S. B. Treiman, Phys. Rev. **C3** (1971) 1921
27) B. R. Holstein, Rev. Mod. Phys. **46** (1974) 789
28) S. Weinberg, Phys. Rev. **112** (1958) 1375
29) D. H. Wilkinson and D. E. Alburger, Phys. Rev. **C13** (1976) 2517
30) S. S. Hanna, Electromagnetic decay of isobaric analogue states, in Isospin in nuclear physics, ed. D. H. Wilkinson (North-Holland, Amsterdam, 1969)
31) D. J. Millener (Oxford University), personal communication (1975)
32) B. M. Preedom and B. H. Wildenthal, Phys. Rev. **C6** (1972) 1633
33) T. T. S. Kuo, Nucl. Phys. **A103** (1967) 71
34) F. P. Calaprice, W. Chung and B. H. Wildenthal, to be published
35) W. Chung and B. H. Wildenthal, to be published
36) A. Genz, A. Richter and B. M. Schmitz, Nucl. Phys. **A267** (1976) 13
37) F. P. Calaprice and D. E. Alburger, to be published
38) N. S. Oakey and R. D. Macfarlane, Phys. Rev. Lett. **25** (1970) 170
39) S. J. Freedman, R. D. Cousins, C. A. Gagliardi, G. T. Garvey and J. F. Greenhalgh, Phys. Lett. **67B** (1977) 165
40) R. D. Macfarlane, N. S. Oakey and R. J. Nickles, Phys. Lett. **34B** (1971) 133

1.E.1:
3.A

Nuclear Physics **A322** (1979) 1–12; © *North-Holland Publishing Co., Amsterdam*

RADIATIVE DECAYS OF UNBOUND HIGH-SPIN STATES IN ^{24}Mg (II)

L. K. FIFIELD, E. F GARMAN, M. J. HURST, T. J. M. SYMONS †, F WATT, C. H. ZIMMERMAN †† and K. W. ALLEN

Nuclear Physics Laboratory, University of Oxford, England

Received 7 February 1979

Abstract: Known negative-parity levels at 11.59 (5^-), 12.44 (7^-), 13.06 (5^-), and 13.76 (5^-) MeV in ^{24}Mg have been studied as resonances in the ^{20}Ne(α, γ)^{24}Mg reaction, and their radiative and α-particle decay widths deduced. The 12.44 MeV level is identified as the 7^- member of a $K^\pi = 0^-$ band by virtue of a strongly enhanced E2 γ-ray transition to the 10.03 MeV 5^- level. The 13.06 MeV level exhibits a strongly enhanced γ-ray transition to a probable 3^- level at 10.33 MeV, indicating the existence of a new negative-parity rotational band in ^{24}Mg. Known 4^+ levels at 12.05, 12.12, 12.16, 12.51 and 13.05 MeV have also been studied as ^{20}Ne(α, γ)^{24}Mg resonances in a search for the 4^+ member of a proposed excited $K^\pi = 0^+$ band via an enhanced E2 transition to the 8.65 MeV 2^+ level. No such transition was observed, but the 12.05 MeV level was identified as the second 4^+ $T = 1$ level in ^{24}Mg. In addition, γ-ray decay schemes and angular distributions provided the following information on the spins and parities of three sharp resonances near 14 MeV in ^{24}Mg: 14.10, $(2, 4)^+$; 14.146, 4^+ (3^-, 5^-) and 14.32, 4^+.

E | NUCLEAR REACTIONS ^{20}Ne(α, γ), E = 2.7–6.0 MeV; measured $\sigma(E_\gamma, E_i, \theta_\gamma)$. ^{24}Mg deduced levels, J, π, T, γ-ray branching ratios, radiative widths, α-particle widths. Enriched gas target.

1. Introduction

In a previous paper [1]) we have discussed the particle and radiative decays of a number of positive-parity states between 11.8 and 14.5 MeV in ^{24}Mg in the light of information obtained from the ^{20}Ne(α, γ)^{24}Mg reaction. These states could, by virtue of their having either high spin or non-zero isospin, be associated unambiguously with theoretical counterparts in a recent large-basis shell-model calculation [2]) despite their high excitation energies. Such an association is not at present possible for high-spin negative-parity states in the same region of excitation energy, owing to the formidably large shell-model bases involved when configurations involving a hole in the 1p shell or a particle in the 1f-2p shell are included. There is, however, some evidence [3]) for the existence of two negative-parity rotational bands in ^{24}Mg, and in this paper we present information obtained from the ^{20}Ne(α, γ)^{24}Mg reaction which provides convincing evidence for the reality of these bands. In addition, since the known 5^- levels at 13.06 [ref. [4])] and 13.76 [ref. [5])] MeV belong to neither of

† Present address: Lawrence Berkeley Laboratory, Berkeley, California 94720, USA.
†† Present address: Department of Physics, University of Edinburgh, Edinburgh, Scotland.

the proposed negative parity bands, we have studied their radiative decay properties in a search for additional band structure in ^{24}Mg.

We have also studied the radiative decay properties of five 4^+ levels between 12.05 and 13.05 MeV, and of levels at 14.10, 14.146 and 14.32 MeV. The motivation for studying the 4^+ levels was the proposal [6]) that there may be an excited $K^\pi = 0^+$ band in ^{24}Mg built on the 6.44 MeV 0^+ level. This was founded on the observation [6]) of an enhanced E2 transition between the 8.65 (2^+) and 6.44 MeV levels. In the present work we have used the ^{20}Ne(α, γ)^{24}Mg reaction to search for a similarly enhanced transition to the 8.65 MeV level from one of the known [7]) 4^+ levels between 12 and 13 MeV level.

Finally, levels near 14 MeV were investigated because an earlier angular correlation study [5]) employing the ^{16}O(^{12}C, $\alpha\alpha$)^{20}Ne reaction had indicated the existence of at least three unresolved levels in the vicinity of the 14.15 MeV (8^+, $K^\pi = 2^+$) level. Four narrow levels between 14.08 and 14.16 MeV were clearly resolved in the present work, and all four have been studied in detail. Results for the 14.08 (6^+) and 14.153 (8^+) MeV levels were presented in the previous paper [1]); here we discuss the 14.10 and 14.146 MeV levels, together with another new level at 14.32 MeV.

2. Experimental procedure

A differentially pumped gas target was employed in all the measurements reported here. A description of the target may be found in ref. [8]), and details of the experi-

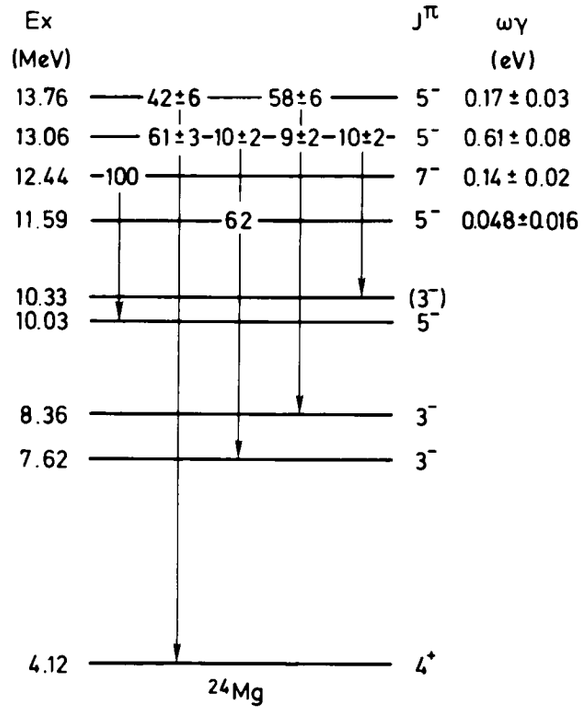

Fig. 1. Gamma-ray decay schemes for negative-parity levels in ^{24}Mg which have been studied in the present work as resonances in the ^{20}Ne(α, γ)^{24}Mg reaction. Only the dominant γ-ray branch of the 11.59 MeV level was observed, and the branching ratio has been taken from ref. [3]). Values of $\omega\gamma = (2J+1)\Gamma_\gamma\Gamma_{\alpha_0}/\Gamma$ are listed for each level, where Γ_γ is the total γ-ray width of the level concerned.

mental procedure relevant to the measurement of resonance strengths, γ-ray angular distributions and decay schemes of resonances in the ^{20}Ne(α, γ)^{24}Mg reaction are given in the previous paper [1]). Complete γ-ray yield curves for the ^{20}Ne(α, γ)^{24}Mg and ^{20}Ne(α, $\alpha'\gamma$)^{20}Ne reactions spanning the region of excitation from 11.8 to 14.4 MeV in ^{24}Mg may also be found in ref. [1]), together with a table of all the resonances observed.

3. Negative-parity levels: results and discussion

Gamma-ray decay schemes and values of $\omega\gamma$ ($= (2J+1)\,\Gamma_\gamma\Gamma_{\alpha\,0}/\Gamma$) are shown in fig. 1 for the four negative-parity levels which were investigated in the present work. As an indication of the quality of the data from which these decay schemes were derived, on-resonance and off-resonance γ-ray spectra for the 12.44 MeV (7^-) level are shown in fig. 2. Table 1 summarises the information on the electromagnetic decay properties of the four levels derived from these data. Previous information on the

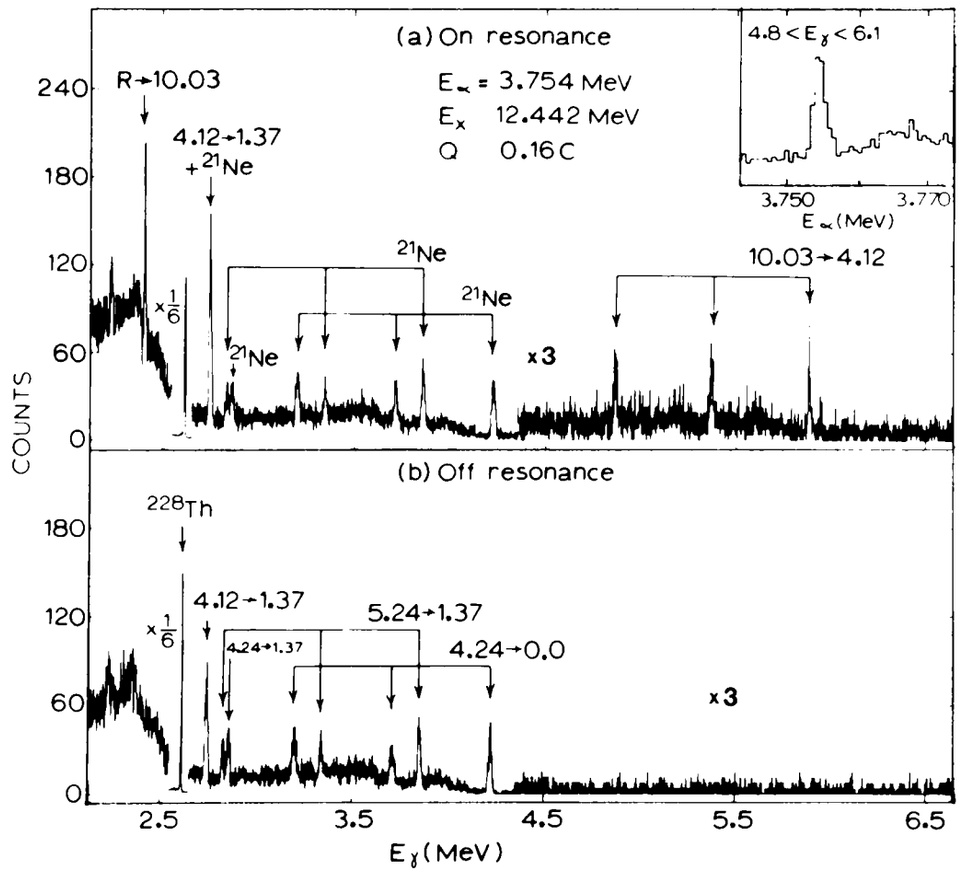

Fig. 2. Spectra of γ-rays at the 3.754 MeV resonance, and 15 keV below resonance. The 85 cm^3 Ge(Li) detector was positioned 9 cm from the target at 125° to the incident beam. Q is the accumulated charge of ^{4}He^{++} for the on-resonance spectrum, and the off-resonance spectrum has been normalised to the same total charge. Peaks are labelled with the transition in ^{24}Mg, and peaks labelled ^{21}Ne arise from the ^{21}Ne(α, nγ)^{24}Mg reaction and are identified in (b). The inset shows the relevant portion of the γ-ray yield curve taken at a target pressure of 200 μm. All energies are in MeV.

TABLE 1

Electromagnetic transition rates for negative-parity levels in ^{24}Mg

K_i^π	K_f^π	E_i (MeV)	E_f (MeV)	J_i^π	J_f^π	$M\lambda$ [a]	$B(M\lambda)_{exp}$ (W.u.)	$B(M\lambda)_{rot}$ [d] (W.u.)
0^-	0^-	8.36	7.55	3^-	1^-	E2	< 200 [b]	
		10.03	8.36	5^-	3^-	E2	20^{+8}_{-5} [b]	(20)
		12.44	10.03	7^-	5^-	E2	51 ± 10 [c]	21
0^-	0^+	8.36	0.0	3^-	0^+	E3	10.5	(10.5)
		10.03	1.37	5^-	2^+	E3	11.0	15.9
		12.44	4.12	7^-	4^+	E3	< 38	18.0
3^-	3^-	9.30	7.62	(4^-)	3^-	E2	29 ± 6 [b]	(29)
		11.59	7.62	(5^-)	3^-	E2	4.6 ± 1.4 [c]	7.0
		11.59	9.30	(5^-)	(4^-)	E2	37 ± 11 [c]	27
		13.06	4.12	5^-	4^+	E1	$(8.4 \pm 1.1) \times 10^{-5}$	
(1^-)	3^-	13.06	7.62	5^-	3^-	E2	0.35 ± 0.08	
(1^-)	0^-	13.06	8.36	5^-	3^-	E2	0.66 ± 0.16	
(1^-)	(1^-)	13.06	10.33	5^-	(3^-)	E2	22 ± 4	
		13.76	4.12	5	4^+	E1	$5 \times 10^{-5} > B(E_1) \geqq 10^{-5}$ [c]	
		13.76	8.36	5^-	3^-	E2	$2.3 > B(E_2) \geqq 0.5$ [c]	

[a]) E1 transitions not shown for members of the $K^\pi = 0^-$ and 3^- bands.

[b]) Ref. [3]).

[c]) Present work, using lifetimes of 22 ± 6 fs [ref. [3])] and 16 ± 4 fs [ref. [9])] for the 11.59 and 12.44 MeV levels respectively.

[d]) The rotational-model predictions are proportional to $(J_i \lambda K_i K_f - K_i | J_f K_f)^2$, and are normalized to the transition rates in parentheses.

[e]) Assuming $\Gamma_{\alpha_0}/\Gamma > 0.3$. See text.

TABLE 2

Alpha-particle widths of negative-parity levels in ^{24}Mg

E_i (MeV)	J_i^π	K_i^π	Channel	Γ_α (eV)	θ_α^2 [a]
11.59	(5^-)	(3^-)	α_0	0.005 ± 0.002	0.001 ± 0.0004
12.44	7^-	0^-	α_0	0.027 ± 0.008	0.020 ± 0.006
13.06	5^-	(1^-)	α_0	< 1000	< 0.7
			α_1	7 ± 1	0.05 ± 0.01
13.76	5^-		α_0	$960 < \Gamma\alpha_0 < 3200$ [b]	$0.13 < \theta_\alpha^2 < 0.44$
			α_1	$0.4 < \Gamma\alpha_1 < 2.4$ [b]	$1.1 \times 10^{-4} < \theta_\alpha^2 < 6.4 \times 10^{-4}$

[a]) $\theta_\alpha^2 = \Gamma_\alpha / \Gamma_\alpha^{s.p.}$, where the single particle width, $\Gamma_\alpha^{s.p.} = 2\hbar^2 P_L / \mu R^2$ where μ is the reduced mass, $R = 1.2(20^{1/3} + 4^{1/3})$ fm, $P_L(kR)$ is the penetrability factor for α-particles of wave number k and angular momentum L.

[b]) Assuming $\Gamma_{\alpha_0}/\Gamma > 0.3$. See text.

lower-lying members of the proposed [3]) $K^\pi = 0^-$ and 3^- bands is also included, and the predictions of the simple rotational model are presented for comparison. Alpha-particle widths for the same set of levels are presented in table 2, together with spectroscopic factors derived from the observed widths using simple Coulomb

penetrabilities. Below, we discuss individually the four levels and their relevance to rotational band structure in ^{24}Mg.

3.1. THE 12.44 MeV LEVEL AND THE $K^\pi = 0^-$ BAND

The 12.44 MeV level has been tentatively proposed [3]) as the 7^- member of a $K^\pi = 0^-$ band built on the 7.55 MeV 1^- level. This suggestion was founded upon the observation in the ^{12}C(^{16}O, $\alpha\gamma$)^{24}Mg reaction [3]) of a weak γ-ray decay from a level near 12.4 MeV through the suggested 5^- member of the $K^\pi = 0^-$ band. Recently, this weak γ-ray decay mode has been confirmed, and employed in a measurement [9]) of the lifetime of the 12.44 MeV level by the Doppler shift attentuation method (DSAM). It is now possible, therefore, to deduce values for both the radiative width Γ_γ and the α-particle width Γ_α of the 12.44 MeV level by combining the value of $\omega\gamma$ measured in the present work with this recently measured lifetime.

Prior to the present work, the existence of a $K^\pi = 0^-$ band in ^{24}Mg rested upon a preferred but not unambiguous 5^- assignment [3]) to the 10.03 MeV level. With the measurement here of the radiative width of the 12.44 → 10.03 MeV transition, the tentative nature of this assignment is removed, since any other spin-parity combination would imply an abnormally large reduced transition probability for either the 12.44(7^-) → 10.03 or the 10.03 → 8.36(3^-) MeV transition. It then follows that both these transitions are strongly enhanced, which in turn firmly established the 8.36 (3^-), 10.03 (5^-) and 12.44 (7^-) MeV levels as members of a $K^\pi = 0^-$ band. The relative in-band transition probabilities are not, however, well reproduced by the simple rotational model prescription.

From table 1, it can be seen that the 3^- and 5^- members of the $K^\pi = 0^-$ band exhibit strongly enhanced E3 γ-ray transitions [3,10]) to members of the ground state rotational band, indicating that the intrinsic structure of the 0^- band probably arises from a collective deformation of the ^{24}Mg ground state. A similarly enhanced transition from the 7^- level to the 4.12 MeV 4^+ level would correspond to only 5 % of the total γ-ray width of the 7^- level. Unfortunately, the statistics of the present measurement are not sufficient to demonstrate the existence or absence of such a weak branch.

Turning to table 2, we note that Tribble, Garvey and Comfort [11]) have shown that the 3^- member of the band at 8.36 MeV has a predominantly sd^7-pf "particle" structure. If the band picture is a valid one, then this intrinsic structure should be common within the band. As a consequence, members of the $K^\pi = 0^-$ band are expected to have appreciable reduced widths for decay into the ^{20}Ne ground state plus an α-particle. A similar situation exists in ^{20}Ne, where a $K^\pi = 0^-$ "particle" band occurs at rather low excitation. The measured α-particle spectroscopic factors [12]) for the members of this band in ^{20}Ne are very large ($\sim$ 0.5).

In the present work we have measured the α-particle width of the 12.44 MeV (7^-, $K^\pi = 0^-$) level in ^{24}Mg, and have derived the α-particle spectroscopic factor

shown in table 2. In principle, similar information may be obtained from the study of reactions which transfer an α-particle to the ^{20}Ne ground state, such as the ^{20}Ne(^{7}Li, t)^{24}Mg reaction. This reaction is found [13-15]) to selectively populate the states in the $K^{\pi} = 0^{-}$ band, and it would be of interest to compare the spectroscopic factor deduced from the measured width of the 12.44 MeV 7^{-} level with the spectroscopic factor derived from a DWBA analysis of the ^{20}Ne(^{7}Li, t)^{24}Mg data. Unfortunately no such analysis has been published. We note, however, that the absolute value of θ_{γ}^{2} for the 12.44 MeV level in ^{24}Mg, 0.02, is considerably smaller than the equivalent quantities for members of the $K^{\pi} = 0^{-}$ band in ^{20}Ne. Qualitatively at least, a similar difference is observed between the cross sections measured in the α-particle transfer reactions, with the cross sections to levels strongly excited by the ^{16}O(^{7}Li, t)^{20}Ne reaction being an order of magnitude greater than those to levels selectively populated by the ^{20}Ne(^{7}Li, t)^{24}Mg reaction [13]).

Having established the existence of a $K^{\pi} = 0^{-}$ "particle" band in ^{24}Mg, and identified it as far as its 7^{-} member at 12.44 MeV, the question then arises as to the location and properties of the higher-lying members of this band, since spins up to 15^{-} are possible within an sd^{7}-pf basis. It has been suggested [5]), although solely on energy considerations, that the 9^{-} level at 16.55 MeV may be the next member of the band. If so, it would be expected to be preferentially excited by the ^{20}Ne(^{7}Li, t)^{24}Mg reaction. In fact, the most prominent peak in the spectra of both Lepareux *et al.* [14]) and Cobern *et al.* [15]) corresponds to a level at just this excitation energy, which provides more compelling evidence that the 16.55 MeV 9^{-} level belongs to the $K^{\pi} = 0^{-}$ band.

3.2. THE 11.59 MeV LEVEL AND A $K^{\pi} = 3^{-}$ BAND IN ^{24}Mg

The 11.59 MeV level in ^{24}Mg, studied here as a resonance in the ^{20}Ne(α, γ)^{24}Mg reaction, is believed to be the 5^{-} member of a $K^{\pi} = 3^{-}$ band built upon the 3^{-} level at 7.62 MeV. Although the 5^{-} assignment is not unambiguous, the reduced transition probabilities in tables 1 and 2 were derived by assuming it to be correct. The predominant decay mode of the 11.59 MeV level is by γ-ray emission, and its lifetime has been measured [3]) using the ^{12}C(^{16}O, $\alpha\gamma$)^{24}Mg reaction. Combining this lifetime with the value of $\omega\gamma$ for the strongest γ-ray branch measured in the present work, values for both the α-particle width and the partial γ-ray widths may be deduced. The results imply a 16 % α-particle branch which reduces the γ-ray transition rates quoted in ref. [3]) by 16 %. The arguments for the existence of a $K^{\pi} = 3^{-}$ band are unaffected however. In contrast to the $K^{\pi} = 0^{-}$ band, the relative transition rates within the tentative $K^{\pi} = 3^{-}$ band are reproduced rather well by the simple rotational model prescription (see table 1).

The band head of the proposed 3^{-} band is the 7.62 MeV level, which was also investigated by Tribble *et al.* [11]) and found to have a predominantly p^{-1}-sd^{9} "hole" structure. Consequently, members of the band built upon this level are not expected

to have large α-particle reduced widths, and it can be seen from table 2 that this is indeed the case. Again, there is an analogous "hole" band in ^{20}Ne, a $K^\pi = 2^-$ band built upon the 4.97 MeV level. The members of this band in ^{20}Ne have very small reduced α-particle widths [12]). However, the demonstration of a weak α-particle branch from the 11.59 MeV level does raise the possibility of an unambiguous determination of its spin via a particle-particle angular correlation measurement employing the ^{12}C(^{16}O, α)^{24}Mg reaction [4, 5]).

3.3. THE 13.06 MeV LEVEL AND A POSSIBLE NEW BAND IN ^{24}Mg

The 5^- level at 13.06 MeV has been observed previously in the ^{12}C(^{16}O, α)^{24}Mg reaction [4]) and decays predominantly by α-particle emission. Its γ-ray decay properties (see fig. 1) were investigated here in order to explore the possibility of further negative-parity band structure in ^{24}Mg.

The most notable feature of the decay of the 13.06 MeV 5^- level is the transition to a level at 10334 ± 4 keV. This latter level is listed in the most recent compilation of Endt and Van der Leun [7]), and has been observed in both inelastic electron scattering [16]) and inelastic proton scattering [17, 18]), although there appears to be some confusion concerning its spin. In the inelastic electron scattering work [16]) it was not resolved from the nearby 2^+ level at 10355 keV, but the dependence of the form factor on momentum transfer limited the spin and parity of the second member of the doublet to 3^- or 4^+, with 4^+ preferred. However, the angular distribution of inelastically scattered protons [18]) populating a level at 10328 ± 7 keV, although consistent with a 3^- assignment, was inconsistent with 4^+. There is also rather strong evidence for an $l_p = 1$ component in the angular distribution of neutrons populating a state at $\sim$ 10.35 MeV via the ^{23}Na(d, n)^{24}Mg reaction [19]), which would again favour the 3^- assignment. We note that the present results also argue weakly against a 4^+ assignment, since the E1 strength of the 13.06 $\rightarrow$ 10.33 MeV transition would then be 10^{-3} W.u., which is stronger than any known isospin forbidden E1 transition in this mass region, although it does not exceed the recommended upper limit [20]) for such transitions. Hence, the weight of the evidence is strongly in favour of a 3^- assignment to the 10.33 MeV level. If this assignment is correct, then the 13.06 $\rightarrow$ 10.33 MeV γ-ray transition is an E2 transition with a strength of 22 W.u., which would clearly identify the 13.06 and 10.33 MeV levels as members of a new rotational band in ^{24}Mg. The moment of inertia of this band is reasonable and lies midway between the moments of inertia of the $K^\pi = 0^+$ and the $K^\pi = 0^-$ bands. The position of the band head has not been established, but the 8.44 MeV 1^- level would be an excellent candidate. Independent evidence that this level, together with the 8.86 MeV 2^- level, may be the start of a $K^\pi = 1^-$ band comes from a recent ^{23}Na(^{3}He, d)^{24}Mg study by Garrett *et al.* [22]). Unfortunately, no information was obtained from the present work on a possible 10.33 $\rightarrow$ 8.44 MeV transition since the region of the spectrum where the corresponding γ-ray would

be found was obscured by Compton events from a ^{228}Th source placed close to the germanium detectors for energy calibration purposes. It would be of some interest to study the decay of the 10.334 MeV level in more detail, either using the ^{23}Na(^{3}He, dγ)^{24}Mg reaction which appears to populate it [22]), or by more extensive work on the γ-ray spectrum of the 13.06 MeV level using the ^{20}Ne(α, γ)^{24}Mg reaction.

3.4. THE 13.76 MeV LEVEL

The 13.76 MeV 5^- level has been previously observed in the ^{16}O(^{12}C, α)^{24}Mg reaction. It was observed in the present work as a weak resonance in both the ^{20}Ne(α, γ)^{24}Mg and ^{20}Ne(α, α')^{20}Ne reactions. Although an accurate value for $\Gamma_{\alpha 0}/\Gamma$ is not available for this level, we estimate from the data presented in ref. [5]) that $\Gamma_{\alpha 0}/\Gamma > 0.3$. This then leads to the limits on the electromagnetic and α-particle transition rates given in tables 1 and 2. In principle, a more accurate value of $\Gamma_{\alpha 0}/\Gamma$ could be obtained by studying the proton decay channels via proton induced reactions on ^{23}Na at $E_p = 2163$ keV.

From table 1, it can be seen that there is no evidence for any strongly enhanced transition in the γ-ray decay scheme of the 13.76 MeV level. On the other hand, the level does have a large reduced width for the decay into the ^{20}Ne ground state plus an α-particle. This large reduced width appears to be manifested in the ^{20}Ne(^{7}Li, t)^{24}Mg reaction also, since there is a prominent peak at approximately the correct energy in the spectra of both Lepareux *et al.* [14]) and Cobern *et al.* [15]).

4. The 4^+ states between 12 and 13 MeV

Decay schemes and $\omega\gamma$ values for five known 4^+ levels between 12.05 and 13.05 MeV in ^{24}Mg are shown in fig. 3. None of these levels exhibited an enhanced E2 transition to the 2^+ level at 8.65 MeV which would indicate the continuation of the proposed [6]) excited $K^\pi = 0^+$ band built on the 6.44 MeV level. Limits on the strength of such a transition from the levels studied are given in table 3. The 4^+ member of this band, if it exists, must lie below 12 MeV; possible candidates are the 4^+ levels at 11.22 and 11.69 MeV which were not studied in the present work.

However, from the information in fig. 3 we may identify the 12.05 MeV 4^+ level as the second 4^+ $T = 1$ level in ^{24}Mg, since the M1 transition between it and the 4.12 MeV level has a strength of 0.20 W.u. and its α-particle width is extremely small (6.5 eV). It is almost certainly the analogue of the 2.563 MeV level in ^{24}Na, although the spin of the ^{24}Na level has not been definitely established [23]). Similarly, the 12.64 MeV 4^+ level, which has been studied in detail with the ^{23}Na(p, γ)^{24}Mg reaction [7]), is probably the analogue of the 3.126 MeV level in ^{24}Na. In the shell-model calculations of Kelvin, Watt and Whitehead [2]) employing the Chung-Wildenthal interaction [24]) with Coulomb corrections, the second and

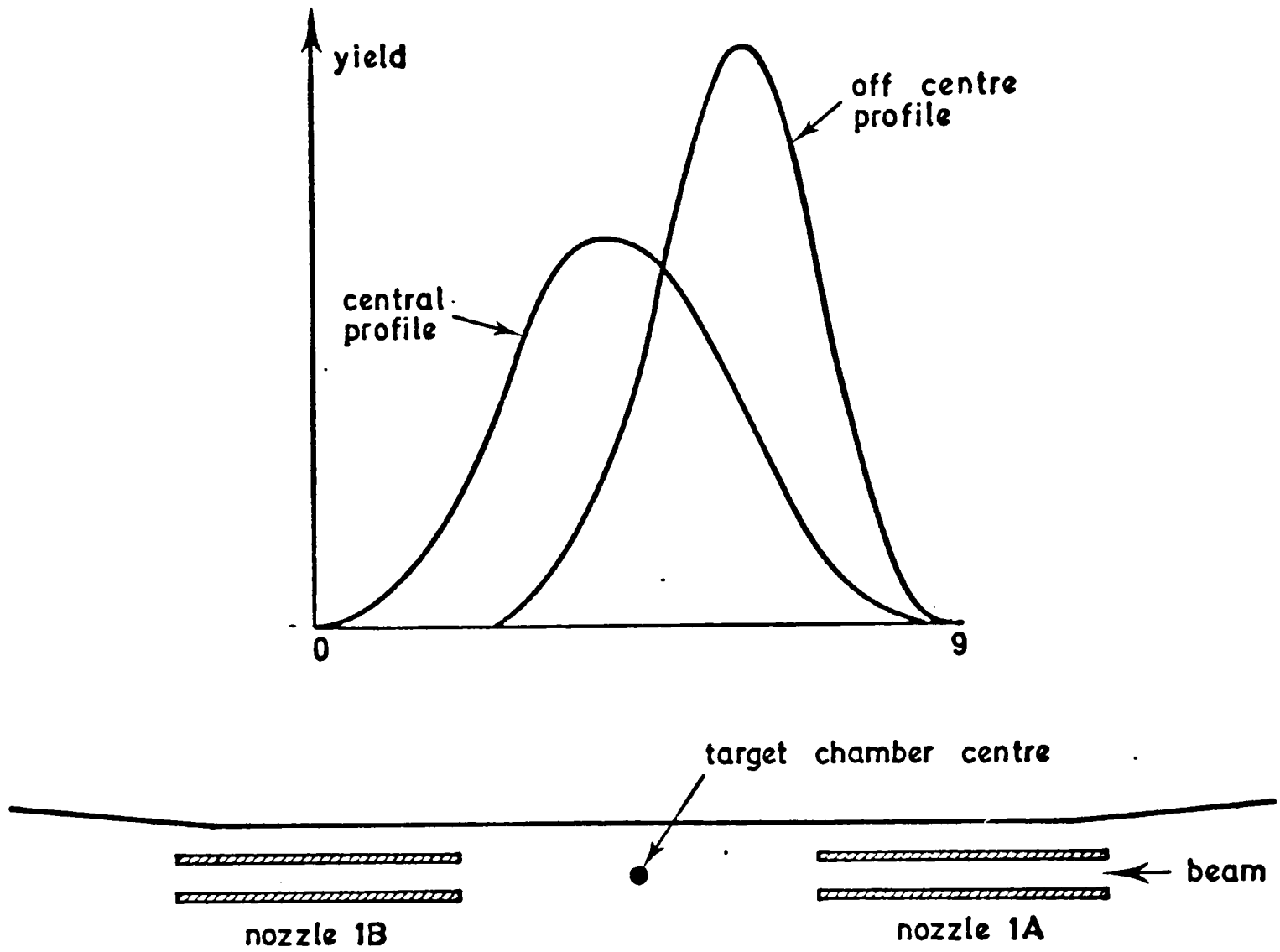

Fig.2.4.1 Gamma-ray yield profile as a function of position in the target chamber for a centrally positioned resonance and an off-centre case. The nominal beam energies are 6923.4 and 6922.05 keV for a nominal resonance energy of 6920 keV. The gas pressure is 760μ.

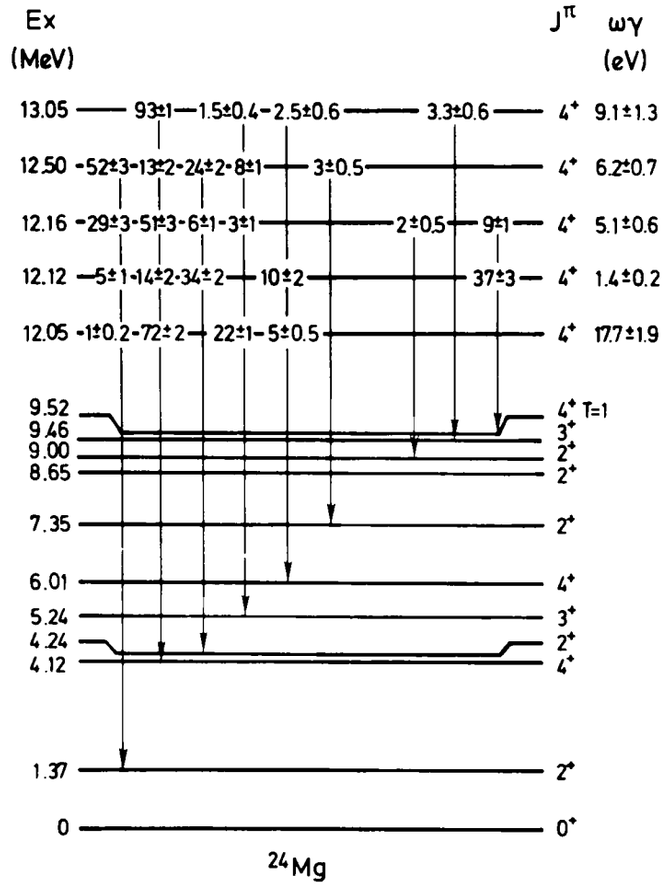

Fig. 3. Gamma-ray decay schemes for known 4^+ levels between 12.05 and 13.05 MeV in ^{24}Mg. These levels were excited as resonances in the ^{20}Ne(α, γ)^{24}Mg reaction, and the resonance strengths $\omega\gamma$ and decay schemes were deduced from on-resonance γ-ray spectra taken with an 85 cm^3 Ge(Li) detector.

TABLE 3

Limits on E2 transition strengths from 4^+ states in ^{24}Mg to the 8.65 MeV 2^+ level

Transtion $E_i(J_i^\pi) \rightarrow E_f(J_f^\pi)$	Branching ratio [a] (%)	Transition strength [b] (W.u.)
$12.05(4^+) \rightarrow 8.65(2^+)$	< 0.4	< 7.4
$12.12(4^+) \rightarrow 8.65(2^+)$	< 3.2	< 3.0
$12.16(4^+) \rightarrow 8.65(2^+)$	< 1.1	< 3.4
$12.51(4^+) \rightarrow 8.65(2^+)$	< 1.8	< 4.4
$12.63(4^+) \rightarrow 8.65(2^+)$	< 1.0 [c]	< 3.1
$13.05(4^+) \rightarrow 8.65(2^+)$	< 0.2 [c,d]	< 2.1

[a]) All limits are derived from 3 standard deviations of the number of counts within the region of the γ-ray spectrum at which the $R \rightarrow 8.65$ peak would be expected.

[b]) Using values of $(2J+1)\,\Gamma_{\gamma_0}\Gamma_\gamma/\Gamma$ from the present work. For the 12.63 MeV level, this was estimated from the yield curve to be 4.6 ± 1.5 eV. Values of $(2J+1)\,\Gamma_p\Gamma_x/\Gamma$, where x = γ, p_1, α_0 were taken from refs. [27,28]) for the 12.05, 12.63 and 13.05 MeV levels.

[c]) Ref. [6]).

[d]) Also using $(2J+1)\Gamma_{\gamma_0}\Gamma_{\gamma_1}/\Gamma = 5.9 \pm 1.0$ eV measured in the present work.

third 4^+ $T = 1$ levels in ^{24}Mg occur at 12.100 and 12.685 MeV, which continues the tendency noted in the previous paper [1]) for the predicted $T = 1$ levels to lie $\sim$ 100 keV above their experimental counterparts.

We note also that the values of $\omega\gamma$ deduced in the present work from on-resonance γ-ray spectra are appreciably smaller than those deduced by Highland and Thwaites [25]) from γ-ray yield curves. This difference is most extreme for the 13.05(4^+) and 14.08(6^+) MeV levels where our $\omega\gamma$ values are a factor of three smaller than those of ref. [25]).

5. Levels near 14 MeV

Decay schemes and values of $\omega\gamma$ for the levels at 14.10, 14.146 and 14.32 MeV are shown in fig. 4. Gamma-ray angular distributions have been measured for each of

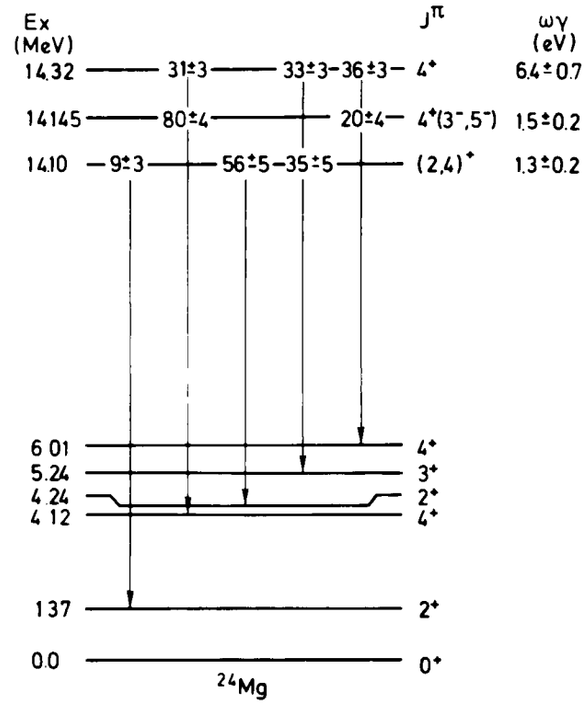

Fig. 4. Gamma-ray decay schemes and resonance strengths for the levels at 14.10, 14.146 and 14.32 MeV which have been investigated with the ^{20}Ne(α, γ)^{24}Mg reaction. The spin and parity assignments indicated for these three levels were deduced from the data presented in this figure and from γ-ray angular distribution measurements.

these levels. The results of fits to the distributions of the strongest transitions, together with the decay schemes and resonance strengths, allow the limits on the spins and parities of the three levels indicated in fig. 4. A unique assignment is obtained for the 14.32 MeV level only. An earlier ^{16}O(^{12}C, $\alpha\alpha$)^{20}Ne angular correlation measurement [5]), with an energy resolution of 100 keV, indicated the existence of at least three unresolved levels with spins of 4, 6 and 8 between 14.05 and 14.20

MeV. The 6^+ level is almost certainly the 14.08 MeV level discussed in the previous paper, while the 8^+ contribution arises from the well known 14.15 MeV 8^+ $K^\pi = 2^+$ state. The 4^+ contribution to the angular correlation must then have arisen from either or both of the levels at 14.10 and 14.145 MeV discussed here.

6. Summary and conclusions

The present work has added considerably to our knowledge of negative-parity band structure in ^{24}Mg. The reality of the $K^\pi = 0^-$ band proposed by Branford *et al.* [3]) has been conclusively demonstrated by the measurement of the partial decay widths of the 7^- level at 12.44 MeV. New information has also been obtained for the suggested $K^\pi = 3^-$ band, and in particular, the demonstration of a weak α-particle decay branch from the 11.59 MeV level opens the possibility of an unambiguous determination of its spin and parity via a particle-particle angular correlation measurement. If such a measurement were performed and found to confirm the presently tentative 5^- assignment to the 11.59 MeV level, then the 3^- band in ^{24}Mg would rest upon much firmer foundations than it does at present.

In addition, we have produced strong evidence for the existence of a new band in ^{24}Mg, of which the probable 3^- level at 10.33 MeV and the 5^- level at 13.06 MeV would be members. This band may be a $K^\pi = 1^-$ band built upon the 1^- level at

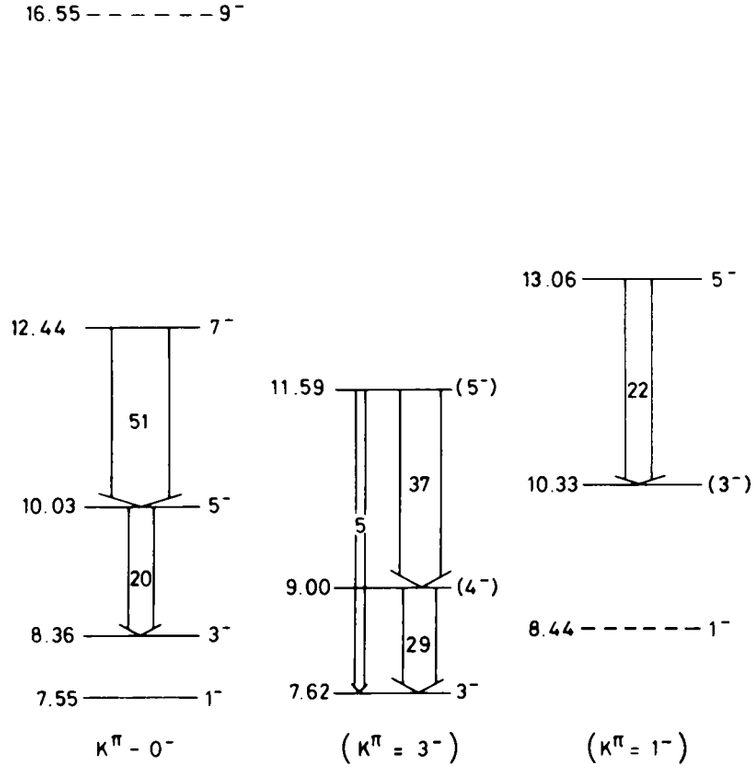

Fig. 5. Negative-parity band structure in ^{24}Mg. In-band E2 transition rates are given in Weisskopf units.

8.44 MeV. Fig. 5 summarises the present state of our knowledge of negative-parity band structure in ^{24}Mg.

Finally, although it appears that reliable shell-model calculations for negative-parity levels in ^{24}Mg are prohibitively difficult at the present time, an alternative approach may lie in the picturesquely named "nuclear helicopter" model of Pilt and Wheatley [26]). This cluster model approach, in which two correlated α-particles move in a simple potential, has had rather startling success in reproducing the spectrum of positive-parity levels in ^{24}Mg. It would be of considerable interest to apply this approach to negative-parity levels. The $K^\pi = 0^-$ band in particular could well be susceptible to such a treatment.

References

1) L. K. Fifield, M. J. Hurst, T. J. M. Symons, F Watt, C. H. Zimmerman and K. W. Allen, Nucl. Phys. **A309** (1978) 77
2) D. Kelvin, A. Watt and R. R. Whitehead, J. of Phys. **G3** (1977) 1539, and private communication
3) D. Branford, N. Gardner and I. F Wright, Phys. Lett. **36B** (1971) 456
4) A. Gobbi, P. R. Maurenzig, L. Chua, R. Hadsell, P. D. Parker, M. W. Sachs, D. Shapira, R. Stokstad, R. Wieland and D. A. Bromley, Phys. Rev. Lett. **26** (1971) 396
5) L. K. Fifield, R. W. Zurmühle and D. P Balamuth, Phys. Rev. **C8** (1973) 2217
6) D. Branford, L. E. Carlson, F. C. P. Huang, N. Gardner, T. R. Ophel and I. F Wright, Austral. J. Phys. **29** (1976) 139
7) P M. Endt and C. van der Leun, Nucl. Phys. **A310** (1978) 1
8) F Watt, L. K. Fifield, M. J. Hurst, T. J. M. Symons, C. H. Zimmerman and K. W. Allen, Nucl. Instr. **151** (1978) 163
9) I. F Wright, L. K Fifield, A. R. Poletti and B. E. Cooke, to be published
10) O. Titze, Z. Phys. **220** (1969) 66
11) R. E. Tribble, G. T. Garvey and J. R. Comfort, Phys. Lett. **44B** (1973) 366
12) F Ajzenberg-Selove, Nucl. Phys. **A190** (1972) 1
13) R. Middleton, in Int. Conf. on nuclear reactions induced by heavy ions, Heidelberg (North-Holland, Amsterdam, 1970) p. 263
14) M. Lepareux, N. Saunier, C. Gerardin, M. Wery, A. Foti, G. Pappalardo and A. Strazzeri, Lett. Nuovo Cim. **8** (1973) 725
15) M E. Cobern, D. J. Pisano and P. D. Parker, Phys. Rev. **C14** (1976) 491
16) A. Johnston and T. E. Drake, J. Phys. **A7** (1974) 898
17) C. E. Moss, Nucl. Phys. **A269** (1976) 429
18) B. Zwieglinski, G. M. Crawley, H. Nann and J. A. Nolen, Jr., Phys. Rev. **C17** (1978) 872
19) S. M. Tang, B. D. Sowerby and D. M. Sheppard, Nucl. Phys. **A125** (1969) 289
20) P M Endt and C. van der Leun, Nucl. Data **13A** (1974) 67
21) J. H. Anderson and R. C. Ritter, Nucl. Phys. **A128** (1969) 305
22) J. D. Garrett, H. T. Fortune, R. Middleton and W. Scholz, Phys. Rev. **C18** (1978) 2032
23) A. S. Keverling Buisman and P. J. M. Smulders, Nucl. Phys. **A228** (1974) 205
24) W Chung, Ph.D. thesis, Michigan State University, 1976 (unpublished)
25) G. J. Highland and T. T. Thwaites, Nucl. Phys. **A109** (1968) 163
26) A. A. Pilt and C. Wheatley, Phys. Lett. **76B** (1978) 11
27) Z. E. Switkowski, R. O'Brien, A. K. Smith and D. G. Sargood, Austral. J. Phys. **28** (1975) 141
28) P. M. Endt and C. van der Leun, Nucl. Phys. **A214** (1973) 1

1.E.1:
3.A

Nuclear Physics **A309** (1978) 77–105;

RADIATIVE DECAYS OF UNBOUND HIGH SPIN STATES IN ^{24}Mg

(I). Positive parity states

L. K. FIFIELD, M. J. HURST, T. J. M. SYMONS †, F WATT,
C. H. ZIMMERMAN †† and K. W. ALLEN

Nuclear Physics Laboratory, University of Oxford, England

Received 26 June 1978

Abstract: The ^{20}Ne(α, γ)^{24}Mg reaction has been used to measure radiative decay rates for known high spin levels at 12.86(6^+), 13.44(6^+) and 14.15(8^+) MeV in ^{24}Mg, and for previously unidentified levels at 12.00, 13.04 and 14.08 MeV. Gamma-ray angular distributions indicate that the 12.00 and 14.08 MeV levels are probably 6^+ levels, while the 13.04 MeV level is the lowest 0^+ $T = 1$ state. A new level at 11.005 MeV, populated in the radiative decay of the 14.08 MeV level, is most likely the lowest 5^+ $T = 1$ state in ^{24}Mg. Alpha-particle widths have also been measured for several of these levels and for the known 6^+ level at 13.85 MeV using the ^{20}Ne(α, α′γ)^{20}Ne reaction and previously determined branching ratios. The results for both radiative and particle decay widths are compared with recent shell-model calculations performed within a full $(sd)^8$ basis.

E NUCLEAR REACTIONS ^{20}Ne(α, γ), ^{20}Ne(α, α′γ), E = 3.0–6.0 MeV; measured $\sigma(E_\alpha, E_\gamma, \theta_\gamma)$. ^{24}Mg deduced levels, J, π, T, γ-ray branching ratios, radiative widths, α-particle widths. Windowless gas target.

1. Introduction

With the development of shell-model codes [1]) capable of untruncated calculations throughout the 2s-1d shell, there has been renewed interest in the spectroscopy of nuclei near the middle of the shell. At present, much of the interest centres on the form of residual interaction to be used in such calculations. The earlier "realistic" residual interactions of Kuo [2]) and Kuo and Brown [3]), in which attempts were made to generate an effective interaction within the sd shell from the nucleon-nucleon force, have now been largely superseded by the new semi-empirical effective interactions of Preedom and Wildenthal [4]) (PW) and Chung and Wildenthal [5]). This latter interaction has been further extended by the Glasgow group [6]) to include an empirically determined Coulomb interaction, and we shall refer to this as the CWC interaction. To date, extensive calculations with the CWC interaction have been performed only for the mass-24 nuclei, which may therefore be regarded as the testing ground for this new interaction. Paradoxically, the ^{24}Mg nucleus is more suited to this role than the "simpler" nuclei near the beginning of the 2s-1d shell, since its spectrum appears to be remarkably free of the intruder states which plague the interpretation of the spectra

† Present address: Lawrence Berkeley Laboratory, Berkeley, California 94720, USA.
†† Present address: Department of Physics, University of Edinburgh, Edinburgh, Scotland.

of the lighter nuclei. In the present work we have sought to extend the spectroscopic information available for comparison with the calculations by studying the electromagnetic (EM) properties of high spin states and low-lying $T = 1$ states in ^{24}Mg using the ^{20}Ne(α, γ)^{24}Mg reaction.

A considerable body of information on positive-parity high spin states in ^{24}Mg has been built up from studies of the $^{12}C + ^{16}O \rightarrow ^{24}Mg + \alpha$ reaction [7-9]. Lifetimes of bound and quasi-bound levels have been determined [7,8] using the ^{12}C(^{16}O, $\alpha\gamma$)^{24}Mg reaction and the Doppler shift attentuation method (DSAM), and the corresponding EM transition rates confirm the existence of low-lying $K^\pi = 0^+$ and 2^+ rotational bands. Both bands have been identified as far as their 8^+ members which lie at 13.21 and 14.15 MeV respectively. However, although the 13.21 MeV level decays exclusively by emitting γ-rays, its lifetime is very short and has not yet been determined with sufficient accuracy to allow meaningful comparison with the calculations. The 14.15 MeV level on the other hand decays through both γ-ray and α-particle channels [9]) and only an upper limit on its lifetime has been established using the DSAM [7]). This level is, however, accessible to investigation using the ^{20}Ne(α, γ)^{24}Mg reaction, which is in principle capable of providing a considerably more accurate measurement of its EM decay rate than has so far been possible for the lower 8^+ level at 13.21 MeV. We have excited the 14.15 MeV level as a resonance in the ^{20}Ne(α, γ)^{24}Mg reaction, and our results, which are in excellent agreement with the shell-model calculations using the PW interaction, have already been presented in letter form [10]). Here we will go into more detail and discuss the results in the light of the more recent calculations employing the new CWC interaction.

In addition to the 8^+ levels, the ^{16}O(^{12}C, α)^{24}Mg reaction selectively populates a number of other levels between 11.8 and 14.4 MeV in ^{24}Mg. Using α-α and α-α-γ angular correlation techniques, 6^+ levels have been identified [9]) at 12.83, 13.42 and 13.84 MeV, with another level at $\approx$ 14.1 MeV also most probably having spin and parity 6^+. Three of these four levels are accessible to the ^{20}Ne(α, γ)^{24}Mg reaction since they have appreciable α-decay branches to the ^{20}Ne ground state, and their EM decay properties can thereby be measured and compared with the calculations. It is interesting to note that both the PW and CWC interactions predict [6]) that the third 6^+ level in ^{24}Mg should lie near 12.0 MeV, and we have undertaken a search for such a level.

In addition to measurements of EM decay widths, it has been possible to measure α-particle decay widths for several of the above states using the resonant yield of 1.63 MeV γ-rays from the ^{20}Ne(α, $\alpha'\gamma$)^{20}Ne reaction and known α-decay branching ratios. These may be compared with results of calculations by Kelvin, Watt and Whitehead [11]), who have recently developed a technique for calculating reduced widths for α-decay.

One of the features of the CWC interaction is the inclusion of empirically determined Coulomb corrections. Since these corrections were derived from a rather limited data set, the excitation energies of low-lying $T = 1$ states in ^{24}Mg are of

considerable importance in testing the accuracy of these corrections, and in extending the data set from which they were derived. Prior to the present work, only the analogues of the ^{24}Na-^{24}Al ground states and first two excited 1^+ states had been identified with certainty. However, the lowest 6^+ $T = 1$ and 0^+ $T = 1$ states in ^{24}Mg are predicted to lie within the region covered in the present work, and the ^{20}Ne(α, γ)^{24}Mg reaction should prove a useful tool in locating these states. Furthermore, since the lowest 5^+ $T = 1$ level has a calculated excitation energy of 11.17 MeV [ref. [6])], it might well be populated by a strong isospin allowed M1 transition from one of the higher 6^+ $T = 0$ levels.

Within the region of excitation energy investigated here, the heavy ion induced reactions indicate the existence of a number of high spin negative-parity levels. We have also studied these levels as resonances in the ^{20}Ne(α,γ)^{24}Mg reaction, but a discussion of the results will be deferred to a second publication.

2. Experimental method

A differentially pumped gas target was employed throughout this work with the attendant advantages of very low γ-ray background and high energy resolution. Since full details of this target have been presented elsewhere [12]), only a brief description will be given here. The target assembly was built into a 25 cm diameter stainless steel flange and consisted of a 5 cm long tube containing the target gas with 4 cm long nozzles at each end restricting the flow of gas out of the tube. Gas escaping from these nozzles was pumped away by a liquid helium cooled cryopump. The target gas pressure was maintained constant by a servo-controlled needle valve with the feedback signal derived from a capacitance manometer which measured the target pressure.

Neon gas, enriched to greater than 99.99 % in ^{20}Ne, was used in all the measurements. A total of 15 atm. litres in a 20 litre storage volume served as the reservoir for the target, and at a target pressure of 1 Torr this reservoir emptied in 6 h. Recycling was accomplished by warming the cryopump above 20 °K and pumping the evolved gas back into the storage volume using a liquid helium cooled cryofinger.

Beams of α-particles were obtained from the Oxford single-ended Van de Graaff accelerator. Typical beam currents ranged from 5μA of ^{4}He$^+$ at 3 MeV down to 2μA at 6 MeV with greater than 99.6 % of the beam transmitted through the target to the Faraday cup, which was located 3 m beyond the target. This ensured a very low level of γ-ray background from nuclear reactions induced in material other than the target gas. At the higher energies, the usable beam current was limited by high counting rates in the γ-ray detectors due to the intense flux of 1.63 MeV γ-rays from the ^{20}Ne(α, $\alpha'\gamma$)^{20}Ne reaction.

For the yield curve measurements, γ-rays were detected in a 7.6 × 7.6 cm NaI(Tl) crystal, positioned with its front face 1 cm from the centre of the target. A target gas pressure of 0.2 Torr was employed; the corresponding target thickness ranged from

2 keV at 3 MeV to 1.2 keV at 6 MeV. Yield curves were measured using an automatic beam energy modulation technique [13]) in which the beam energy was varied continuously over a typical energy range of 60 keV. The nuclear magnetic resonance (NMR) frequency of a probe in the accelerator analysing magnet served to monitor the instantaneous beam energy. Single-channel analysers (SCA) were used to set gates about various regions of the γ-ray energy spectrum, and a simple pile-up rejection system was employed to prevent pulse pile-up from contributing a background in the higher energy γ-ray gates. The outputs from the SCA units, together with the digitised Faraday cup current, were fed into an interface between the NMR frequency counter and a Laben 8192 channel analyser. This interface scaled the number of pulses at each of its eight inputs as a function of NMR frequency, thereby building up a series of yield curves, one for each γ-ray gate, in different areas of the analyser memory. At the end of a run, which usually involved several sweeps over the chosen energy range, the resulting spectra were transferred to a computer where the γ-ray yield in each gate was normalised to the beam charge accumulated in each frequency interval. Yield curves over an extended region could then be obtained by joining normalised yield curves from individual runs.

For the γ-ray decay scheme, resonance strength, and angular distribution measurements, two germanium detectors were employed to provide high resolution γ-ray spectra. An 85 cm^3 Ge(Li) detector, fixed at either 125° or 135°, was used to monitor the position of the resonance in the target by providing an accurate measurement of the Doppler shifted energy of a secondary γ-ray transition. The determinations of resonance strengths and decay schemes were made from the spectra measured with this detector since its relative detection efficiency for γ-rays with energies up to 11.5 MeV had been accurately determined. The second detector was a 60 cm^3

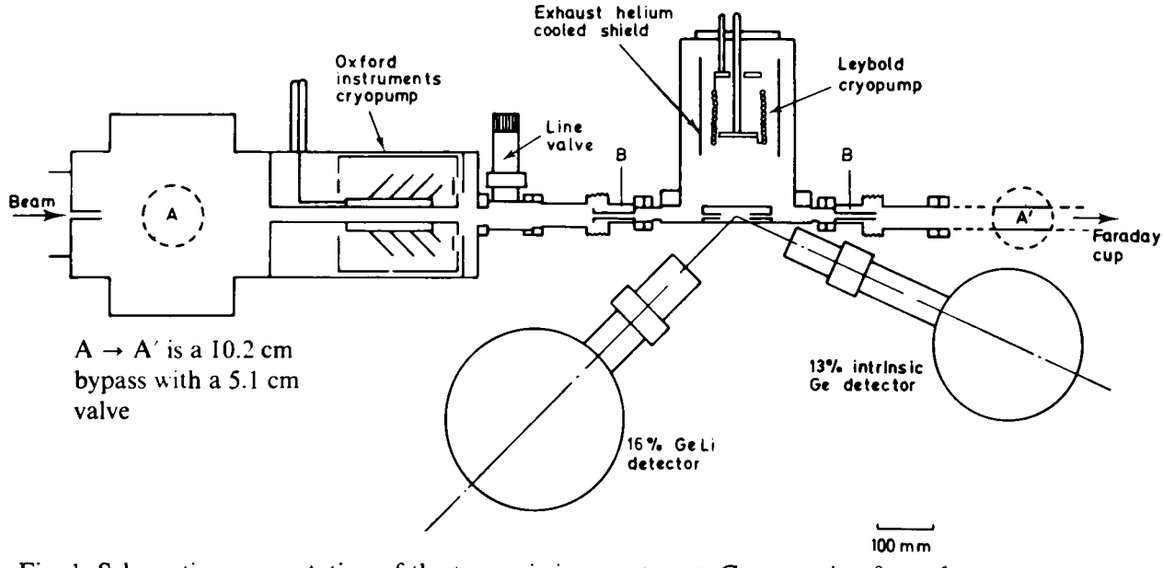

Fig. 1. Schematic representation of the transmission gas target. Gas escaping from the target nozzles is pumped away by the Leybold cryopump, while the region beyond the differential pumping apertures B is maintained at high vacuum by the annular Oxford Instruments cryopump.

intrinsic germanium detector which could be positioned at angles between 25° and 90° to the beam direction for the measurement of γ-ray angular distributions. Distances from the centre of the target to the front faces of the detectors ranged from 8 to 14 cm for various runs. The gas target and a typical detector geometry are depicted schematically in fig. 1.

Detector gains were maintained constant during most of the runs by Laben gain stabilisers using peaks from a ^{228}Th source and from a precision pulser. The pulser was also useful in making corrections for dead time losses. A pair of pulses arriving within 4 μs of one another were prevented from contributing to the γ-ray spectrum by a simple pile-up rejection circuit. Energy calibration of the γ-ray spectrum was accomplished by taking spectra with sources of ^{60}Co, ^{228}Th and Am-^{10}B, the latter in the presence of a substantial quantity of iron and paraffin to provide 7631.1 and 7645.5 keV γ-rays from the ^{56}Fe(n, γ)^{57}Fe reaction.

Target gas pressures of 1 Torr were used in the majority of measurements of γ-ray spectra. Since almost all the resonances studied had natural widths less than 1.5 keV, and the beam energy resolution was better than 1.5 keV, such pressures ensured that the resonance was located completely within the target provided that the mean resonance position was approximately central in the target. The yield of γ-rays was then effectively that from a thick target. However, the source of resonant γ-rays was extended along the beam direction and it was necessary to correct the observed yields before extracting resonance strengths or fitting γ-ray angular distributions. Details of this correction procedure are given in ref. [12]). All γ-ray angular distributions and resonance strengths reported here have been corrected for extended target effects.

Measurements of $\omega\gamma[=(2J+1)\Gamma_\gamma\Gamma_{\alpha_0}/\Gamma]$ for the resonances studied were made by comparison of the yield of resonant γ-rays with the yield of 8.64 MeV γ-rays at the 6.93 MeV (2^+ $T=1$) resonance in the ^{16}O(α, γ)^{20}Ne reaction. A number of measurements with oxygen as the target gas were made at the 6.93 MeV resonance in order to reproduce the various detector geometries employed in the ^{20}Ne(α, γ)^{24}Mg measurements. In each case, care was taken to measure the yield at the reference resonance with as nearly as possible the same target thickness and resonance position as pertained to the corresponding ^{20}Ne(α, γ)^{24}Mg measurements. This ensured that the extended target corrections were very similar in the two cases, thereby keeping uncertainties to a minimum. A value of 19.7$\pm$1.6 eV was adopted for $\omega\gamma$ of the reference resonance [14]). The $\omega\gamma$ of a ^{20}Ne(α, γ)^{24}Mg resonance is then

$$\omega\gamma = \frac{\varepsilon}{\varepsilon_R}\frac{E}{E_R}\left(\frac{20}{24}\times\frac{20}{16}\right)^3\frac{Y}{Y_R}\omega\gamma_R,$$

where R denotes the reference resonance, E the lab α-particle energy, ε the lab stopping power at energy E in units of keV/atom · cm^2 taken from the tables of Northcliffe and Schilling [15]), and Y the yield of γ-rays corrected for extended target

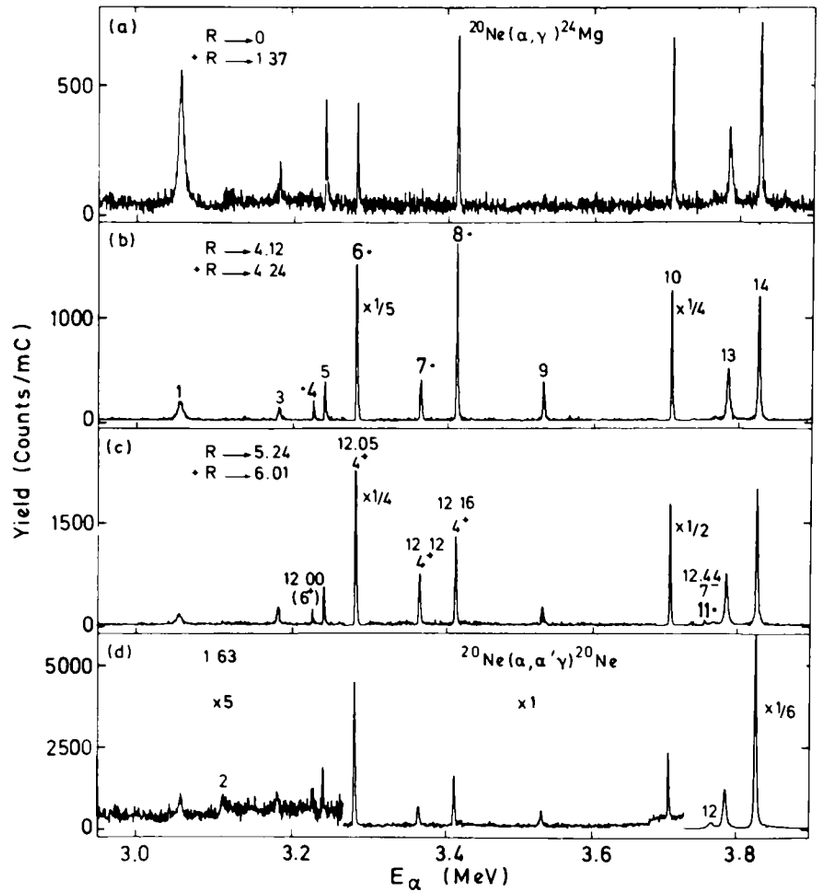

Fig. 2. Yield of γ-rays from the bombardment of isotopically enriched ^{20}Ne gas with α-particles over the range of beam energy from 2.95 to 3.9 MeV. Curves (a), (b) and (c) are the yields of γ-rays in three different regions of the spectrum from the NaI detector. The full energy and escape peaks of the indicated transitions in ^{24}Mg fall within these regions. Curve (d) is the yield of γ-rays in the region of the full energy peak of the 1.63 MeV γ-ray from the ^{20}Ne(α, $\alpha'\gamma$)^{20}Ne reaction. Resonances are numbered with increasing excitation energy, and γ-ray spectra have been measured with a Ge(Li) detector for those marked with an asterisk and with their excitation energy, spin and parity.

and for angular distribution effects. The numerical factor in brackets accounts for the different lab to c.m. conversion factors in the ^{20}Ne(α, γ)^{24}Mg and ^{16}O(α, γ)^{20}Ne reactions.

3. Results: yield curves

Yields of γ-rays from the ^{20}Ne(α, γ)^{24}Mg and ^{20}Ne(α, $\alpha'\gamma$)^{20}Ne reactions as a function of α-particle energy are shown in figs. 2–4. The yields in each of three γ-ray gates are shown in parts (a), (b) and (c) of figs. 2–4, respectively, and the transitions in ^{24}Mg accepted by the different gates are indicated; the yield of γ-rays in the 1.63 MeV photopeak which arises from the ^{20}Ne(α, $\alpha'\gamma$)^{20}Ne reaction is shown in part (d) of figs. 2–4. Table 1 summarises the excitation energies, widths and the extent of previous information for the numbered resonances. It can be seen that of the 54 resonances observed, 17 have not been observed previously in either the α-particle

detector. Since both measurement and calculation of the gas pressure profile were impracticable, a constant pressure region, bounded by regions of linear pressure drop to zero, was assumed*, with a total length of 13cm. Results were found not to depend significantly on the length of the constant pressure region, which for high target pressures was taken to be the full 13cm with a step change to zero pressure.

A computer programme DISDEL exists to perform these calculations and for a given beam energy it will calculate the correction factor to be applied to the observed intensity in a detector in order to obtain the intensity that would have been observed from an equivalent point target.

In addition, the mean Doppler shift of a given γ-ray can be calculated, and if this energy does not agree with the value measured by the appropriate detector then the assumed beam energy must be incorrect. The programme is able to iterate over the calculation to choose a beam energy for which measured and predicted γ-ray energy agree. This is necessary because a beam energy change of 1 keV corresponds typically to a movement of the resonance profile of 1cm whereas the analysing magnet calibration is not reliable to better than 5 keV. In order to estimate accurately the position of the resonance profile, the energy of the chosen γ-ray must be known accurately, and for this reason a secondary transition is usually chosen (in ^{20}Ne the $1.63MeV(2^+) \rightarrow 0.00MeV(0^+)$). In chapters four and five however, several cases will be described where this method had to be modified.

* This assumption was born out by tests on the angular distribution of the 10.27MeV state, and is reasonable in view of the ratio of the diameters of the target chamber and nozzles (15mm & 3mm).

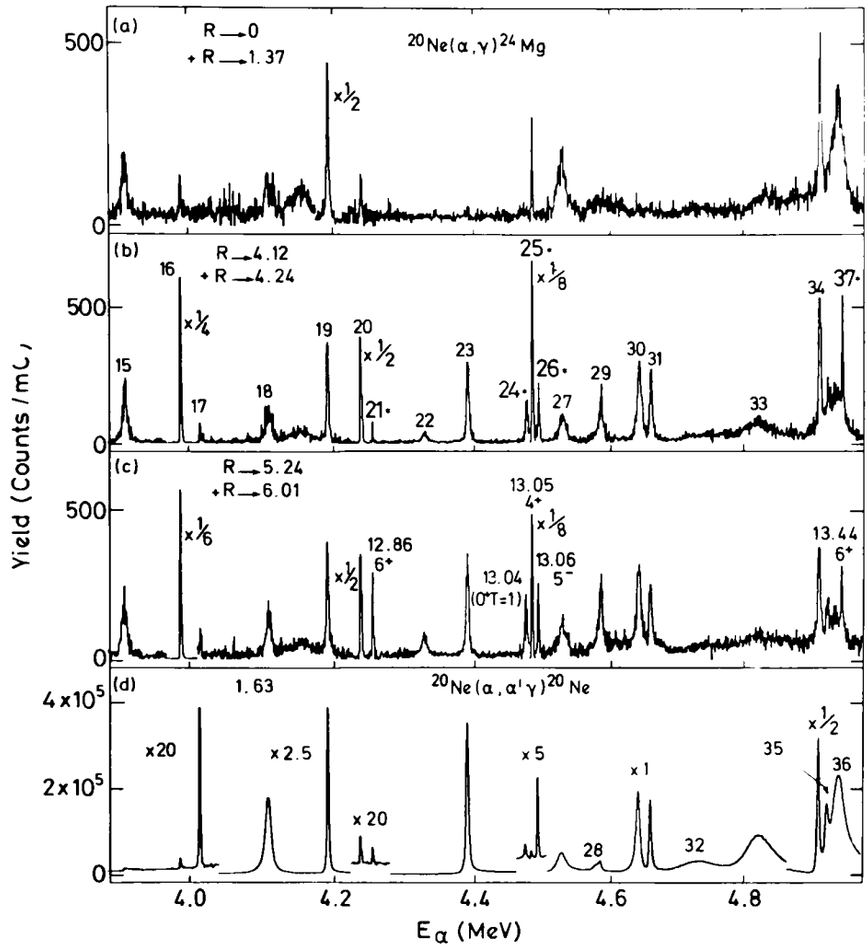

Fig. 3. As for fig. 2, but for beam energies between 3.9 and 4.95 MeV.

induced or proton induced reactions. For those resonances which have been observed previously, the excitation energies and widths quoted by Endt and Van der Leun [16]) are generally in good agreement with those measured in the present work.

Since the emphasis in the present work was on the radiative decays of high spin states, no attempt has been made to study all of the resonances observed. In particular, states which exhibited appreciable γ-ray decay strength to the ground or first excited state of ^{24}Mg were not considered further.

4. The 8^+ $K^\pi = 2^+$ level at 14.15 MeV

Yield curves spanning a region of excitation in ^{24}Mg which encompasses the 14.15 MeV (8^+ $K^\pi = 2^+$) level are shown in fig. 5. The main features of these yield curves are a prominent resonance (no. 50) in the yield of γ-rays to the 4.12 MeV (4^+) level at $E_\alpha = 5.799$ MeV, a very strong ^{20}Ne(α, α'γ)^{20}Ne resonance (no. 51) at $E_\alpha = 5.801$ MeV, and a very weak resonance in the yield of 4.0–4.7 MeV γ-rays at $E_\alpha = 5.807$ MeV. This latter resonance corresponds to the 14.15 MeV 8^+ level in ^{24}Mg. The presence of the (α, α') resonance necessitated the use of reduced beam

TABLE 1

Resonances in $^{20}Ne(\alpha, \gamma)^{24}Mg$ and $^{20}Ne(\alpha, \alpha)^{20}Ne$ observed in the present work

No.	E_x [a] (keV)	E_x (present) [b] (keV)	E_x (previous) [c] (keV)	J^π [c]	Γ (present) (keV)	Γ (previous) [c] (keV)	Reactions [d]
1	3054	11859	11863 ± 4	1^-	7.0 ± 0.3	8 ± 2	A
2	3109	11905			5.5 ± 2.2		
3	3181	11965	11966 ± 2	2^+	2.8 ± 0.3	1.8 ± 0.4	A, B
4	3224	12001		$6^+(4^+)$ [e]	< 1		
5	3240	12014	12016 ± 2	3^-	< 1	0.7 ± 0.2	A, B
6	3281	12048	12050 ± 2	4^+	< 1	< 0.02	A, B
7	3366	12119	12118 ± 2	4^+	1.9 ± 0.3	< 2	B, C
8	3415	12160	12167 ± 5	4^+	0.9 ± 0.3		A
9	3530	12256	12259 ± 2	3^-	1.8 ± 0.3	0.6 ± 0.2	B
10	3707	12403	12405 ± 2	2^+	< 1	< 0.1	A, B
11	3754	12442	12420 ± 30	7^-	< 1		C
12	3766	12452	12462 ± 5	1^-	5.7 ± 0.4	7 ± 2	A, B
13	3786	12469	12477 ± 5	2^+	3.8 ± 0.3	5 ± 1	A, B
14	3829	12505	12506 ± 4	4^+	2.3 ± 0.3	1	A, B
15	3915	12576	12581 ± 5	2^+	6.2 ± 0.6	6 ± 1	A, B
16	3988	12637	12638 ± 2	4^+	< 1	0.03 ± 0.02	A, B
17	4015	12660	12660 ± 2	3^-	0.9 ± 0.3	< 0.5	A, B
18	4109	12738	12738 ± 2	2^+	8.3 ± 0.5	5 ± 1	A, B
19	4193	12808	12807 ± 2	2^+	2.3 ± 0.3	1.2 ± 0.2	A, B
20	4240	12847	12846 ± 2	2^+	< 1	0.2 ± 0.1	B
21	4257	12861	12830 ± 30 [f]	6^+ [f]	< 1		C
22	4329	12921	12921 ± 2		6.7 ± 0.6	5.5 ± 0.5	B
23	4391	12973	12978 ± 13		3.3 ± 0.3		A
24	4475	13043	(13044 ± 2)	0^+ $T = 1$ [c]	2.3 ± 0.4		B
25	4483	13050	13050 ± 2	4^+	< 1	0.09 ± 0.03	A, B
26	4492	13057	13070 ± 50	5^-	< 1		C
27	4528	13087	13088 ± 2	$(2^+, 3^-)$	11.9 ± 0.6	6 ± 0.5	A, B
28	4582	13132			9 ± 2		
29	4588	13137	13138	2^+	5.4 ± 0.5	< 10	B
30	4643	13183	13184 ± 2	2^+	5.6 ± 0.4	6.5 ± 0.5	B
31	4661	13198	13200		2.7 ± 0.4	< 10	B
32	4731	13256	13261		36 ± 3	50	B
33	4824	13334			33 ± 3		
34	4915	13410	13407 ± 5	$(1^-, 2^+)$	2.8 ± 0.3		A
35	4928	13420	13419 ± 2	2^+	3.2 ± 0.7	4.1 ± 0.7	B
36	4942	13432	13434 ± 10		15 ± 2.5		A
37	4950	13439	13420 ± 30 [f]	6^+ [f]	< 1		C
38	5003	13483	13482		1.2 ± 0.3	1	B
39	5124	13584	13584		21 ± 2.3	23 ± 3	B
40	5232	13674	13677 ± 2		4.8 ± 0.8	7.8 ± 1	B
41	5285	13718			4.3 ± 0.3		
42	5340	13764	13750 ± 30	5^- [f]	3.2 ± 0.4		C
43	5378	13795			4.4 ± 0.4		
44	5444	13850	13840 ± 30 [f]	6^+ [f]	< 1		C
45	5486	13885			12 ± 1.8		
46	5650	14022	14025 ± 5	1^-	6.2 ± 0.7		A
47	5715	14076			24 ± 5		

TABLE 1 (continued)

No.	E_x [a] (keV)	E_x (present) [b] (keV)	E_x previous) [c] (keV)	J^π [c]	Γ (present) (keV)	Γ (previous) [c] (keV)	Reactions [d]
48	5720	14080	14080 ± 5	$6^+(4^+)$ [e]	< 1		A, C
49	5740	14097	14100 ± 5	(4^+) [e]	1.4 ± 0.4		A, C
50	5799	14146	14144 ± 5	$(3^-, 4^+, 5^-)$ [c]	1.8 ± 0.4		A, C
51	5801	14148			6.2 ± 0.7		
52	5807	14153	14152 ± 3	8^+			C
53	5913	14241			11.3 ± 1.4		
54	6014	14325	14328 ± 5	4^+ [e]	< 1		A

[a]) Error ± 5 keV unless otherwise indicated.
[b]) Error ± 4 keV unless otherwise indicated.
[c]) From Endt and van der Leun [16]) unless indicated otherwise.
[d]) Reactions in which state has been observed previously: A, ^{20}Ne(α, γ)^{24}Mg, ^{20}Ne(α, α′)^{20}Ne, or ^{20}Ne(α, α)^{20}Ne; B, ^{23}Na(p, x) where x = p, γ or α; C, ^{12}C(^{16}O, α)^{24}Mg or ^{16}O(^{12}C, α)^{24}Mg.
[e]) Present work.
[f]) Ref. [9]).

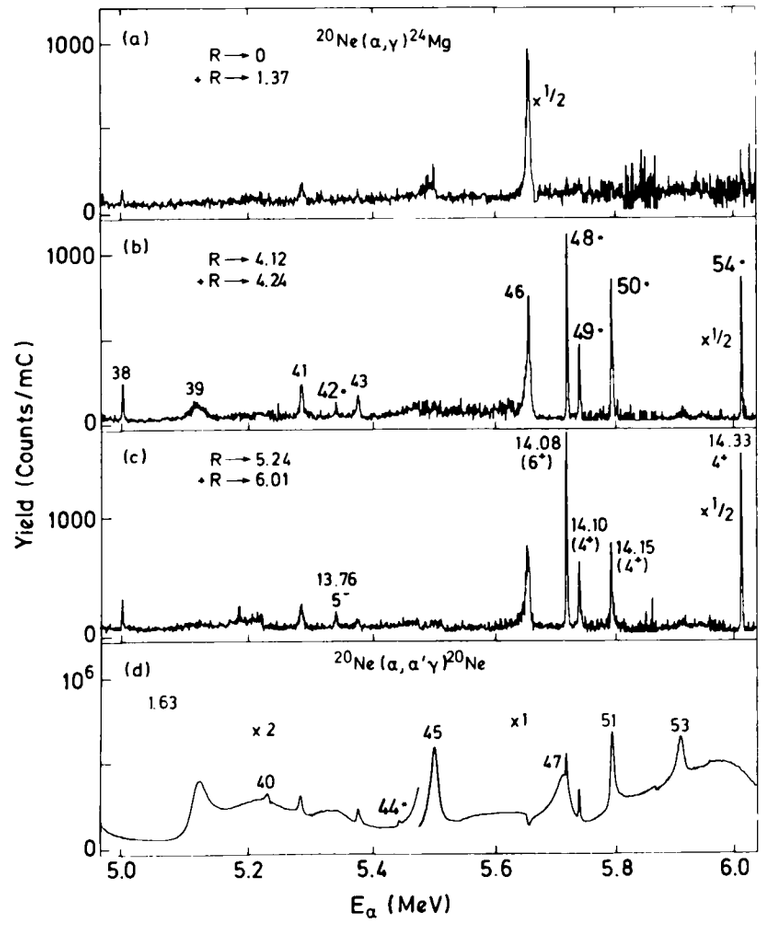

Fig. 4. As for fig. 2, but for beam energies between 4.95 and 6.0 MeV.

currents of $\approx$ 1 μA of $^4He^+$ in order to keep the counting rates in the γ-ray detectors within reasonable limits.

In order to measure the resonance yield from the 8^+ level, γ-ray spectra were measured on- and off-resonance and are shown in fig. 6. Although there are a number of γ-rays which occur in both spectra, most of which are due to the $^{21}Ne(\alpha, n\gamma)^{24}Mg$ reaction on the tiny fraction of residual ^{21}Ne in the target gas (less than 0.01 %), the 14.15 $\rightarrow$ 9.52 MeV and 9.52 $\rightarrow$ 6.01 MeV transitions are clearly visible in the on-resonance spectrum only, and the areas of these two peaks were used in determining the resonance yield of the R $\rightarrow$ 9.52 MeV transition.

The insets in fig. 6 show the region of γ-ray energy near 6 MeV, where the 6.04 MeV γ-ray from the weaker R $\rightarrow$ 8.11 MeV (6^+) transition is clearly visible in the on-resonance spectrum; the extracted branching ratio of (29 ± 5) % is in good agreement with the more accurate value of Branford *et al.* [7]).

The position of the resonance in the target was determined from the Doppler shift of the γ-ray from the 9.53 $\rightarrow$ 6.01 MeV transition. Uncertainties in this Doppler shift due to statistics and to uncertainty in the unshifted γ-ray energy influenced the corrections for extended target effects and were propagated through into the uncertainty on $\omega\gamma$. A final value of 0.24 ± 0.04 eV was obtained for $\omega\gamma (= 17\Gamma_\gamma(\Gamma_{\alpha_0}/\Gamma))$

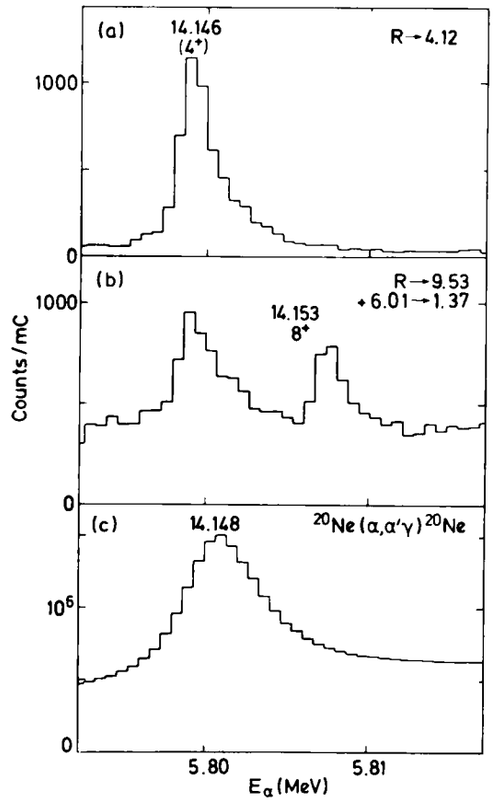

Fig. 5. Yield of γ-rays as a function of α-particle energy in the neighbourhood of the 14.153 (8^+, $K^\pi = 2^+$) level in ^{24}Mg. Curve (a) is the yield from the region of the γ-ray spectrum between 8.7 and 10.5 MeV, curve (b) the yield from 4.0 to 4.7 MeV, and curve (c) the yield in the 1.63 MeV full energy peak.

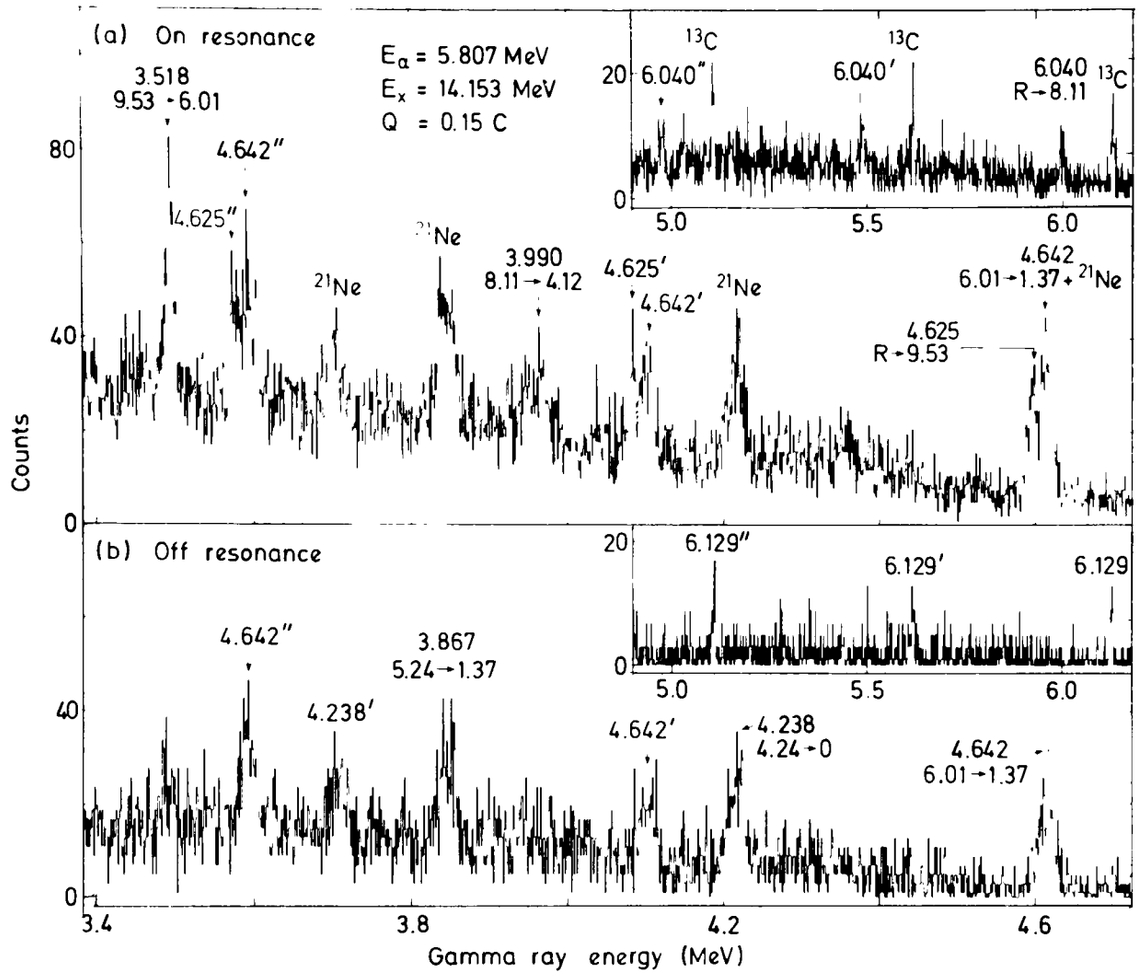

Fig. 6. Partial spectra of γ-rays (a) on the 5.807 MeV (8^+) resonance and (b) 18 keV above this resonance. The 85 cm^3 Ge(Li) detector was at 135° and 13 cm from the centre of the target and the target pressure was 1 Torr. The insets show the region of the spectrum between 5 and 6 MeV, and full energy peaks are labelled with their unshifted γ-ray energy and the corresponding transition in ^{24}Mg. All energies are in MeV Single and double escape peaks are denoted by single and double primes. Peaks in the on-resonance spectrum labelled ^{21}Ne and ^{13}C are due to the ^{21}Ne(α, nγ)^{24}Mg and ^{13}C(α, nγ)^{16}O reactions respectively, and are identified in (b). Q is the accumulated charge in Coulombs of ^{4}He^{++} and the off-resonance spectrum has been normalised to the same total charge.

of the R → 9.53 MeV transition from analysis of the above data. Taken together with the value [9]) 0.22±0.04 for Γ_{γ_0}/Γ, this implies a radiative width of 64±17 meV for the in-band 14.15 (8^+) → 9.53 (6^+) MeV transition in ^{24}Mg.

At the time of our earlier report of these results, the only calculations within a complete (2s-1d)^8 basis which were available utilised the PW effective interaction. More recently, similar calculations have been carried out by Kelvin, Watt and Whitehead [11]) using the new CWC interaction. The results for all three known 8^+ states are presented and compared with experiment and the earlier calculation in table 2. It is apparent at once that the PW interaction gives a remarkable account of the E2 transition rates for all three levels. The CWC interaction on the other hand fails quite dramatically to account for the $8_3 \rightarrow 6_1$ transition rate which it predicts

TABLE 2

Comparison of calculated and observed E2 transition rates for 8^+ states in ^{24}Mg

State	E_x (MeV)	Transition	E2 transition rate (W.u.)		
			PW	CWC	exp
8_1	11.86	$8_1 \rightarrow 6_1$	3.8	3.5	$3.0^{+1.8}_{-0.8}$ [a])
8_2	13.21	$8_2 \rightarrow 6_1$	16.8	5.5	17.5^{+19}_{-6} [b])
8_3	14.15	$8_3 \rightarrow 6_1$	0.9	9.8	0.8 ± 0.2 [c])
		$8_3 \rightarrow 6_2$	7.6	7.6	9.1 ± 2.4

[a]) Ref. [8]). [b]) Ref. [7]). [c]) Present work.

to be strongly enhanced and an order of magnitude stronger than the observed rate. It does, however, give the correct in-band transition rate. The indications are that the $8_2 \rightarrow 6_1$ transition rate is underpredicted by about the amount that the $8_3 \rightarrow 6_1$ is overpredicted, although the uncertainties in the lifetime of the 13.21 MeV (8_2^+) level make a quantitative comparison difficult. Thus, despite the fact that the set of excitation energies employed in fitting the CWC interaction is substantially larger and covers a broader mass range than the set used in deriving the PW interaction, the latter gives a much better account of the E2 transition rates from 8^+ states in ^{24}Mg (which represent an extrapolation beyond the mass range of its data set) than does the former. Similar differences between the CWC and PW interactions occur [11]) for the lowest 9^+ and 10^+ states in ^{24}Mg, but these states have so far eluded all attempts to locate them. On the other hand, the two interactions are in excellent accord over the properties of the lower lying members of the $K^\pi = 0^+$ and 2^+ bands. The states with $J \geqq 8$ are therefore uniquely sensitive to the interaction one uses, and hence it becomes that much more interesting to locate and measure the properties of the states with $J \geqq 9$.

5. States with $J^\pi = 6^+$

5.1. EXPERIMENTAL RESULTS

Of the four known or probable 6^+ states between 11.8 and 14.4 MeV in ^{24}Mg, three have been studied in the present work as resonances in the ^{20}Ne(α, γ)^{24}Mg reaction, while the fourth has been observed as a weak resonance in the ^{20}Ne(α, $\alpha'\gamma$)^{20}Ne reaction. In addition, we have located a new level at 12.00 MeV which is an excellent candidate for the third 6^+ level in ^{24}Mg, predicted [6]) by the shell-model calculations to lie near this excitation energy but not previously identified. Each of these levels will be discussed in turn below. Their γ-ray decay schemes and resonance strengths are summarised in fig. 7, while the corresponding transition rates are listed in table 3.

TABLE 3

Experimental and calculated transition rates for 6^+ levels in ^{24}Mg

State	E_x (MeV)			Transition	$M\lambda$	$B(M\lambda)$ (W.u.)		
	exp	PW	CWC			exp [a])	PW [b])	CWC [b])
6_1	8.11	8.25	8.27	$6_1 \rightarrow 4_1$	E2	35^{+40}_{-12} [c])	25	22
6_2	9.53	9.60	9.31	$6_2 \rightarrow 4_1$	E2	$0.8^{+0.8}_{-0.3}$ [c])	0.2	0.04
				$6_2 \rightarrow 4_2$	E2	24^{+24}_{-8}	11.6	13.6
6_3	12.00	11.98	11.85	$6_3 \rightarrow 4_1$	E2	> 0.18	0.73	0.28
				$6_3 \rightarrow 4_2$	E2	> 0.21	0.005	0.02
				$6_3 \rightarrow 4_3$	E2	> 0.94	2.8	0.6
				$6_3 \rightarrow 4_4$	E2	$< 1.3 \times (6_3 \rightarrow 4_3)$	3.0	4.1
				$6_3 \rightarrow 5_3 (T = 1)$	M1	> 0.17		0.11
6_4	12.86	12.47	12.12	$6_4 \rightarrow 4_1$	E2	0.04 ± 0.01	0.09	0.31
				$6_4 \rightarrow 4_2$	E2	0.80 ± 0.12	1.07	1.47
				$6_4 \rightarrow 4_3$	E2	2.9 ± 0.7	1.4	2.6
				$6_4 \rightarrow 4_4$	E2	11.2 ± 2.1	2.6	0.3
				$6_4 \rightarrow 5_3 (T = 1)$	M1	< 0.04		0.58
6_5	13.44	12.96	12.85	$6_5 \rightarrow 4_1$	E2	0.98 ± 0.19	0.03	0.04
				$6_5 \rightarrow 4_2$	E2	< 0.4	0.06	0.2
				$6_5 \rightarrow 4_3$	E2	< 1.4	2.3	3.0
				$6_5 \rightarrow 4_4$	E2	< 7.3	2.8	3.2
				$6_5 \rightarrow 5_3 (T = 1)$	M1	< 0.1		0.006
6_6	13.85	13.71	14.09	$6_6 \rightarrow 4_1$	E2	[d])	0.07	0
				$6_6 \rightarrow 4_2$	E2		1.4	1.7
				$6_6 \rightarrow 4_3$	E2		0.1	0.2
				$6_6 \rightarrow 4_4$	E2		0.4	1.0
				$6_6 \rightarrow 5_3 (T = 1)$	M1			0.17
6_7	14.08	14.24	14.86	$6_7 \rightarrow 4_1$	E2	0.66 ± 0.14 [e])	0.15	[f])
				$6_7 \rightarrow 4_2$	E2	1.5 ± 0.4	0.01	
				$6_7 \rightarrow 4_3$	E2	< 0.5	0	
				$6_7 \rightarrow 4_4$	E2	0.5 ± 0.2	1.5	
				$6_7 \rightarrow 5_3 (T = 1)$	M1	0.14 ± 0.03		

[a]) Present work unless otherwide indicated. Upper limits are 3 standard deviation limits.
[b]) Ref. [11]). [c]) Ref. [7]).
[d]) The 13.85 MeV level was not observed as a ^{20}Ne$(\alpha, \gamma)^{24}$Mg resonance.
[e]) Using $\Gamma_\alpha/\Gamma = 0.85 \pm 0.15$.
[f]) Calculated transition rates not available.

The level at 12.00 MeV. On-resonance and off-resonance γ-ray spectra for this new level are shown in fig. 8; the only decays observed from the resonance proceed to known 4^+ states in ^{24}Mg, and to a previously unidentified level at 11.01 MeV which is discussed below with reference to the 14.08 MeV level. Angular distributions were measured for the R → 4.12 and R → 6.01 MeV transitions. Measurement of the Doppler shifted energy of the γ-ray from the 4.12 → 1.37 MeV transition in the monitor detector served to define the position of the resonance in the target. The

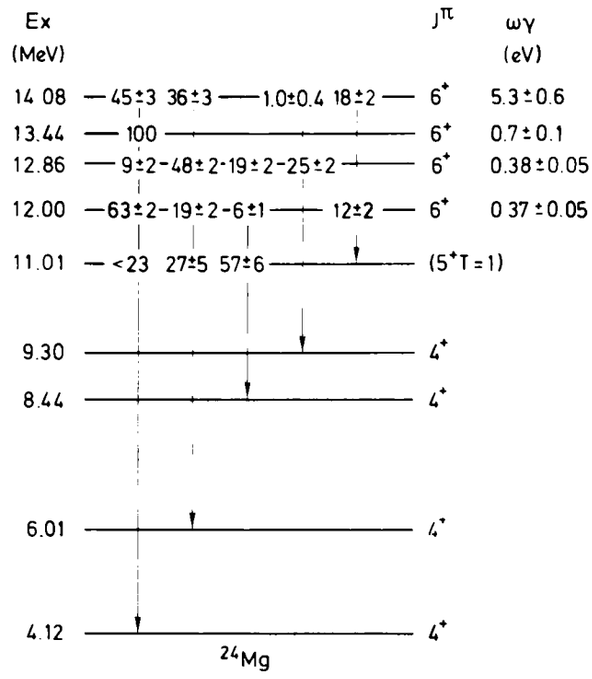

Fig. 7. Gamma-ray decay schemes and resonance strengths of known or probable 6^+ levels studied in the present work. The decay scheme of the 11.01 MeV level was derived from the spectrum of the 14.08 MeV level, but the branching ratio to the 8.44 MeV level derived from the spectrum of the 12.00 MeV level (53 ± 10 %) is in good agreement.

background contribution of 2.75 MeV γ-rays from the ^{21}Ne(α, nγ)^{24}Mg reaction was subtracted using the off-resonance spectrum which was taken within a few keV of the resonance energy. It is apparent from fig. 8 that the off-resonance yield was very small compared with the on-resonance yield for this resonance, but for some of the resonances at higher bombarding energy this was not the case. The necessity for background subtraction introduced an additional uncertainty into the determination of the resonance position which, in turn, increased the uncertainty in the corrected γ-ray yield.

The corrected angular distributions for the 12.00 MeV level are shown in fig. 9, together with χ^2 plots for the R $\rightarrow$ 4.12 MeV transition. Spin 5 is seen to be ruled out at the 0.1 % confidence level, while spins of 4 and 6 give equally good fits, in the case of 6 for a mixing ratio δ(E2 M3) of zero. Although spins 2 and 3 are ruled out at 1 % confidence, they cannot be ruled out at 0.1 %. However, spin 2 may be excluded since it requires an unreasonably large M3 enhancement of > 750 W.u. For spin 3, the M2 enhancement is > 1 W.u. which, while large, does not exceed the recommended upper limit of 3 W.u. [ref. [17])]. The angular distribution of the R $\rightarrow$ 6.01 MeV transition is very similar to that of the R $\rightarrow$ 4.12 MeV transition, and yields similar mixing ratios for spin hypotheses of 3, 4 and 6. Hence, although $J^\pi = 3^-$ and 4^+ cannot be ruled out for the 12.00 MeV level, the absence of decays to levels with $J < 4$, and the close similarity of the angular distributions of the R $\rightarrow$ 4.12 and R $\rightarrow$ 6.01 MeV transitions, make $J^\pi = 6^+$ the more likely

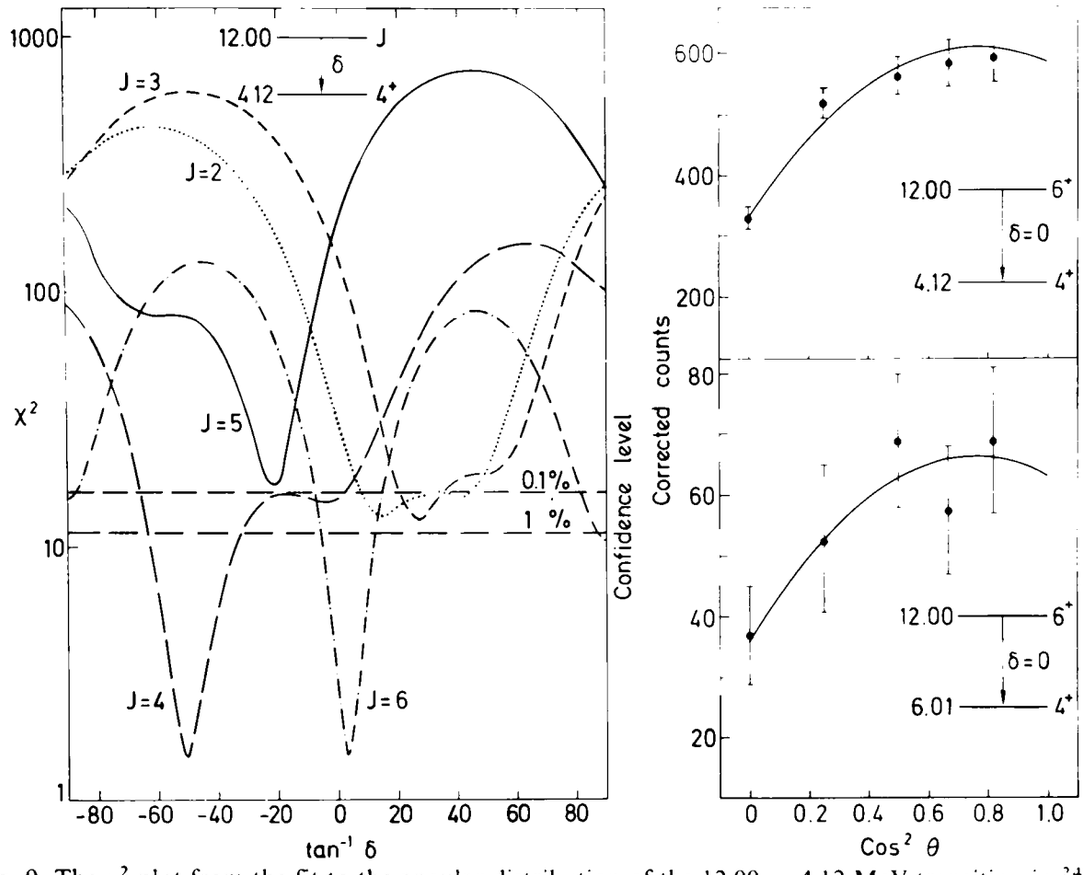

Fig. 9. The χ^2 plot from the fit to the angular distribution of the 12.00 → 4.12 MeV transition in ^{24}Mg. The angular distributions of both the 12.00 → 4.12 and 12.00 → 6.01 MeV transitions are also shown, and the solid lines are best fits for $J = 6$ and $\delta = 0$.

γ-decay of the 9.30 MeV level identifies it as the level observed [20]) in ^{24}Al β-decay and assigned spin and parity $(3, 4)^+$. From the value of the radiative width for the 12.86 → 9.30 MeV transition the 3^+ assignment may be rejected as implying an unreasonably large M3 strength for this transition, leaving 4^+ as the only possible assignment for the 9.30 MeV level.

The level at 12.86 MeV was also observed as a ^{20}Ne(α, α′γ)^{20}Ne resonance, and the quantity $(2J+1)\Gamma_{\alpha_1}\Gamma_{\alpha_0}/\Gamma$ was determined from the resonance yield of 1.63 MeV γ-rays. Since the branching ratio $\Gamma_{\alpha_0}/\Gamma_{\alpha_0}+\Gamma_{\alpha_1}$ is known, the partial α-decay widths of the 12.86 MeV level may be deduced, and are given in table 4.

The level at 13.44 MeV. Again, a definitive spin and parity assignment of 6^+ and a value for the ratio $\Gamma_{\alpha_0}/\Gamma_{\alpha_1}$ have been established previously from α-α angular correlation measurements [9]). The 13.44 MeV level was found to γ-decay only to the lowest 4^+ state at 4.12 MeV.

Extraction of the inelastic scattering yield for this resonance was complicated by the presence of a broad resonance (no. 36) upon which the 13.44 MeV level appeared as a shoulder. Therefore, the yield of 1.63 MeV γ-rays from the 13.44 MeV level was obtained from the yield curve rather than from the on-resonance γ-ray spectrum. The region of the yield curve around the 13.44 MeV level was decomposed into its

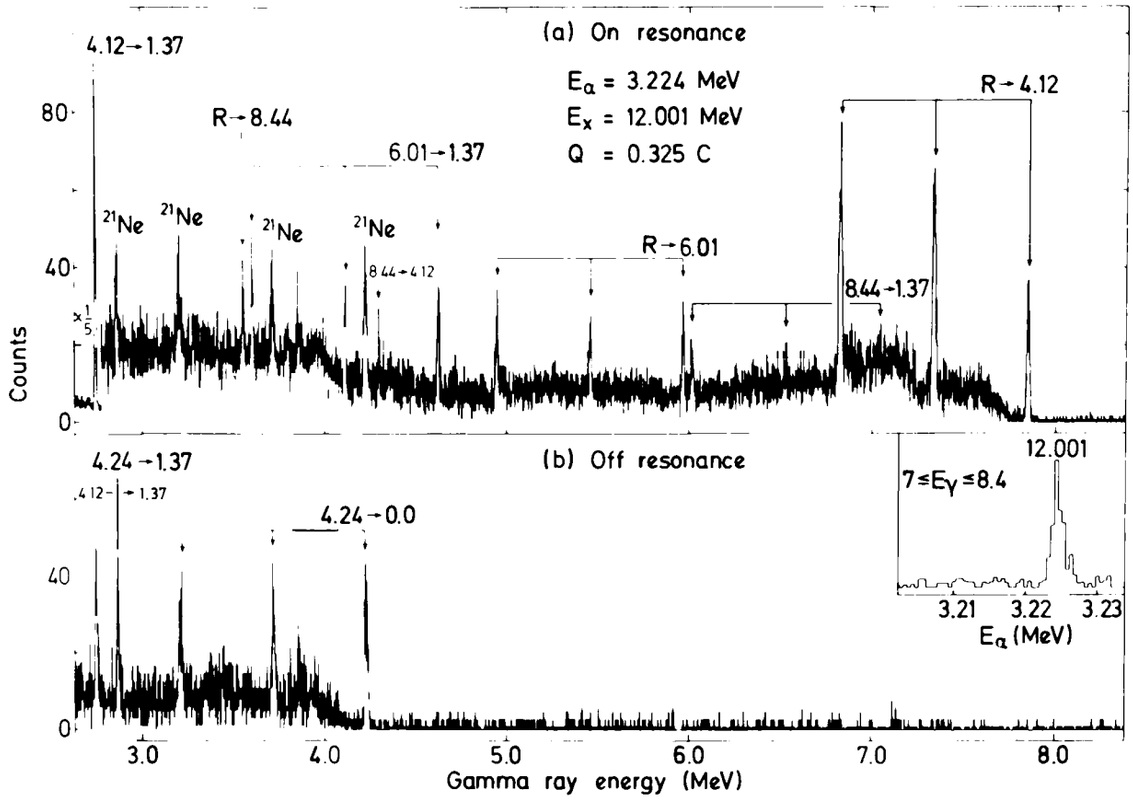

Fig. 8. Spectra of γ-rays at the 3.224 MeV resonance, and 15 keV below resonance. The 85 cm^3 Ge(Li) detector was positioned 9 cm from the target at 125° to the incident beam. Q is the accumulated charge of $^4He^{++}$ for the on-resonance spectrum, and the off-resonance spectrum has been normalised to the same total charge. Peaks are labelled with the transition in ^{24}Mg, and peaks labelled ^{21}Ne arise from the ^{21}Ne(α, nγ)^{24}Mg reaction and are identified in (b). The inset shows the relevant portion of the yield curve taken at a target pressure of 200 μm.

assignment, and in subsequent discussion we shall assume that the 12.00 MeV level has $J^\pi = 6^+$.

Previous published information on this state is limited to the observation [18]) in the ^{12}C(^{16}O, α)^{24}Mg reaction of a level at 12.00 MeV which is very strongly excited at a beam energy of 46.0 MeV. Very recently, however, Young *et al.* [19]) have used this reaction to populate the 12.00 MeV level and have measured the angular correlation of the α-particles from the subsequent decay to the ^{20}Ne ground state. The resulting correlation is well described by approximately equal admixtures of $J = 6$ and $J = 3$, the latter arising from the known 3^- state at 12.016 MeV, and provides strong support for a 6^+ assignment to the 12.00 MeV level observed in the present work. It is probable that the 6^+ component in the angular correlation is comparatively weak because the dominant decay mode of the 12.00 MeV level is γ-ray emission (see subsect. 5.2).

The level at 12.86 MeV. This level is known to have $J^\pi = 6^+$ from α-α angular correlation measurements [9]) employing the ^{16}O(^{12}C, $\alpha\alpha$)^{20}Ne reaction. In the present work, γ-ray decays to the 4^+ levels at 4.12, 6.01 and 8.44 MeV and to a level at 9.30 MeV were observed and are indicated in the γ-ray spectrum of fig. 10. The subsequent

For angular distribution measurements two detectors were employed. One detector (13% intrinsic germanium) was used to measure the intensity at different angles, while the other (16% Ge(Li)) was kept fixed usually at 135° or 145° to the beam direction. The Doppler shift measured by the fixed monitor enabled the determination of the resonance profile to be independent of the position of the other detector, and it also provided a continuous check on the profile, enabling the effects of possible drifts in beam energy to be determined.

Although in principle this method could be used to measure resonance strengths absolutely, systematic uncertainties in stopping power, gas pressure distribution and beam current measurement would make the final error considerable, so measurements were made relative to a resonance of known strength. The resonance chosen for most of this work was the 6.93 MeV T=1 resonance (E_x=10.27 MeV) with $J^{\pi}=2^+$. The $\omega\gamma$ for the primary decay mode of this resonance has been measured on several occasions [In76a; Sn78]. In Chapter four the work performed on this state is described, and the $\omega\gamma$ was measured relative to the 5.06 MeV T=0 resonance (E_x=8.78 MeV) with $J^{\pi}=6^+$, whose strength has been measured by Rogers et al. [Ro71f].

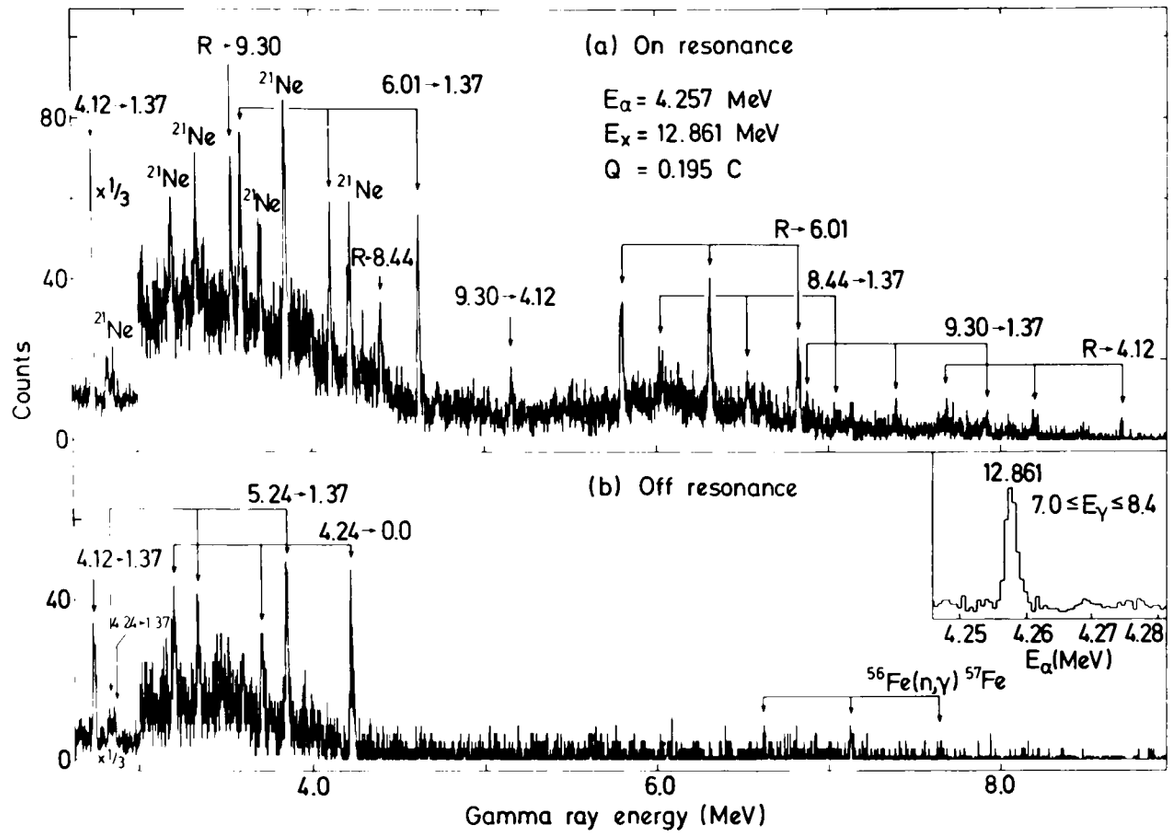

Fig. 10. As for fig. 8, but for the 4.257 MeV resonance. The α-particle energy was 18 keV higher for the off-resonance spectrum than for the on-resonance spectrum.

two component resonances, and the resulting number of 1.63 MeV γ-rays from the 13.44 MeV level alone was compared with the number at the peak of the 12.86 MeV level in order to determine the quantity $(2J+1)\Gamma_{\alpha_1}\Gamma_{\alpha_0}/\Gamma$. The partial α-decay widths of the 13.44 MeV level are given in table 4.

The level at 13.85 *MeV.* This level decays almost exclusively by α-particle emission to the 1.63 MeV level in ^{20}Ne, a property which necessitated an α-α-γ angular correlation measurement [9]) to determine its spin and parity as 6^+ rather than the simpler α-α angular correlation method applicable to states with an appreciable branch to the ^{20}Ne ground state. For the same reason, the 13.85 MeV level was not observed as a ^{20}Ne(α, γ)^{24}Mg resonance in the present work. It was, however, observed as a weak resonance in the ^{20}Ne(α, α′γ)^{20}Ne reaction. The resonant yield of 1.63 MeV γ-rays was extracted from the yield curve by comparison with the yield at the resonance corresponding to the 12.86 MeV (6^+) level. The resulting partial α-particle decay widths for the 13.85 MeV level are given in table 4.

The level at 14.08 MeV. Angular correlation measurements employing the ^{16}O(^{12}C, α)^{24}Mg reaction indicated that at least three levels were contributing to the peak in the α-particle spectrum at the expected position of the 14.15 MeV 8^+ level. In addition to the 8^+ level, levels with possible J^π assignments of 6^+ and 4^+ were proposed, with the 6^+ level lying somewhat lower in excitation energy than the 8^+

TABLE

Alpha particle widths of

Level	E_x (MeV)	$\omega\gamma_\alpha$ [a] (eV)	Γ_α/Γ [b]	Ground-Γ_α (eV)
6_3	12.00	[c]		> 0.022
6_4	12.86	2.4 ± 0.3	0.35 ± 0.04	0.33 ± 0.04
6_5	13.44	15 ± 5	0.23 ± 0.03	1.6 ± 0.6
6_6	13.85	40 ± 10	0.03 ± 0.01	3.0 ± 1.3
6_7	14.08	1160 ± 165	> 0.7 [f]	$250 < \Gamma_\alpha < 1000$
8_1	11.86			$< 1.2 \times 10^{-4}$ [i]
8_2	13.21			$< 2.2 \times 10^{-3}$ [i]
8_3	14.15		0.22 ± 0.04	0.075 ± 0.016 [j]

[a]) $\omega\gamma_\alpha = (2J+1)\Gamma_\alpha\Gamma_\alpha/\Gamma$

[b]) Derived from the present work and from α-particle branching ratios in ref. [9]). Errors were estimated from

[c]) $\vartheta_\alpha^2 = \Gamma_\alpha/(2\hbar^2 P_L/\mu R^2)$, where μ is the reduced mass of the ^{20}Ne+α system, $R = r_0\,(20^{1/3}+4^{1/3})$ fm,

[d]) Ref. [11]).

[e]) The 12.00 MeV level was not observed as a ^{20}Ne(α, α′)^{20}Ne* resonance.

[f]) See text.

[g]) Calculations are not available for this level.

[h]) Using $\Gamma_\alpha/\Gamma = 0.85 \pm 0.15$.

[i]) Ref. [9]).

[j]) Derived from known α-particle and γ-ray branching ratios [9]) using our measured value of Γ_γ.

level. The experimental resolution of these measurements was 100 keV. The much higher energy resolution of the present work has allowed us to resolve the individual levels, and sharp states were observed at 14.08, 14.10, 14.146 and 14.153 (8^+) MeV. Gamma-ray decay schemes and angular distributions were measured for the three lower levels. These showed that only the 14.08 MeV level is a candidate for the 6^+ level suggested by the ^{16}O(^{12}C, α)^{24}Mg measurements, while both the 14.10 and the 14.146 MeV levels are most likely 4^+ levels. The 14.08 MeV level was found to decay to the 4^+ levels at 4.12 and 6.01 MeV and to a previously unobserved γ-decaying level at 11.01 MeV. On- and off-resonance γ-ray spectra for the 14.08 MeV level are shown in fig. 11, and the γ-ray angular distributions are shown in fig. 12, together with the results of fitting the R → 4.12 MeV transition for various spin hypotheses. Clearly, the only acceptable spin hypotheses are 4^+ with δ(E2/M1) = -0.85 ± 0.10 and 6^+ with δ(M3/E2) consistent with zero. A strong preference for the 6^+ over the 4^+ assignment is indicated by the results of the angular correlation study of states in this region, and supporting evidence from the present work is provided by the similarity of the R → 4.12 and R → 6.01 MeV angular distributions. Unfortunately, the 6^+ level suggested by the angular correlation work cannot be regarded as definitely established, and we must allow the possibility of a 4^+ assignment to the 14.08 MeV level. In subsequent discussion we will, however, assume that this level has $J^\pi = 6^+$.

4

6^+ and 8^+ levels in ^{24}Mg

state transitions		Transitions to 1.63 MeV state		
$\vartheta^2_{2_1}$ [c])	$A^2_{\gamma L}$ [d])	Γ_{2_1} (eV)	$\vartheta^2_{2_1}$ [c])	$A^2_{\gamma L}$ [d])
$> 7.6 \times 10^{-3}$	5.1×10^{-3}			
$(4.0 \pm 0.5) \times 10^{-3}$	8.6×10^{-3}	0.54 ± 0.08	0.10 ± 0.02	3.5×10^{-4}
$(3.5 \pm 1.3) \times 10^{-3}$	3.5×10^{-3}	4.9 ± 1.7	0.03 ± 0.01	2.5×10^{-3}
$(2.6 \pm 1.1) \times 10^{-3}$	2.2×10^{-2}	100 ± 40	0.13 ± 0.05	1.1×10^{-4}
$0.13 < \vartheta^2_{2_1} < 0.51$	[g])	105 ± 25 [h])	0.06 ± 0.014	[g])
$< 3.4 \times 10^{-2}$	2.7×10^{-3}			
$< 1.6 \times 10^{-3}$	2.8×10^{-3}			
$(3.7 \pm 0.8) \times 10^{-3}$	8.0×10^{-3}	0.18 ± 0.05 [j])	$(6.9 \pm 1.9) \times 10^{-3}$	2.5×10^{-2}

data in ref. [9]).
$P_L(kR)$ is the penetrability factor for relative orbital angular momentum L and wave number k.

Limits on the spin and parity of the 11.01 MeV level may then be obtained from analysis of the angular distribution of the R → 11.01 MeV transition. Acceptable fits were obtained for $J = 5$ with $\delta \approx 0$ and $J^\pi = 6^+$ with $\delta(\text{E2/M1}) = 1.26 \pm 0.33$. Any higher value of the spin is extremely unlikely since the 11.01 MeV level is observed to decay to 4^+ levels, and a 4^+ assignment requires an unreasonably large M3 component in the R → 11.01 MeV transition. A 5^- assignment to the 11.01 MeV level would require a 3.8 mW.u. transition from the 14.08 MeV level, which exceeds the recommended upper limit [17]) for isospin forbidden E1 decays. A 6^+ assignment similarly requires a 32 W.u. E2 transition from the 14.08 MeV level, which, while not ruled out, is rather unlikely. Hence the most likely spin and parity assignment for the 11.01 MeV level is 5^+. The transition from the 14.08 MeV level would then be a strong 0.12 W.u. M1 transition. This strength is characteristic of a $\Delta T = 1$ transition, making the 11.01 MeV level an excellent candidate for the first 5^+ $T = 1$ state in ^{24}Mg. It should be emphasized, however, that this conclusion rests upon the assumption of a 6^+ assignment to the 14.08 MeV level. The uncertainty in the spin of the 14.08 MeV level could be removed by a remeasurement of the ^{16}O(^{12}C, $\alpha\alpha$)^{20}Ne angular correlation with improved energy resolution.

The 14.08 MeV level was also observed as a ^{20}Ne(α, $\alpha'\gamma$)^{20}Ne resonance, and the resonant yield was extracted from a series of spectra taken at 0.7 keV intervals across

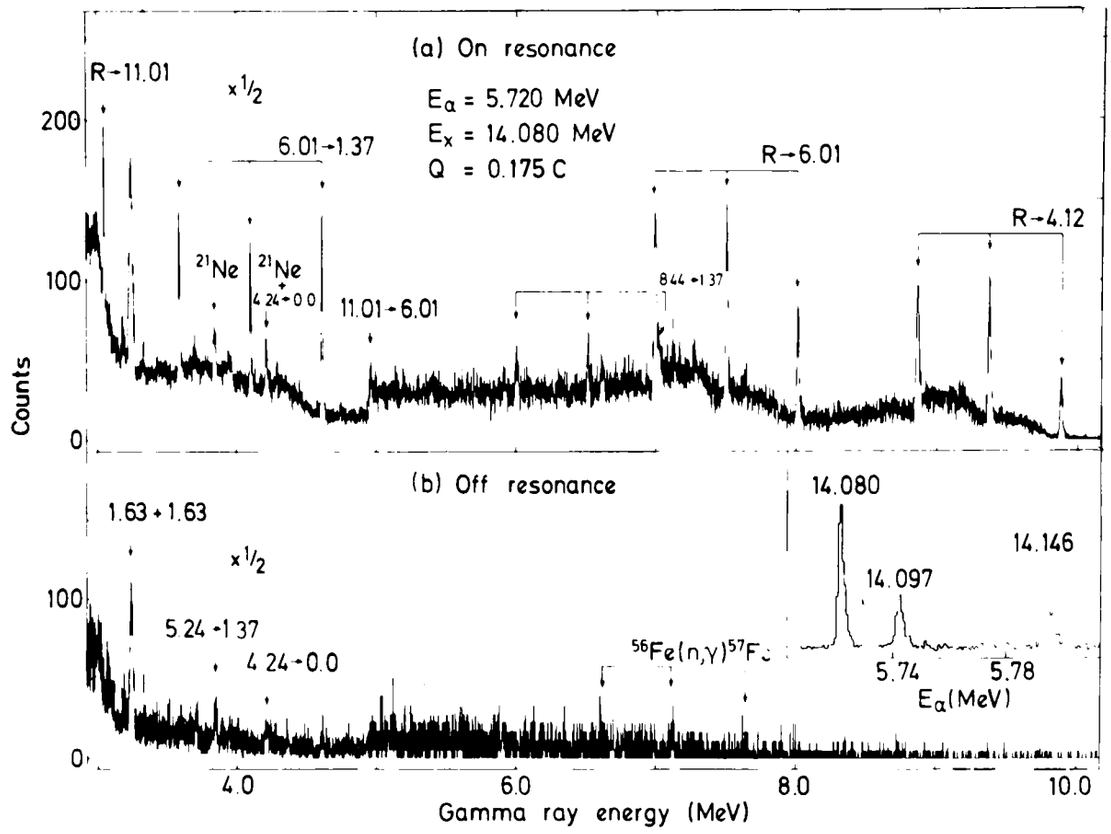

Fig. 11. As for fig. 8, but for the 5.72 MeV resonance, with the Ge(Li) detector 13 cm from the centre of the target and at 135° to the incident beam. The off-resonance spectrum was taken 7 keV below the on-resonance spectrum.

the resonance at a target pressure of 0.3 Torr. Corrections were applied for the loss of yield in such a thin target due to energy spread and straggling of the beam. The resulting α-particle widths are given in table 4.

5.2. DISCUSSION OF 6^+ $T = 0$ LEVELS

Electromagnetic transitions. A summary of the experimental information on E2 transition rates from 6^+ levels in ^{24}Mg is presented in table 3. For the 12.00 MeV level, only lower limits are listed because the quantity Γ_α/Γ has not yet been measured, and as we shall see below there are good reasons to believe that this ratio could be substantially less than unity. Also listed in table 3 are excitation energies and E2 transition rates calculated [6, 11]) with both the PW and CWC interactions.

We note first that, since there is a one-to-one correspondence between experimental and calculated levels, the shell-model calculations are predicting correctly the density of 6^+ levels in this region of excitation energy. From this fact we can probably conclude that 6^+ intruder states from outside the $(sd)^8$ basis are not important below 14 MeV in ^{24}Mg. Note also that the PW interaction gives a better account of the observed

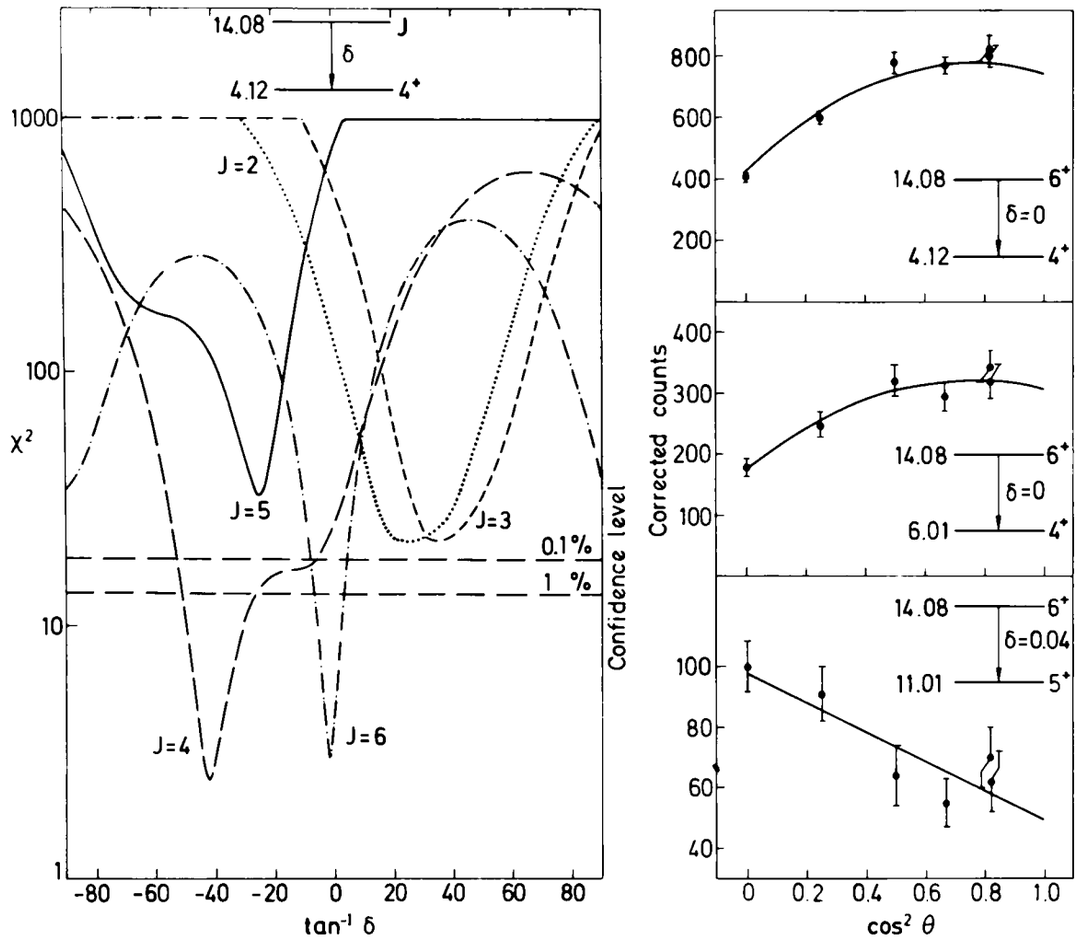

Fig. 12. The χ^2 plot from the fits to the angular distribution of the 14.08 → 4.12 MeV transition. The angular distributions for this transition and two other transitions are also shown, together with the best fits for the indicated spins and mixing ratios.

excitation energies than does the CWC interaction, the RMS deviations between calculation and experiment being 254 and 487 keV, respectively.

Secondly, the predicted electromagnetic transition rates for the third and higher 6^+ levels are markedly lacking in any notable features. All the calculated transition rates are weak, and in particular there is no hint of a $K^\pi = 4^+$ band arising from the (84) representation of SU(3) which gives rise [21]) to the well-known $K^\pi = 0^+$ and 2^+ bands. Experimentally, however, there is one outstanding feature, namely the 11 W.u. transition between the 12.86 (6_4) and 9.30 (4_4) MeV levels, which may indicate additional band structure in ^{24}Mg. The calculations spread approximately the same total transition strength to the 4_4 level over four 6^+ levels rather than concentrating it in a single level.

As far as the weaker transitions are concerned, it would be surprising if quantitative agreement between calculations and experiment were obtained. We know, for example, that there are deviations of a factor of two or more for the cross-band transitions between members of the $K^\pi = 2^+$ and $K^\pi = 0^+$ bands. Nevertheless,

the transitions from the 12.86 MeV level to the three lowest 4^+ states are reproduced rather well by both interactions. For the 12.00 MeV level, a quantitative comparison must await a measurement of the α-particle decay branching ratio (Γ_α/Γ), but we note that a reasonable value of about 0.3 would bring two of the three observed transitions into good agreement with the calculations employing the PW interaction, but not with those using the CWC interaction. For the higher lying 6^+ levels at 13.44 and 14.08 MeV on the other hand, there is little correspondence between measured and calculated transition rates apart from the qualitative observation that all are rather weak.

Alpha-particle widths. Alpha-particle widths of 6^+ and 8^+ levels in ^{24}Mg are summarised in table 4. With the exception of the 11.86 and 13.21 MeV 8^+ levels, all the values are from the present work using branching ratios from ref. [9]) where appropriate. The spectroscopic factors, ϑ_α^2, were derived from the measured widths using a radius parameter r_0 of 1.2 fm; increasing r_0 to 1.4 fm decreases ϑ_α^2 by a factor between 4 and 10 depending on the transition. Theoretical calculations by Kelvin *et al.* [11]), using wave functions generated with the CWC interaction, are tabulated in the final column. The quantity A_{NL}^2 is as defined by Ichimura *et al.* [22]), and when calculated with harmonic oscillator wave functions should be approximately equal to ϑ_α^2. The N and L are the oscillator quantum numbers for the c.m. of the α-particle, where $2N+L = 8$ if the same oscillator length parameters are used for the internal structure of the α-particle and for the sd shell wave functions. In deriving $\vartheta_{\alpha_0}^2$ for the 14.08 MeV level, we have assumed a conservative upper limit of 30 % on an α-particle branch to the 1.63 MeV level in ^{20}Ne, and have used $\Gamma_{\alpha_0}/\Gamma = 0.85 \pm 0.15$ in deriving $\vartheta_{\alpha_1}^2$.

Looking first at the ground-state decays, we note that with our particular choice of r_0, the experimental spectroscopic factors lie between 10^{-3} and 10^{-2}, and the calculations follow the same trend. The exception is the 14.08 MeV level, which appears to have a large ground-state spectroscopic factor if the 6^+ assignment is correct, but for which calculations are not available. For the 14.15 MeV (8^+) level, the rather satisfactory agreement between measured and calculated spectroscopic factors for the ground-state decay also extends to the excited state decay. However, this is certainly not the case for the 6^+ levels, where the excited state spectroscopic factors are an order of magnitude or more times larger than those for the ground-state transitions and the calculated values.

One aspect of table 4, concerning the 12.00 MeV level, merits further comment. The calculated reduced width for the ground-state α-decay corresponds to a partial width of 0.015 eV, which is considerably smaller than the predicted PW radiative width of 0.08 eV. It is probable therefore that the 12.00 MeV level will decay predominantly by γ-ray emission, and an independent measurement of its α-particle decay branching ratio is required before its radiative width can be determined from the value of $\omega\gamma$ measured in the present work. Such a measurement, employing the ^{12}C(^{16}O, α)^{24}Mg reaction, is in progress at another laboratory [19]).

6. The $T = 1$ states

6.1. EXPERIMENTAL RESULTS

The lowest 0^+, 5^+ and 6^+ $T = 1$ states in ^{24}Mg are predicted [6]) to lie at 13.12, 11.17 and 13.51 MeV, respectively, by the shell-model calculations employing the CWC interaction. In the present work we have located the 0^+ level at 13.04 MeV, and as noted in 5.1 above, the 5^+ level has probably been identified at 11.01 MeV. However, no resonance with the expected properties of the 6^+ $T = 1$ level has been observed, although information from other reactions indicates that it is probably to be found at 13.37 MeV. Below, we consider each level in turn.

The state at 13.04 MeV. This level corresponds to a weak resonance ($\omega\gamma$ = 0.73 ± 0.09 eV) at 4.475 MeV, which was observed to decay only to the $J = 1$ levels at 7.55, 7.75, 8.44, 9.83 and 9.97 MeV. The decay scheme immediately suggests a 0^+ assignment to the 13.04 MeV level, and this was reinforced by analysis of the angular distributions of the R → 9.83 and 9.83 → 0 MeV transitions shown in fig. 13. Equally good fits are obtained for the three possible assignments ($J = 0$, 1 or 2) consistent with the decay scheme and resonance strength. However, the fit for $J = 1$ implies an unreasonably large M2 enhancement of > 1500 W.u. for the R → 9.83 MeV transition, leaving $J^\pi = 0^+$ or 2^+ as possible assignments. The strength of the R → 9.83

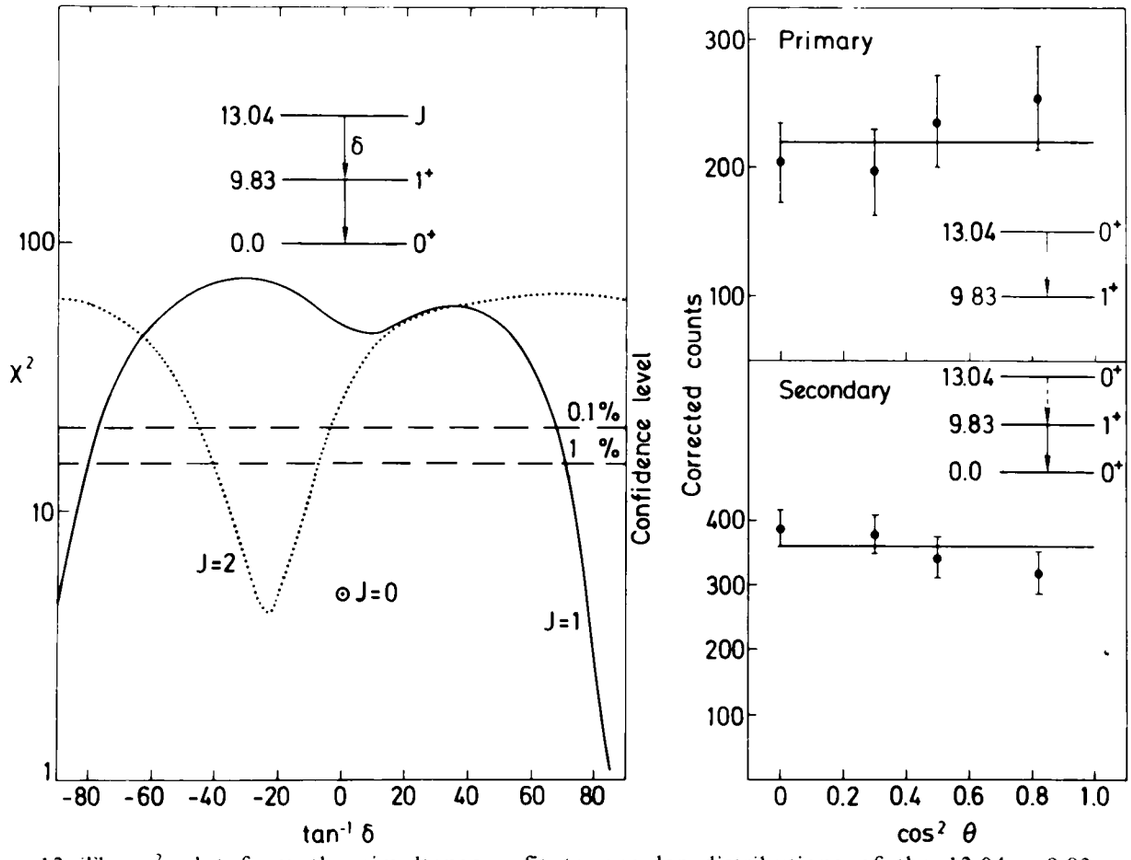

Fig. 13. The χ^2 plot from the simultaneous fit to angular distributions of the 13.04 → 9.83 and 9.83 → 0.0 MeV transitions, together with the angular distributions and the best fit for spin zero.

MeV transition corresponds to a 0.44 or a 0.09 W.u. M1 transition for $J = 0$ and $J = 2$ respectively, both of which exceed the recommended upper limit [17]) for isospin retarded M1 transitions. Hence we conclude that the 13.04 MeV level has $T = 1$. It follows that a 2^+ assignment to this level is unlikely since the isospin allowed M1 transitions to the low-lying 2^+ states at 1.37 and 4.24 MeV are not observed, in spite of the much larger energy available to these transitions. Therefore, $J^\pi = 0^+$ is the most probable assignment for the 13.04 MeV level, and in future discussion we will assume this to be the case.

The state at 11.01 MeV. This level, which decays predominantly by γ-ray emission to 4^+ levels, was observed to be fed by a 3.07 MeV γ-ray from the probable 6^+ $T = 0$ level at 14.08 MeV. The evidence in favour of it being the lowest 5^+ $T = 1$ level is summarised in subsect. 5.1.

The state at 13.37 MeV. The signature of the lowest 6^+ $T = 1$ level in ^{24}Mg is expected to be a strong γ-ray transition to the lowest 5^+ $T = 0$ level at 7.81 MeV, with a predicted radiative width of 0.14 eV. A careful search was made for a resonance with this property in the ^{20}Ne(α, γ)^{24}Mg reaction in the vicinity of 13.4 MeV in ^{24}Mg, but with a negative result. Thus we conclude that the 6^+ $T = 1$ level probably has a very small α-particle width. Such a result is not unexpected, since the two nearby 6^+ $T = 0$ levels with which mixing might occur have α-particle widths of only 0.3 and 1.5 eV.

However, there is evidence in the literature for the observation of the 6^+ $T = 1$ level in both the ^{23}Na(p, γ)^{24}Mg and the ^{16}O(^{12}C, $\alpha\gamma$)^{24}Mg reactions, although these observations have not been interpreted in this way. In two recent studies [23,24]) of the former reaction, a resonance at 1748 keV (13.365 MeV in ^{24}Mg) was observed to decay with a 26 % γ-ray branch to the 7.81 MeV (5^+) level. The other dominant γ-ray branch fed a level at 10.58 MeV which has the properties expected [11]) of the second 5^+ $T = 0$ level in ^{24}Mg. Neither set of authors allowed the possibility of a 6^+ assignment to the 13.365 MeV level owing to the observation of a weak branch to the 1.37 MeV (2^+) level. However, since the branching ratio quoted in ref. [23]) differs by a factor of three from that in ref. [24]), it is probable that this branch can be attributed to a 15 keV wide resonance at 1735 keV.

Supporting evidence for the identification of the 13.365 MeV level as the 6^+ $T = 1$ level is provided by the observation [9]) of a state at 13.34 ± 0.03 MeV in the ^{16}O(^{12}C, α)^{24}Mg reaction with parity $(-1)^J$ and for which the only observed decay mode was γ-ray emission. As expected of a $T = 1$ state, this level was very weakly populated and as a consequence it was unfortunately not possible to determine its γ-ray decay scheme. The only difficulty in identifying this level with that observed in the ^{23}Na(p, γ)^{24}Mg reaction arises from the total width of 1.6 ± 0.7 keV quoted by Meyer *et al.* [23]) for the 1748 keV resonance. If correct, this would be inconsistent with the ^{16}O(^{12}C, $\alpha\gamma$)^{24}Mg observations, but since the value of Γ is comparable with the experimental resolution and the error is large, an independent measurement of this width is clearly desirable. Further measurements on the 1748 keV resonance in the

^{23}Na(p, γ)^{24}Mg reaction are underway, including a measurement of the γ-ray angular distribution and a careful determination of its width.

6.2. DISCUSSION OF $T = 1$ LEVELS

Excitation energies. Fig. 14 shows the level scheme of known or inferred $T = 1$ levels in ^{24}Mg and their probable analogues in ^{24}Na, together with the CWC predictions [6]). The comparison between calculated and experimental energies is based upon binding energies relative to ^{16}O. The rather large underbinding of 178 keV for

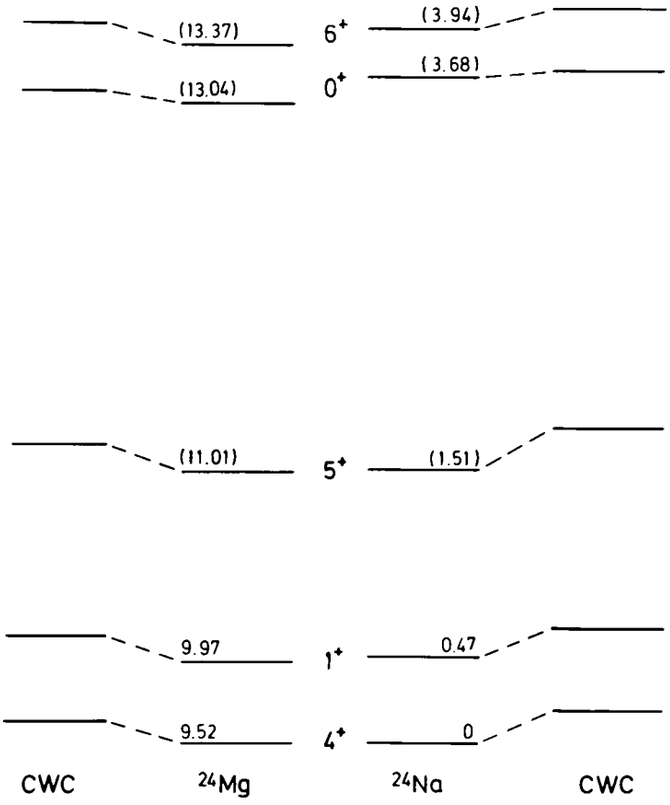

Fig. 14. Measured and calculated energy spectra of $T = 1$ levels in ^{24}Mg and ^{24}Na, where we have aligned the observed 4^+ $T = 1$ level at 9.52 MeV in ^{24}Mg with the ^{24}Na ground state. The positions of the calculated levels were determined by comparing calculated and experimental binding energies relative to ^{16}O. Levels in parentheses do not have their spins definitely established.

the ^{24}Na ground state has already been noted by Kelvin, Watt and Whitehead [6]), who suggest that it may arise from an underestimation of the Coulomb correction for ^{24}Na in the derivation [5]) of the nuclear two-body matrix elements of the CW interaction. A somewhat smaller underbinding of the analogue states in ^{24}Mg would then also be expected and this is certainly observed. However, if this systematic effect is removed by lowering the calculated energies by 118 and 142 keV in ^{24}Mg and ^{24}Na, respectively (the average underbindings for the five levels shown), then the rms deviation between calculation and experiment becomes an impressive 32 keV for

^{24}Mg, while for ^{24}Na it is 69 keV. We also note from fig. 14 that the excited levels in ^{24}Na generally lie higher than their counterparts in ^{24}Mg. The calculations exhibit the same trend, although with the exception of the 5^+ level the calculated Coulomb energy differences are somewhat smaller than the experimental ones.

Electromagnetic transition rates. Table 5 summarises the available information on the electromagnetic decays of $T = 1$ levels in ^{24}Mg. We have assumed for the purposes of this discussion that the levels at 11.01 and 13.37 MeV are indeed the 5^+ and 6^+ $T = 1$ levels, and that the level at 10.58 MeV populated in the decay of the 13.37 MeV level is the second 5^+ $T = 0$ level. The calculations are those of Kelvin, Watt and Whitehead [11]) using the CWC interaction.

Of these five $T = 1$ levels, only the 0^+ and 1^+ levels have had their electromagnetic transition rates measured. For the 0^+ level, the measured rates of the transitions to each of the three lowest 1^+ levels in ^{24}Mg are seen from table 5 to be reproduced remarkably well by the calculations. It is somewhat puzzling therefore that similar agreement between measured and calculated rates is not found for the transition between the 9.97 MeV (1^+ $T = 1$) level and the ground state, where the rate deduced from inelastic electron scattering [25]) is a factor of three greater than the calculated rate.

TABLE 5

Electromagnetic transition strengths of $T = 1$ levels in ^{24}Mg

E_x (MeV)	J^π	Transition	B(M1) (W.u.)		Branching ratio	
			exp	calc [c])	exp	calc [c])
9.52 [a])	4_5^+ $T = 1$	$4_5 \rightarrow 4_1$		2.1×10^{-2}	49 ± 6	57
		$4_5 \rightarrow 4_2$		1.4×10^{-2}	6 ± 1	11
		$4_5 \rightarrow 4_3$		1.3	39 ± 5	28
		$4_5 \rightarrow 3_1$		3.1×10^{-3}	3.8 ± 0.4	4.2
9.97 [b])	1_3^+ $T = 1$	$1_3 \rightarrow 0_1$	0.22 ± 0.02	0.07	90 ± 10	62
11.01 [c])	5_3^+ $T = 1$	$5_3 \rightarrow 4_1$		5.6×10^{-4}	< 23	2
		$5_3 \rightarrow 4_2$		0.02	27 ± 5	35
		$5_3 \rightarrow 4_3$		0.16	57 ± 6	36
		$5_3 \rightarrow 6_1$		0.08	< 15	14
13.04 [c])	0_6^+ $T = 1$	$0_6 \rightarrow 1_1$	0.07 ± 0.01	0.09	36 ± 3	40 [f])
		$0_6 \rightarrow 1_2$	0.44 ± 0.07	0.52	52 ± 4	53
		$0_6 \rightarrow 1_3$	0.11 ± 0.02	0.07	12 ± 2	7
13.37 [d])	6_6^+ $T = 1$	$6_6 \rightarrow 5_1$	> 0.007	0.04	26 ± 3	27 [f])
		$6_6 \rightarrow 5_2$	> 0.16	0.82	74 ± 3	73

[a]) Data from Endt and Van der Leun [16]).
[b]) B(M1) from Johnston and Drake [25]). Branching ratio from Endt and Van der Leun.
[c]) Present work.
[d]) Data from Meyer *et al.* [23]) and Boydell and Sargood [24]).
[e]) Calculations of Kelvin, Watt and Whitehead [11]) using the CWC interaction. (1 W.u. = $1.79\mu_N^2$.)
[f]) Calculated and experimental branching ratios are normalised to 100 for the transitions shown. Branches were also observed from the 13.04 MeV level to the 1^- levels at 7.55 ($(6 \pm 2)\%$) and 8.44($(13 \pm 2)\%$) MeV.

CHAPTER 3

THE NUCLEUS ^{20}Ne

3.1 Introduction

In chapter one it was stated that the independent particle shell model has been successful in accounting for the properties of the excited states of light nuclei provided that only a few ($\lesssim 8$) valence particles or holes need be considered and that the model space can conveniently be truncated so as to reduce the problem to manageable proportions. The model is also successful in predicting the spin and parity of nuclear ground states over a much larger mass range, only failing when the assumption of a spherical potential well is known to be invalid.

The simple shell model has some notable failures. In particular it cannot account for the nature of even the lowest excited states of nuclei in the rare-earth and actinide regions of the periodic table, where the energy levels resemble the rotational bands of molecules and E2 transition strengths of many (~100) single particle units are observed. Even in light nuclei near a closed shell, where the shell model should be at its best, the significant E2 γ-decay of the first excited state of ^{17}O cannot be explained, since this decay ought to involve only a neutron.

An explanation of these phenomena is provided by the collective model, which pictures a deformed nucleus experiencing bulk rotational or vibrational excitation with consequent enhanced transition strengths due to the many particles involved.

For the 4^+ and 5^+ $T = 1$ levels, only branching ratios are available from experiment, while for the 6^+ state, lower limits on the transition strengths are also available from the measured value [23]) of $(2J+1)\Gamma_\gamma\Gamma_p/\Gamma$. The calculations are seen to reproduce the measured branching ratios very well for each of these three levels. In the case of the 11.01 and 13.37 MeV levels this agreement lends additional support to the identification of them as the lowest 5^+ and 6^+ $T = 1$ levels in ^{24}Mg. Further support for the 6^+ $T = 1$ assignment to the 13.37 MeV level comes from the lower limits on the reduced transition probabilities given in table 5. The strength of the transition to the 10.58 MeV level requires that either the initial or final state must have $T = 1$, since the lower limit in table 5 already exceeds the recommended upper limit [17]) of 0.03 W.u. for isospin retarded M1 transitions. Similar arguments hold if this transition is E1 rather than M1. If J is less than 6, then the lower limits are increased by a factor $13/(2J+1)$. Since there is no counterpart in ^{24}Na of the 10.58 MeV level in ^{24}Mg it follows that the 13.37 MeV level must have $T = 1$.

7. Summary and conclusions

Kelvin, Watt and Whitehead [6]) have shown that the new CWC interaction is clearly superior to the PW interaction as far as energy spectra in mass-24 nuclei are concerned. However, an improvement in the prediction of excitation energies, many of which were included in the fitting procedure, does not necessarily imply that the wave functions will give a better account of other nuclear properties. To test the wave functions, we must turn to a comparison between experiment and the model calculations for other properties, such as electromagnetic transition rates, which are sensitive to details of the nuclear wave functions. In the present work we have obtained a considerable body of information on the radiative and α-particle widths of a number of positive-parity states which may be employed in such a comparison. These states, although they occur at high excitation energy, may nevertheless be identified with levels generated by the shell-model calculations by virtue of having either high spin or non-zero isospin. The subsequent comparison between the observed and calculated properties of these states has highlighted some interesting features of the shell-model calculations.

(i) For radiative transitions between levels of the $K^\pi = 0^+$ and 2^+ bands with spins less than 8, the new CWC and the older PW interactions yield similar transition rates [10, 11]) which reproduce the measured in-band transition rates reasonably well and the cross-band transition rates somewhat less well. For the $J = 8$ levels, however, the predictions of the two calculations are markedly different and surprisingly it is the PW interaction which yields results in excellent agreement with experiment.
(ii) The PW interaction also appears to give a better account of the 6^+ levels studied here. The excitation energies of these particular levels are more accurately reproduced by the PW interaction than by the CWC interaction, and the indications are that the radiative transition rates of the third 6^+ level are also better accounted for by the

former interaction. Neither interaction, however, is able to reproduce the observed decay rate of the strongly enhanced $6_4 \rightarrow 4_4$ transition.

(iii) Alpha-particle widths have been measured for several of the 6^+ levels and for the 14.15 MeV 8^+ level, and α-particle spectroscopic factors extracted. Comparison may only be made with spectroscopic factors calculated with the CWC interaction, since calculations with the PW interaction are not available. We find that satisfactory agreement between calculated and experimental spectroscopic factors is obtained for transitions to the ^{20}Ne ground state, but that transitions to the 1.63 MeV level from 6^+ states are in general substantially stronger than the calculated values. The transition from the 14.15 MeV 8^+ level to the 1.63 MeV level in ^{20}Ne is, however, well reproduced by the calculations.

(iv) The lowest 0^+, 5^+ and 6^+ $T = 1$ levels in ^{24}Mg have probably been identified at 13.04, 11.01 and 13.37 MeV, respectively. Again, calculations employing the CWC interaction are the only ones available. We find that the calculated excitation energies are $\approx$ 100 keV higher than the observed energies, but this discrepancy can probably be attributed to the use of an incorrect binding energy for ^{24}Na in the derivation of the CWC interaction. However, the relative spacings of the known $T = 1$ levels in ^{24}Mg are very accurately reproduced by the calculations. Of the electromagnetic transition rates, absolute values have been measured for only the 0^+ level, although γ-ray branching ratios are available for the 5^+ and 6^+ levels. In each case, the transition rates or branching ratios calculated using the CWC interaction are in remarkable agreement with the experimental values. This agreement also extends to the γ-ray branching ratios of the 4^+ $T = 1$ level at 9.52 MeV. In fact, the only property of the known $T = 1$ levels which is not well reproduced by the calculations is the rate of the transition from the 1^+ $T = 1$ level (9.97 MeV) to the ^{24}Mg ground state, which is a factor of three larger than the calculated value.

In summary then, we have seen that the older PW interaction is in general as good as the new CWC interaction in reproducing electromagnetic transition rates of $T = 0$ levels in ^{24}Mg, and in certain cases, most notably the 8^+ member of the $K = 2^+$ band, is markedly better. However, the CWC interaction appears to account very well for both the excitation energies and radiative decays of low-lying $T = 1$ states in ^{24}Mg.

We wish to express our gratitude to Drs. Kelvin, Watt and Whitehead for permission to quote the results of their calculations prior to publication. We are also grateful to them, and to Dr. I. F. Wright for several useful discussions, and we thank E. F. Garman for assistance with the experiments.

References

1) R. R. Whitehead, Nucl. Phys. **A182** (1972) 290
2) T. T. S. Kuo, Nucl. Phys. **A103** (1967) 71
3) T. T. S. Kuo and G. E. Brown, Nucl. Phys. **85** (1966) 40
4) B. M. Preedom and B. H. Wildenthal, Phys. Rev. **C6** (1972) 1633

5) W. Chung, Thesis, Michigan State University, 1976, unpublished
6) D. Kelvin, A. Watt and R. R. Whitehead, J. of Phys. **G3** (1977) 1539
7) D. Branford, A. C. McGough and I. F. Wright, Nucl. Phys. **A241** (1975) 349
8) D. Branford, M. J. Spooner and I. F. Wright, Particles and Nuclei **4** (1972) 231
9) L. K. Fifield, R. W. Zurmühle and D. P. Balamuth, Phys. Rev. **C8** (1973) 2217
10) L. K. Fifield, M. J. Hurst, T. J. M. Symons, F. Watt and K. W. Allen, Phys. Letts. **69B** (1977) 45
11) D. Kelvin, A. Watt and R. R. Whitehead, to be published
12) F. Watt, L. K. Fifield, M. J. Hurst, T. J. M. Symons, C. H. Zimmerman and K. W. Allen, Nucl. Instr. **151** (1978) 163
13) M. R. Wormald and J. Takacs, Nucl. Instr. **113** (1974) 263
14) P. D. Ingalls, Nucl. Phys. **A265** (1976) 93
15) L. C. Northcliffe and R. F. Schilling, Nucl. Data **7A** (1970) 233
16) P. M. Endt and C. van der Leun, Nucl. Phys. **A214** (1973) 1
17) P. M. Endt and C. van der Leun, Nucl. Data **13A** (1974) 67
18) J. L. C. Ford, J. Gomez del Campo, R. L. Robinson, P. H. Stelson and S. T. Thornton, Nucl. Phys. **A226** (1974) 189
19) K. C. Young, Jr., J. M. Lind, D. P. Balamuth and R. W. Zurmuhle, Bull. Amer. Phys. Soc. **27** (1978) 520, and private communication
20) C. Detraz, Nucl. Phys. **A188** (1972) 513
21) M. Harvey, in Advances in nuclear physics, vol. 1 (Plenum, NY, 1968) p. 67
22) M. Ichimura, A. Arima, E. C. Halbert and T. Terasawa, Nucl. Phys. **A204** (1973) 225
23) M. A. Meyer, J. P. L. Reinecke and D. Reitmann, Nucl. Phys. **A185** (1972) 625
24) S. G. Boydell and D. G. Sargood, Austral. J. Phys. **28** (1975) 369
25) A. Johnston and T. E. Drake, J. of Phys. **A7** (1974) 898

Journal of
Physics G
Nuclear
Physics

A study of the reaction $^{16}O(^{3}He, p)^{18}F$

H M Sen Gupta, M J Hurst and F Watt

Nuclear Physics Laboratory, University of Oxford, Keble Road, Oxford OX1 3RH, UK

Reprinted from Journal of Physics G: Nuclear Physics **2** 935–949 (1976)

Journal of Physics G: Nuclear Physics
Covering theoretical and experimental topics in nuclear and particle physics, weak, strong and electromagnetic interactions, and those aspects of cosmic rays relevant to nuclear and particle physics.

Published by The Institute of Physics, Bristol and London
Bristol Publishing Office: Techno House, Redcliffe Way, Bristol BS1 6NX (England)

J. Phys. G: Nucl. Phys., Vol. 2, No. 12, 1976. Printed in Great Britain.

A study of the reaction $^{16}O(^3He, p)^{18}F$

H M Sen Gupta†, M J Hurst and F Watt
Nuclear Physics Laboratory, University of Oxford, Keble Road, Oxford OX1 3RH, UK

Received 28 June 1976

Abstract. The $^{16}O(^3He, p)^{18}F$ reaction has been studied at 18 MeV and angular distributions have been measured for observed levels up to 10 MeV. The distributions for the 2p–0h positive parity states have been analysed in terms of the DWBA theory for a two-nucleon stripping process and good agreement has been obtained in most cases up to a centre-of-mass angle of 90 Eleven new levels in ^{18}F have been observed between E_x = 7 MeV and 10 MeV. Tentative J^π assignments have been made for some of them.

NUCLEAR REACTIONS $^{16}O(^3He, p)^{18}F$, E = 18 MeV; measured $\sigma(E_p, \theta)$. ^{18}F; deduced levels. DWBA analysis.

1. Introduction

The odd–odd nucleus ^{18}F, with two particles outside the closed ^{16}O shell, has been the subject of a great deal of interest during the last decade (Rolfs *et al* 1973a, b, c, d, e, Sens *et al* 1973a, b and references therein). The low-lying levels arise from three basic configurations, namely 2p–0h positive parity states, 4p–2h positive parity states leading to pronounced rotational bands and 3p–1h (including some small 5p–3h admixture) negative parity states which may also exhibit some rotational structure. At energies well above the Coulomb barrier two-nucleon transfer reactions should proceed mainly by a direct reaction mechanism. In the (^{3}He, p) reaction the transferred deuteron may be either in a ^{1}S or ^{3}S state and so the reaction $^{16}O(^3He, p)^{18}F$ would be expected to lead readily to the excitation of (2p–0h) states in ^{18}F. The present work was undertaken to study the level properties of ^{18}F through the $^{16}O(^3He, p)$ reaction.

This reaction has been studied previously by Pühlhofer and Bock (1967), Mangelson *et al* (1968) and Polsky *et al* (1969). A survey of earlier work is given by Mangelson *et al*. Several levels up to E_x = 3·8 MeV and 6·9 MeV were studied by Pühlhofer and Bock (1967) and Polsky *et al* (1969) respectively; angular distributions were analysed in terms of the DWBA method based on a 'pseudo-single-stripping' of a mass-2 particle and this proved adequate in some cases for the identification of transferred angular momenta. A more thorough DWBA analysis was carried out by Mangelson *et al* (1968) using a microscopic two-particle transfer theory. Their energy resolution (~ 140 keV), however, was not sufficient to resolve several well established levels in ^{18}F (for example, the triplet at E_x ~ 1 MeV).

† Permanent address: Department of Physics, University of Dacca, Dacca, Bangladesh.

In the present work all of the known levels up to 5·6 MeV and many between 5·6 and 10 MeV have been resolved. Angular distributions have been obtained for the majority of observed levels and DWBA analyses were carried out for 2p–0h positive parity states for which the wavefunctions were available.

2. Experimental arrangement

The targets used in this experiment were prepared by the evaporation of tungsten oxide (enriched in ^{16}O) on to thin carbon foils (8 $\mu g\ cm^{-2}$). Elastic scattering studies using 6 MeV ^3He ions from the Oxford tandem Van de Graaff generator were carried out at angles of 11·25°, 26·25° and 41·25°. DWBA analyses using several optical-model potentials showed that at 11·25° the theoretical elastic scattering cross section for 6 MeV ^3He ions is well represented by the classical Rutherford scattering formula. The results from the Rutherford scattering at 11·25°, together with the scattering data at the other two angles, yielded an effective target thickness of $23 \pm 5\ \mu g\ cm^{-2}$.

A beam of 18 MeV ^3He ions from the tandem generator was used in conjunction with the Oxford multiple-angle magnetic spectrograph to study the reaction $^{16}O(^3He, p)^{18}F$. Data were taken at angles from 11·25° to 123·75° in 7·5° intervals (corresponding to channels $2 \rightarrow 12$, $14 \rightarrow 18$) covering the excitation energy range in ^{18}F of $0 \rightarrow 10$ MeV in channel 2 to $0 \rightarrow 6{\cdot}3$ MeV in channel 18. The reaction was recorded using Ilford 25 μm L4 emulsions covered with 0·0135 in mylar absorber foils to block heavier particles from competing reactions. The total charge collected was 2000 μC.

3. Plate scanning

The photographic plates on which the reaction data were recorded were examined by the University of Bradford automatic scanner (Stephenson and Dale 1971). The proton energy spectrum for each channel was recorded on magnetic tape and a printed copy of the associated track length spectra, which provides an indication of the quality of the tracks observed by the scanner, was used to check the validity of the proton count recorded in any particular group. In some cases, where a plate section contained only one group (e.g. the ground-state group at backward angles) it was scanned manually. The number of events recorded by the scanner for 12 MeV proton tracks in 25 μm Ilford L4 emulsion is reported to be within 2% of the value obtained from manual estimates (Stephenson and Dale 1971). Several automatic–manual cross checks were made and these tests showed that the errors in the absolute cross sections associated with the automatic scanning process were small compared with the error introduced by the uncertainty in target thickness. The relative errors in the angular distribution of specific groups introduced by the automatic scanning process were thought to be negligible.

4. Data extraction

The proton energy spectra for each channel were transferred to the Oxford PDP-10 computer for analysis. Extraction of cross sections was achieved using established

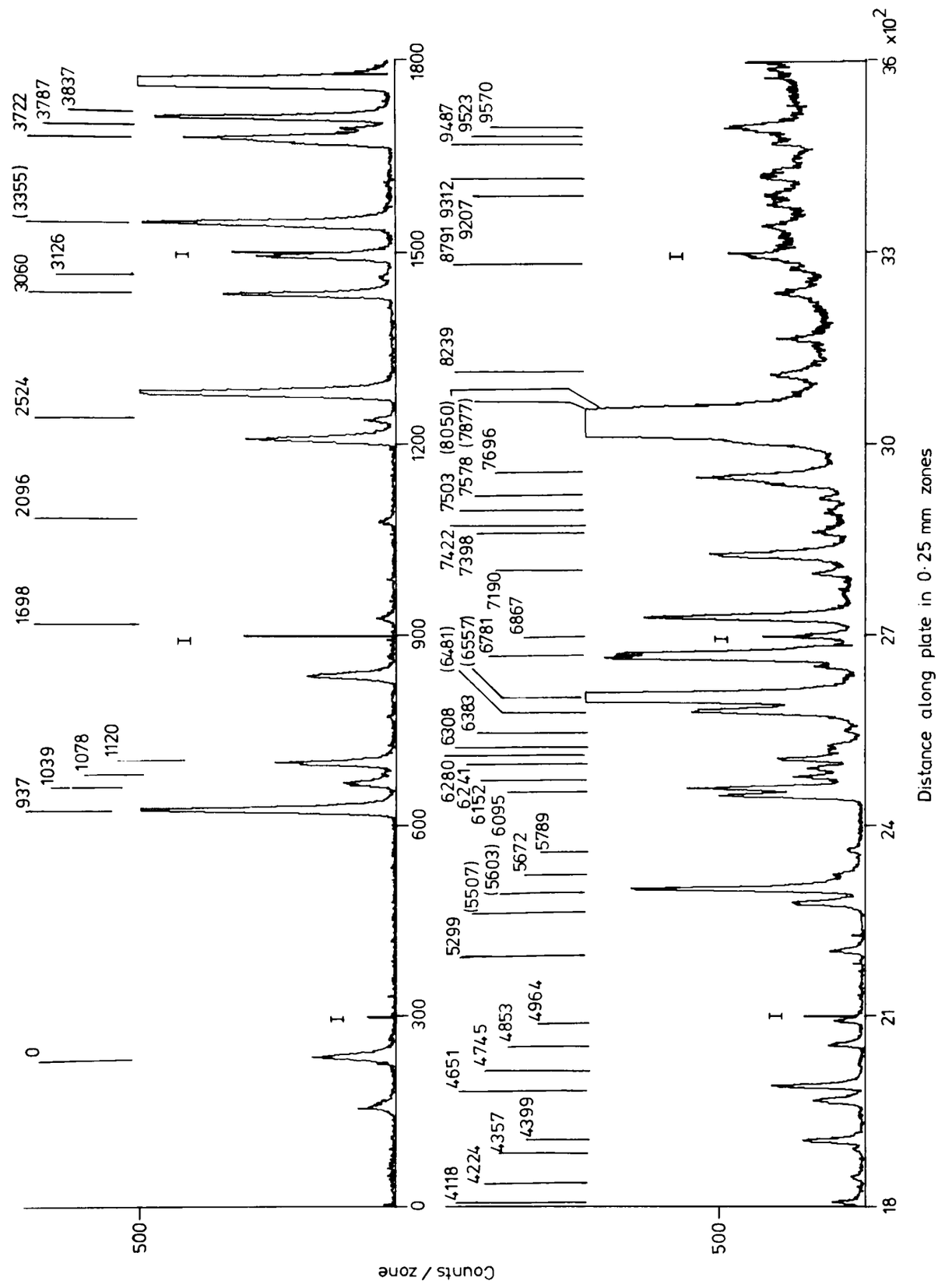

Figure 1. The proton spectrum from $^{16}O(^3He, p)^{18}F$ at a laboratory angle of 26·25°. $E(^3He) = 18$ MeV. The ^{18}F excitation energies are derived from an internal calibration (see table 1). Where excitation energies have been marked in brackets, the associated proton groups are masked by contaminant peaks at this particular angle. The index lines marked on the plates for calibration purposes are marked with an I.

spectrum handling programs. A plot of the proton groups present in channel 4 (laboratory angle 26·25°) is shown in figure 1. The $^{16}O(^3He, p)$ proton groups are labelled by their associated ^{18}F energy levels. Unmarked proton groups are from the $^{12}C(^3He, p)^{14}N$ contaminant reaction except for the broad peak in channel 3040 caused by proton knock-on. Extraction of peak areas from isolated groups was achieved by summation with either linear or parabolic background subtraction. For partially resolved groups, e.g. close doublets or peaks with overlapping contaminant lines, iterative double gaussian fitting with suitable background subtraction was employed. The angular distribution results are shown in figures 2–5. The errors associated with the angular distribution results, where larger than the statistical errors, are due to the effects of close or overlapping groups or a poor associated track length spectrum.

Each channel was calibrated internally in energy using a parabolic fit to about eight well established and accurately known energy levels in ^{18}F between excitation levels of 0 and 7 MeV. The energy levels used as calibration points for the energies quoted in table 1 are shown underlined. Inspection of table 1 shows that the extracted interpolated energies of the remaining known narrow states agreed to within 5 keV in most cases.

Table 1.

Present energy (keV)	Previous energy†‡ (keV)	$J^\pi; T$‡	Dominant configuration (see text)	σ_{max}§ (mb sr^{-1})	$\sigma_{average}$§ (12° → 55°)	Γ (kev)‖
0 ± 1	0	1⁺; 0	2p–0h	3·60	1·40	
937 ± 1	937	3⁺; 0	2p–0h	5·37	2·94	
1039 ± 1	1042	0⁺; 1	2p–0h	0·95	0·56	
1078 ± 3	1081	0⁻; 0	3p–1h	0·08	0·07	
1120 ± 1	1122	5⁺; 0	2p–0h	1·62	1·14	
1698 ± 1	1701	1⁺; 0	4p–2h	0·55	0·23	
2096 ± 5	2101	2⁻; 0	3p–1h	0·44	0·21	
2524 ± 1	2524	2⁺; 0	4p–2h	0·21	0·17	
3060 ± 1	3060	2⁺; 1	2p–0h	3·70	1·62	
3126 ± 6	3135	1⁻; 0	3p–1h	0·12	0·06 ± 0·02	
3355 ± 1	3357	3⁺; 0	4p–2h	0·61	0·37	
3722 ± 2	3724	1⁺; 0	4p–2h	0·79	0·51	
3787 ± 1	3787	3⁻[a]	3p–1h	0·22	0·16	
3837 ± 1	3836	2⁺; 0	2p–0h	3·85	2·03	
4118 ± 2	4119	3⁺; 0	2p–0h	0·33	0·26	
4224 ± 2	4229	2⁻[a]	3p–1h	0·28	0·15	
4357 ± 5	4361	1⁺; 0	2p–0h	0·12	0·08	
4399 ± 1	4402	4⁻[a]	3p–1h	0·92	0·76	
4651 ± 1	4650	4⁻; 1	2p–0h	1·44	0·96	
4745 ± 10	4739	0⁺; 1		0·04 ± 0·02	—	
4853 ± 2	4849	1(⁻); 0[a]	3p–1h	0·53	0·45	
4964 ± 2	4957	2⁺; 1	2p–0h	0·35	0·29	
5299 ± 2	5301	4⁺; 0	4p–2h	0·45	0·38	
5507 ± 3	5501	3⁻[a]	3p–1h	0·08	0·05	
5603 ± 3	5599	(4⁺): 1	(2p–0h)	3·72	1·79	
	5606	1⁻: 1	3p–1h[¶]			
5672 ± 3	5674	1⁻: 1	3p–1h[¶]	0·34	0·17	
5789 ± 3	5785	2⁻[a]	3p–1h	0·13	0·09	
6095 ± 1	6095	4⁻: 0	3p–1h[¶]	2·65	1·15	

Table 1. (continued)

Present energy (keV)	Previous energy†‡ (keV)	$J^\pi; T$‡	Dominant configuration (see text)	σ_{max}§ (mb sr^{-1})	$\sigma_{average}$§ (12° → 55°)	Γ (kev)‖
6152 ± 3	6135	$0^+;1$	4p–2h[d]	0·98	0·60	12^{+6}_{-12}
	6161	$3^+;1$	2p–0h[d]			
6241 ± 4	6240	$3^-;1$[a]	3p–1h[¶]	1·53	1·12	
	6261	1^+[b]				
6280 ± 5	6280	$2^+;1$	4p–2h[d]	0·72	0·38	
6308 ± 5	6309	3^+[b]	4p–2h[d]	0·50	0·38	
6383 ± 3	6385	2^+[b]	2p–0h	0·18	0·11	
6481 ± 3	6483	3^+	4p–2h	0·08	0·06 ± 0·02	
6557 ± 4	6565	5^+	4p–2h	0·20	0·09	
6781 ± 1	6780	$4^+;0$	2p–0h	3·95	2·60	22^{+6}_{-8}
6867 ± 4	6871	$3^{(-)}, 4^-$[c]		0·62	0·43	
7190 ± 4	7194			0·40	0·35	
7398 ± 3	7395	$(3^+, 4^+)$	(2p–0h)	0·65	0·36	22 ± 8
7422 ± 5	—			0·13 ± 0·05	0·08 ± 0·03	< 15
7503 ± 5	—	$(3^+, 4^+)$	(2p–0h)	0·37	0·16	43 ± 9
7578 ± 4	—			0·34	0·22	18^{+6}_{-8}
7696 ± 7	—			3·45	2·06	41 ± 8
7877 ± 4	7872	$(2^-);0$		1·32	0·71	32 ± 5
8050 ± 7	—			1·14	0·60	30 ± 10
8239 ± 6	—	$(3^+, 4^+)$	(2p–0h)	1·03	0·65	34 ± 5
8791 ± 6	—			0·2 at 30	—	20^{+5}_{-10}
9207 ± 9	—		(2p–0h)	0·92	0·37	35 ± 8
9312 ± 10	—			1·40	0·98	80 ± 20
9487 ± 10	9494	$(6^-);0$		0·13	—	< 12
9523 ± 40	—			0·6 ± 0·2	—	55 ± 25
9570 ± 10	—			1·20	—	33 ± 7

† The states underlined in column 2 were the calibration points used for the energies extracted in column 1.
‡ Unless otherwise stated, the values given in columns 2 and 3 are from Ajzenberg-Selove (1972).
§ Errors are 25% unless stated.
‖ Where values are not given, these are less than 10 keV.
¶ May have a significant 5p–3h admixture (Ellis and Engeland 1970).
[a]Lindgren *et al* (1972); [b]Rolfs *et al* (1973a); [c]Rolfs *et al* (1973d); [d]Sens *et al* (1973a, b).

The intrinsic energy resolution associated with the experiment was found by examination of many known sharp states in channels 2 to 4 to be consistently 22 ± 3 keV.

The criteria used for the identification of new states and the confirmation of existing states were

(*a*) the excitation energies of levels in ^{18}F derived from proton energy measurements in at least three channels were required to be consistent within 10 keV and

(*b*) the proton groups observed in these channels had similar widths.

5. DWBA analysis

The DWBA theory of direct two-nucleon transfer reactions has been given by Glendenning (1965) and others. The analyses presented here were carried out neglecting finite

Table 2. Eigenvalues and eigenfunctions of ^{18}F used in the DWBA analysis.

J^π	Energy (MeV)		Expansion coefficients					
	Theory[a]	Expt[b]	$(d_{5/2})^2$	$(d_{5/2}d_{3/2})$	$(d_{5/2}s_{1/2})$	$(d_{3/2})^2$	$(d_{3/2}s_{1/2})$	$(s_{1/2})^2$
				$T = 0$ states				
1^+	0·0	0·0	0·592	−0·667		−0·049	0·158	0·421
1^+	4·1	3·725	−0·512	0·090		0·101	0·080	0·844
1^+	6·1	4·361	0·483	0·490		−0·143	−0·636	0·319
2^-	2·7	3·838		0·569	0·715		0·406	
2^-	6·9	6·383		0·806	−0·583		−0·103	
3^+	0·9	0·937	0·522	−0·243	0·818	0·021		
3^+	4·9	4·115	0·796	−0·204	−0·569	0·007		
3^+4^+	5·9	6·777		1·000				
5^+	1·4	1·119	1·000					
				$T = 1$ states				
0^+	1·2	1·041	0·914			0·278		0·296
2^+	2·9	3·061	0·746	0·099	0·614	0·103	−0·215	
2^+	5·2	4·964	−0·651	−0·002	0·751	−0·001	−0·112	
4^+	4·5	4·652	0·945	0·327				
4^+	6·0[c]	7·12[e]	−0·269	0·963				
4^+	8·48[d]	7·12[e]	−0·300	0·954				

[a] Normalized to ground state. The amplitudes are from Rolfs *et al* (1973b) except where stated otherwise.
[b] Levels in ^{18}F are as stated by the respective authors.
[c] Freed and Ostrander (1968).
[d] Kuo and Brown (1966).
[e] Level refers to ^{18}O.

range and nonlocality effects and using the code DWUCK due to Kunz which was run on the IBM 360/195 computer of the Rutherford High Energy Laboratory. The spectroscopic amplitudes for the even parity 2p–0h states are shown in table 2. The amplitudes are taken from Kuo and Brown (1966), Freed and Ostrander (1968) and Rolfs *et al* (1973b) for the two-particle states in *jj* coupling formalism with the two-body Hamiltonian given either by the Kuo–Brown or Tabakin interaction.

The optical-model potential used in the analyses was of the form

$$U(r) = -V(1 + e^x)^{-1} - iW(1 + e^{x'})^{-1} + i4W_D(d/dx')(1 + e^{x'})^{-1} + V_C(r)$$

where

$$x = (r - r_0A^{1/3})/a \qquad x' = (r - r_0'A^{1/3})/a'$$

and $V_C(r)$ is the Coulomb potential due to a uniformly charged sphere of radius $R_C = r_CA^{1/3}$.

Three sets of ^{3}He potential and two sets of proton potential were used (table 3). Following the notation of Mangelson *et al* (1968), set 6 is the average of two ^{3}He potentials used by Hiebert *et al* (1967) in their study of the ^{16}O(d, ^{3}He)^{15}N reaction. The potential set 9 is the average of potentials obtained from the fitting of the ^{3}He–^{16}O elastic scattering data of Artemov *et al* (1965). The set taken from Polsky *et al* (1969) was used by them to reproduce the ^{16}O(^{3}He, p) angular distribution associated with the 1120 keV level in ^{18}F. The proton potential 11 is the standard Perey potential (Perey 1963) while the set 12 has its geometrical parameters arbitrarily reduced by 10%. The bound-state wavefunctions were calculated separately for each

The ^{20}Ne nucleus lies in an important mass region for studying the apparently conflicting claims of these two models since, with only four particles outside an ^{16}O core, it is possible to restrict the model space to just the s-d shell by assuming the core to be inert. The problem remains tractable even when limited core excitation is allowed, and so it is reasonable to expect the shell model to explain most features of this nucleus without the need for excessive calculational effort.

In 1958 Elliott[El58] showed how collective motion could be described in the nuclear shell model by using the SU(3) classification scheme and a long range quadrupole-quadruole interaction. In particular he showed that for ^{20}Ne a $K^{\pi}=0^{+}$ band was expected, consisting of states at excitations of 0.0, 1.6, 3.9, 7.4 and 10.3 MeV. The predicted energy spacings are significantly less than those predicted by the J(J+1) rule of the simple rotational model. In 1961 Litherland et al.[Li61] demonstrated that indeed the first three states of ^{20}Ne do fit a rotational band hypothesis, the evidence being their strongly enhanced E2 transition strengths. Similarly he showed that the other low lying levels could also be assigned to bands. Since then the 6^{+} and 8^{+} members of the ground state band have been identified, and also several other bands have been suggested.

To date the compilation[Aj78] identifies 6 rotational bands which include all the 14 known states in ^{20}Ne up to an excitation of 8.5 MeV. A further 14 states above this energy are also assigned to these bands. In addition a $K^{\pi}=1^{-}$ band has been suggested [Me75] and evidence reported in Chapter 4 when discussing the 11.27MeV(1^{-};T=1) state supports the idea that the 8.85MeV(1^{-}) and 9.32MeV(2^{-}?) states are the first two

Table 3. Parameters of the optical-model potentials.

	Label	V (MeV)	r_0 (fm)	a (fm)	W (MeV)	W_D (MeV)	r'_0 (fm)	a' (fm)	r_C (fm)
$^3He + ^{16}O$	6	180·0	1·08	0·784	15·6		2·12	0·468	1·40
	9	220·0	1·11	0·653	7·1		2·11	0·815	1·40
	Polsky	156·0	1·05	0·829	6·0		2·40	0·592	1·40
$p + ^{18}F$	11	42·6	1·25	0·65		8·4	1·25	0·47	1·25
	12	42·6	1·11	0·58		8·4	1·11	0·42	1·11
n or p	Bound state	[a]	1·25	0·65					1·25

[a] Adjusted; see text.

of the nucleons transferred. The well shape was assumed to be of Woods–Saxon form with radius parameter $r_0 = 1{\cdot}25$ fm and diffuseness $a = 0{\cdot}65$ fm. The well depths were adjusted so as to give each nucleon a separation energy equal to half the separation energy of the n–p pair; the n–p binding energy for $S = 0$, $T = 1$ transfer was taken to be lower by 2·22 MeV.

6. Results and discussion

In the present study only the 2p–0h states are expected to be populated by the two-nucleon direct stripping process while excitations of other configurations (4p–2h or 3p–1h) can arise only through the small components of core excitation in the ^{16}O ground-state wavefunction or complicated processes such as two-step reaction and compound nuclear mechanisms. Shell-model calculations of the level spectra and level properties of mass-18 nuclei have been carried out by many authors (Halbert *et al* 1971 and references therein) based on a closed ^{16}O core as well as core excitations. Described and discussed below are the angular distributions for separate groups of levels.

6.1. The 2p–0h states

The measured angular distributions to states which are known to have mainly 2p–0h configurations are shown in figure 2 together with DWBA fits. A summary of known 2p–0h states is shown in table 1. As expected, inspection of figure 2 or table 1 shows that in general the cross sections for the 2p–0h states are larger than those for 4p–2h and 3p–1h states.

In agreement with the $^{20}Ne(^3He, p)$ work of Garrett *et al* (1971) it was found that a single set of optical-model parameters could not reproduce all of the angular distributions satisfactorily; most are, however, well accounted for by the potential sets shown in figure 2. It is further to be noted that the imaginary part of the ^3He potential has a much larger radius than that of the real part (table 3) which suggests that the reaction takes place at the surface of the nucleus. A similarly larger radius of the ^3He imaginary potential was needed in the DWBA analyses of the $^{12}C(^3He, \alpha)$, $^{16}O(^3He, \alpha)$ and $^{20}Ne(^3He, p)$ reactions (Fuchs and Oeschler 1973, Garrett *et al* 1971).

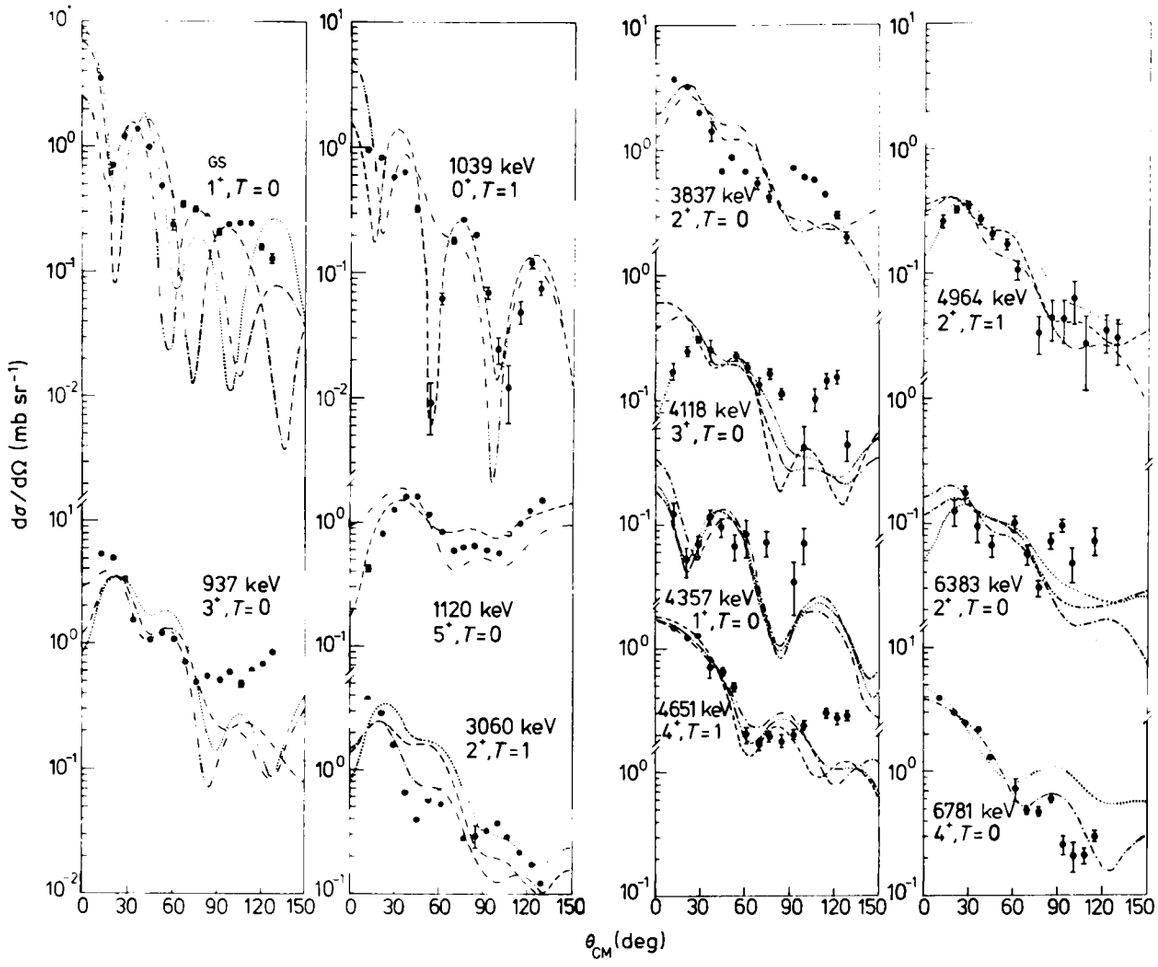

Figure 2. The proton angular distribution of 2p–0h states following the $^{16}O(^3He, p)^{18}F$ reaction at 18 MeV. —···—···, Polsky-12; – – –, Polsky-11; —·—·—, 6–12; ····, 9–11.

From inspection of figure 2 it can be seen that satisfactory fits were obtained up to about 90° for most of the 2p–0h states. The absence of deep minima in some of the angular distributions together with the increase in cross section at around 90° may be explained by the addition of a Hauser–Feshbach contribution (not shown in the diagram); a small contribution may also come from higher-order processes. It was found that for the 4357 keV level a more satisfactory fit was obtained by assuming that two L values contribute incoherently. Such a sum is considered only when the two contributions are of comparable magnitude (Glendenning 1965). The changes in the shape of the fit other than at the minima were insignificant however.

Shell-model calculations based on an inert ^{16}O core (e.g. Rolfs *et al* 1973b) predict three $J^- = 0^-$, $T = 1$ states in ^{18}F arising from dominant $(d_{5/2})^2$, $(s_{1/2})^2$ and $(d_{3/2})^2$ configurations respectively. The first two 0^+, $T = 1$ states have been identified as the 1039 and 6135 keV levels while the third has not yet been observed (it is predicted to be around $E_x = 16$ MeV). The $0^+ \rightarrow 0^-$, $T = 1$ two-particle transfers in $(^3He, p)$ reactions in (sd) shell nuclei are characterized by a pronounced minimum around 50° in the angular distribution (Betts *et al* 1971), a feature not observed in $0^+ \rightarrow 1^+$ transitions. In agreement with this general result, the angular distribution leading to the 1039 keV level has a deep minimum around 55° and the DWBA calculations

with one of the parameter sets (Polsky-11) reproduce this feature. Another deep minimum is found around 100° and it would be interesting to see if this is seen in other $0^+ \rightarrow 0^+$ transitions in other reactions. Separate angular distributions for the 6135 keV level could not be obtained as it was not resolved from the 6161 keV level.

The 4357 keV level was previously assumed to have $J = 2,3$ from γ ray studies (Ajzenberg-Selove 1972) while a later work (Rolfs *et al* 1973a) assigns $J^\pi = 1^+$ in agreement with shell-model calculations (Rolfs *et al* 1973b). The present DWBA analysis using the Rolfs wavefunction for $J^\pi = 1^+$ is in good agreement with the observed angular distribution. In previous (^{3}He, p) experiments (Mangelson *et al* 1968, Polsky *et al* 1969) this level was not resolved from the 4399 ($J^\pi = 4^-$) keV level.

6.2. The 4p–2h states

The measured angular distributions to states which are thought to be predominantly 4p–2h are shown in figure 3. A summary of these states is shown in table 1. Most of the angular distributions shown do not possess the characteristics of a direct stripping process (i.e. no tendency to fall off in intensity at higher angles, no sharp minima and no large forward peak) and so DWBA analyses were not generally attempted.

Two models have been proposed to explain the 4p–2h states; these are the weak coupling model (Arima *et al* 1967, Zucker 1969, Benson and Flowers 1969) and the strong coupling model (Bassichis *et al* 1965). In the weak coupling model, the particle wavefunctions are assumed to be substantially the same as the wavefunctions of the ^{20}Ne ground-state rotational band $J^\pi = 0^+, 2^+$ and 4^+ coupled to two holes (^{14}N ground state, $[(1p_{1/2})^{-2}]J^\pi = 1^+$) giving $J^\pi = (1^+)$, $(1^+, 2^+, 3^+)$ and $(3^+, 4^+, 5^+)$ respectively. The level at 1698 keV (1^+) in ^{18}F has been associated with the first 1^+ level of the above configuration. (Recent shell-model calculations (Millener 1972) in fact show this state to have greater than 90% 4p–2h contribution.) The 2524 (2^+), 3355 (3^+), 5299 (4^+) and 6557 (5^+) keV levels have been associated with the 2^+, 3^+ and the 4^+, 5^+ members of the first and second triplets respectively (Middleton *et al* 1968, Sens *et al* 1973b). Controversy exists for the remaining two levels of the weak coupling model ($J^\pi = 1^+, 3^+$). The 4224 keV level was suggested as a candidate for the above 1^+ level by Middleton *et al* (1968) which later was found to have $J^\pi = 2^-$ (Rolfs *et al* 1973d). The 3722 keV level ($J^\pi = 1^+$) suggested by Sens *et al* (1973b) is believed to be a 2p–0h state (Rolfs *et al* 1973b). Recent shell-model calculations (Millener 1972) show this state to have 65% 2p–0h character. A DWBA fit for this level using the 2p–0h wavefunctions of Rolfs *et al* (1973b) was undertaken (figure 3). However, on the strength of the extremely poor two-particle fit it might appear that a more valid dominant configuration is 4p–2h. In previous (^{3}He, p) studies this level was not considered to have a dominant (2p–0h) configuration (Polsky *et al* 1969) while in the experiment of Mangelson *et al* (1968) it was not resolved. The association of the missing 4p–2h, 3^+ state with the 6308 keV level does not seem to be on a firm basis (Sens *et al* 1973b). According to the shell-model calculations of Rolfs *et al* (1973b) this is classed as a 2p–0h state. In the present experiment the 6308 keV level was not sufficiently resolved from the 6280 keV level for the extraction of accurate cross sections.

In the strong coupling model, several low-lying levels have been proposed as members of the $K^\pi = 1^+$ rotational band. The levels at 1698 (1^+), 2524 (2^+), 3355 (3^+), 5299 (4^+) and 6557 (5^+) keV have been identified on the basis of γ ray transition

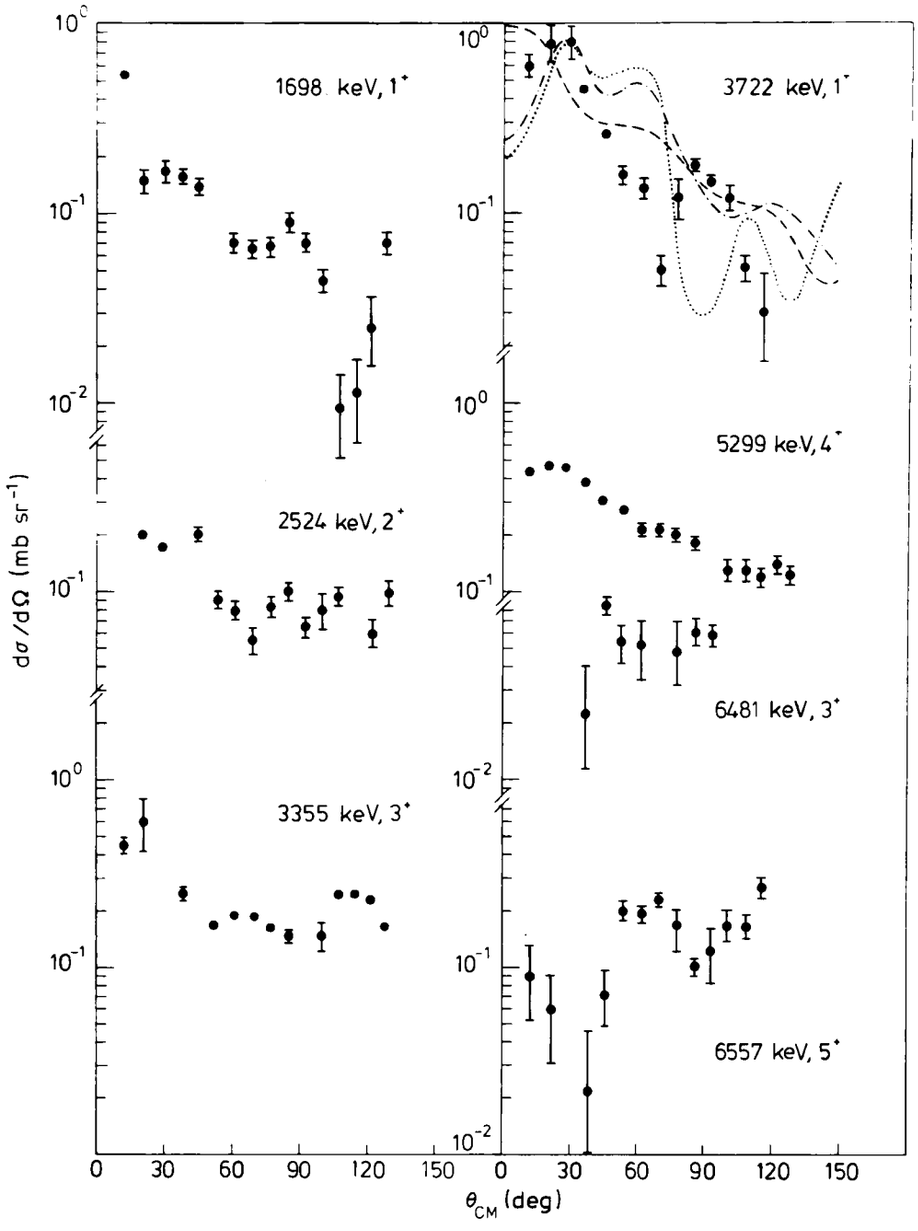

Figure 3. The proton angular distribution of 4p–2h states following the $^{16}O(^3He, p)^{18}F$ reaction at 18 MeV.

probabilities as members of this band (Rolfs *et al* 1973c). The identification of the 3355 keV level with the $J^\pi = 2^+$, 2p–0h configuration by Freed and Ostrander (1968) is therefore probably incorrect. Further confirmation that this level is of 4p–2h character emerges from its strong excitation in the $^{14}N(^7Li, t)$ reaction (Middleton *et al* 1968) and the lack of direct stripping process characteristics (figure 3) in the present experiment.

The 4745 keV level is a member of the $J^\pi = 0^+$, $T = 1$ triad of mass 18 (^{18}O:3632 keV and ^{18}Ne:3576 keV). This level, which was not resolved in the (^3He, p) and (α, d) reactions of Mangelson *et al* (1968), is very weakly excited both in the present work and in that of Polsky *et al* (1969). The angular distribution of protons feeding this level was not extracted because of the small cross section ($40 + 20\ \mu b\ sr^{-1}$). The 3632 keV level in ^{18}O is likewise very weakly excited in the $^{16}O(t, p)$ reaction (Middleton and Pullen 1964), while in the $^{20}Ne(p, t)$ reaction (Falk

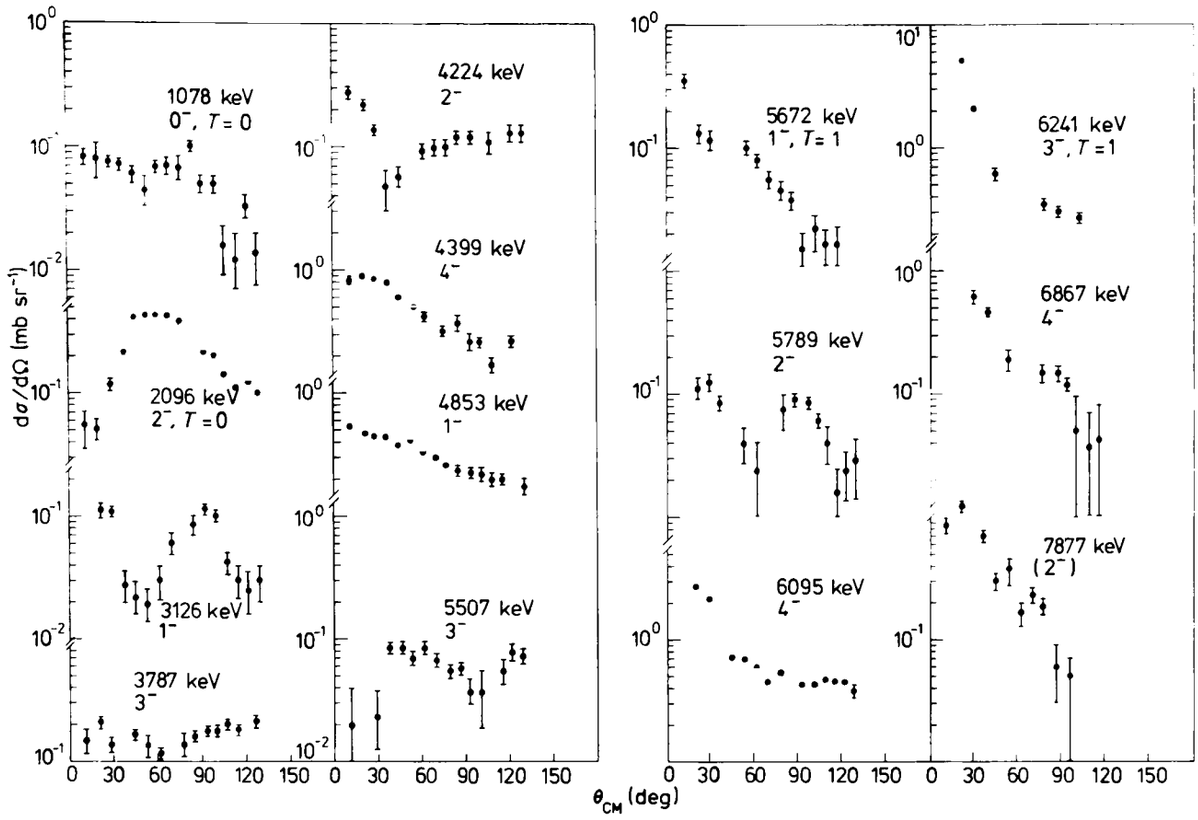

Figure 4. The proton angular distribution of 3p–1h states following the $^{16}O(^3He, p)^{18}F$ reaction at 18 MeV.

et al 1970, L'Ecuyer *et al* 1970) the 3576 keV level was not resolved. The identification of the 4745 keV level as a 2p–0h state (Kuo and Brown 1966) seems to be incorrect on the grounds of two-particle transfer intensity considerations.

6.3. The 3p–1h negative parity states

The measured angular distributions to states which are thought to have 3p–1h character are shown in figure 4. A further listing of these states is shown in table 1. The negative parity states in ^{18}F can arise from 3p–1h configuration with a small 5p–3h contribution (Poletti 1967, Ellis and Engeland 1970) or from the 2p–0h $(d_{5/2}f_{7/2})$ or $(s_{1/2}f_{7/2})$ configurations. The latter configuration is excluded for low-lying levels for several reasons (Rolfs *et al* 1973d). Selective excitation of the negative parity levels in the $^{15}N(^6Li, t)$ reaction (Lindgren *et al* 1972), strong excitation of some of the levels in neutron pick-up from ^{19}F (Ajzenberg-Selove 1972) and weak excitation in $(^3He, p)$ and (α, d) on ^{16}O all point to the 3p–1h nature of the states.

In the weak coupling approximation (Poletti 1967, Ellis and Engeland 1970) the particle wavefunctions are assumed to be substantially the same as those of ^{19}F and the hole wavefunctions are assumed to be the same as the ground-state wavefunctions of ^{15}N or ^{15}O. Several negative parity states in ^{18}F are thus generated by coupling a $(1p_{1/2})^{-1}$ configuration to the members of the ground-state rotational band of ^{19}F, most of which have been identified experimentally (Lindgren *et al* 1972). The strong coupling model has also been successful in describing the negative parity states (Rolfs *et al* 1973d). The 1078 (0^-), 2096 (2^-) and 4399 (4^-) keV levels have

been shown to be members of a $K^\pi = 0^-$ rotational band exhibiting the expected $J(J + 1)$ energy progression and enhanced E2 in band transitions. Evidence for a $K^\pi = 1^-$ band and a second $K^\pi = 0^-$ band exists although E2 in band transition strengths have not been measured.

The following characteristics may be noted in the (^{3}He, p) reaction (figure 4). The negative parity levels are weakly excited and in general the angular distributions have a non-stripping character. The magnitudes of the cross sections due to compound nuclear contributions are expected to follow a $J(J + 1)$ rule and, with one or two exceptions, the cross sections of the negative parity states show this behaviour. The shapes of the distributions, however, are not explained by Hauser–Feshbach calculations (not shown) and thus it appears that the negative parity levels populated in the (^{3}He, p) reaction arise from a combination of several processes and that, as expected, the direct stripping process probably plays a minor part.

The angular distribution of protons leading to the level at 3126 keV, derived from present studies, is not consistent with the 1^+, 2p–0h assignment of Freed and Ostrander (1968) and for the above reasons these results confirm the $J^\pi = 1^-$, 3p–1h assignment catalogued in Ajzenberg-Selove (1972).

6.4. *Levels of unknown configuration including new states*

Eleven new levels have been observed in the present experiment in the excitation region 7 to 10 MeV. Angular distributions of some of them together with distributions of some states with no firm spin–parity assignments are shown in figure 5. The distributions associated with levels nearer to 10 MeV are not shown because at this energy the associated proton group is observed in only a small number of channels

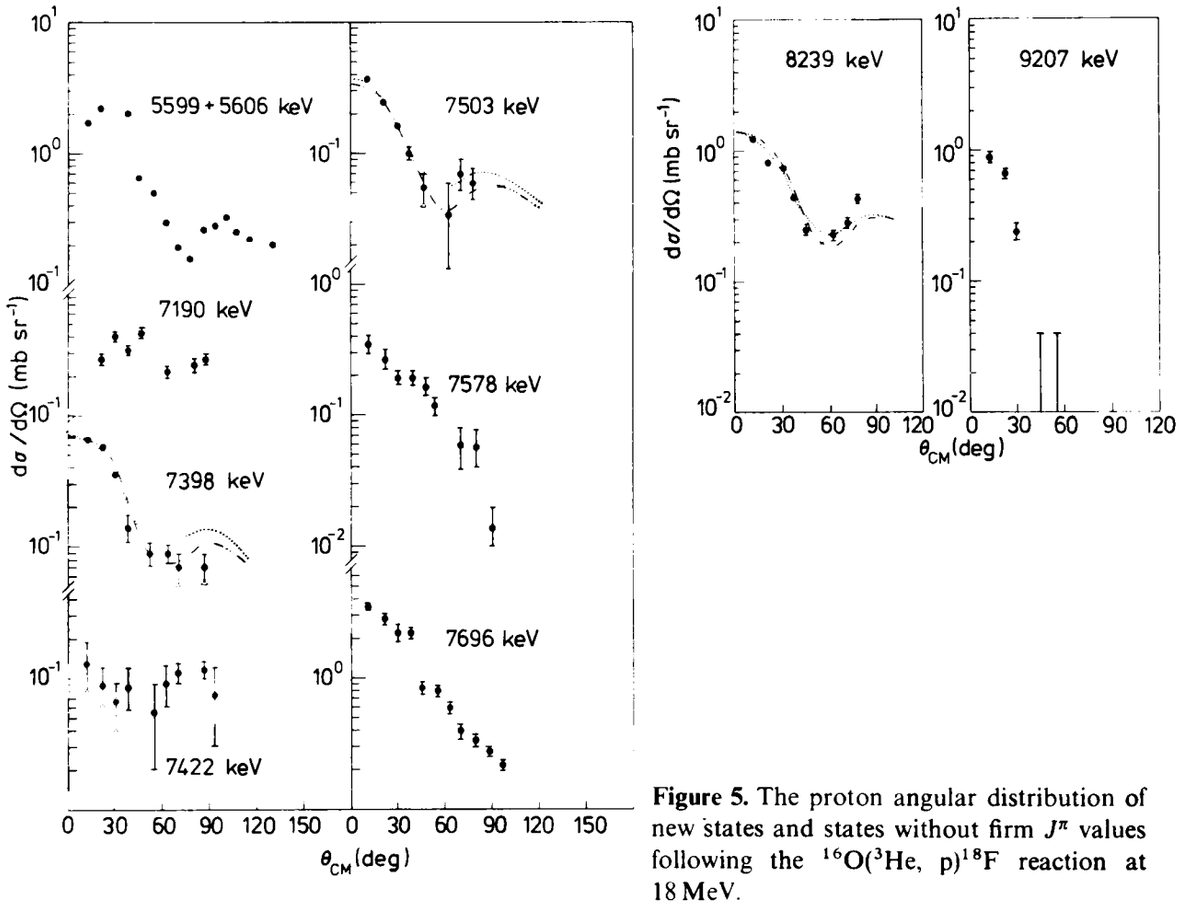

Figure 5. The proton angular distribution of new states and states without firm J^π values following the ^{16}O(^{3}He, p)^{18}F reaction at 18 MeV.

due to kinematic effects. Because of the varied nature of the states covered in this section, a level by level discussion follows.

The energies, cross sections and widths of the relevant states in this section are listed in table 1. The 5599/5606 keV doublet, populated very strongly, was not resolved and therefore a DWBA fit was not attempted. If, however, we assume that the upper level (1^-) is weakly populated then the angular distribution associated with this state shows the characteristic minimum at 70° of the 4^+ level at 4651 keV, thus confirming the tentative assignment of (4^+) to the 5599 keV level catalogued in Ajzenberg-Selove (1972).

Of the 6240, 6261, 6280 and 6309 keV quadruplet only the 6240, 6280 and 6309 keV levels were observed. The resolution of the present experiment was not sufficient to enable accurate angular distributions of the 6280 and 6309 keV levels to be extracted.

The angular distribution associated with the 7190 keV level, besides being weakly excited, does not appear to have a direct stripping character and is therefore more likely not to have a 2p–0h configuration.

The 7398, 7503 and 8239 keV levels all have similar angular distributions, characterized by a direct stripping nature. These distributions have been fitted by two-particle DWBA for $L = 4$ transitions using the wavefunctions for the 7·12 MeV ($J^\pi = 4^+$) level in ^{18}O, which has a dominant $d_{5/2}d_{3/2}$ configuration (Kuo and Brown 1966, Freed and Ostrander 1968) and have shown good agreement. One of these levels (which therefore also seem to have a dominant $(d_{5/2}d_{3/2})$ configuration) may hence be the analogue of the 7·12 MeV state in ^{18}O. Tentative assignments for these levels are therefore $J^\pi = 3^+, 4^+$ (the 5^+ is ruled out with the above configuration).

The 7422 keV level is the weak member of the barely resolved 7398/7422 keV doublet. Although the angular distribution is difficult to extract accurately it appears nevertheless to have little structure and hence the level does not seem to be of 2p–0h nature.

The 7578 and 7696 keV levels have similar angular distributions which are not characteristic of any particular configuration.

The 8050 and 8791 keV levels, although excited strongly at the forward angles, are masked by contaminants in the majority of channels and therefore are not included in the angular distribution diagram.

The 9207 keV level is the last of the newly observed levels to yield a useful angular distribution as a result of the increasing kinematic shift with energy in higher channels. The angular distribution has a striking change in cross section of a factor 50 between 12° and 55°, characteristic of a 2p–0h, $J^\pi = 0^+$ state (cf the angular distribution of the 0^+, 1039 keV state in figure 2).

The 9312 (possibly of doublet nature), 9523 and 9570 keV peaks are broad states and therefore probably of low spin. The sharp state at 9487 keV has been observed only once previously (Rivet *et al* 1966) and assigned 6^- on rather weak grounds. The excitation energy and the sharpness of this state make it a possible candidate for the 6^+ member of the 4p–2h, $K^\pi = 1^+$ band.

7. Conclusion

The angular distributions associated with the 2p–0h positive parity states in ^{18}F are fairly well accounted for by the DWBA theory for two-nucleon stripping

(Glendenning 1965), at least up to 90°. In agreement with previous studies on light nuclei, a single set of optical-model parameters could not reproduce all the angular distributions. Some of the levels are strongly excited showing that certain configurations (having two-nucleon correlations) are selectively populated in the (^{3}He, p) reaction. Cross sections to states arising mainly from core excitation (such as predominantly 4p–2h positive parity and 3p–1h negative parity states) which are in general weaker than the predominantly 2p–0h states, display a variety of angular distribution shapes showing that in these cases the (^{3}He, p) reaction cannot be explained by a single-step mechanism. For the (3p–1h) states, Hauser–Feshbach calculations do not account for the non-stripping character of the distributions, although, in agreement with the compound nuclear mechanism, high spin states in general are more strongly excited than the low spin ones and appear to follow a $J(J+1)$ dependence. Eleven new levels have been observed between $E_x = 7$ and 10 MeV. An accurate measurement of absolute cross sections has been made with an energy resolution much improved on previous ^{16}O(^{3}He, p) studies and the data collected should be useful for future detailed structure calculations.

Acknowledgments

The authors wish to thank Dr D Roaf for his valuable assistance in operating the multiple-angle spectrograph and in the processing of the photographic emulsions, Dr D Sinclair for his help with the DWBA computations and Professor K W Allen and Dr A A Pilt for their interest in this work.

We also wish to thank Professor G Brown for the use of the Bradford University automatic scanner, Mr D N Slater for his assistance with the scanner during the plate analysis and Mrs P Ravenhill for the manual scanning needed to complete the work.

Dr H M Sen Gupta wishes to thank the Royal Society for financial support and the University of Dacca for granting leave. M J Hurst acknowledges financial support from the Science Research Council.

References

Ajzenberg-Selove F 1972 *Nucl. Phys.* A **190** 1–196

Arima A, Horiuchi H and Sebe T 1967 *Phys. Lett.* **24B** 129–31

Artemov K P, Gol'dberg V Z, Islamov B I, Rudakov V P and Serikov I N 1965 *Sov. J. Nucl. Phys.* **1** 450–2

Bassichis W H, Giraud B and Ripka G 1965 *Phys. Rev. Lett.* **15** 980–2

Benson H G and Flowers B H 1969 *Nucl. Phys.* A **126** 332–54

Betts R R, Fortune H T, Garrett J D, Middleton R, Pullen D J and Hansen O 1971 *Phys. Rev. Lett.* **26** 1121–4

Ellis P J and Engeland T 1970 *Nucl. Phys.* A **144** 161–90

Falk W R, Kidney R J, Kulisic P and Tandon G K 1970 *Nucl. Phys.* A **157** 241–62

Freed N and Ostrander P 1968 *Nucl. Phys.* A **111** 63–80

Fuchs H and Oeschler H 1973 *Nucl. Phys.* A **202** 396–402

Garrett J D, Middleton R, Pullen D J, Andersen S A, Nathan O and Hansen O 1971 *Nucl. Phys.* A **164** 449–83

Glendenning N K 1965 *Phys. Rev.* **137** B102–13

Halbert E C, McGrory J B, Wildenthal B H and Pandya S P 1971 *Adv. Nucl. Phys.* vol 4 eds M Baranger and E Vogt (New York, London: Plenum) pp 315–442
Hiebert J C, Newman E and Bassel R H 1967 *Phys. Rev.* **154** 898–920
Kuo T T S and Brown G E 1966 *Nucl. Phys.* **85** 40–86
L'Ecuyer J, Gill R D, Ramavataram K, Chant N S and Montague D G 1970 *Phys. Rev.* C **2** 116–24
Lin C L and Yoshida S 1964 *Prog. Theor. Phys.* **32** 885–903
Lindgren R A, Gutbrod H H, Fulbright H W and Markham R G 1972 *Phys. Rev. Lett.* **29** 798–801
Mangelson N F, Harvey B G and Glendenning N K 1968 *Nucl. Phys.* A **119** 79–96
Middleton R, Polsky L M, Holbrow C H and Bethge K 1968 *Phys. Rev. Lett.* **21** 1398–401
Middleton R and Pullen D J 1964 *Nucl. Phys.* **51** 63–76
Millener D J 1972 University of Oxford *DPhil Thesis*
Perey F G 1963 *Phys. Rev.* **131** 745–63
Poletti A R 1967 *Phys. Rev.* **153** 1108–13
Polsky L M, Holbrow C H and Middleton R 1969 *Phys. Rev.* **186,** 966–77
Pühlhofer F and Bock R 1967 *Phys. Lett.* **25B** 117–9
Rivet E, Pehl R H, Cerny J and Harvey B G 1966 *Phys. Rev.* **141** 1021–32
Rolfs C, Berka I and Azuma R E 1973d *Nucl. Phys.* A **199** 306–27
Rolfs C, Berka I, Trautvetter H P and Azuma R E 1973e *Nucl. Phys.* A **199** 328–50
Rolfs C, Charlesworth A M and Azuma R E 1973a *Nucl. Phys.* A **199** 257–73
Rolfs C, Kieser W E, Azuma R E and Litherland A E 1973b *Nucl. Phys.* A **199** 274–88
Rolfs C, Trautvetter H P, Azuma R E and Litherland A E 1973c *Nucl. Phys.* A **199** 289–305
Sens J C, Pape A and Armbruster R 1973b *Nucl. Phys.* A **199** 241–56
Sens J C, Rietsch F, Pape A and Armbruster R 1973a *Nucl. Phys.* A **199** 232–40
Stephenson J and Dale P W 1971 *Nucl. Instrum. Meth.* **91** 365–76
Zuker A P 1969 *Phys. Rev. Lett.* **23** 983–7

1.E.1:
2.G

Nuclear Physics **A295** (1978) 451–462; © *North-Holland Publishing Co., Amsterdam*

A STUDY OF THE (τ, α) REACTION ON ^{50}Cr

M. A. ZAMAN and H. M. SEN GUPTA

Department of Physics, University of Dacca, Dacca, Bangladesh

and

F. WATT and M. J. HURST

Nuclear Physics Laboratory, Keble Road, Oxford, England

Received 3 August 1977
(Revised 1 November 1977)

Abstract: The ^{50}Cr$(\tau, \alpha)^{49}$Cr reaction has been studied at E_τ = 16.0 MeV using the Tandem Van de Graaff accelerator and the multichannel magnetic spectrograph of the Nuclear Physics Laboratory, Oxford. Twenty-nine levels up to an excitation of $\approx$ 6.8 MeV have been observed, including a few analogues. The angular distributions have been analyzed in terms of the DWBA theory of direct reaction. The J^π limits and spectroscopic factors are obtained for various levels.

E | NUCLEAR REACTION ^{50}Cr(τ, α), E = 16 MeV; measured $\sigma(E_x, \theta)$. ^{49}Cr deduced levels, l, C^2S, J, π. Enriched target.

1. Introduction

The ^{49}Cr nucleus with four protons and five neutrons outside the "closed" ^{40}Ca core is accessible only to a few nuclear reactions. The level properties of this nucleus have been studied through the single-neutron pickup reactions on ^{50}Cr [refs. [1–3])] and the (α, n) reaction on ^{46}Ti [refs. [4, 5])]. A few levels were observed by Whitten and McIntyre [1]) in the (p, d) reaction on ^{50}Cr and the angular distributions were studied for the ground and the first excited states and no detailed analysis is reported. The (τ, α) reaction on ^{50}Cr was studied by David *et al.* [2]) and Blumenthal *et al.* [3]). The latter authors made the l_n assignments for the angular distributions leading to some low-lying levels and several J^π assignments to levels from the $(\tau, \alpha\gamma)$ angular correlation studies. Some of the l_n assignments in the two works are contradictory (levels at 1.07, 1.54 and 2.42 MeV, for example). The spectroscopic factors were extracted only by David *et al.* It was thought worthwhile to make another study of the ^{50}Cr(τ, α) reaction.

The present work is concerned with the (τ, α) reaction on ^{50}Cr at E_τ = 16 MeV and the angular distributions were measured for all the twenty-nine levels observed up to $E_x \approx$ 6.8 MeV. Many more levels were observed in this experiment than by

members of such a band. Medsker et al.[Me75] also suggest other possible members of this band and of other bands, but as yet no firm evidence has been provided for these assignments. The bands so far identified are shown in figure 3.1.1.

One method by which the assignment of particular states to such bands can be made is by their population in reactions suspected to be selective for states of the required type. For example the two states at 9.03MeV(4^+) and 12.14MeV(6^+) are strongly populated in the 8-particle transfer reaction $^{12}C(^{12}C,\alpha)^{20}Ne$ whereas the three states at 9.99MeV(4^+), 10.79MeV(4^+) and 12.59MeV(6^+) are not. This supports the contention that the two states seen belong to an 8-particle 4-hole band based on the 0^+ state at 7.19MeV, as such states would be expected to be preferred by this reaction, which is believed to have a direct component at the bombarding energies employed. Reactions which are called selective are, however, not always as selective as might be desired, due to compound nuclear contributions, and so assignments cannot always be made with confidence. Furthermore, the comparison of measured spectroscopic strengths with model predictions is subject to uncertainties in the understanding of the reaction mechanism.

An alternative basis for assigning states to bands relies on the enhanced E2 electromagnetic transition probability between states in a band due to the collective nature of the states concerned. An enhancement is predicted by the simple rotational model but a more successful quantitative prediction can be made using the shell model. The γ-decay strength of a bound state can be deduced from the lifetime of the state and from its branching ratios for the different γ-decay modes available. Measurements of γ-decay strengths for virtual states

David *et al.* [2]) and the properties of many of the new levels, such as l_n transfer, J^π limits and spectroscopic factors, are given. Finally, the level spectrum in ^{49}Cr was compared with that given by the spherical shell-model calculations of Ginocchio [6]) based on the $(f_{\frac{7}{2}})^n$ configuration and the Coriolis coupling model of Malik and Scholz [7]) and Zurmühle *et al.* [4]).

2. Experimental procedure

The experiment was carried out with a beam of 16 MeV ^{3}He particles from the Tandem Van de Graaff accelerator of the Nuclear Physics Laboratory, Oxford. The target was prepared by the vacuum evaporation of Cr_2O_3 (isotopically enriched to 99 % ^{50}Cr) onto a thin carbon backing of thickness $\approx$ 10 $\mu g \cdot cm^{-2}$. The scattered particles were magnetically analysed in a multiple gap magnetic spectrograph, the applied magnetic field strength being 10.18 kG. The scattered particles were recorded in 25 μm thick Ilford K − 1 and L4 emulsion at 14 angles between 11.25° and 108.75° in steps of 7.5°. The plates were scanned at Dacca for groups of α-particles and the energy spectra were obtained at different angles. A typical spectrum at 18.75° is shown in fig. 1. The energy resolution (FWHM) is $\approx$ 22 keV.

To establish the absolute cross section scale, the target thickness was measured from a subsidiary experiment on the elastic scattering of 6 MeV ^{3}He particles from

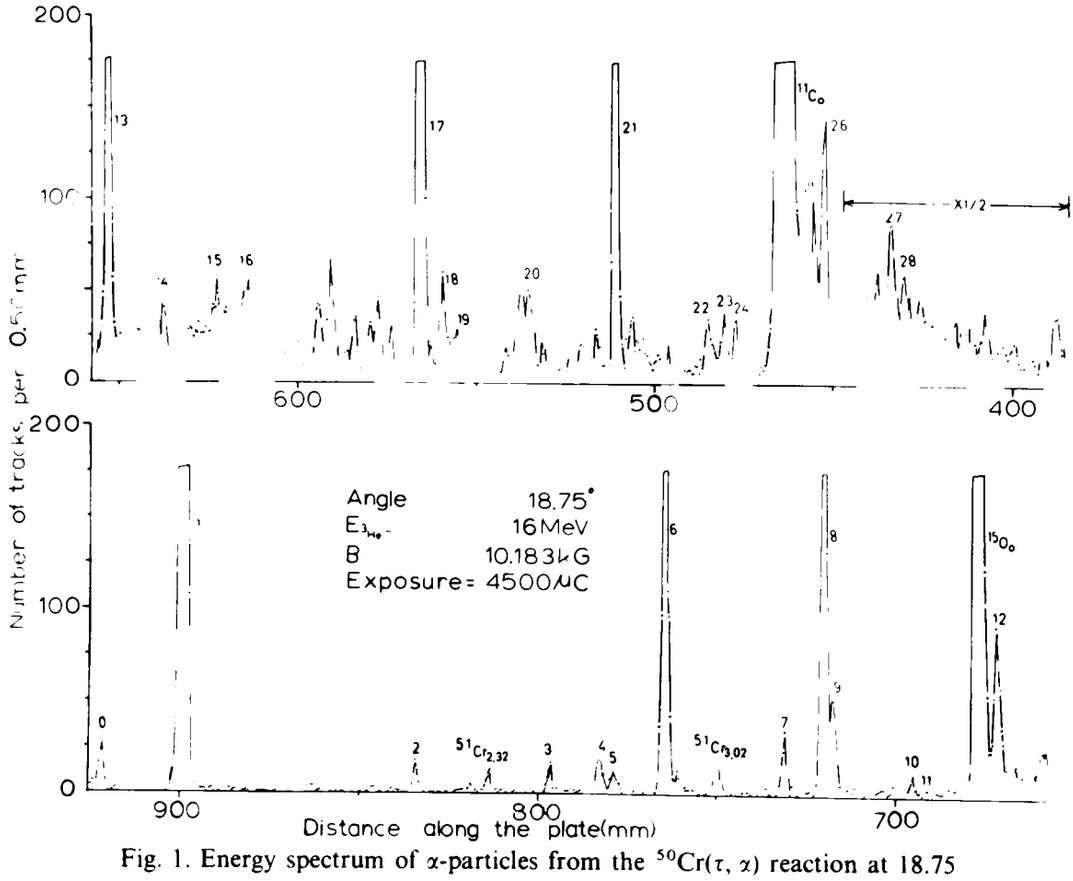

Fig. 1. Energy spectrum of α-particles from the ^{50}Cr(τ, α) reaction at 18.75°

the same target. A short exposure of 0.0504 μC was taken at a magnetic field of strength 5.11 kG and the yields of the elastic group at 11.25 and 18.75° were measured from which the effective thickness of the ^{50}Cr target was found to be $\approx 30\ \mu g \cdot cm^{-2}$ by assuming the scattering to be Rutherford at these angles. The absolute cross section of the (τ, α) reaction is believed to be accurate to within 20 %.

3. DWBA analysis

The DWBA calculations in the local zero-range approximations were carried out by one of the authors (H.M.S.G.) using the code DWUCK due to Kunz with the IBM 360/195 computer of the Rutherford High Energy Laboratory. The optical model potential used in the calculations was of the standard Woods-Saxon form for both the real and imaginary parts of the ^3He particles and α-particles potentials. A Coulomb potential arising from a uniformly charged spherical nucleus of radius $R_C = r_C A^{\frac{1}{3}}$ was added to the above potential. The (real) potential of the bound neutron was assumed to be of the Woods-Saxon type including a Thomas-Fermi spin-orbit term as given by

$$V_0 \frac{\lambda}{45.2} \frac{1}{r} \frac{d}{dr} f(r, r_0, a)\, \boldsymbol{l} \cdot \boldsymbol{s},$$

with $\lambda = 25$; the $f(r, r_0, a)$ is the Woods-Saxon form factor. The neutron well depth was adjusted to reproduce the binding energy of the levels.

The optical model parameters [2]) used in the DWBA analyses are listed in table 1. The real depths approximately satisfy the condition $V_\alpha \approx V_\tau + V_n$. The spectroscopic factors were extracted using the normalization constant $N = 23$.

TABLE 1

Optical model parameters

Potential	V_0 (MeV)	r_0 (fm)	a (fm)	W_0 (MeV)	r_I (fm)	a_I (fm)	$V_{s.o.}$ [a])	r_C (fm)	Ref.
τ	142.4	1.362	0.650	12.69	1.755	0.781	8.05	1.4	[2])
α	183.7	1.40	0.560	26.0	1.48	0.560		1.4	[2])
neutron	[b])	1.25	0.65				$\lambda = 25$		

[a]) The radial form factor is the same as that for the real part of the central potential with $r_{s.o.} = r_0$ and $a_{s.o.} = a$.

[b]) Adjusted to reproduce the binding energy.

4. Results and discussion

4.1. THE ANGULAR DISTRIBUTIONS

In the present work, twenty-nine levels, including a few analogues, were observed

TABLE

Summary of the results

Group	Excitation (MeV)			$\sigma_{max}(\theta)$ (mb sr) [a]	l-values		
	[a]	[b]	[c]		[a]	[b]	[d]
0	0	0	0	0.071	3	3	(3)
1	0.272	0.27	0.272	3.85	3	3	3
2	1.072	1.07	1.085	0.037	(5)	(5)	0
3	1.542	1.57	1.563	0.072	n.s.	n.s.	(1)
4	1.698	1.71	1.704	0.031	1	1	(1)
5	1.725	1.74	1.742	0.026	1	1	
6	1.981	1.98	1.982	0.93	2	2	2
			2.169				
7	2.42	2.43	2.433	0.070	3	3	(2)
			2.504				
8	2.582	2.58	2.580	0.537	0		0
9	2.613	2.61	2.614	0.18	1		1
10	2.91			0.020	n.a.		
11	2.98			0.015	n.a.		
			3.187 [e]				
12	3.224	3.24		0.22	3		3
13	3.504	3.51		0.56	3		3
14	3.72			0.085	3		
15	3.93	3.93		0.12	1		(1)
16	4.05			0.09	0		
17	4.766	4.76		1.50	3		3
18	4.851			0.11	3		
19	4.92			0.22	1		
20	5.19			0.10	2		(2)
21	5.569	5.57		0.72	2		2
22	5.99			0.066	n.a.		
23	6.03			0.055	n.a.		
24	6.07			0.068	n.a.		
25	6.41 6.43	6.43		1.09	0		(0)
26	6.465	6.47		1.62	0		0
27	6.78	6.76		0.25	0		0
28	6.81			0.23	3		

[a]) Present work. [b]) The $^{50}Cr(\tau, \alpha)$ reaction at 18 MeV (ref. [3])); column 12 has been taken from their
[c]) The $^{46}Ti(\alpha, n)$ reaction [5]). [f]) β-decay work [12, 13]). [g]) The J^{π} values are consistent

up to an excitation of $\approx$ 6.8 MeV. The angular distributions were measured for all the groups and the spectroscopic factors were extracted for many of them. The results are summarized in table 2; also included are the results from previous $^{50}Cr(\tau, \alpha)$ works [2, 3]) and the $^{46}Ti(\alpha, n)$ work [4, 5]). The measured angular distributions are shown in figs. 2 and 3 with a comparison to the DWBA calculations. The angular distributions of some of the levels were not analysed, as either the cross sections are missing at forward angles (due to the presence of a contaminant or to

2

for levels of ^{49}Cr

C^2S		J^π		
[a])	[d])	[e])	[b])	[a])
0.10	0.19		$\frac{5}{2}^-$ [f])	[g])
5.22	3.80	$\frac{7}{2}^-$	$\frac{7}{2}^-$	[g])
	0.2	$\frac{9}{2}^-$	$(\frac{5}{2}^-, \frac{9}{2}^-)$	$\frac{9}{2}^-$
	0.05	$\frac{11}{2}^-$	$(\frac{5}{2}^-, \frac{7}{2}^-, \frac{11}{2}^-)$	
0.054			$(\frac{1}{2}^-, \frac{3}{2}^-)$	[g])
	0.1			
0.046			$\frac{3}{2}^-$	[g])
1.63	2.0		$\frac{3}{2}^+$	[g])
0.08	0.18		$\frac{5}{2}^-$	[g])
		$\frac{13}{2}^-$		
0.97	1.3		$\frac{1}{2}^+$	[g])
0.21	0.13		$\frac{3}{2}^-$	[g])
		$(\frac{11}{2}, \frac{13}{2}, \frac{15}{2})^-$		
0.30	0.22		$\frac{5}{2}^-$	[g])
0.72	0.57		$(\frac{5}{2}^-, \frac{7}{2}^-)$	[g])
0.13				$(\frac{5}{2}, \frac{7}{2})^-$
0.05	0.06		$\frac{1}{2}^-$	[g])
0.09				$\frac{1}{2}^+$
3.27	1.7		$\frac{7}{2}^-$	[g])
0.18				$\frac{5}{2}^-, (\frac{7}{2})^-$
0.10				$\frac{3}{2}^-, (\frac{1}{2})^-$
0.13	0.32			$(\frac{3}{2})^+$
1.04	2.1		$\frac{3}{2}^+$	[g])
0.51	0.3		$\frac{1}{2}^+$	[g])
0.89	0.64		$\frac{1}{2}^+$	[g])
0.18	0.18		$\frac{1}{2}^+$	[g])
0.68				$(\frac{5}{2}, \frac{7}{2})^-$

$(\tau, \alpha\gamma)$ reaction. [e]) The $^{46}Ti(\alpha, n)$ reaction [4]). [d]) The $^{50}Cr(\tau, \alpha)$ reaction at 18 MeV (ref. [2])).
with the compilation of Blumenthal *et al.* [3]).

an emulsion disturbance) or the data are available only over a narrow range of angles. Such levels are marked n.a. in table 2.

The levels at 2.17, 2.50 and 3.19 MeV observed in the $^{46}Ti(\alpha, n)$ reaction [4, 5]) are not excited in the single-neutron pickup reactions on ^{50}Cr (this work and ref. [2])). The levels at 2.91, 2.98, 3.72, 4.05, 4.85, 4.92, 5.99, 6.03, 6.07 and 6.81 MeV observed in the present experiment were not reported earlier; the spectroscopic properties of some of them (marked n.a. in table 2) could not, however, be given. The doublet

at 1.698 and 1.725 MeV reported by Blumenthal *et al.* [3]), but not resolved in ref. [2]), is clearly separated in our work and the $l = 1$ assignment to both the levels is in agreement with their work [2, 3]).

The levels at 1.07 and 1.54 MeV are weakly excited in the (τ, α) reaction and the l-assignments to them are respectively 0 and (1) according to David *et al.* [2]). In agreement with Blumenthal *et al.* [3]), the angular distribution leading to the latter group is not characteristic of a direct single-step process and that for the former could not be fitted with $l \leqq 3$. A tentative $l = 5$ assignment is consistent with $J^{\pi} = \frac{9}{2}^{-}$ given by the ^{46}Ti(α, n) angular correlation studies [5]). If this l-assignment is correct, then the other possible spin value of $\frac{5}{2}^{-}$ (ref. [4]) should be excluded. However, a direct pickup process from the 1h orbital is rather unlikely.

The $l = 3$ assignment to the level at 2.42 MeV in our work is in agreement with that of Blumenthal *et al.* [3]), but is in disagreement with the tentative $l = 2$ assignment

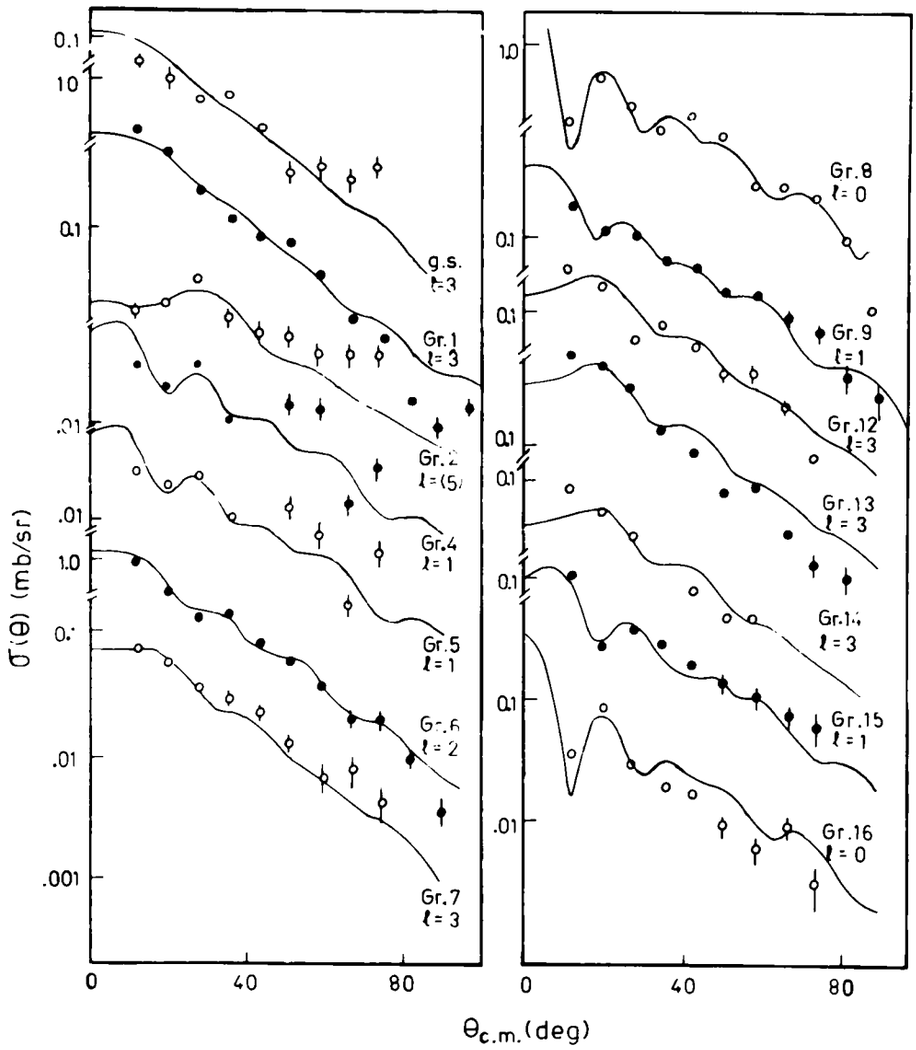

Fig. 2 The (τ, α) angular distributions fitted with the DWBA curves; the error bars represent the statistical errors.

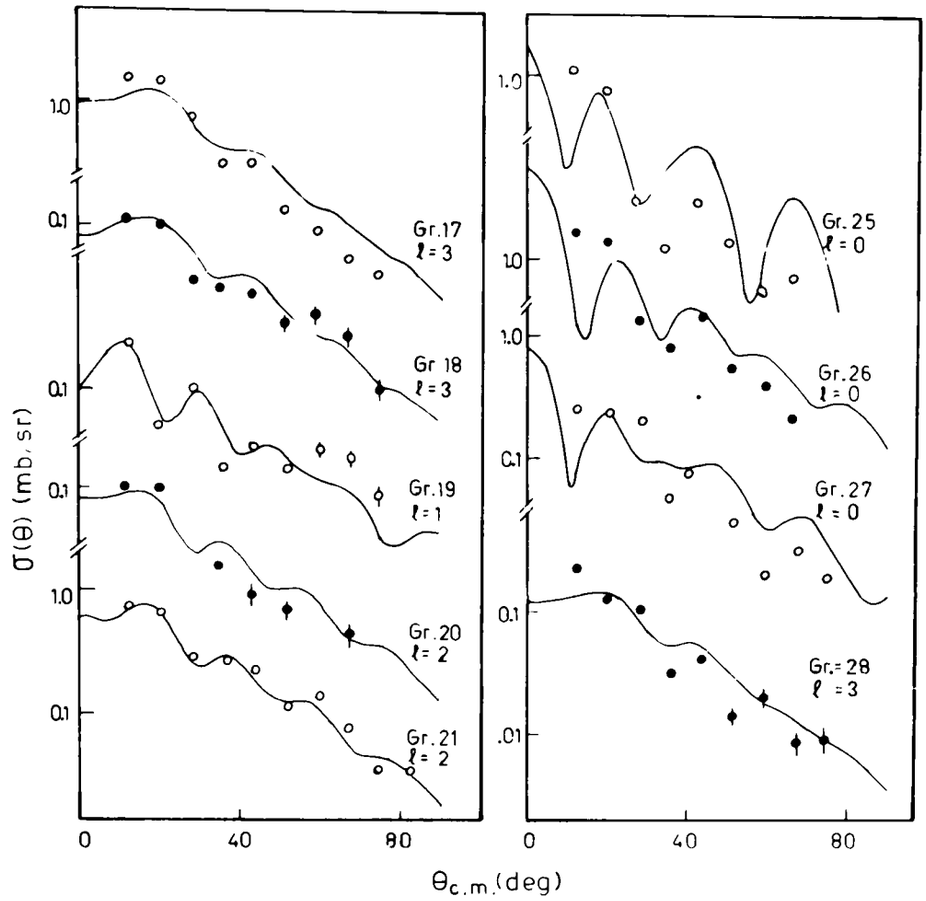

Fig. 3. As in fig. 2.

made by David *et al.* [2]). Some of the tentative assignments of l-values of David *et al.* (the g.s., 3.93, 5.19 and 6.41-6.43 MeV levels) are confirmed in the present experiment. These l-values are consistent with the known J^π values of the g.s. and the levels at 3.93 and 6.41-6.43 MeV (table 2); the J^π of the other level (5.19 MeV) is suggested to be $\frac{3}{2}^+$ in our work.

The single-particle strengths are usually distributed over a few levels (the $l_n = 3$ transitions in particular) as shown in fig. 4. This is consistent with the fact that being in the middle of the $f_{\frac{7}{2}}$ shell, the ^{50}Cr is not a good shell-model nucleus.

All $l = 0$ and 2 transitions are assumed to belong to the 2s and $1d_{\frac{3}{2}}$ states, respectively, and except where the J^π values are known to be $\frac{1}{2}^-$ and $\frac{5}{2}^-$ (table 2) all $l = 1$ and 3 transitions are, respectively, treated as the $2p_{\frac{3}{2}}$ and $1f_{\frac{7}{2}}$ shell-model states.

A total of nine $l = 3$ distributions have been identified in the present work (table 2 and fig. 4), as against five (including one tentative) by David *et al.* [2]). Of these the 4.77 MeV level is the analogue of the g.s. of ^{49}V [$J^\pi = \frac{7}{2}^-$ (ref. [8]))]. The summed spectroscopic factor for the $1f_{\frac{7}{2}}$, $T_<$ state comes to be 6.8 using $N = 23$. In view of the lack of a proper normalization constant, a comparison with the sum-rule limit is not meaningful. One can, however, make an approximate comparison of the ratio of the $\sum C^2S$ for the $T_>$ and $T_<$ component of a shell-model state with that of the shell-model limit. The observed values of the above ratio for the $1f_{\frac{7}{2}}$, $1d_{\frac{3}{2}}$

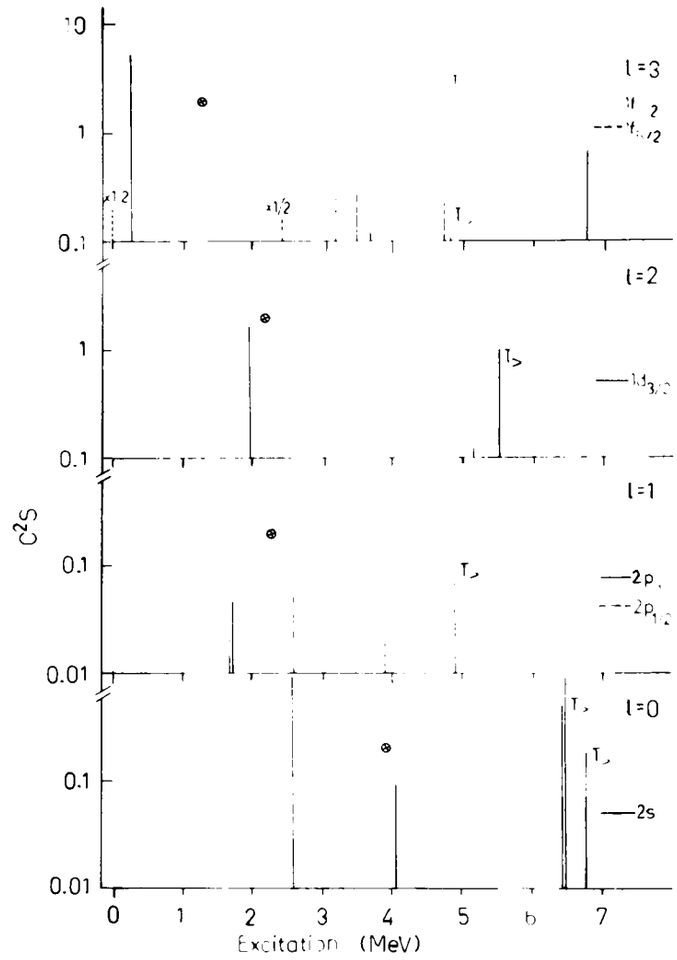

Fig. 4 The spectral distribution of single-particle strength; the centre of gravity of the respective $T_<$ states are shown.

and 2s states are, respectively, ≈ 0.4, ≈ 0.6 and ≈ 0.65, being close to the expected values of 0.3, 0.5 and 0.5. The measured ratio can be further improved by using a different prescription for the bound state geometry, the variable radius procedure for example [2, 9]).

Only one level (namely at 3.93 MeV) with $J^\pi = \frac{1}{2}^-$ has been identified in the ^{46}Ti(α, nγ) work [4]). This is weakly excited in the (τ, α) reaction (this work and ref. [2])).

From simple shell-model considerations the 2p and $1f_{\frac{5}{2}}$ shell-model states should not be populated in the single-neutron pickup experiments on ^{50}Cr. It is, however, possible that the ^{50}Cr with ten nucleons outside the "closed" ^{40}Ca core has a rather diffuse Fermi surface and the excitation of the 2p and $1f_{\frac{5}{2}}$ shells is therefore not surprising. Even in ^{40}Ca and ^{48}Ca, the two best shell-model nuclei in this region, the $l = 1$ transitions have been observed in many single-nucleon pickup experiments [10, 11]).

In addition to the four analogue states observed in a previous (τ, α) work [2]), two levels at 4.85 and 4.92 MeV have been tentatively identified in this experiment as analogues of the respective parent levels in ^{49}V at 0.152 and 0.749 MeV [ref. [8])].

These are not as prominent as the remaining analogues; nevertheless, the relative spacings and the l_n values are consistent with the relative level spacings and the J^π values of the parent levels. The results of the analogue states are summarized in table 3 for a comparison with the corresponding levels excited in the ^{50}Cr(t, α)

TABLE 3

Summary of the results for the analogue states in ^{49}Cr

	^{50}Cr(τ, α)^{49}Cr [a]			^{50}Cr(t, α)^{49}V [c]					
E_x^A (MeV)	E_x [b] (MeV)	l_n	C^2S	E_x^p (MeV)	l_p	C^2S	J^π	$\frac{C^2S(\tau,\alpha)}{C^2S(t,\alpha)}$	ΔE_C (MeV)
4.766	0	3	3.27	0	3	2.96	$\frac{7}{2}^-$	1.10	8.12
4.851	0.085	3	0.18	0.091	3	0.21	$\frac{5}{2}^-$	0.86	8.11
4.92	0.154	1	0.10	0.152	1	0.12	$\frac{3}{2}^-$	0.83	8.12
5.569	0.803	2	1.04	0.749	2		$\frac{3}{2}^+$		8.17
6.41	1.64								
6.43	1.66	0	1.40	1.647	0	1.54	$\frac{1}{2}^+$	0.91	
6.465	1.699								
6.78	2.01	0	0.18	1.999	0	0.12	$\frac{1}{2}^+$	1.5	8.13

[a]) Present work.
[b]) Excitation in "^{49}V" obtained with the 4.766 MeV level as the ground-state analogue.
[c]) Bachner *et al.* [8]).

reaction [8]). The spectroscopic factors in the two reactions leading to the parent levels and their analogues have in general a satisfactory resemblence except for the 6.78 MeV level ($J^\pi = \frac{1}{2}^+$). The 2s state presents a difficulty in that there is no single analogue of the 1.65 MeV level in ^{49}V; instead three levels, namely, 6.41, 6.43 and 6.47 MeV in ^{49}Cr appear at about the expected excitation and we have assumed that the 2s, $T_>$ strength is distributed over these levels. It may be noted that the present work confirms the tentative $l = 0$ assignment made by David *et al.* [2]) for the 6.41-6.43 MeV doublet and further that the angular distributions of γ-rays in the ^{50}Cr(τ, αγ) reaction [3]) relating the levels 6.41-6.43 MeV and 6.47 MeV are characteristic of $J^\pi = \frac{1}{2}^+$; they further have similar γ-decay properties.

Finally, the Coulomb displacement energy ΔE_C for the isobaric pair of nuclei ^{49}V-^{49}Cr comes to be 8.12 MeV for the g.s. analogue; the ΔE_C values for the other levels are shown in table 3. The slight variation in the values of ΔE_C may be attributed to the slight dependence of the Coulomb displacement energy matrix elements on the different shell-model states.

4.2. THE LEVEL SPECTRUM

The observed level spectrum of ^{49}Cr is compared with that of the available theories [4, 6, 7]) in fig. 5.

The level spectrum due to Ginocchio [6]) is from the conventional spherical shell-

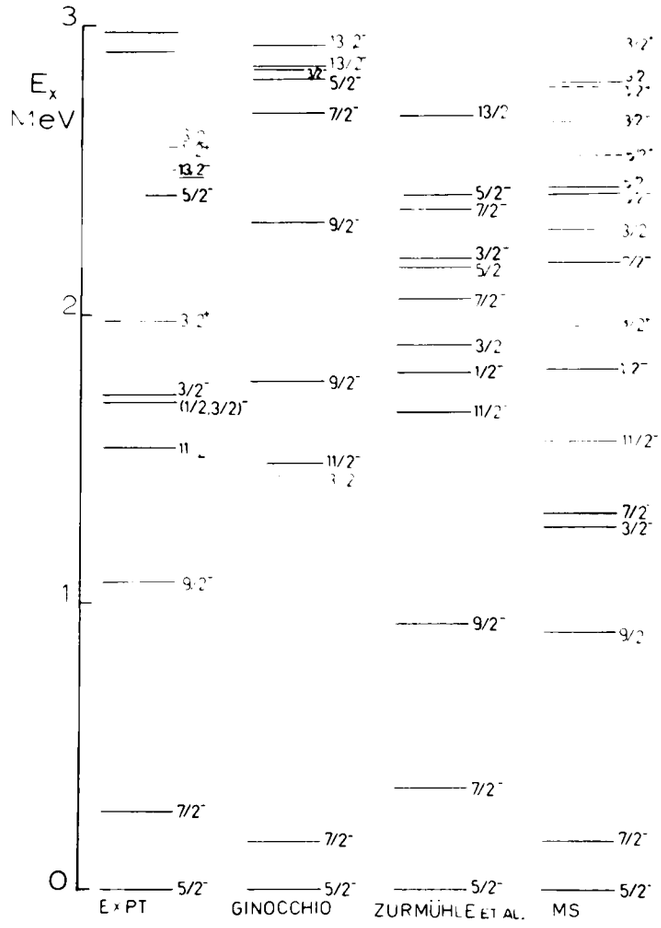

Fig. 5. Comparison of the experimental level spectrum of ^{49}Cr with different theoretical calculations. The broken lines and the J^π values that are underlined are from refs. [3-5]).

model calculations with the nine extra-core nucleons outside ^{40}Ca distributed only in the $1f_{\frac{7}{2}}$ shell and the two-body matrix elements were given by the experimental level spectra of ^{42}Ca, ^{42}Sc and ^{50}Ti (all having two nucleons in the $f_{\frac{7}{2}}$ shell). The calculations by Malik and Scholz [7]) are based on the collective model including a large Coriolis coupling between rotational bands. The other calculations due to Zurmühle *et al.* [4]) while otherwise similar to those of Malik and Scholz include the excited proton configurations, where necessary, to generate wave functions having good isopin.

The observed level spectrum is characterized by a doublet near the ground state followed by a gap of about 1 MeV †. This feature is reproduced in all calculations except the one by Ginocchio [6]), where the second excited state has $J^\pi = \frac{3}{2}^-$ and the level with $J^\pi = \frac{9}{2}^-$ appears much higher than the observed position. The $J^\pi = \frac{11}{2}^-$ level is correctly reproduced by all the three theoretical calculations.

It has been suggested [3,4]) that these four levels (ground and the first three excited states) with $J^\pi = \frac{5}{2}^-$, $\frac{7}{2}^-$, $\frac{9}{2}^-$ and $\frac{11}{2}^-$ may be members of the g.s. rotational band;

† This characteristic feature is present in the nuclei ^{45}Ca, ^{47}Ti, ^{51}Mn and ^{53}Mn, all having N or $Z = 25$.

both the band mixing calculations [4, 7]) successfully reproduce the levels with the correct spin sequence. The $J^\pi = \frac{9}{2}^-$ and $\frac{11}{2}^-$ levels appear with a reversal in position in the shell-model calculation [6]) and an additional $\frac{9}{2}^-$ level is predicted by this model which is not observed. The next member, $J^\pi = \frac{13}{2}^-$, of the proposed band may be either of the levels at 2.50 MeV [ref. [5])] and 2.69 MeV [ref. [4])] observed in the $^{46}Ti(\alpha, n\gamma)$ reaction. The $J^\pi = \frac{13}{2}^-$ level at $\approx$ 2.7 MeV predicted by Zurmühle *et al.* [4]) and one of the levels around $E_x \approx 3$ MeV given by Ginocchio [6]) may be the desired member of the band under discussion.

The doublet 1.698-1.725 MeV with the angular distributions typical of $l_n = 1$ are the best candidates for the $\frac{1}{2}^-$-$\frac{3}{2}^-$ doublet predicted by the band mixing calculations of Zurmühle *et al.* [4]). It is possible that the $\frac{1}{2}^-$ and $\frac{3}{2}^-$ levels calculated by Malik and Scholz [7]) at $\approx$ 2 MeV (with a much larger separation) correspond to the doublet under discussion. The extra $\frac{3}{2}^-$ at $\approx$ 1.2 MeV predicted by them is not observed.

The positive-parity levels are calculated only by Malik and Scholz [7]). The relative positions are given and the $\frac{3}{2}^+_1$ level is normalized to the observed level at $\approx$ 2 MeV (fig. 5). The observed $\frac{1}{2}^+$ level is well reproduced in these calculations [7]).

5. Conclusion

Twenty-nine levels are observed in the present experiment, as against eighteen by David *et al.* [2]). The l_n values, J^π limits and C^2S values are given for many of the levels including some new ones found in the present work. Several analogue states observed in a previous (τ, α) work are also found in the present work; in addition, two levels at 4.85 and 4.92 MeV are tentatively identified as analogues. The relative level spacings and the l_n values are consistent with the level spacings and the known J^π values of the parent levels. The spectroscopic factors for the corresponding levels from the (τ, α) and (t, α) reaction on the same target nucleus ^{50}Cr bear in general a reasonable proportionality. The observed level spectrum is better given by the band mixing calculations of Zurmühle *et al.* [4]) than the other band mixing calculations of Malik and Scholz [7]) and the spherical shell-model calculations of Ginocchio [6]).

Adequate information on the low-spin states ($J \leqq \frac{7}{2}$) is thus given by the single-neutron pickup reaction, but a study of the high-spin states selectively populated in the multi-nucleon transfer reactions using heavy ions seems promising.

The authors wish to thank Dr. D. Roaf for invaluable advice in running the magnetic spectrograph and processing the plates. They are thankful to Professor P. D. Kunz for the DWUCK code and Dr. D. Sinclair for instructions in the DWBA analyses. One of the authors (M.A.Z.) is grateful to the University of Dacca. Dacca for a fellowship. Another author (H.M.S.G.) acknowledges a grant from the Royal Society; he appreciates the hospitality of Professor K. W. Allen at the Nuclear

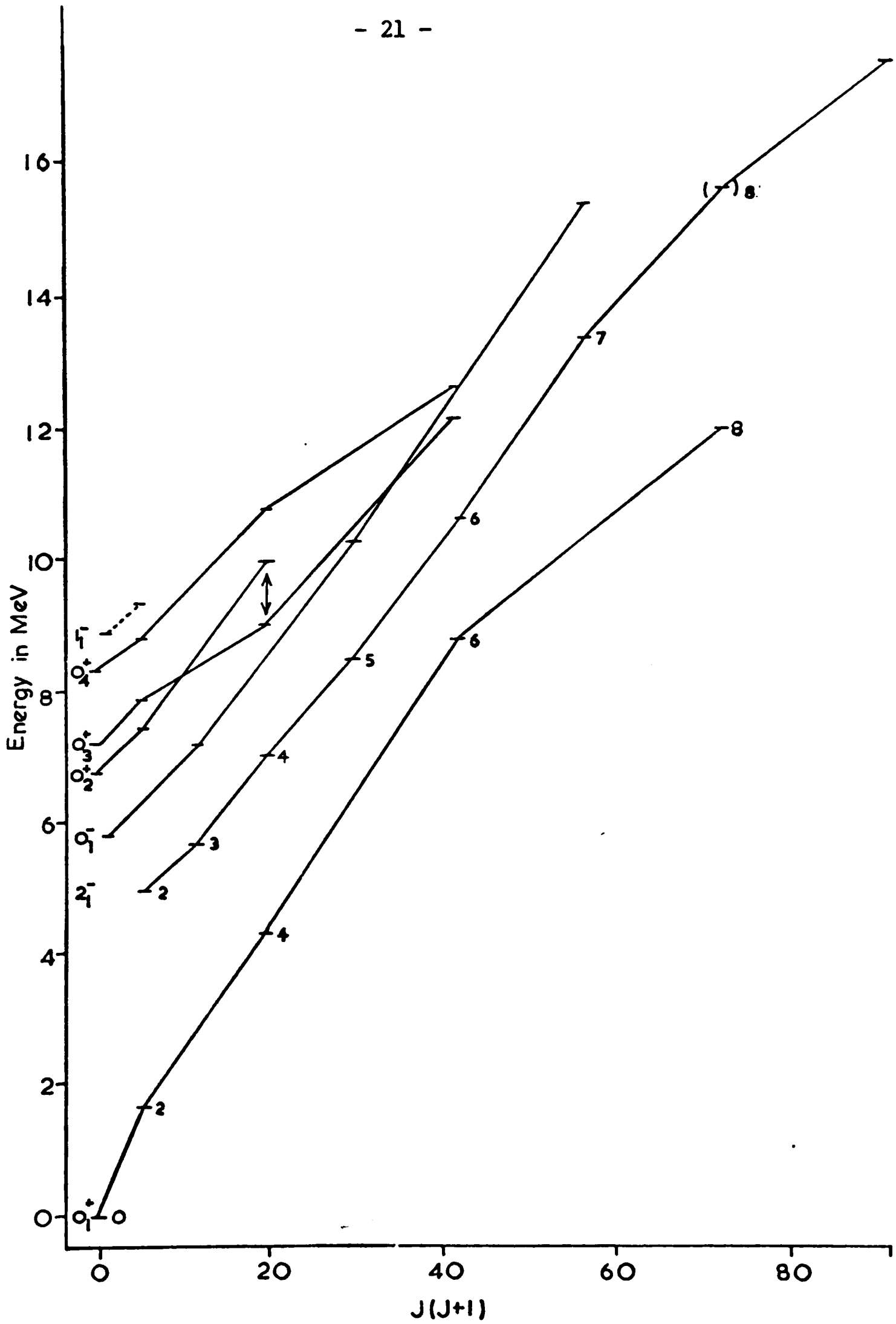

Fig.3.1.1 Plot of energy against J(J+1) for states assigned to bands in ^{20}Ne. The values of K^π are given at the start of each band, and the values of J are marked on the first two bands only.

Physics Laboratory, Oxford. M. J. H. acknowledges support from the Science Research Council.

References

1) C. A. Whitten and L. C. McIntyre, Phys. Rev. **160** (1967) 997
2) P. David, H. H. Duhm, R. Bock and R. Stock, Nucl. Phys. **A128** (1969) 47
3) D. A. Blumenthal, R. W. Zurmühle and P. D. Balamuth, Phys. Rev. **C4** (1971) 415
4) R. W. Zurmühle, D. A. Hutcheon and J. J. Weaver, Nucl. Phys. **A180** (1972) 417
5) Z. P Sawa, J. Blomqvist and W. Gullholmer, Nucl. Phys. **A205** (1973) 257
6) J. N. Ginocchio, Phys. Rev. **144** (1966) 952
7) F B. Malik and W. Scholz, Phys. Rev. **150** (1966) 919; also private communication quoted in ref. [3])
8) D. Bachner, R. Santo, H. H. Duhm, R. Stock and S. Hinds, Nucl. Phys. **A106** (1968) 577
9) A. R. Majumder, M. S. Chowdhury, H. M. Sen Gupta and A. Guichard, Nucl. Phys. **A238** (1975) 1
10) R. Bock, H. H. Duhm and R. Stock, Phys. Lett. **18** (1965) 61
11) R. J. Peterson, Phys. Rev. **170** (1968) 1003
12) B. Crosemann and H. T. Easterday, Phys. Rev. **90** (1953) 1124
13) R. H. Nussbawn, A. H. Wapstra, G. J. Nijgh, L. Ornstein and N. F Verster, Physica **20** (1954) 165

J. Phys. G: Nucl. Phys., Vol. 4, No. 3, 1978. Printed in Great Britain. © 1978

A study of the $^{15}N(\alpha,\gamma)^{19}F$ reaction for bombarding energies between 5·2 and 8·4 MeV. I. Yield curves and gamma decay schemes

T J M Symons, L K Fifield, M J Hurst, F Watt, C H Zimmerman and K W Allen

Nuclear Physics Laboratory, Keble Road, Oxford OX1 3RH, UK

Received 25 August 1977

Abstract. The $^{15}N(\alpha,\gamma)^{19}F$ reaction has been studied for α-particle bombarding energies from 5·2 to 8·4 MeV using a differentially-pumped gas target. Forty-two resonances have been identified in the gamma ray yield, of which 32 have been observed to decay by gamma emission to known states in ^{19}F. The remaining ten resonances were found to arise from the $^{15}N(\alpha,\alpha'\gamma)^{15}N$ and $^{15}N(\alpha,p\gamma)^{18}O$ reactions. Decay schemes, widths and values of $\omega\gamma$ have been measured for many of these states. The data obtained are compared with previous published work on the ^{19}F nucleus.

NUCLEAR REACTIONS $^{15}N(\alpha,\gamma)$, $E = 5{\cdot}2$–$8{\cdot}4$ MeV; measured $\sigma(E)$, Γ, $\omega\gamma$, γ branching. ^{19}F; deduced levels, J, π, Γ_γ. Windowless gas target.

1. Introduction

Historically, ^{19}F has played a central role in the development of our understanding of light nuclei. The small number of active nucleons outside the ^{16}O closed core allowed the first full intermediate-coupling shell-model calculation to be made for this nucleus by Elliott and Flowers (1955). This was soon followed by a description of the low-energy spectrum in terms of rotational bands based on the $\frac{1}{2}^+$ ground state and the $\frac{1}{2}^-$ first excited state (Paul 1957). Subsequently, the analysis of shell-model wavefunctions in terms of the SU(3) model has allowed considerable insight into the relation between microscopic and collective models for nuclei in this mass range (Harvey 1964). An interesting recent development has been the suggestion that there may be considerably more three- and four-particle clustering of the active nucleons than is suggested by the simple shell model (Buck *et al* 1975, Buck and Pilt 1977).

A considerable experimental effort has been proceeding in parallel with these theoretical studies. The experimental data available up to 1972 have been summarised by Ajzenberg-Selove (1972), and an excellent critical review of the positive parity levels has been given by Rogers (1973). More recently, both direct three- (Hamm *et al* 1976, Van der Borg *et al* 1976) and four- (Middleton 1970, Pilt *et al* 1976) particle transfer reactions have been used to populate levels in ^{19}F. Both the SU(3) and cluster models predict that these reactions should selectively populate members

of the low-lying positive and negative parity bands respectively. These reactions have indeed proved to be highly selective especially at high bombarding energies (10 MeV/nucleon), this selectivity persisting to quite high excitation in ^{19}F for both reactions. However, by themselves the transfer data are inadequate since our understanding of the reaction process is insufficient for any but the most general statements to be made regarding the nature of the states populated. On the other hand, compound nuclear reactions with light projectiles do provide very much more detailed information that is generally model independent, although these reactions are, of course, far less selective of a particular configuration.

This paper describes a study of the region of excitation from 8·2 to 10·6 MeV in ^{19}F using the ^{15}N(α,γ)^{19}F reaction. This reaction has been used extensively at lower energies to investigate the radiative decays of unbound states in ^{19}F. The principal motivation for this work was to obtain detailed information regarding the electromagnetic decays of the states seen in many-particle transfer reactions. Although this energy region has been studied carefully using the ^{18}O(p,γ)^{19}F reaction, there were strong reasons for believing that the proton widths of the high-spin states should be very much smaller than the corresponding α widths and that radiative α capture should provide a useful complementary technique. The experimental difficulties with radiative α capture at energies greater than a few MeV are well known (see, for example, Rolfs and Litherland (1975)) and will be discussed only briefly in §2.

In the experiments performed, several new high-spin states were indeed observed, as has already been reported (Symons *et al* 1976, Fifield *et al* 1977). However, many other states were populated, and the purpose of this paper is to provide a concise description of these other levels. Although angular distribution measurements were not made in this series of experiments, the observed gamma decay widths allow limits to be set on the spin and parity assignments for many of the levels. Some of the states have also been observed in proton-induced reactions and, where appropriate, comparisons will be made between the two sets of data.

2. Experimental methods

2.1. Accelerator and beam line

The Q value for radiative capture of alpha particles by ^{15}N is 4·013 MeV, and the reaction may be used to populate levels in ^{19}F above this energy. As the bombarding energy is raised, both the average density and natural widths of the resonances observed will increase. However, for bombarding energies up to 8·4 MeV, the highest energy reached in this study, the resonances remain for the most part well separated. Under these circumstances, a single state will be populated at a particular bombarding energy. This, of course, is dependent on the ability of the accelerator to resolve states that may be separated by a few keV only. It is also necessary that the accelerator should produce an intense beam, since typical capture cross sections are of the order of a few microbarns. In all the experiments described here, we have used the ^{4}He$^+$ beam from the single-ended Oxford injector van de Graaff accelerator. This machine satisfies both of the requirements described above, since the spread in energy of the analysed beam is less than 1 keV at 5 MeV, and steady beams of 20 μA or more may readily be obtained from the radio-frequency ion source up to 9 MeV bombarding energy.

Since the capture gamma ray yield is so small, it is necessary to minimise the production of gamma rays and fast neutrons from nuclear reactions with contaminants in the beam line and target material. In unfavourable circumstances, this background may entirely obscure the weaker capture gamma rays. In particular, above 5·1 MeV bombarding energy, 6·13 MeV gamma rays from the prolific $^{13}C(\alpha,n\gamma)^{16}O$ reaction dominate the high-energy spectrum unless strict precautions are taken to eliminate carbon from the system.

For earlier work at Oxford (e.g. Alexander *et al* 1972), a clean beam line was constructed using stainless steel throughout and a hydrocarbon free pumping system. However, with water-cooled solid targets, it proved difficult to eliminate residual carbon from the gold backings. This placed an effective upper limit of 5 MeV on the bombarding energy that could be used.

However, the study of capture resonances at higher energies has become routine following the development at Oxford of a differentially cryopumped gas target. This system has been described in detail elsewhere (Allen *et al* 1976) and was used for all the experiments described in this paper. Briefly, the design and operation of the system were as follows.

The target chamber, which is shown in figure 1, consisted of a thin-walled stainless steel tube, 19 cm in length, at each end of which were coaxially mounted tantalum nozzles 2·5 cm long by 3 mm internal diameter. The beam entered and left the cell through these nozzles, the dimensions of which were chosen as a compromise between the requirement that there should be 100% transmission of the beam, and that the gas flow out of the target should be minimised. In this we were aided by the low emittance of the beam from the accelerator.

The necessarily high pumping speeds were provided by liquid-helium-cooled cryopumps mounted in the differential pumping regions on either side of the target chamber. Differential pumping apertures were also provided between the regions pumped by the cryopumps and the remainder of the beam line.

Nitrogen-15 gas, enriched to 99·6% purity, was fed into the chamber through a servo-controlled valve, the servo signal being provided by the output from a capacitance manometer which measured the pressure in the chamber. Since the ^{15}N gas accumulated on the cryopump surfaces during an experiment, it was necessary to warm

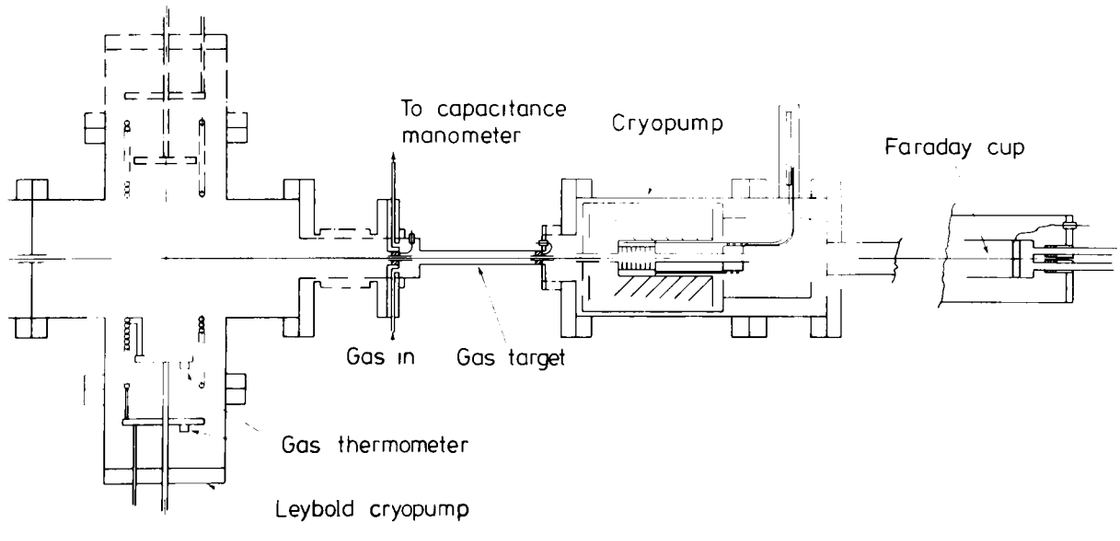

Figure 1. Layout of the transmission gas target.

up the cryopumps at intervals to return this gas to the storage volume. This was accomplished by incorporating a small liquid helium cooled cryofinger into the storage volume itself.

After transmission through the target, the beam was stopped in a well shielded Faraday cup 3 m from the chamber. Under optimum focusing conditions, more than 99·9% of the incident beam passed through the target chamber.

2.2. *Measurement of the excitation function*

The yield of gamma rays was measured as a function of beam energy using a 10·2 × 10·2 cm NaI(Tl) detector mounted 3 cm from the beam axis. The beam energy was varied automatically by modulating the field in the analysing magnet (Wormald and Takacs 1974), the energy stabilisation system then forcing the machine energy to follow this changing field. Gamma ray pulses from the detector were sorted into seven energy intervals using single-channel analysers, and the data recorded in different subgroups of a multichannel analyser memory using an interface which set up a correspondence between channel number in the memory and the frequency of the nuclear magnetic resonance (NMR) probe used to measure the field in the analysing magnet. An eighth subgroup was used to store the digitised output from the beam current integrator, so that each channel of the yield curve could be normalised to the same incident charge. Typically, the beam energy was varied over a range of 100 keV in a single run, and the separate sections, after normalisation, were joined off-line to produce the total excitation function over the energy range studied.

2.3. *Measurement of the natural widths of resonances*

In principle, the natural widths of the resonances observed may be extracted from the gamma ray yield curves, provided that the instrumental width is small compared with the natural width. In practice, however, several features of the experimental data limited the accuracy that could be obtained.

Using the notation of Gove (1959), the gamma ray yield as a function of energy may be written as

$$Y = n \int_0^{E_1} \int_0^{t} \int_0^{'} \sigma(E) w(E_i, E, x) g(E_b, E_i)\, dE\, dx\, dE_i \qquad (1)$$

where $g(E_b, E_i)$ represents the probability that an incident particle has energy E_i when the beam has nominal energy E_b, $w(E_i, E, x)$ represents the probability that a particle of incident energy E_i has an energy E at a distance x through a target of thickness t and $\sigma(E)$ is the Breit–Wigner cross section for the yield from an isolated resonance.

If one is to obtain the width of a resonance by fitting this expression to the experimental data, then it is important to have reliable forms for the two distribution functions, g and w.

There are two contributions to the beam energy distribution function. The first arises from the energy spread of the accelerated beam. For the Oxford injector this is of the order of 1 part in 5000. The form of the distribution is not known and, as an approximation, it was assumed to be gaussian. The second contribution comes from the thermal motions of the molecules in the target, since to first order the

effective energy of an incident α particle in the laboratory is given by

$$E = \tfrac{1}{2} MV^2 - MV v_z$$

where V is the velocity of the incoming α particle and v_z is the component of velocity of the target molecule along the beam axis in the direction of the incident beam.

Using simple kinetic theory, one may show that the effect of the translational motion is to introduce an effective gaussian spread in the beam energy, with a width of 0·47 keV at room temperature for a 6 MeV α particle beam. Similar analyses lead to widths of 0·36 and 0·66 keV from the rotational and vibrational degrees of freedom respectively. Adding these three contributions in quadrature to the expected intrinsic beam energy spread at 6 MeV, one expects an energy resolution of the order of 1·3 keV in the laboratory frame.

If this intrinsic resolution is to be attained, then it is essential that the relation between the NMR frequency and beam energy should remain constant during a run which may last for up to two hours. It is also important that the NMR frequency should follow the changing field accurately.

The energy loss distribution (w) is difficult to obtain accurately. For a thick target, in which each α particle undergoes many interactions while passing through the gas, the distribution will be gaussian, with the width increasing as the square root of the energy lost. However, in the experiments described here, the target thickness was typically of the order of 4 keV or less. This is comparable with the maximum energy that may be lost by an α particle in a single collision with an atomic electron, which is 3 keV at 6 MeV. Fluctuations in the energy loss are then important, and the distribution is asymmetrical, depending on the exact form of the interaction cross section between the particle and the atomic electrons. This problem was first considered by Landau (1944), who obtained an analytic form for the distribution in the limit of very thin samples, using an approximate form for the cross section. Landau's methods have been extended by Symon (1952), and by Vavilov (1957) into the regime between the thin and thick sample cases.

All these methods assume an approximate form for the cross section, and neglect effects due to the discrete binding energies of the different atomic electrons. Recently, Cobb *et al* (1976) have developed a Monte-Carlo program to integrate directly the cross sections derived by Fano (1963). This may be expected to yield more reliable results than the analytic methods for thin samples. In the results discussed here, the target thicknesses were in a range where the differences between the Symon theory and Monte-Carlo results are small. Nevertheless, it was considered that the latter distributions should be used. In order to incorporate the Monte-Carlo results into a least-squares fitting program, the Monte-Carlo program was run for a series of different beam energies and target thicknesses within the region of interest. The distributions obtained were then parametrised using a simple analytic function. The expression for the yield given in (1) was then integrated numerically to generate artificial yield curves. As a test of the program, it was first applied to the $T = \frac{3}{2}, \frac{3}{2}^+$ resonance in the $^{15}N(\alpha,\gamma)^{19}F$ reaction at 4·61 MeV. This resonance is known to have a natural width of 8 eV (Wormald and Wright 1969), which will not contribute to the width of the peak observed in the yield curve. The fit obtained is shown in figure 2 and accounts well for the asymmetric shape of the yield curve. At this energy, the fitted pressure (0·066 Torr) was 20% higher than the actual pressure in the target (0·055 Torr), indicating that the Monte-Carlo program was giving rather too low

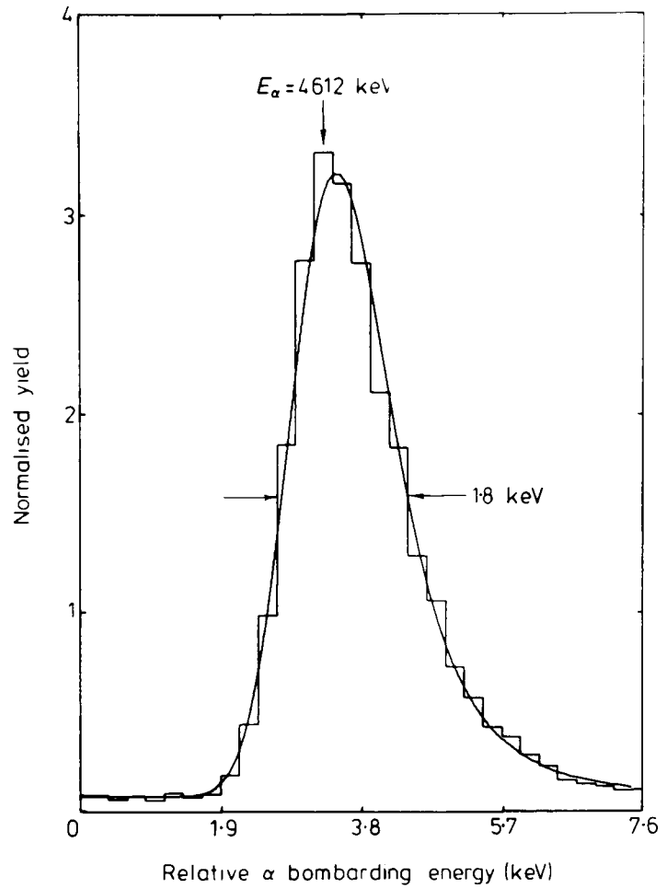

Figure 2. Theoretical fit to the yield curve obtained over the 4·61 MeV $\frac{3}{2}^+$ resonance in the $^{15}N(\alpha,\gamma)^{19}F$ reaction.

a stopping power. However, fits to sharp resonances at higher bombarding energies usually agreed to within 10% with the nominal gas pressure.

The program was then used to extract the natural widths of many of the resonances observed between 5 and 8 MeV bombarding energy. A limitation in the usefulness of the method is due to uncertainties in the beam energy distribution. Since both the beam spread and the natural width of the resonances add approximately in quadrature to give the observed width it was impossible to be sure whether any slight broadening in a particular resonance profile was due to the width of the resonance or a systematic shift in the NMR calibration during a run, or to the poor tracking of the magnetic field by the NMR system. For this reason, only limits on the natural width were obtained for resonances which could be adequately explained by a beam width of 2 keV or less.

2.4. *Measurement of gamma decay spectra*

When a resonance in the gamma ray yield had been located, the decay spectrum was measured using an 85 cm^3 Ge(Li) detector. The detector was mounted 14 cm from the centre of the target chamber at an angle of 55° to the beam axis. This angle was chosen in order to minimise effects of the gamma ray anisotropy on the observed intensity, since at 55° $P_2(\cos\theta)$ vanishes and no correction needs to be applied to pure dipole transitions.

Initially, spectra were recorded in an 8192-channel analyser and were then transferred to the PDP10 computer for off-line analysis. The spectra were taken with the target pressure set at 0·22 Torr as in the yield curve measurements. Several off-resonance spectra were also recorded to permit identification of background peaks in the spectrum. All the gamma rays observed in the spectrum above 1 MeV energy were identified as coming from one of the following sources.

(1) The capture process itself;

(2) inelastic α particle reactions with the ^{15}N target;

(3) reactions with aluminium contamination in the tantalum nozzles;

(4) reactions with residual ^{13}C in the beam line and nozzles;

(5) naturally occurring isotopes present in the walls of the target room, such as ^{40}K and ThC″;

(6) thermal neutron capture in the iron of the target chamber;

(7) reactions with residual ^{14}N in the target gas.

The relative intensities of the different primary transitions were extracted from the peak areas using the relative efficiency function of the Ge(Li) detector. This was generated by interpolation, using pairs of gamma rays of known relative intensity. These were obtained from radioactive sources, from well known resonances in the $^{15}N(\alpha,\gamma)^{19}F$ reaction, and from resonances in the $^{27}Al(p,\gamma)^{28}Si$ reaction.

2.6. *Decay strengths*

The maximum gamma ray yield from a resonance of natural width Γ, using a target of thickness T keV, may be derived from the Breit–Wigner cross section, and is found to be

$$Y_{\max} = \frac{4\pi\lambda\!\!\!^{-2}_{\alpha}}{S}\omega\gamma \tan^{-1} T/\Gamma$$

where $\omega\gamma$ is defined to be

$$\frac{2J+1}{2}\frac{\Gamma_\alpha\Gamma_\gamma}{\Gamma}$$

for the $^{15}N(\alpha,\gamma)^{19}F$ reaction, $\lambda\!\!\!^{-}_{\alpha}$ is the Compton wavelength for the incident α particle in the centre-of-mass frame and S is the stopping power of the target material per ^{15}N nucleus.

Clearly, this expression has a limiting value when $T \gg \Gamma$ of $(2\pi^2/S)\lambda\!\!\!^{-2}_{\alpha}\omega\gamma$. Therefore, measurement of the gamma ray intensity provides a direct measurement of $\omega\gamma$. Furthermore if, as is often the case, $\Gamma_\alpha \gg \Gamma_\gamma$ and $\Gamma_\alpha \approx \Gamma$, then $\omega\gamma \approx \frac{1}{2}(2J+1)\,\Gamma_\gamma$ and the gamma decay width may be extracted directly from $\omega\gamma$. Rather than make an absolute measurement of $\omega\gamma$ for each resonance, it is usual to compare the relative intensities of the gamma rays from different resonances with that of one carefully measured standard resonance. In this way, systematic errors arising from incorrect calibration of the beam current integrator, uncertainties in the α particle stopping power and other quantities may be minimised.

In the experiment described here, measurements of $\omega\gamma$ were made relative to the gamma ray yield from the $\frac{5}{2}^+$, $T = \frac{3}{2}$ resonance at 4·47 MeV. The value of $\omega\gamma$ for this resonance has been taken as 17·4 ± 2·1 eV (Rogers 1976).

2.7. Spin and parity assignments

From the measured value of $\omega\gamma$ of a resonance level, it is possible to extract values for the quantity $(2J + 1)\Gamma_\gamma$ as follows. For levels in ^{19}F below 10·4 MeV in excitation, α particle and proton emission are the only possible particle decay modes, and hence $\Gamma = \Gamma_\alpha + \Gamma_p + \Gamma_\gamma$. Most of the resonances observed in the present work have not been observed in either the ^{18}O(p, γ)^{19}F or ^{18}O(p, α)^{15}N reactions, indicating that $\Gamma_p \ll \Gamma_\alpha$. If we then make the reasonable assumption that $\Gamma_\gamma \ll \Gamma$, then $\omega\gamma = \frac{1}{2}(2J + 1)\Gamma_\gamma$. To the extent that this assumption is invalid, the value of Γ_γ will be *underestimated* by this procedure. For those resonances which have been observed in the proton-induced reactions, it is a simple matter to include the effect of the proton partial width if either of the quantities

$$\frac{(2J + 1)\Gamma_p\Gamma_\gamma}{2\Gamma} \quad \text{or} \quad \frac{(2J + 1)\Gamma_p\Gamma_\alpha}{2\Gamma}$$

has been measured.

Once the value of $(2J + 1)\Gamma_\gamma$ has been determined, electromagnetic decay strengths of the various decay branches may be extracted for a given value of the resonance spin and parity, J^π, and expressed in some suitable reduced form such as the Weisskopf unit (Wu). These decay strengths may be used to place sensible limits on the values of J^π by comparison with the recommended upper limits on the decay strengths of transitions of given multipolarity as tabulated, for example, by Endt and van der Leun (1974). Although this method rarely provides unique J^π assignments, it is essentially model independent. The remaining ambiguities may often be resolved by gamma ray angular distribution measurements, but such measurements are beyond the scope of the present work.

3. Experimental results

3.1. Yield curves

The gamma ray yield was measured for α-particle bombarding energies between 5·2 and 8·4 MeV using the methods described in §2.2. The results obtained are illustrated in figures 3(*a*)–(*d*), where the yield curves for gamma rays of between 3·5 and 5 MeV and of greater than 5 MeV are shown. In general, high-spin resonances, which decay by a cascade of low-energy gamma rays, will be seen more strongly in the 3·5 to 5 MeV gate than in the high-energy gate. Examples are the resonances at 6·65 and 7·38 MeV.

It may be noted that there are discontinuities in the yield curves at various energies. These arise where the background level changed between two runs as a result of slight variations in beam focusing conditions. In total, some 42 prominent resonances were observed. These have been numbered in the figure, and this numbering scheme will be adhered to in the remainder of the paper. In addition to the resonances marked, there was evidence for several weak underlying resonances with widths of the order of 50 keV or more. An example is the broad state centred at approximately 5830 keV. No attempt has been made to study these broad states in detail.

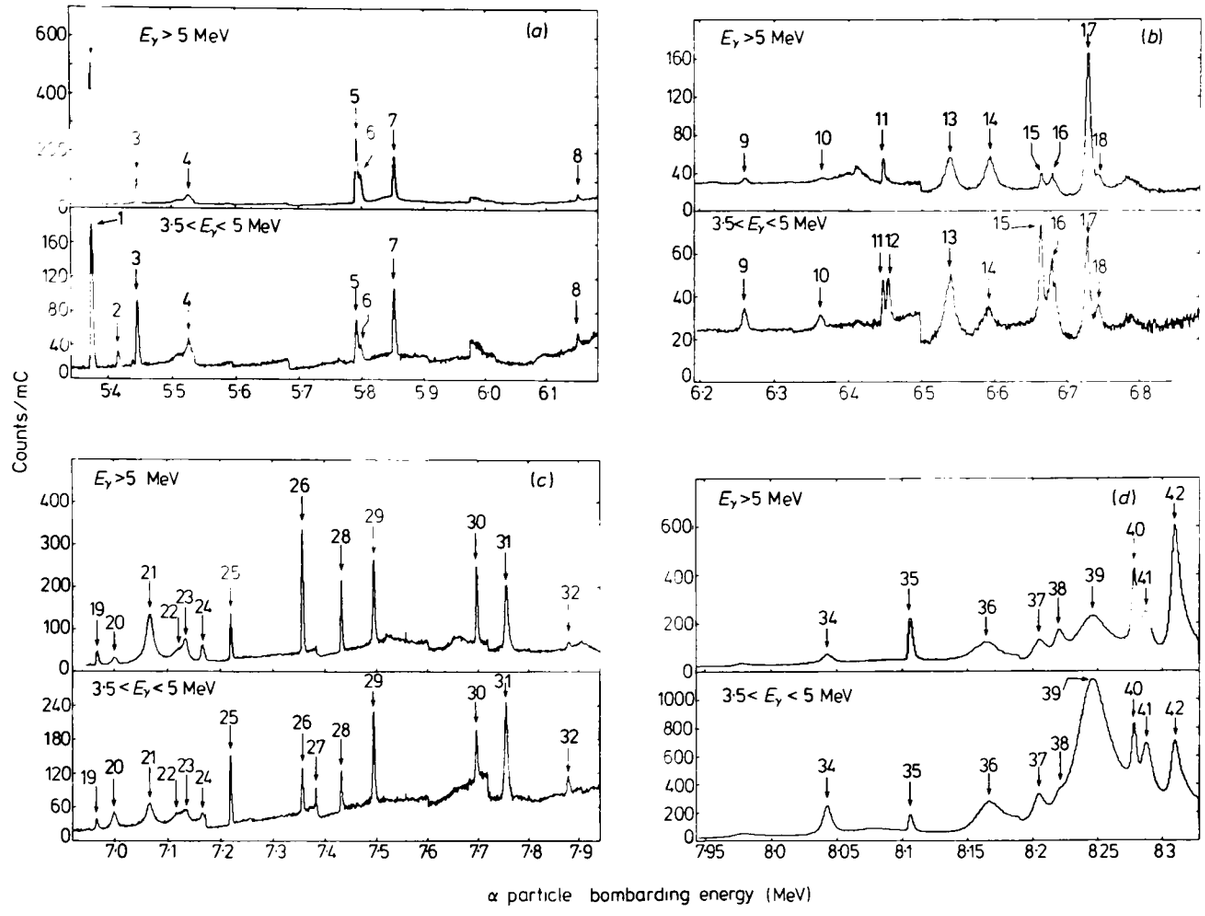

Figure 3. Gamma ray yield curves obtained from the bombardment of $^{15}N_2$ gas by α particles in the range of energies from 5·3 to 8·4 MeV.

3.2. Gamma decay spectra

Gamma ray spectra were recorded at all the resonances with the exception of resonance number 1, which has been studied in detail in previous work using solid targets (Underwood 1972). The Ge(Li) detector was mounted in the configuration described in §2.4, and the gas pressure was maintained at 0·22 Torr for all the separate runs. Subsequently, the spectra were analysed and capture gamma ray transitions identified from 32 of the 41 resonances studied. Typical spectra obtained on resonance are shown in figures 4 and 5 together with an off-resonance spectrum. The relative intensities of the transitions were then extracted using the Ge(Li) detector relative efficiency curve. It was also possible to extract the energies of the resonances from the gamma decay energies. In almost all cases this provided more accurate excitation energies than could be obtained from the α-particle bombarding energies. The relative intensities obtained are shown in figure 6 together with the excitation energies of the states.

3.3. Widths of resonances

For many of the resonances observed it was possible to extract the natural width directly using the procedures described in §2.5. A typical example was resonance number 13, for which the yield curve together with the fit obtained is shown in figure 7. In the case of sharp resonances, only upper limits could be obtained for

can be made using capture reactions, and provide a direct measure of the validity of a band hypothesis, the quality of the agreement between theory and experiment giving a measure of the success of the calculated wave-functions in describing the band members.

The four in-band transitions for the ground state band have all been measured, a remeasurement of the $8^+ - 6^+$ transition strength being reported in Chapter 5 (also Hurst et al.[Hu80]). Transition strengths in the $K^\pi=2^-$ band have also been reported up to the decay of the 6^- state. It was not possible to extend the measurements to the 7^- member in the work reported in this thesis because the excitation of 13.33MeV required too high a beam energy(E_α=10.76MeV). No transition strengths in the 0^- band are known. The 5^- member has a width of 145KeV, making it totally unsuitable for study with the gas target and, although the 3^- member at 7.17MeV has a width of only 8KeV, this is still rather broad and the expected enhanced E2 decay would have an energy of 1.4MeV which might be difficult to observe due to the background caused by Compton scattering of 1.63MeV γ-rays from the decay of the first excited state populated in competing decay branches. In fact we searched for this state, but without success.

For the other bands the same problems apply. The high-spin states are usually at too high an excitation, and for those which are accessible, the total width is often too great and the energy of the enhanced γ-ray transition is too small. The 12.14MeV(6^+,$K^\pi=0^+_3$) level was observed as a resonance in the $^{16}O(\alpha,\alpha_2\gamma)^{16}O$ reaction which produces 6.13MeV γ-rays, but no capture γ-rays were observed. The 9.03MeV(4^+,$K^\pi=0^+_3$) level was seen as a resonance and a value was obtained for the total width, but the decay spectrum was not studied as it was

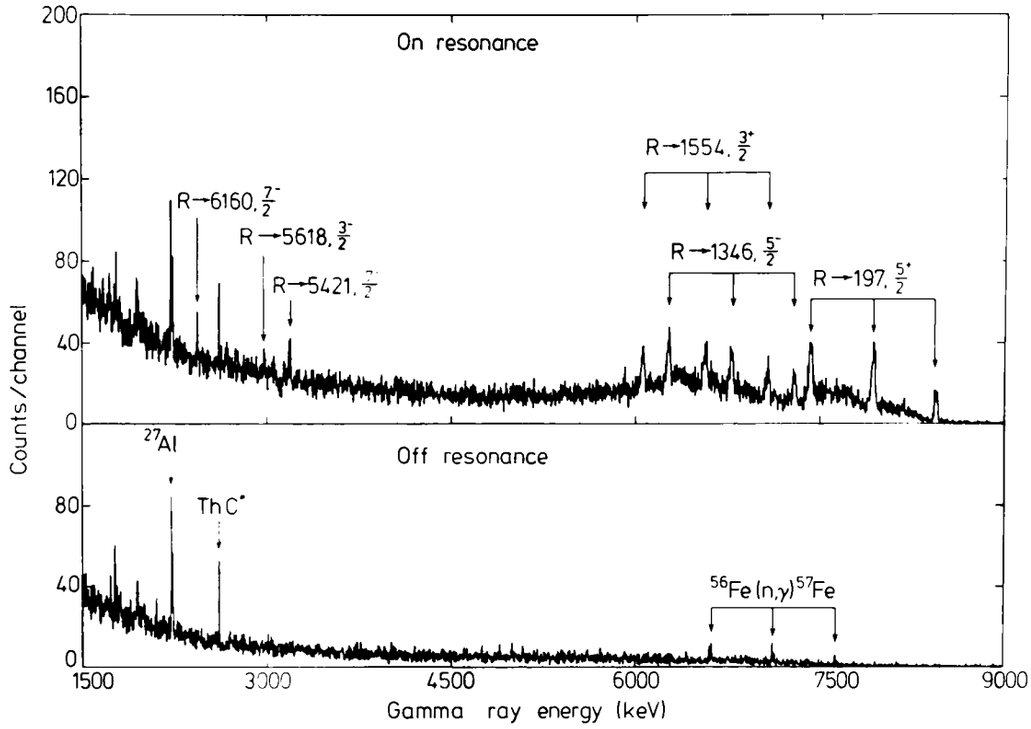

Figure 4. Gamma decay spectrum from the 5·784 MeV resonance in the $^{15}N(\alpha,\gamma)^{19}F$ reaction, obtained using a 85 cm^3 Ge(Li) detector.

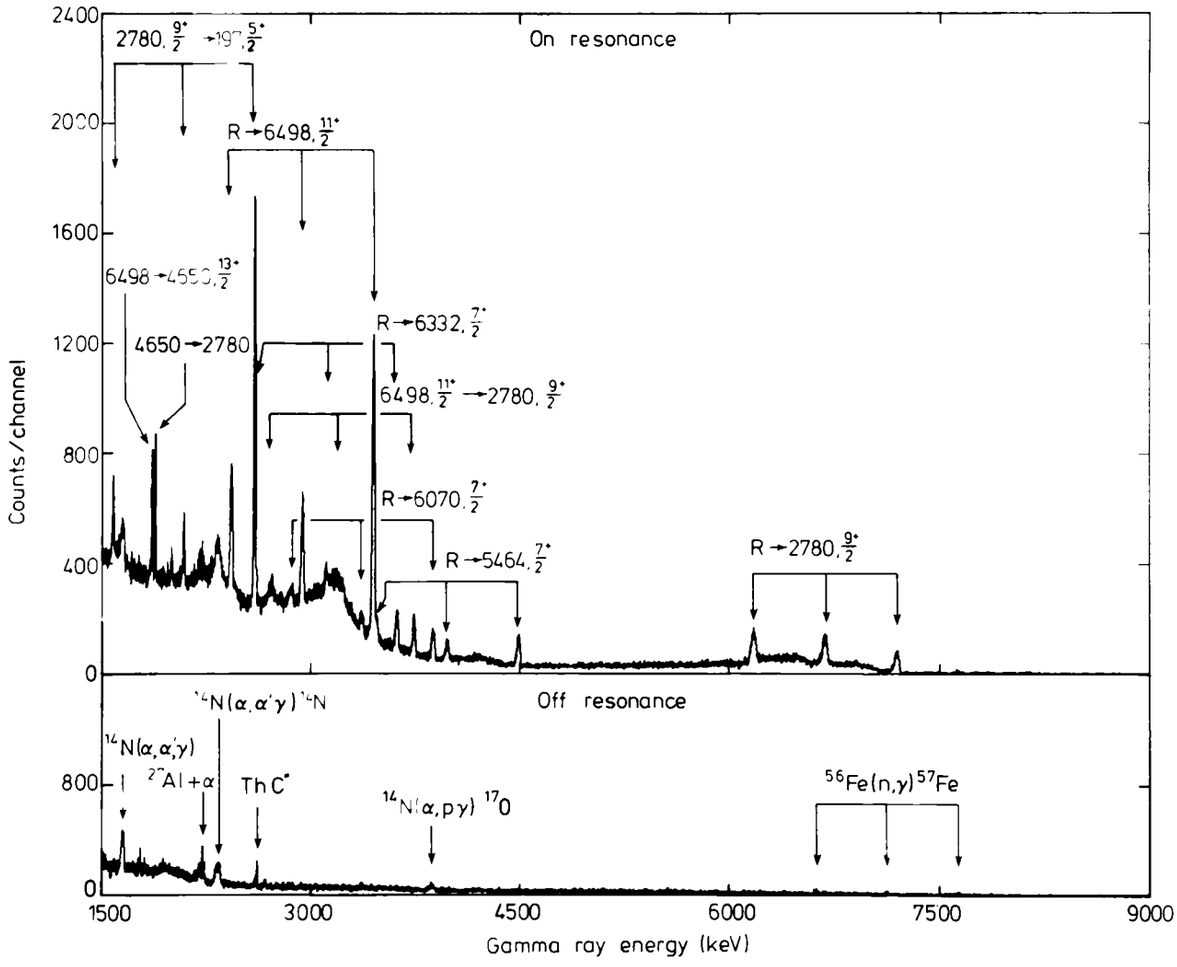

Figure 5. Gamma decay spectrum from the 7·491 MeV resonance in the $^{15}N(\alpha,\gamma)^{19}F$ reaction.

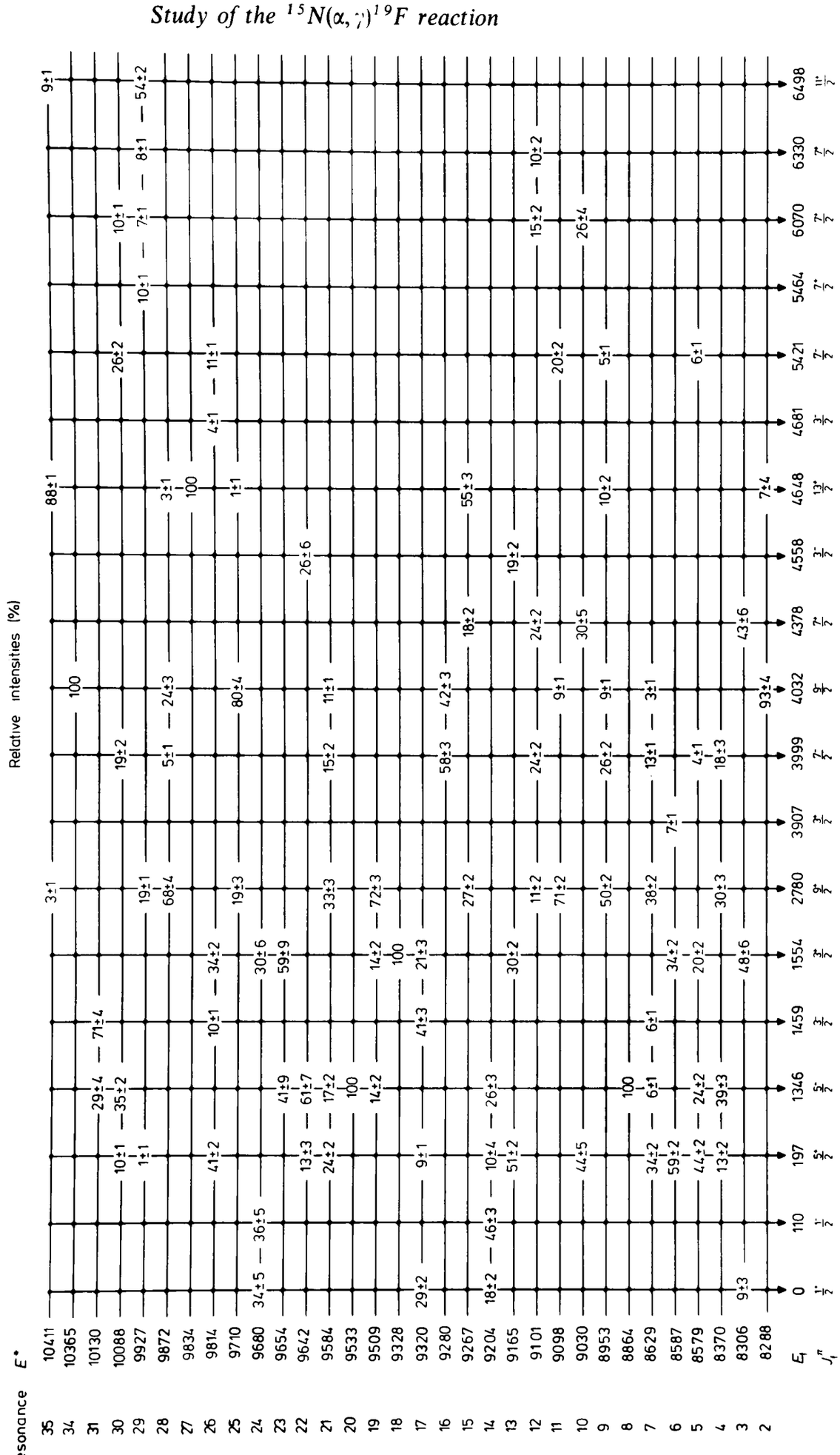

Figure 6. Relative intensities at 55° of the decays of resonances observed in the $^{15}N(\alpha,\gamma)^{19}F$ reaction.

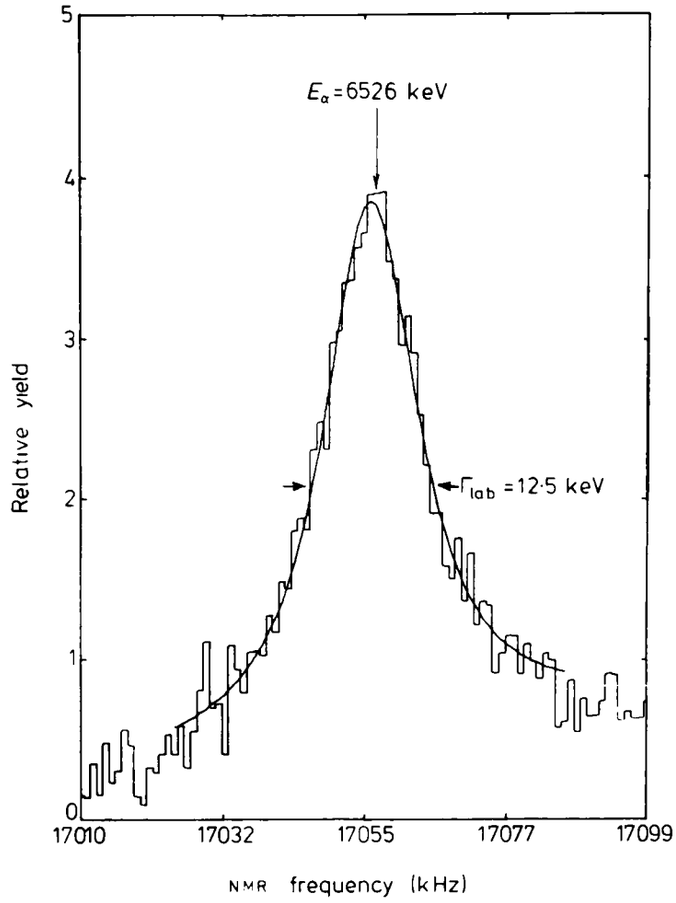

Figure 7. Calculated and experimental yield curves for the 6·526 MeV resonance in the $^{15}N(\alpha,\gamma)^{19}F$ reaction.

widths, and secondly, the program used was unable to fit overlapping resonances. In these latter cases an estimate of the width could usually be made. The widths of the resonances studied are tabulated in table 1.

3.4. $\omega\gamma$ measurements

Values of $\omega\gamma$ have been extracted for all the resonances from which capture gamma rays were observed. In most cases, these values were derived from the spectra accumulated at a target pressure of 0·22 Torr. This corresponds to a target thickness of approximately 3 keV in the energy range studied here. Thus the thick-target approximation is hardly valid even for sharp resonances where the upper limit that may be placed on the width of the resonance is of the order of 1 keV. Therefore, corrections were made assuming the widths shown in table 1, and the errors on $\omega\gamma$ increased accordingly. However, for several of the sharp high-spin states, further measurements of $\omega\gamma$ were made using a target pressure of 0·66 Torr corresponding to a target thickness of 10 keV. Clearly, the thick-target approximation is more reliable in these cases. The values of $\omega\gamma$ obtained are shown in table 1 and may be used in conjunction with the table of decay schemes to obtain the $\omega\gamma$ values for individual transitions. It must be emphasised once again that these values refer to measurements at 55° and contain no corrections for angular distribution effects.

Table 1. Properties of capture resonances.

Resonance	E^* (keV)	E_α (keV)	Γ (keV)	$\omega\gamma$ (55°) (eV)	J^π
2	8288 ± 4	5415 ± 5	<1	0·58 ± 0·1	$\frac{13}{2}^-$
3	8306 ± 4	5439 ± 5	<1	2·1 ± 0·5	$\frac{5}{2}^+$
4	8370 ± 4	5520 ± 5	7·5 ± 1·5	0·54 ± 0·2	$\frac{7}{2}, \frac{5}{2}^+$
5	8579 ± 4	5784 ± 5	~1	5·1 ± 1·3	$\frac{5}{2}$
6	8587 ± 3	5794 ± 4	2·1 ± 0·1[a]	1·6 ± 0·35	$\frac{3}{2}$
7	8629 ± 4	5487 ± 5	<1	2·5 ± 0·4	$\frac{7}{2}^+$
8	8864 ± 4	6145 ± 5	<1	0·2 ± 0·05	$<\frac{9}{2}$
9	8953 ± 3	6261 ± 4	~1	0·85 ± 0·2	$\frac{11}{2}^-, (\frac{9}{2}^+)$
10	9030 ± 5	6356 ± 5	4·2 ± 1	0·53 ± 0·26	$\frac{5}{2}, \frac{7}{2}$
11	9098 ± 4	6442 ± 5	0·57 ± 0·03[a]	0·48 ± 0·15	$\frac{7}{2}^+$
12	9101 ± 4	6445 ± 5	~1	0·40 ± 0·1	$\frac{7}{2}, \frac{9}{2}$
13	9165 ± 5	6526 ± 6	9·9 ± 1·5	1·4 ± 1	$\frac{1}{2}, \frac{3}{2}$
14	9204 ± 7	6576 ± 6	10·2 ± 1·5	1·5	$\frac{3}{2}$
15	9267 ± 4	6656 ± 5	2 ± 1	0·15 ± 0·04	$\frac{11}{2}^+, \frac{9}{2}^+$
16	9280 ± 5	6672 ± 6	<1·5	0·38 ± 0·09	$\frac{7}{2}, \frac{9}{2}$
17	9320 ± 4	6722 ± 5	3·4 ± 1	3·4 ± 1·7	$\frac{1}{2}^+$
18	9329 ± 4	6735 ± 5	~6	—	$<\frac{5}{2}$
19	9509 ± 4	6963 ± 5	<1	0·7 ± 0·2	$\frac{5}{2}^+, \frac{7}{2}^+$
20	9533 ± 6	6993 ± 7	6·3 ± 1·5	0·5	$\frac{3}{2}, \frac{5}{2}, \frac{7}{2}$
21	9584 ± 4	7057 ± 5	9·6 ± 1·5	5·2 ± 3	$\frac{7}{2}$
22	9642 ± 6	7131 ± 7	~8	~1	$\frac{3}{2}, \frac{5}{2}$
23	9654 ± 6	7146 ± 6	~6	~2	$\frac{3}{2}, \frac{5}{2}$
24	9680 ± 6	7179 ± 7	~4	~1	$\frac{1}{2}, \frac{3}{2}$
25	9710 ± 4	7217 ± 5	<1	4 ± 0·7	$\frac{9}{2}^+, \frac{11}{2}$
26	9814 ± 4	7349 ± 5	<1·5	3·5 ± 0·8	$\frac{5}{2}^+$
27	9834 ± 3	7376 ± 4	<1	0·51 ± 0·1	$\frac{11}{2}, \frac{13}{2}, \frac{15}{2}$
28	9872 ± 3	7422 ± 4	~1·5	3·6 ± 0·6	$\frac{9}{2}^+, \frac{11}{2}^-$
29	9926 ± 3	7491 ± 4	~1	19·3 ± 3·0	$\frac{9}{2}^+$
30	10088 ± 5	7696 ± 6	<1·5	2·37 ± 0·5	$\frac{5}{2}, \frac{7}{2}$
31	10130 ± 6	7749 ± 6	3·2 ± 1	1·3 ± 0·4	$\frac{3}{2}, \frac{5}{2}$
34	10365 ± 4	8047 ± 5	3 ± 1·5	0·9 ± 0·4	$\frac{7}{2}, \frac{9}{2}, \frac{11}{2}$
35	10411 ± 3	8105 ± 4	<1·5	15·0 ± 3·0	$\frac{11}{2}^+, \frac{13}{2}^+$

[a] These values are from the measurements of Yagi (1962).

3.5. Spin assignments

We have discussed in §2.7 how the transition strengths measured may be used to put strong limits on the spins and parities of the states that have been observed. The limits obtained are shown in table 1. In some cases there is evidence from other nuclear reactions that may be used to put further restrictions on the possible spin assignments. In these cases, the values that may be eliminated in this way are shown in brackets. This will be discussed further in the next section.

3.6. Resonances in $^{15}N(\alpha,\alpha'\gamma)^{15}N$ and $^{15}N(\alpha,p\gamma)^{18}O$

Nine of the resonances seen at high bombarding energy were found to be resonances in either the $^{15}N(\alpha,\alpha'\gamma)^{15}N$ or $^{15}N(\alpha,p\gamma)^{18}O$ reactions. The excitation energies and widths of the states observed are shown in table 2. Six of these resonances may be identified with energy levels already known in this region. Comparisons of excitation energies and widths with those quoted by Ajzenberg-Selove (1972) are given

Table 2.

Resonance	E_x (keV)	E^* (keV)		Γ (keV)	
		This work	Other[a]	This work	Other[a]
32	7875 ± 5	10231 ± 4	10231 ± 3	<1	4·3
33	7976 ± 6	10308 ± 4	10306 ± 3	–	9·2
36	8173 ± 5	10469 ± 4	—	13·8 ± 1·5	
37	8204 ± 5	10488 ± 4	—	6·0 ± 1·0	–
38	8220 ± 5	10501 ± 4	10496 ± 1	5·4 ± 1·0	6·2 ± 0·5
39	8245 ± 5	10521 ± 4	—	18 ± 2	
40	8277 ± 5	10546 ± 4	10541 ± 1	2·5 ± 1	2·5 ± 0·2
41	8286 ± 5	10554 ± 4	10554 ± 3	5·0 ± 1·5	7·6 ± 2
42	8306 ± 5	10560 ± 4	10566 ± 1	3·7 ± 1	5·2 ± 0·5

[a] Values taken from Ajzenberg-Selove (1972).

in the table. The remaining three resonances, numbers 36, 37 and 39, have not been reported previously.

4. Discussion

4.1. Comparison with light-ion reactions

It was mentioned in the introduction that the region of excitation that we have been considering in ^{19}F has been studied with several other nuclear reactions. Of particular relevance are the studies of the ^{18}O(p,γ)^{19}F, ^{18}O(p,p)^{18}O, ^{18}O(p,α)^{15}N and ^{18}O(^{3}He,d)^{19}F reactions. Since α particle and proton decay are the only particle channels available below 10 MeV, it might be expected that these reactions should be complementary to the ^{15}N(α,γ)^{19}F study. That this is indeed the case is demonstrated in figure 8, where the states reported in this region are listed together with their spin assignments. It may be noticed that although many of the states had been observed previously, there are some 23 new levels. In addition, several of the previously known states were not observed in this study. Perhaps the most significant difference between the two sets of data is that, without exception, states of spin greater than $\frac{7}{2}$ have *only* been observed in the present study. This is not unexpected, since most models of the ^{19}F nucleus, such as the (sd) shell model predict that the reduced proton widths of these states should be very small indeed.

Some more specific details may be provided for individual resonances where our results have provided new information in addition to that deduced from previous work.

4.1.1. Resonance 2. This resonance was observed by Underwood *et al* (1974) in the ^{15}N(α,γ)^{19}F reaction using solid targets. They were able to limit the possible spin and parity of this level to $\frac{9}{2}^-$ or $\frac{13}{2}^-$ from an angular distribution measurement of the primary decay to the 4032 keV $\frac{9}{2}^-$ level. The observation of a 7 ± 4% branch to the 4648 keV $\frac{13}{2}^+$ level in the present work eliminates the $\frac{9}{2}^-$ assignment since it would imply a very large M2 strength of greater than 100 Wu.

4.1.2. Resonance 3. This state was populated in the $^{18}O(^3He,d)^{19}F$ reaction (Schmidt and Duhm 1972), and given a spin assignment of $\frac{5}{2}^+$. This is confirmed by our work, since any other assignment would imply very large M2 strengths.

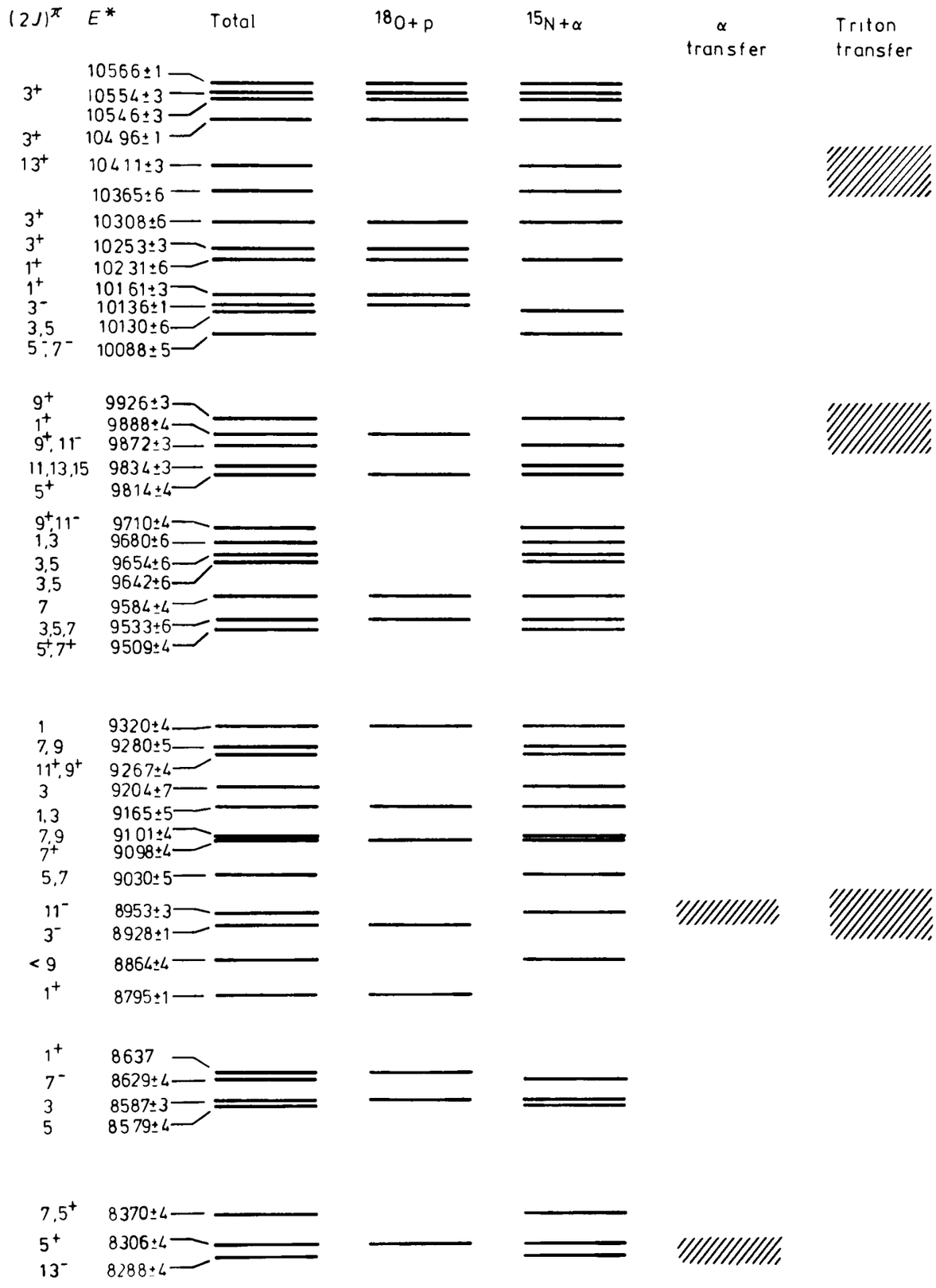

Figure 8. Energy level diagram for the ^{19}F nucleus.

4.1.3. Resonance 6. A state at this energy has been observed in the $^{18}O(p,\gamma)^{19}F$ reaction (Wormald 1969, Nelson and Hudspeth 1962, Huang *et al* 1963), and in the $^{18}O(p,\alpha)^{15}N$ and $^{18}O(p,p)^{18}O$ reactions by Yagi (1962). However, the relative intensities measured are in disagreement with those quoted by Nelson and Hudspeth, although very much better agreement is obtained with the more recent $^{18}O(p,\gamma)^{19}F$ work of Wormald using Ge(Li) detectors. From the ratio of $\omega\gamma(p,\gamma)$ to $\omega\gamma(\alpha,\gamma)$ one may deduce that $\Gamma_\alpha/\Gamma_p = 0{\cdot}026 \pm 0{\cdot}008$ in good agreement with the value $0{\cdot}032 \pm 0{\cdot}002$ deduced by Yagi from the $^{18}O(p,\alpha)^{15}N$ cross section.

4.1.4. Resonance 9. This state was observed as a resonance in the $^{15}N(\alpha,\gamma)^{19}F$ reaction by Underwood *et al* (1974). It was assigned as $\frac{11}{2}^+$ on the basis of the angular distribution of the primary decay to the 2780 keV $\frac{9}{2}^+$ state. Using the gas target, we have observed several new branches. In particular, the observation of decays to the $\frac{7}{2}^-$ levels at 3999 keV and 5421 keV is inconsistent with the previous assignment, since they would imply M2 strengths of greater than 100 Wu. Recent work at Oxford using a modified version of the gas target which allows the measurement of angular distributions has shown that $\frac{11}{2}^-$ is the only assignment consistent with all the experimental data (Fifield *et al* 1977).

4.1.5. Resonance 11. This state has been observed previously as a resonance in the $^{18}O(p,\gamma)^{19}F$ reaction by Wormald (1969) and by Allen *et al* (1965), and in the $^{18}O(p,\alpha)^{15}N$ and $^{18}O(p,p)^{18}O$ reactions by Yagi (1962). The relative gamma ray intensities measured in this study are in good agreement with those measured using the $^{18}O(p,\gamma)^{19}F$ reaction, although it should be noted that several additional weak branches were observed by Wormald. From the two capture reactions one may deduce a value $0{\cdot}1 \pm 0{\cdot}04$ for Γ_γ/Γ_p. This is in rather poor agreement with the value 120 ± 20 deduced from the $^{18}O(p,\alpha)^{15}N$ cross section by Yagi (1962). If one accepts our value for this ratio, together with the total width of $0{\cdot}57 \pm 0{\cdot}03$ keV measured by Yagi, this leads to values of $0{\cdot}052 \pm 0{\cdot}03$ keV and $0{\cdot}52 \pm 0{\cdot}03$ keV for Γ_γ and Γ_p respectively.

4.1.6. Resonance 13. This resonance almost certainly corresponds to that observed in $^{18}O(p,p)^{18}O$ by Yagi (1962), since the excitation energy (9166 keV) agrees with our value to within 1 keV. However, the width quoted by Yagi as $5{\cdot}8 \pm 0{\cdot}3$ keV is in very poor agreement with our value of $9{\cdot}9 \pm 1{\cdot}5$ keV.

4.1.7. Resonance 17. This state has been observed as a resonance in proton capture by Nelson and Hudspeth (1962) and by Huang *et al* (1963). Unfortunately, no branching ratios are available from these studies and little comparison may be made with the present work.

4.1.8. Resonance 26. This state has been observed as a resonance in the $^{18}O(p,\gamma)^{19}F$ reaction by Wormald (1969) and by Nelson and Hudspeth (1962). It has also been seen in the $^{18}O(p,\alpha)^{15}N$ reaction, and in elastic proton scattering by Sellin *et al* (1969) and by Karadzhev *et al* (1964). The yields from the radiative proton and α capture may be used to obtain a value for Γ_γ/Γ_p of $0{\cdot}55 \pm 0{\cdot}16$. This is in fair agreement with the value of 0·83 deduced by Sellin *et al*.

4.2. Comparison with many-particle transfer reactions

The usefulness of three-and four-particle transfer reactions in selecting states with relatively simple configurations has been reviewed by Anyas Weiss *et al* (1974). Using the notation of the SU(3) model, then in the case of ^{19}F, one may expect α particle transfer to pick out members of the $K^\pi = \frac{1}{2}^-$ band dominated by the (81) SU(3) representation with four particles in the (sd) shell. Similarly, triton transfer may be expected to populate the ground-state $K^\pi = \frac{1}{2}^+$ (60) band and at higher excitation states belonging to the (sd^2pf) (70) representation. Clearly, the data obtained in these reactions are extremely valuable in locating these states. However, two points should be borne in mind. Firstly, although much may be learnt about the dominant configuration of the states seen, rather a small amount of information may reliably be extracted regarding their quantum numbers, although some information has been obtained from a DWBA analysis of the data from the $^{16}O(\alpha,p)^{19}F$ reaction by van der Borg *et al* (1976). Here, the value of reactions such as (α,γ) is that they provide model-independent information regarding the spins and parities of the states if angular distribution measurements are made. In addition, the measurement of one or more transition rates from each state provides additional data that may be compared with theoretical predictions. Angular distribution measurements have not been made for the series of experiments described here, but are now in progress with a modified version of the gas target and have already been reported in Letter form.

The second important point is that the resolution of high-energy particle transfer reactions is rather poor, particularly when solid-state detectors are used to identify the reaction products. Even when a magnetic spectrograph is used, the resolution is unlikely to be very much better than 30 keV. The resolution obtained in the present study is of the order of 1 keV and the importance of this is illustrated graphically in figure 9, where the results of two three-particle transfer experiments are superimposed on the gamma ray yield curve corresponding to an excitation energy of approximately 9·8 MeV in the ^{19}F nucleus. Four sharp resonances are observed in this energy region and it is likely that contributions to the transfer reaction yield may come from more than one of the states.

These two features of the α capture reaction, namely the model-independent information on spins and parities and the high resolution, have proved invaluable in the identification of specific states observed in the transfer reactions. In this identification one is aided by the high-spin selectivity of the transfer reaction. In α particle transfer, for example, states are strongly excited at 8·29 and 8·95 MeV. There is little doubt that the levels populated are the $\frac{13}{2}^-$ state at 8·288 MeV (resonance 2) and the $\frac{11}{2}^-$ state at 8·956 MeV (resonance 9) and that these two levels must carry appreciable components of the (81) $L = 6$ strength expected in this region. As a further example, states at 8·95, 9·9 and 10·4 MeV are selectively populated in triton transfer reactions. The 10·4 MeV level is almost certainly the 10·411 MeV state (resonance 35) seen in the present work. This state has subsequently been assigned $\frac{13}{2}^+$ from γ ray angular distribution measurements (Symons *et al* 1978) and is believed to be the second $\frac{13}{2}^+$ level predicted by $(sd)^3$ shell-model calculations. At 9·9 MeV there are three high-spin states observed in the present work. The most likely candidates for the state observed in the triton transfer reactions are the 9834 keV state (resonance 27) and the 9879 keV state (resonance 28), with the measured excitation energy indicating a preference for the latter. Population of the 9926 keV $\frac{9}{2}^+$ state is unlikely since its excitation and measured γ decay scheme make it an excellent candidate

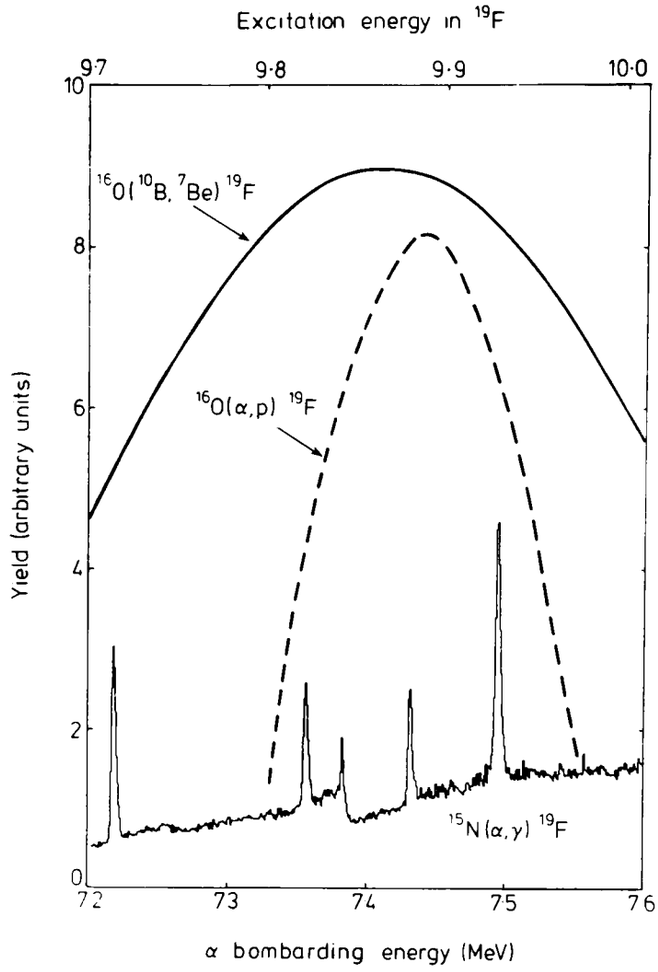

Figure 9. Comparison of results from this study with those from three particle transfer reactions for the region of excitation around 9·8 MeV in ^{19}F

for the isobaric analogue of the $\frac{9}{2}^+$ state at 2·3 MeV in ^{19}O. The 8·95 MeV level must, in the absence of other high-spin states in this region, be identified with the 8·953 MeV level which was also populated in α transfer, indicating an appreciable contribution of the (sd^2pf) (70) amplitude in its wavefunction in addition to the $(p^{-1}sd^4)$ (81) contribution, as discussed by Fifield *et al* (1977).

4.3. Summary

The ^{15}N$(\alpha,\gamma)^{19}$F reaction has been used to study states in ^{19}F between 8 and 10·4 MeV excitation. The high resolution of the gas target and its very low gamma ray background have allowed us to measure decay schemes, resonance strengths and other relevant parameters for a large number of capture resonances. In many cases this information has then enabled strong limits to be placed on the spins and parities of these states. However, it is clear that for a satisfactory comparison of these data with the results of other experiments and with theoretical calculations, more rigorous spin assignments are necessary, especially for the high-spin states. A series of angular distribution measurements using a modified gas target is in progress at this laboratory; preliminary results have already been reported by Fifield *et al* (1977).

Acknowledgments

The authors are grateful to Dr A Pakkanen for help in running some of the experiments, and to Drs D J Millener and A A Pilt for many useful discussions on ^{19}F.

References

Ajzenberg-Selove F 1972 *Nucl. Phys.* A **190** 1
Alexander T K *et al* 1972 *Nucl. Phys.* A **197** 1
Allen K W *et al* 1976 *Nucl. Instrum. Meth.* **134** 1
Allen J P *et al* 1965 *Phys. Rev.* **140** 1245
Anyas Weiss A N *et al* 1974 *Phys. Rep.* **12** 202
Buck B, Dover C B and Vary J P 1975 *Phys. Rev.* C **11** 1803
Buck B and Pilt A A 1977 *Nucl. Phys.* A **280** 133
Cobb J H, Allison W W M and Bunch J N 1976 *Nucl. Instrum. Meth.* **133** 315
Elliott J P and Flowers B H 1955 *Proc. R. Soc.* A **229** 536
Endt P M and van der Leun C 1974 *Nuclear Data* A **13** 67
Fifield L K *et al* 1977 *Phys. Lett.* **68B** 125
Fano U 1963 *Ann. Rev. Nucl. Sci.* **13** 1
Gove H E 1959 *Nuclear Reactions* vol I (Amsterdam: North-Holland) p 259
Hamm M *et al* 1976 *Phys. Rev. Lett.* **36** 846
Harvey M 1964 *Nucl. Phys.* **52** 542
Huang K *et al* 1963 *J. Phys. Soc. Japan* **18** 646
Karadzhev K U *et al* 1964 *Sov. Phys.-JETP* **47** 1185
Landau L D 1944 *Sov. J. Phys.* **8** 207
Middleton R 1970 *Proc. Int. Conf. on Nuclear Reactions with Heavy Ions, Heidelberg* (Amsterdam: North-Holland) p 263
Nelson J W and Hudspeth E L 1962 *Phys. Rev.* **125** 301
Paul E B 1957 *Phil. Mag.* **2** 311
Pilt A A *et al* 1976 *Nucl. Phys.* A **273** 189
Rogers D W O 1973 *Nucl. Phys.* A **207** 455
——1976 *Can. J. Phys.* **54** 938
Rolfs C and Litherland A E 1975 *Nuclear Spectroscopy* (New York: Academic) p 143
Schmidt C and Duhm H H 1962 *Nucl. Phys.* **29** 665
Sellin D L *et al* 1969 *Ann. Rev. Phys.* **51** 461
Symon K 1952 *High Energy Particles* ed Bruno Rossi (New York: Prentice-Hall) p 37
Symons T J M *et al* 1976 *Phys. Lett.* **63B** 409
——1978 to be published
Underwood B Y 1972 *DPhil Thesis* Oxford University
Underwood B Y *et al* 1974 *Nucl. Phys.* A **225** 253
Vavilov P V 1957 *Sov. Phys.-JETP* **5** 920
Wormald M R 1969 *PhD Thesis* Manchester University
Wormald M R and Takacs J 1974 *Nucl. Instrum. Meth.* **113** 263
Wormald M R and Wright I F 1969 *Proc. Int. Conf. on the Properties of Nuclear States, Montreal* (Montreal: Montreal University Press) 4.24
Van der Borg K, De Meijer R J and Van der Woude A 1976 *Nucl. Phys.* A **273** 172
Yagi K 1962 *J. Phys. Soc. Japan* **17** 604

studied in detail by Alexander et al.[Al72b]. They were not able to observe the low energy 1.2MeV E2 decay to the 7.83MeV 2^+ state.

In addition to enabling assignments of states to bands to be made, knowledge of electromagnetic transition strengths also enables isospin assignments to be made. Although direct reactions can be useful in isospin assignments due to the ability to compare spectroscopic strengths in mirror reactions[egMi74], it is desirable to demonstrate that the γ-transitions follow the general rules governing the strength of such transitions, as stated by Endt[En74] and Skorka[Sk66]. In particular, an E1 decay which is not strongly suppressed (>0.003 Weisskopf Units) or an enhanced M1 decay (>0.03 Weisskopf Units) is a strong indication of the isovector nature of the transition. In this work previously tentative T=1 assignments have been made definite for the 11.27 and 12.25MeV levels due to the observation of new γ-branches.

The alpha-capture reaction on ^{16}O has already been studied in the beam energy range $3MeV<E_\alpha<9.65MeV$ by a number of groups [Al72a, Pe64b, St78, Ma77, Al72b, In76b, Fi77, Li67, Di71, Ro71o, Ro71f, Da78] using both solid and gas targets. Pearson and Spear[Pe64b] carried out an initial survey of the reaction using a solid target and subsequent work has been performed with more specific purpose, searching for particular states or resolving inconsistencies between the earlier capture work and data from other reactions[egMa77]. Even much of the gas target work has suffered from ^{13}C contamination due to hydrocarbons in the beam-line and the technique of Alexander et al.[Al72a] of using the inverse reaction $^4He(^{16}O,\alpha)^{20}Ne$ in order to study the 8^+ member of the ground state band still suffered from the same γ-rays due to inelastic scattering of the ^{16}O beam.

THE RADIATIVE WIDTH OF THE 8^+ MEMBER OF THE $K^\pi = 2^+$ BAND IN ^{24}Mg

L.K. FIFIELD, M.J. HURST, T.J.M. SYMONS, F. WATT and K.W. ALLEN
Nuclear Physics Laboratory, Keble Road, Oxford, UK

Received 2 May 1977

The radiative width of the 14.15 MeV, 8^+, $K^\pi = 2^+$ level in ^{24}Mg has been measured using the ^{20}Ne$(\alpha, \gamma)^{24}$Mg reaction and a differentially cryopumped gas target. The result, $\Gamma_\gamma = 85 \pm 23$ meV, implies E2 strengths of 9.1 ± 2.4 and 0.8 ± 0.2 W.u. for the transitions to the 9.53 (6^+, $K^\pi = 2^+$) and 8.11 (6^+, $K^\pi = 0^+$) MeV levels, respectively. These are in excellent agreement with the predictions of recent large basis shell model calculations.

The extent to which rotational band structure persists in deformed light nuclei as the nuclear spin increases has been the subject of considerable theoretical [1–3] and experimental [4, 5] interest in recent years. In ^{24}Mg there are two well known positive parity bands which are believed to have the structure of eight particles in the 2s–1d shell outside an ^{16}O core, namely $K^\pi = 0^+$ and 2^+ bands built on the ground state and 4.24 MeV (2^+) state, respectively. Both bands have been identified only as far as the 8^+ members, and in-band E2 γ-ray transition strengths, which serve as an indicator of band structure, have been measured [5] up to the 8^+ member of the ground-state band and up to the 7^+ member of the $K^\pi = 2^+$ band. With the development of the Glasgow shell model code, it has become possible to calculate the excitation energies and electromagnetic transition rates within these bands using an untruncated $(sd)^8$ basis, and to extend the calculations to levels with $J > 8$ which have not yet been located experimentally. One would hope to determine from such calculations whether the band structure persists up to the $(sd)^8$ spin 12 limit, or only up to some critical lower spin value. The results, as reported recently by Watt, Kelvin and Whitehead [1], favour the latter possibility with the critical spin value lying between $J = 8$ and $J = 10$. In both bands, the in-band E2 γ-ray transitions from the 8^+ members are predicted to be substantially weaker than the strongly enhanced transitions between lower members of the bands, and above $J = 9$ the band structure effectively disappears.

In so far as the properties of the bands have been determined experimentally, they are in reasonable agreement with the calculations. This applies to the excitation energies, to the strongly enhanced in-band E2 γ-ray transitions, and to the relatively weak cross-band transitions. However, the crucial test of the calculations, and hence of their predictive power with respect to the states with $J > 8$, lies in the measurement of the in-band transition rates from the two 8^+ states at 13.21 ($K^\pi = 0^+$) and 14.15 ($K^\pi = 2^+$) MeV. Although the lifetime of the 13.21 MeV level has been measured [5] by the Doppler shift attenuation method, the experimental uncertainty is large owing to the difficulties associated with measuring lifetimes of a few fs, and the result is not sufficiently accurate to verify the predicted fall-off in E2 transition strength. For the 14.15 MeV level, only a lower limit of 3 W.u. has been established [5] for the in-band E2 transition to the 9.53 MeV (6^+, $K^\pi = 2^+$) level using the same technique. However, whereas the 13.21 MeV level decays only by γ-ray emission, the decay strength of the 14.15 MeV level is shared between γ-ray emission and α-particle emission to the ground and 1.63 MeV states in ^{20}Ne. This allows the possibility of measuring the radiative width of the 14.15 MeV level (but not of the 13.21 MeV level) by studying it as a resonance in the ^{20}Ne$(\alpha, \gamma)^{24}$Mg reaction. The purpose of this letter is to report the result of such a measurement which is sufficiently accurate to allow meaningful comparison with the theoretical calculations.

This measurement employed a differentially cryopumped gas target [6, 7], with beams of α-particles obtained from the Oxford 10 MV Van de Graaff accelerator. The use of the gas target ensured that the level of background γ-rays was low, and in particular that the yield of 6.13 MeV γ-rays from the prolific ^{13}C$(\alpha, n\gamma)^{16}$O reaction was negligible. This was an

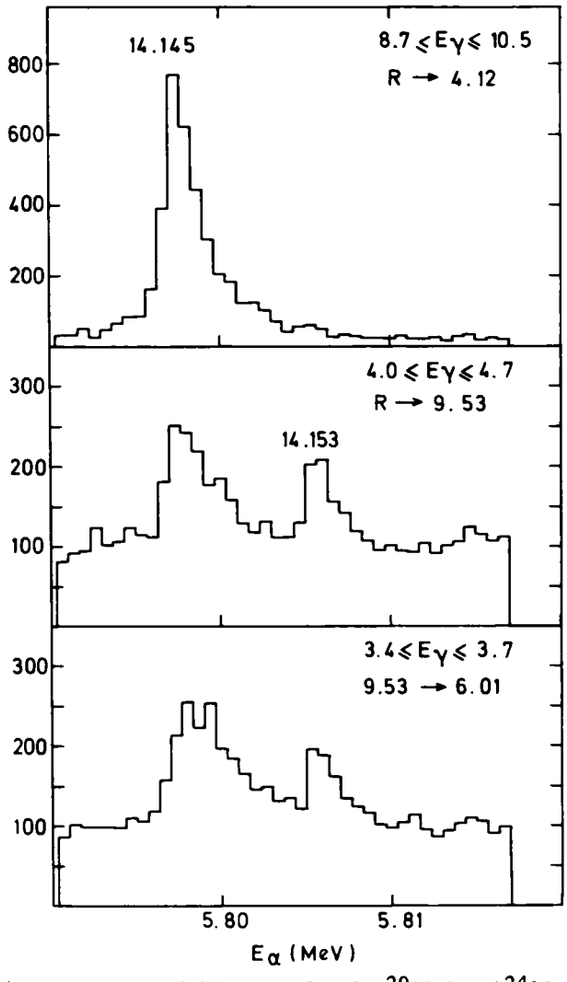

Fig. 1. Gamma-ray yield curves for the ^{20}Ne(α, γ)^{24}Mg reaction in the vicinity of E_α = 5.8 MeV. The three curves shown were obtained with gates set about the indicated regions of the γ-ray energy spectrum, and the resonances are labelled by the corresponding excitation energy in ^{24}Mg. All energies are in MeV. The 8^+ resonance would be expected to appear only in the lower two gates.

essential requirement in the present work since the 14.15 MeV level γ decays by a cascade of γ-rays all with energies substantially less than 6.1 MeV.

In order to locate the 14.15 MeV (8^+) level as a resonance, γ-ray yield curves were measured in the vicinity of E_α = 5.8 MeV using a 7.6 × 7.6 cm NaI(Tl) crystal and an automatic beam energy modulation technique. A target gas pressure of 0.2 torr, corresponding to a target thickness of 1.2 keV, was used in order both to emphasize sharp resonances and to reduce the counting rate from the extremely prolific ^{20}Ne(α, α′γ)^{20}Ne reaction. The result, in the form of three yield curves with gates set about the indicated regions of the γ-ray spectrum, is shown in fig. 1. A prominent sharp resonance at E_α = 5.797 MeV is evident in the high-energy gate, and corresponds to a resonance observed previously by Highland and Thwaites [8]. In the present work it was found to decay predominantly through the 4.12 MeV (4^+) level, which rules it out as a candidate for the 8^+ level. However, the 14.15 MeV (8^+) level is clearly visible in the two lower-energy gates as a weak resonance at an α-particle energy 8 keV above the 5.797 MeV resonance.

Having located the 8^+ resonance, its γ-ray decay scheme was measured by taking spectra on and off resonance with an 85 cm^3 Ge(Li) detector at 135° to the beam direction and 13 cm from the centre of the target. For these measurements, the target gas pressure was increased to 1 torr to ensure an effective thick target yield. The 8^+ resonance was located centrally in the target chamber by first locating the much stronger 5.797 MeV resonance using a yield curve taken at a pressure of 1 torr, and then increasing the beam energy by 8 keV. The resulting on-resonance spectrum clearly exhibited the γ-rays corresponding to decays through the 9.53 and 8.11 MeV 6^+ levels, whereas the off-resonance spectrum taken at a beam energy 18 keV above the resonance did not. Furthermore, the γ-ray branch to the 9.53 MeV (6^+, $K^\pi = 2^+$) level carried (71 ± 5)% of the γ-ray decay strength, and the excitation energy was determined to be 14153 ± 4 keV, both in good agreement with previous measurements [5].

The resonance strength, $\omega\gamma = (2J + 1)(\Gamma_\gamma\Gamma_{\alpha_0}/\Gamma)$, was determined by comparison of the yield of γ-rays from the $R \rightarrow 9.53$ MeV and $9.53 \rightarrow 6.01$ MeV transitions with the yield of 8.64 MeV γ-rays from the 6.93 MeV resonance in the ^{16}O(α, γ)^{20}Ne reaction. Care was taken to measure the yield from the reference resonance with as nearly as possible the same target thickness and resonance position as in the ^{20}Ne(α, γ)^{24}Mg measurement. Relative stopping powers were taken from ref. [9], and small corrections were applied for differences in the angular distributions of γ-rays from the two resonances and for the extended nature of the γ-ray emitting region along the beam direction [7]. Using a value of 19.7 ± 1.6 eV for ωγ of the reference resonance [10], ωγ of the $R \rightarrow$ 9.53 MeV transition was determined to be 0.24 ± 0.04 eV.

Before Γ_γ can be derived from ωγ, a knowledge of Γ_{α_0}/Γ is required. This latter quantity has been meas-

Table 1
E2 transition rates for members of the $K^\pi = 2^+$ band in ^{24}Mg.

	E_i (MeV)	J_i^π	E_f (MeV)	J_f^π	$B(E2)_{exp}$ [a] (W.u.)	$B(E2)_{Th}$ [b] (W.u.)
In band						
$K_i = 2, K_f = 2$	5.24	3^+	4.24	2^+	34 ± 6	34
	6.01	4^+	4.24	2^+	16 ± 3	9.5
	7.81	5^+	5.24	3^+	28 ± 5	14.4
	7.81	5^+	6.01	4^+	(14 ± 6) [c]	18.3
	9.53	6^+	6.01	4^+	23^{+23}_{-8}	11.6
	12.35	7^+	7.81	5^+	20^{+14}_{-6}	15.0
	14.15	8^+	9.53	6^+	9.1 ± 2.4	7.6
Cross band						
$K_i = 2, K_f = 0$	4.24	2^+	0.0	0^+	1.4 ± 0.3	1.7
	4.24	2^+	1.37	2^+	2.7 ± 0.4	4.8
	5.24	3^+	1.37	2^+	2.1 ± 0.3	2.7
	6.01	4^+	1.37	2^+	1.0 ± 0.2	0.2
	6.01	4^+	4.12	4^+	1.0 ± 1.0	4.3
	7.81	5^+	4.12	4^+	3.9 ± 0.8	1.1
	9.53	6^+	4.12	4^+	$0.8^{+0.8}_{-0.3}$	0.2
	14.15	8^+	8.11	6^+	0.8 ± 0.2	0.9

[a] All values taken from Branford et al. [5] with the exception of the $8^+ \rightarrow 6^+$ transitions.
[b] Ref. [12]. Effective charges 0.5 e.
[c] Assumes a pure E2 transition.

ured [11] using the $^{16}O(^{12}C, \alpha\alpha)^{20}Ne$ and $^{16}O(^{12}C, \alpha\gamma)^{24}Mg$ reactions, but the accuracy was limited by the presence of other states in ^{24}Mg which also α-decay to the ^{20}Ne ground state and which were not resolved from the 14.15 MeV (8^+) level. We estimate that the uncertainty in determining the relative contributions of these unresolved levels to the α–α angular correlation contributes an uncertainty of 20% to the value of Γ_{α_0}/Γ, which we take to be 0.22 ± 0.04. Taken together with the measured value of $\omega\gamma$, this implies a value of 64 ± 17 meV for the radiative width Γ_γ of the in-band 14.15 (8^+) → 9.53 (6^+) MeV transition, which corresponds to an E2 transition strength of 9.1 ± 2.4 W.u.

The available information on electromagnetic E2 transition rates for in-band and cross-band transitions involving the $K^\pi = 2^+$ band in ^{24}Mg is collected in table 1 and compared with $(sd)^8$ shell model predictions [1, 12] using the interaction of Preedom and Wildenthal. It is immediately evident that the predicted fall-off in the in-band transition strength at the 8^+ member is borne out by the present work, and further, that very good quantitative agreement between theory and experiment is obtained for both the in-band and cross-band transitions from the 8^+ level. We conclude that the full basis $(2s-1d)^8$ shell model calculations give a good account of the $K^\pi = 2^+$ band in ^{24}Mg, and of the properties of the 8^+ state in particular. Consequently, these calculations can be used with some confidence to indicate both the whereabouts and the properties of the higher spin states in ^{24}Mg, and should be of considerable assistance in the continuing search for these levels.

We wish to thank Dr. A. Watt and Dr. D. Kelvin for communicating some of their results prior to publication.

References

[1] A. Watt, D. Kelvin and R.R. Whitehead, Phys. Lett. 63B (1976) 385.
[2] S. Pittel, Phys. Lett. 34B (1971) 555.
[3] M. Harvey, in: Advances in nuclear physics, vol. 1, eds. M. Baranger and E. Vogt (Plenum Press, New York, 1968).

[4] T.K. Alexander et al., Nucl. Phys. A179 (1972) 477.
[5] D. Branford, A.C. McGough and I.F. Wright, Nucl. Phys. A241 (1975) 349.
[6] K.W. Allen et al., Nucl. Instr. 134 (1976) 1.
[7] F. Watt et al., to be published.
[8] G.J. Highland and T.T. Thwaites, Nucl. Phys. A109 (1968) 163.
[9] L.C. Northcliffe and R.F. Schilling, Nucl. Data A7 (1970) 233.
[10] P.D. Ingalls, Nucl. Phys. A265 (1976) 93.
[11] L.K. Fifield, R.W. Zurmühle and D.P. Balamuth, Phys. Rev. C8 (1973) 2217.
[12] D. Kelvin, A. Watt and R.R. Whitehead, to be published.

THE SECOND $13/2^+$ STATE IN ^{19}F

T.J.M. SYMONS, L.K. FIFIELD, M.J. HURST, A. PAKKANEN,
F. WATT, C.H. ZIMMERMAN and K.W. ALLEN
Nuclear Physics Laboratory, Oxford, UK

Received 13 July 1976

A cryogenically pumped gas target has been used to study resonances in the $^{15}N(\alpha, \gamma)^{19}F$ reaction for E_α = 5.1 to 8.6 MeV. Gamma-ray intensity and angular distribution measurements for a resonance at E_α = 8.105 MeV, corresponding to a state at 10.411 MeV in ^{19}F, restrict the spin and parity of the state to $11/2^+$ or $13/2^+$. Comparison with shell model calculations indicate that the state is a strong candidate for the second $13/2^+$ (2s, 1d)^3 level in ^{19}F.

The properties of the low-lying positive parity levels of ^{19}F from the $J^\pi = 1/2^+$ ground state to the $9/2^+$ state at 2.78 MeV are well explained by shell model calculations using the basis of three particles in the (2s, 1d) shell and a suitable residual interaction [1–3]. If the shell model wavefunctions of these states are classified according to their spatial and SU(3) symmetry, then their dominant components are found to belong to the (6,0) representation of SU(3) with maximum spatial symmetry. Consequently, these levels have received a natural interpretation in terms of a $K^\pi = 1/2^+$ rotational band.

However, this interpretation is less clear for the $11/2^+$ and $13/2^+$ states. Although a $13/2^+$ level has been identified at 4.65 MeV with the properties expected for a member of the band [16, 17], the shell model calculations predict that the (6,0) strength is split appreciably between the two $13/2^+$ levels that may be constructed using the (2s, 1d)^3 basis. Also, in the shell model it is the *third* $11/2^+$ that is dominated by the (6,0) representation. Insofar as neither of the two $11/2^+$ levels known in ^{19}F has the properties expected of a predominantly (6,0) state, this is in accord with experiment, but the third $11/2^+$ level has not yet been found. In view of the excellent agreement between the shell model calculations and experiment for the lower-lying levels, the location and properties of the $11/2^+_3$ and $13/2^+_2$ levels in ^{19}F are clearly of interest.

The $11/2^+_3$ and $13/2^+_2$ levels are predicted to lie between 8 and 10.5 MeV in excitation, and recently, three-particle transfer reactions have been used to study levels in this energy range. If these reactions are assumed to proceed by direct transfer of a triton cluster then the spectroscopic factors for (2s, 1d)^3 states are directly proportional to the intensity of the (60) component in the wave functions; in addition, the kinematics of these reactions frequently favour the population of high-spin states [8]. The (^{7}Li, α), (α, p) and (^{10}B, ^{7}Be) reactions on ^{16}O targets have all been studied [4, 5, 15] and have indeed been found to be highly selective; in each case, the spectrum between 8 and 10.5 MeV is dominated by the strong population of states at 8.9, 9.9 and 10.4 MeV. However, firm identification of one or more of these levels as (2s, 1d)^3 states has proved difficult, since other configurations such as (sd^{2}pf) and (sd, pf^2) may also be excited in these reactions.

We have used the $^{15}N(\alpha, \gamma)^{19}F$ reaction to study levels in ^{19}F reaction to study levels in ^{19}F between 8.2 and 10.6 MeV. For several reasons, this reaction provides valuable complementary information to that obtained from particle transfer studies. Firstly, the resolution of the capture reaction is typically that of the accelerator ($\approx$ 1 keV), and is very much better than that obtainable from magnetic analysis of the products of a charged particle reaction; secondly, model independent spin assignments may be made in many cases; and thirdly, the measurement of electromagnetic transition rates provides a general test of the shell model wave functions whereas the transfer reactions are sensitive only to a single component in the wave function. In our study we have observed 40 resonances in the γ-ray yield, one of which is presented here as a candidate for the $13/2^+_2$ (2s, 1d)^3 state.

The experiment was carried out using a $^4He^+$ beam accelerated by the 10 MV Oxford single-ended Van de Graaff. The main difficulty with α-capture studies at bombarding energies greater than 5 MeV is the large γ-ray yield from competing nuclear reactions, as the α-particle is well above the Coulomb barrier for all the common light element contaminants. In particular, the reaction $^{13}C(\alpha, n\gamma)^{16}O$ produces a copious yield of 6.13 MeV γ-rays above the threshold at 5.1 MeV, and previous studies at bombarding energies above 5 MeV have been limited to the observation of transitions to the first few excited states of the nucleus for which $E_\gamma > 6$ MeV. High-spin states decay via a cascade of lower-energy γ-rays which are almost impossible to observe using solid targets. For this reason a windowless differentially pumped gas target [6] was used; in this target, the beam was transmitted through a 19 cm long gas cell to a well shielded Faraday cup several metres from the target. The necessarily high pumping speeds were obtained using liquid helium cooled cryopumps, which also provide very clean pumping conditions. Isotopically separated ^{15}N gas, enriched to greater than 99.5% in ^{15}N, was used in these measurements.

A high-spin resonance was located at 8.11 MeV using an automatic beam energy modulation technique [7], and the yield curve obtained is shown inset in fig. 1. For this measurement, the pressure in the target was maintained at 0.2 torr corresponding to a total thickness of 4 keV for 8 MeV α-particles [11]. From analysis of the yield curve it was deduced that the total width of the resonance was less than 1 keV.

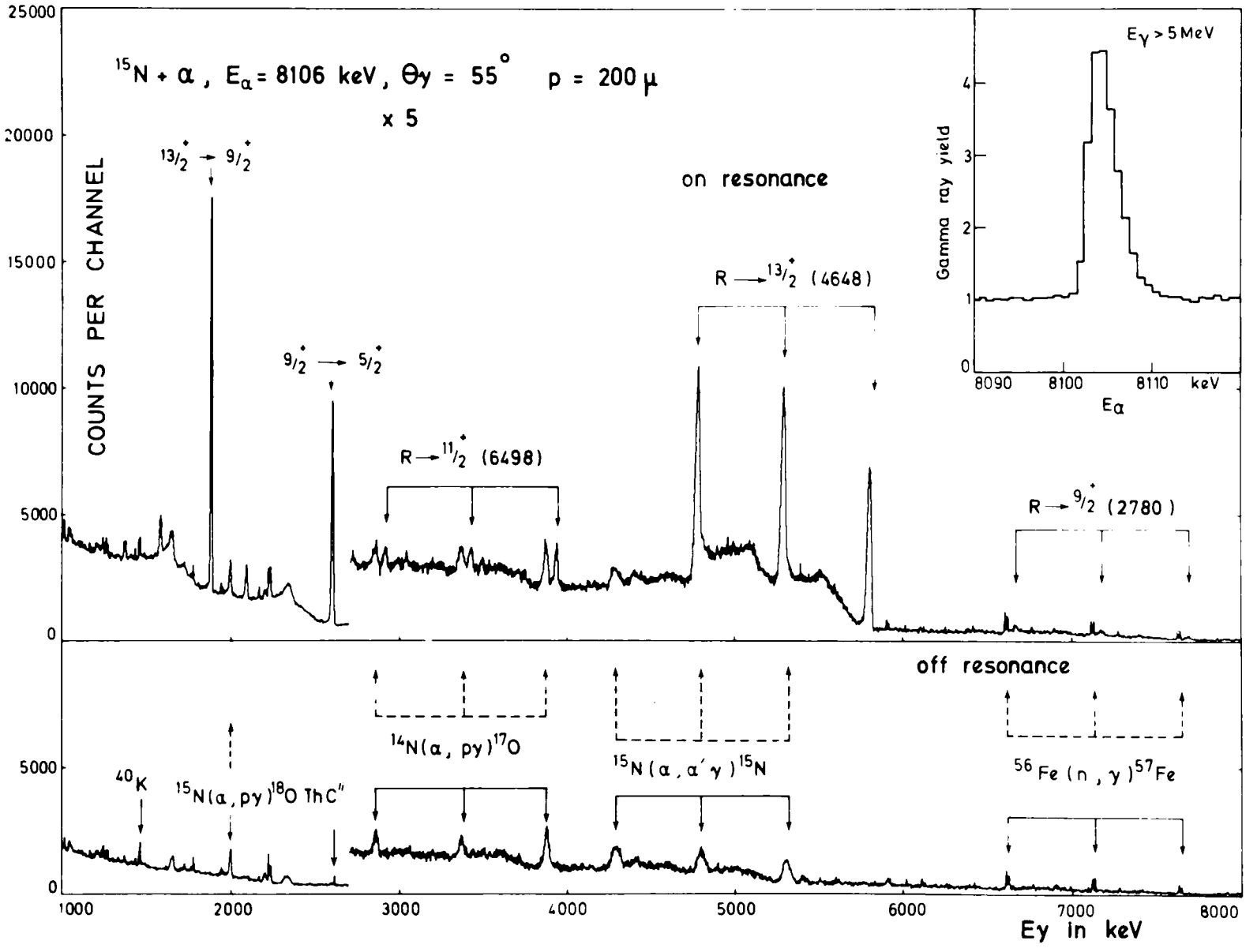

Fig. 1. On and off resonance γ-decay spectra from the E_α = 8.105 MeV resonance in $^{15}N(\alpha, \gamma)^{19}F$.

Gamma-ray spectra were then obtained on and off resonance, using a 16.6% efficient Ge(Li) detector mounted 14 cm from the target at an angle of 55° to the beam axis; the spectra are shown in fig. 1. It can be seen that the capture γ-ray photopeaks were Doppler broadened owing to the extension of the target along the beam axis. In the off-resonance spectrum, γ-rays were present from the reactions $^{14}N(\alpha, p\gamma)^{17}O$, $^{15}N(\alpha, \alpha'\gamma)^{15}N$ and $^{56}Fe(n, \gamma)^{57}Fe$, and also from the naturally occurring radionuclides ThC″ and ^{40}K. These latter γ-rays, together with the neutron capture lines from $^{56}Fe(n, \gamma)^{57}Fe$, provided convenient internal calibration points.

On resonance, strong primary decays were observed to the 4.65 MeV $13/2^+$ and 6.50 MeV $11/2^+$ levels, as well as a weak branch to the 2.78 MeV $9/2^+$ state. The thick target yield from a capture resonance is directly proportional to the quantity $\omega\gamma \equiv (J + 1/2) \times \Gamma_\alpha\Gamma_\gamma/\Gamma)$ [9], and to measure $\omega\gamma$ for the 8.1 MeV resonance, the resonance yield was compared with that of the 4.47 MeV $T = 3/2$ resonance, for which $\omega\gamma$ is 17.4 ± 2.1 eV [10].

The measured value of $\omega\gamma$ derived from a measurement at 55°, using a target pressure of 0.6 torr, was 15.0 ± 3.0 eV, and the best value for the excitation energy derived from the γ-decay sequence was 10411 ± 3 keV. The lower limit on the γ-decay strengths that may be obtained from this value of $\omega\gamma$ immediately restricts the spin of the state to 11/2 or $13/2^+$ since any other choice would require extremely large magnetic quadrupole or octupole transition strengths. If it is assumed that $\Gamma_\alpha \gg \Gamma_\gamma$, then the actual γ-decay strengths may be extracted directly from $\omega\gamma$.

Using a modified version of the gas target, in which the effective target length was reduced, the angular distribution of the transition to the 4.65 MeV $13/2^+$ level was measured between 25° and 90°. By operating the target at a pressure of 0.8 torr, the resonance was localised to a length of approximately 4 cm, and the measurements were made with a 59 cm^3 intrinsic germanium detector mounted with its front face 10 cm from the centre of the target. Under these conditions, corrections to the angular distribution due to the finite length of the target were less than 5% at all angles. As with the $\omega\gamma$ measurement, the position of the resonance within the target was monitored by measuring the Doppler shift of transitions of known energy, using a detector mounted at 135° to the beam axis.

The measured distribution could be fitted by a spin assignment of 13/2 with $\delta = 0.08 \pm 0.08$, or by 11/2 with $\delta = 0.47 \pm 0.06$. The latter value of δ immediately rules out $11/2^-$ as a spin assignment since it would imply an M2 strength of several hundred W.U. for an E1/M2 mixture, and leaves $11/2^+$ and $13/2^+$ as the only reasonable alternatives.

In table 1, the measured transition strengths are compared with the shell model predictions. In the calculation shown, the residual interaction of Preedom and Wildenthal [14] has been used, although calculations have also been made using the Kuo [12] and

Table 1
Experimental electromagnetic transition strengths from the 10.41 MeV state in ^{19}F, compared with shell model predictions using the Preedom and Wildenthal interaction.

Transition $E_{xi} \to E_{xf}$ (MeV)	$13/2^+$				$11/2^+$			
	Exp.		Theor.		Exp.		Theor.	
	$\lvert M(M1)\rvert^2$	$\lvert M(E2)\rvert^2$	$\lvert M(M1)\rvert^2$	$\lvert M(E2)\rvert^2$	$\lvert M(M1)\rvert^2$	$\lvert M(E2)\rvert^2$	$\lvert M(M1)\rvert^2$	$\lvert M(E2)\rvert^2$
10.41 → 4.65 $13/2^+$	0.47 ± 0.10	< 1.4	0.52	0.20	0.46 ± 0.10	25 ± 7	0.56	0.66
10.41 → 6.50 $11/2^+$	0.16 ± 0.03	–	0.24	1.03	0.18 ± 0.03	–	0.002	0.75
10.41 → 2.78 $9/2^+$	–	1.0 ± 0.3	–	0.19	0.010 ± 0.003	–	0.001	0.13

Kuo–Brown [13] interactions, that lead to similar conclusions. For a spin assignment of $13/2^+$, the agreement with the predicted decays of the $13/2^+_2$ level is very good for all the decays that have been measured. In the case of $11/2^+$, however, the calculation is unable to reproduce either the strong M1 transition to the 6.50 MeV $11/2^+$ level, or the extremely strong (25 ± 7 W.U.) E2 transition strength to the 4.65 MeV $13/2^+$ state implied by the large mixing ratio. In this context, it may be noted that the experimentally observed E2 strengths between the low-lying members of the $K^\pi = 1/2^+$ band are, in general, accurately predicted by the shell model.

In conclusion, the agreement between theory and experiment supports the identification of the 10.41 MeV state as the second $(2s, 1d)^3$ $13/2^+$ state in ^{19}F. However, no state observed in the present work exhibits the strong M1 transition to the $13/2^+$ level at 4.65 MeV expected of the third $(2s, 1d)^3$ $11/2^+$ level, and the location of this level remains an outstanding problem in the structure of ^{19}F. The experiment has also illustrated the useful spectroscopic data that may be obtained if radiative α-capture studies are extended to higher bombarding energies than had been practicable using solid targets.

We particularly wish to acknowledge our indebtedness to Dr. D.J. Millener for making available to us his shell model codes and for much helpful and illuminating discussion. We also acknowledge helpful discussions with Dr. A.A. Pilt and correspondence from Dr. A. van der Woude about transfer reactions leading to ^{19}F. Finally we wish to thank Mr. H.R. McK. Hyder and the Van de Graaff operators for their cooperation in maintaining high quality α-particle beams for these experiments.

References

[1] J.P. Elliott and B.H. Flowers, Proc. Roy. Soc. A229 (1955) 536.
[2] D.W.O. Rogers, Nucl. Phys. A207 (1973) 465.
[3] F. Ajzenberg-Selove, Nucl. Phys. A190 (1972) 1.
[4] I. Tserruya, B. Rosner and K. Bethge, Nucl. Phys. A235 (1974) 75.
[5] A. van der Woude, K. van den Borg and R.J. de Meijer, Proc. Sec. Intern. Conf. Clust. Phenom. in Nuclei, Maryland, 1975, p. 431.
[6] K.W. Allen et al., Nucl. Instr. 134 (1976) 1.
[7] M.R. Wormald and J. Takacs, Nucl. Instr. 114 (!(&$) 263.
[8] D.M. Brink, Phys. Lett. 40B (1972) 37.
[9] H.E. Gove and A.E. Litherland, in Nuclear spectroscopy (ed. F. Ajzenberg-Selove) Part A p. 260.
[10] D.W.O. Rogers et al., Can. J. Phys. 54 (1976) 938.
[11] L.C. Northcliffe and R.F. Schilling, Nucl. Data A7 (1970) 233.
[12] T.T.S. Kuo, Nucl. Phys. A103 (1967) 71.
[13] T.T.S. Kuo and G.E. Brown, Nucl. Phys. 85 (1966) 40.
[14] B.M. Preedom and B.H. Wildenthal, Phys. Rev. C6 (1972) 1633.
[15] M. Hamm et al., Phys. Rev. Lett. 36 (1976) 846.
[16] K.P. Jackson et al., Phys. Lett. 30B (1969) 162.
[17] H.G. Bingham, H.T. Fortune, J.D. Garrett and R. Middleton, Phys. Rev. Lett. 26 (1971) 1448.

HIGH-SPIN NEGATIVE PARITY STATES IN ^{19}F

L.K. FIFIELD, T.J.M. SYMONS, C.H. ZIMMERMAN, M.J. HURST, F. WATT and K.W. ALLEN
Nuclear Physics Laboratory, University of Oxford, England

Received 22 March 1977

Levels at 7.17, 8.29, 8.96 and 9.88 MeV in ^{19}F have been assigned spin and parity $11/2^-$, $13/2^-$, $11/2^-$ and $11/2^-$, respectively, from resonance strength and γ-ray angular distribution measurements employing the ^{15}N$(\alpha,\gamma)^{19}$F reaction. An earlier assignment of $11/2^+$ to the 8.96 MeV level is incorrect. The measured properties of the $11/2^-$ states are compared with the results of both SU(3) shell model and cluster model calculations.

Within the framework of the SU(3) shell model, the low-lying negative parity states in ^{19}F up to the $9/2^-$ level at 4.03 MeV are pictured as belonging predominantly to the (81) representation of SU(3) arising from the coupling of a hole in the 1p shell to the ^{20}Ne ground-state band. In addition to reproducing [1] the observed strongly enhanced $J \to J-2$ E2 transition rates, such a description accounts well for the selective population of these levels in the ^{15}N(^{7}Li, t)^{19}F and ^{15}N(^{13}C, ^{9}Be)^{19}F α-particle transfer reactions [2, 3]. Both reactions also strongly populate levels at 8.29 and 8.96 MeV, and these levels have received [2] a natural interpretation as the $11/2^-$ and $13/2^-$ levels arising from the weak coupling of a p-shell hole to the 6^+ level at 8.78 MeV in ^{20}Ne.

Subsequently, a study [4] of the ^{15}N$(\alpha,\gamma)^{19}$F reaction using solid targets strongly suggested a $13/2^-$ assignment to the level at 8.29 MeV. However, the same work indicated a spin and parity assignment of $11/2^+$ for the level at 8.96 MeV, which is inconsistent with the earlier interpretation. Further, a level at 7.17 MeV with a probable spin and parity of $11/2^-$ was discovered [5], and interpreted as the predominantly (81) $11/2^-$ state on the basis of a strongly enhanced E2 transition to the 4.00 MeV ($7/2^-$) level. However, contrary to the expectation for the (81) state, this level was not populated appreciably in α-particle transfer reactions [2, 3]. The situation has been further complicated by recent studies [6, 7] of the ^{16}O$(\alpha, p)^{19}$F and ^{16}O(^{10}B, ^{7}Be)^{19}F triton transfer reactions. The level at 8.96 MeV was again strongly populated in these reactions, whereas the 7.17 and 8.29 MeV levels were not, and a level at approximately 9.90 MeV of unknown spin and parity was also strongly populated.

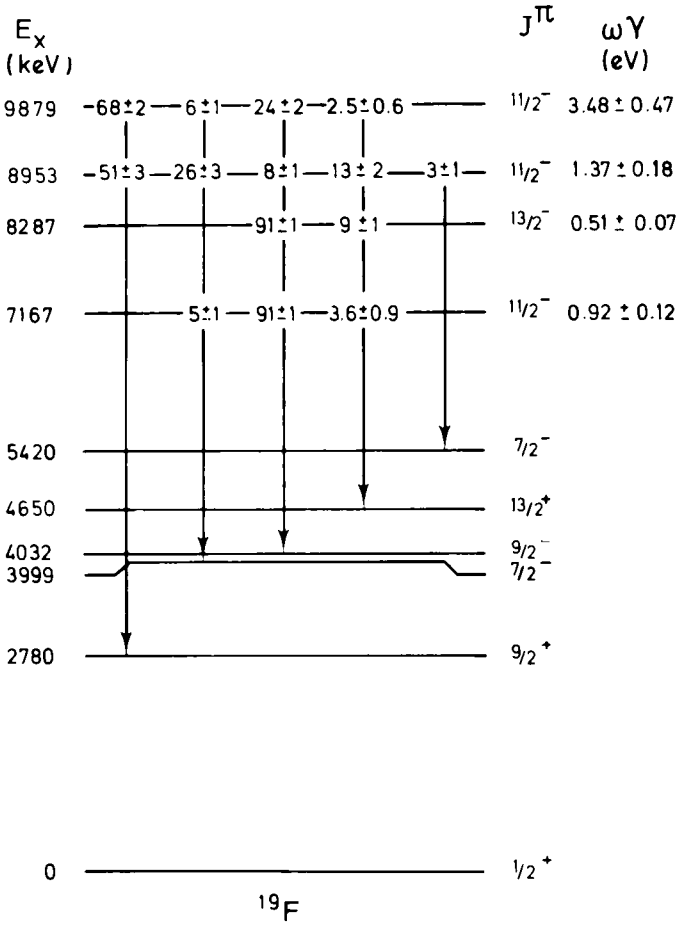

Fig. 1. Decay schemes and values of $\omega\gamma$ for the 7.17, 8.29, 8.96 and 9.88 MeV levels as measured in the present work. The excitation energies of these four states have uncertainties of ±3 keV.

In an attempt to resolve these difficulties, we have studied the levels at 7.17, 8.29, 8.96 and 9.88 MeV using the ^{15}N$(\alpha,\gamma)^{19}$F reaction with a differentially cryopumped gas target. The gas target was similar to one described previously [8], the chief difference being that the effective length was reduced from 19 to 9 cm

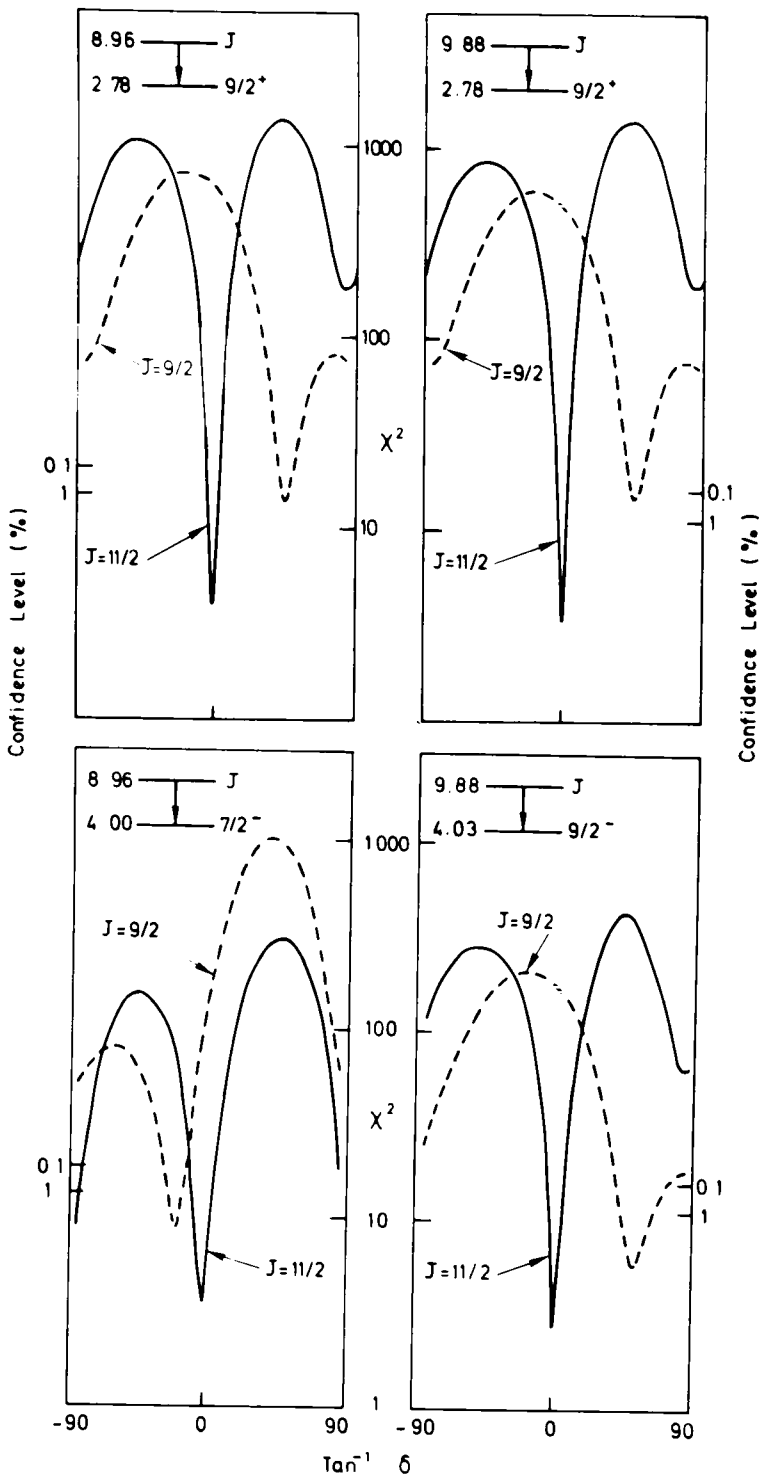

Fig. 2. χ^2 plots for the corrected angular distributions of the two strongest transitions from both the 8.96 and 9.88 MeV levels.

to permit the measurement of γ-ray angular distributions. Resonances were located using a 7.6 cm × 7.6 cm NaI(Tl) crystal and an automatic beam energy modulation technique [9]. Spectra of γ-rays on and off resonance were taken with an 85 cm^3 Ge(Li) detector positioned at 125° and with its front face 11 cm from the centre of the target. The target gas pressures were chosen so that the incident α-particles lost, on average, 8.0 keV in traversing the target [10]. This ensured that the yield of γ-rays from a narrow resonance ($\Gamma < 1$ keV) should be effectively that from a thick target. Accurate measurement of the Doppler shift of one of the secondary γ-ray transitions served to define [11] the precise position of the resonance along the target. Values of $\omega\gamma$ ($= J + \frac{1}{2}\Gamma_\gamma\Gamma_\alpha/\Gamma$) were deduced by comparison of the γ-ray yields from the four resonances with the yield from the 6.93 MeV 2^+ $T=1$ resonance in the $^{16}O(\alpha, \gamma)^{20}Ne$ reaction ($\omega\gamma = 19.7 \pm 1.6$ eV) [12]. Relative stopping powers for oxygen and nitrogen were taken from ref. [10], and corrections were applied for angular distribution effects and for the extended nature of the source of γ-rays (see below).

Gamma-ray angular distributions were also measured for the 8.96 and 9.88 MeV resonances using a 60 cm^3 intrinsic germanium detector which could be positioned at angles between 25° and 90° with its front face 11 cm from the centre of the target. The 85 cm^3 Ge(Li) detector, fixed at 135° and 15 cm from the target, served to define the position of the resonance as in the $\omega\gamma$ measurements. As the source of γ-rays was extended along the beam direction, the observed angular distribution deviated from that of a point target, and it was necessary to correct [11] the raw data before fitting it to the theoretical distributions applicable to a point target. The necessary corrections were less than 10% at all angles.

Gamma-ray decay schemes and $\omega\gamma$ values for the four resonances studied are presented in fig. 1. It is immediately apparent that the observation of branches from the 8.96 MeV level to the $7/2^-$ levels at 4.00 and 5.42 MeV is inconsistent with the earlier $11/2^+$ assignment [4], since it implies M2 strengths of >100 W.u. for both transitions. Instead, the spin and parity of the 8.96 MeV level are limited to $9/2^+$ or $11/2^-$ by the decay scheme and resonance strength measured in the present work. Similarly, the spin and parity of the 9.88 MeV level are also restricted to $9/2^+$ or $11/2^-$. The observation of weak branches to the $13/2^+$ level at 4.65 MeV confirms the $11/2^-$ and $13/2^-$ assignments to levels at 17.7 and 8.29 MeV, respectively. The alternative assignments of $7/2^-$ for the 7.17 MeV level and $9/2^-$ for the 8.29 MeV level, which were consistent with angular distribution measurements [4, 5], would require unreasonably large

3.2 Summary of present work

The clean nature of the cryogenically pumped gas target, together with the possibility of using a thin target, made it worth repeating the survey of Pearson and Spear[Pe64b] with the aim of observing new decay modes of previously known states in ^{20}Ne. In addition there was the possibility of finding new sharp resonances which might have been missed by previous work of inferior resolution, or obscured by contaminant reactions.

The target gas used was oxygen enriched in ^{16}O to reduce background problems due to ^{17}O and ^{18}O, which were stated by the suppliers to be present at levels of 57ppm and 25ppm respectively. Unfortunately the gas became contaminated, presumably due to a leak in the recovery network. This caused a noticeable quantity of ^{17}O and ^{14}N to be introduced, both of which gave rise to troublesome γ-rays from the reactions $^{14}N(\alpha,p\gamma)^{17}O$, $^{14}N(\alpha,\alpha'\gamma)^{14}N$ and $^{17}O(\alpha,n'\gamma)^{20}Ne$.

Various states above an excitation of 7.13 MeV (E_α=3.0 MeV) were selected for study, and a continuous yield curve was measured from E_x=11.1 MeV (E_α=7.96 MeV) to E_x=12.45 MeV (E_α=9.65 MeV).

All the known natural parity states in ^{20}Ne whose total width is less than 15 keV and with energies in the range covered in this thesis are listed in table 3.2.1, where the spin, parity and band assignment of each are indicated. In this table, as elsewhere, beam energies are deduced from excitation energies, using the nuclear mass values of Wapstra and Bos[Wa77]. In addition, for states discussed elsewhere in this thesis, reference to the relevant section is given. Chapter 4 discusses all the T=1 states shown and chapter 5 discusses the T=0

Table 1
Electromagnetic transition rates of $11/2^-$ levels in ^{19}F.

Experiment					SU(3) shell model					Cluster model				
E_x (MeV)	J_i^π	J_f^π	$M\lambda$	$B(M\lambda)$ (W.u.)	E_x (MeV)	J_i^π	J_f^π	$M\lambda$	$B(M\lambda)$ [a] (W.u.)	E_x (MeV)	J_i^π	J_f^π	$M\lambda$	$B(M\lambda)$ [b] (W.u.)
7.17	$11/2_1^-$	$7/2_1^-$	E2	10.0±2.4	7.94	$11/2_1^-$	$7/2_1^-$	E2	1.0	9.12	$11/2_1^-$	$7/2_1^-$	E2	17
		$9/2_1^-$	M1	0.21±0.03	(62)		$9/2_1^-$	M1	0.04	(α)		$9/2_1^-$	M1	0
							$7/2_2^-$	E2	5.2					
8.96	$11/2_2^-$	$7/2_1^-$	E2	8.3±1.4						10.13	$11/2_2^-$	$7/2_1^-$	E2	0
		$9/2_1^-$	M1	0.007±0.001	9.66	$11/2_2^-$	$7/2_1^-$	E2	20	(t)		$9/2_1^-$	M1	0
		$7/2_2^-$	E2	5.1±1.8	(81)		$9/2_1^-$	M1	0.22					
							$7/2_2^-$	E2	0.8					
9.88	$11/2_3^-$	$7/2_1^-$	E2	2.0+0.4										
		$9/2_1^-$	M1	0.033±0.005										

[a] Effective charge 0.5 e. [b] Effective charge 0.045 e.

E3 and M2 enhancements, respectively.

The ambiguities in the spin and parity assignments for the 8.96 and 9.88 MeV levels were resolved by the angular distribution measurements. Fig. 2 shows χ^2 plots for the γ-ray angular distributions of the strongest transitions from the 8.96 and 9.88 MeV levels. In both cases, $11/2^-$ is the only assignment consistent with both the decay scheme and the angular distribution data. In particular, the best fit for $J = 11/2$ to the angular distribution of the 8.96 → 2.78 MeV transition is obtained for a mixing ratio which is consistent with zero. This is in marked contrast to the result, $\delta = 4.4$, on which the $11/2^+$ assignment of ref. [4] was based. The alternative $9/2^+$ assignments are ruled out by the fits to the angular distributions of the 8.96 → 4.00 MeV ($7/2^-$) and 9.88 → 4.03 MeV ($9/2^-$) transitions. Acceptable fits are obtained only for large values of the M2/E1 mixing ratios which imply unreasonably large M2 enhancements of >17 and >100 W.u., respectively. The measured electromagnetic transition rates of the three $11/2^-$ levels at 7.17, 8.96 and 9.88 MeV are summarised in table 1.

Theoretical calculations of the properties of high-spin negative parity states in ^{19}F have recently been carried out within the framework of two quite different models, namely the SU(3) shell model in a $p^{-1}sd^4$ basis [1], and a cluster model [13]. Both calculations predict two $11/2^-$ levels between approximately 8 and 10 MeV in ^{19}F. These may be identified with an α-particle cluster state and a triton cluster state on the one hand, or as states dominated by the (81) and (62) representations of SU(3) on the other. Since the (81) shell model state is expected to be strongly populated in α-particle transfer reactions, it can be associated with the α-particle cluster state, whereas the (62) state does not have a simple cluster structure since it arises mainly from the coupling of a p-shell hole to $T = 1$ states in ^{20}Ne. The triton cluster state cannot be associated with either shell model state, since it is expected to lie predominantly outside the $p^{-1}sd^4$ space employed in the shell model calculations. Hence, the theoretical models indicate the existence of three $11/2^-$ states between 7 and 10 MeV in ^{19}F, and appreciable mixing between these levels might be anticipated.

There is clear evidence for such mixing in the observation that none of the three experimental $11/2^-$ states may be readily identified with a particular model state. This is apparent from table 1, in which the experimental electromagnetic transition strengths for $11/2^-$ levels in ^{19}F are compared with their theoretical counterparts. The 8.96 MeV level, for example, possesses certain of the features of each of the three model states: the large α-particle transfer strength of the α-particle cluster state, the substantial triton transfer strength of the triton cluster state and the 5 W.u. E2 γ-ray transition to the second $7/2^-$ state expected of the (62) model state. Hence, it is clear that further progress towards a detailed understanding of the properties of $11/2^-$ states in ^{19}F must await calculations

which encompass all three states, such as extended SU(3) shell model calculations in which the leading representations of the sd^2pf configuration are added to the basis. These calculations are at present underway in this laboratory.

We wish to thank Drs. D.J. Millener and A.A. Pilt for many useful discussions.

References

[1] D.J. Millener, Oxford University, private communication.
[2] R. Middleton, in: Nuclear reactions induced by heavy ions, Heidelberg (North Holland, 1970) p. 263.
[3] A.A. Pilt et al., Nucl. Phys. A273 (1976) 189.
[4] B.Y. Underwood et al., Nucl. Phys. A225 (1974) 253.
[5] D.W.O. Rogers, W.R. Dixon and R.S. Storey, Can. J. Phys. 51 (1973) 1.
[6] K. van der Borg, R.J. de Meijer and A. van der Woude, Nucl. Phys. A273 (1976) 172.
[7] M. Hamm et al., Phys. Rev. Lett. 36 (1976) 846.
[8] K.W. Allen et al., Nucl. Instr. 134 (1976) 1.
[9] M.R. Wormald and J. Takacs, Nucl. Instr. 113 (1974) 263.
[10] L.C. Northcliffe and R.F. Schilling, Nucl. Data A7 (1970) 233.
[11] F. Watt et al., to be published.
[12] P.D. Ingalls, Nucl. Phys. A265 (1976) 93.
[13] B. Buck and A.A. Pilt, Nucl. Phys. in press.

Table 3.2.1 States in ^{20}Ne Relevant to this Thesis

Beam Energy MeV	Excitation MeV (a)	$J^\pi;T$ (a)	ΓkeV (a)	ΓkeV (b)	K^π (a)	§
3.05	7.17	3^-	8		0^-	
3.07	7.19	0^+	4		0^+_3	
3.36	7.42	2^+	8	6.4 ± 2.4	0^+_2	
3.87	7.83	2^+	2.4	1.4 ± 0.8	0^+_3	
4.65	8.45	5^-	0.013 ± 0.004		2^-	
4.96	8.70	1^-	2.5	2.1 ± 0.8		5.1
5.06	8.78	6^+	0.11 ± 0.02		0^+_1	
5.15	8.85	1^-	19		1^- (b)	4.3
5.37	9.03	4^+	3.2	2.4 ± 1.2	0^+_3	
5.47	9.11	3^-	3.2	<3.2		5.2
5.74	9.32	(2^-) (b)			1^- (b)	4.3
6.93	10.27	$2^+;1$	0.12 ± 0.02 (c)	<1		4.1
7.64	10.84	$2^+;0$	13			
7.95	11.09 (b)	$4^+;1$	<0.5	<1		4.2
8.18	11.27 (b)	$1^-;1$	<0.3	<1		4.3
8.54	11.56	$(0^+,2^+);0$	1.0 ± 0.5	1.3 ± 0.8		5.3
8.99	11.92 (b)	$4^+;0$	0.44 ± 0.15	<1		5.4
9.03	11.95	$8^+;0$	0.035 ± 0.010	<1	0^+_1	5.5
9.26	12.14 (b)	$6^+;0$	0.13 ± 0.07	<1	0^+_3	5.6
9.36	12.22	$2^+;1$	<0.1	<1		4.4
9.40	12.25	$3^-;1$ (b)	~5	<1		4.5
9.58	12.39	$3^-;0$	33 ± 4			
9.60	12.44	$0^+;0$	<8	29		

§ The section of this thesis in which the state is discussed.
a) Data taken from Aj78 except where indicated.
b) Value taken from this work.
c) In76a.

states for which decay spectra were measured. The two T=0 states at 8.85 MeV and 9.32 MeV are discussed briefly in chapter 4 because information about them was obtained through their population by the decay of the 11.27 MeV (1^-;T=1) state. The former was too broad to be suitable for study as a resonance and the latter cannot be populated directly by α-capture due to parity conservation rules. States for which no reference to other chapters is given in the table were, for various reasons, not studied in detail, and a brief discussion of them follows.

An attempt was made to locate the 7.17 MeV (3^-) and 7.19 MeV (0^+) states, but without success. The latter is known [Al72b] to have a very weak γ-strength ($\omega\gamma$=4.35 meV) and it is not surprising that we did not observe it as a resonance without adopting special methods. Since the beam energy required is below the $^{13}C(\alpha,n\gamma)^{16}O$ threshold, little advantage would be gained by using the gas target and so no significant improvement on the work of Alexander et al would be expected. The other state would also be expected to have a significant branch to the 1.63 MeV (2^+) state and so would be expected to be visible in the yield curve presented by Alexander et al in their work on the 0^+ state. Its absence indicates that this state, also, is very weak. This, together with reasons discussed in the previous section, meant that it was not worth spending more time searching for it.

The 2^+ states at 7.42 MeV and 7.83 MeV were both observed in yield curves and fits to these enabled total width estimates of 6.4±2.4 keV and 1.4±0.8 keV respectively to be made in the centre of mass frame of reference. These values are both slightly lower than the values deduced from partial wave analysis by Cameron[Ca53] but are consistent

therewith. The γ-decay properties of these two states have been reported by Alexander et al[Al72b].

No attempt was made to observe the 8.45 MeV (5^-) member of the $K^\pi=2^-$ band as its decay has been well reported previously [Ro71o]. Similarly the 8.78 MeV (6^+) member of the ground state band, although observed, was not studied as its decay strength has been measured absolutely on several occasions [Ro71f, Al72a, Li67, Di71].

The 9.03 MeV (4^+) level was observed in a yield curve, leading to a width estimate of 2.4 ± 1.2 keV which is not inconsistent with the value of 3.2 keV reported by McDermott et al[Mc60]. As explained in the previous section, this resonance was not studied further.

The 2^+ state at 10.840 MeV with a width of 13 keV [Be75] is really too broad for study as the properties of this state are not expected to be of particular significance. The resonance has almost total overlap with the 3^- level at 10.838 MeV which has a width of 45 keV, and separation of the two decay schemes would be difficult. A yield curve was measured over this energy region and an indication of both states was seen but they were not studied further.

At the high energy end of the continuous yield curve that was measured, above the T=1 $2^+/3^-$ doublet, the broad 3^- inelastic resonance at an excitation of 12.39 MeV was seen. Owing to the T=1 assignment made in chapter 4 to the 12.25 MeV state, this state cannot be the analogue of the 1.97 MeV state in ^{20}F as had been suggested by Steck [St78]. No capture γ-rays were observed from this resonance. Above this level, a broad (29 keV) inelastic resonance at $E_x=12.44$ MeV was seen, particularly as a resonance in the inelastic channel populating

the 6.05 MeV (0^+) state in ^{16}O which can only decay by pair production. The resultant positron annihilation radiation gave rise to a clear peak in the yield curve in an energy gate set to cover that energy range. This resonance has since been studied extensively by detecting the inelastically scattered α-particles [Ga80] and has been shown to have $J^\pi=0^+$.

CHAPTER 4

States in ^{20}Ne with T=1

4.1 Introduction

The excitation of the first T=1 state in ^{20}Ne can be predicted from the differences of the Coulomb energies and the mass defects of ^{20}F and ^{20}Ne together with the mass difference between the neutron and hydrogen atom. Pearson and Spear [Pe64b] obtained a value for the excitation of 10.23 MeV using a Coulomb radius derived from several neighbouring isobaric doublets and triplets. This means that in the excitation range covered in this thesis (E_x < 12.5 MeV) the analogues of states in ^{20}F up to 2.3 MeV are expected to appear. These 11 states in ^{20}F are shown in figure 4.1.1 with data on these states coming mainly from Longo et al[Lo73] and Millington et al[Mi74]. The spin and parity assignments of the 1.97 MeV and 2.19 MeV states have not yet been settled.

The analogues of seven of these states have already been definitely identified and a candidate for the analogue of the 0.98 MeV (1^-) state has been proposed. In the work described below, the analogue of this 1^- state is identified unambiguously and the situation regarding the 12.22 MeV (2^+) state is clarified. In addition, the analogue of the 1.97 MeV state is positively identified and found to have $J^\pi=3^-$, reinforcing the tentative spin assignment of the ^{20}F state. Thus all the natural parity T=1 states expected are seen clearly in alpha capture despite the isospin-forbidden nature of this reaction. As described in chapter 1, this is because the observed strength is not dependent on Γ_α provided $\Gamma_\alpha \doteq \Gamma$, and this condition is satisfied for the states here, since, even for energetic allowed dipole transitions, Γ_γ is only a few eV. The

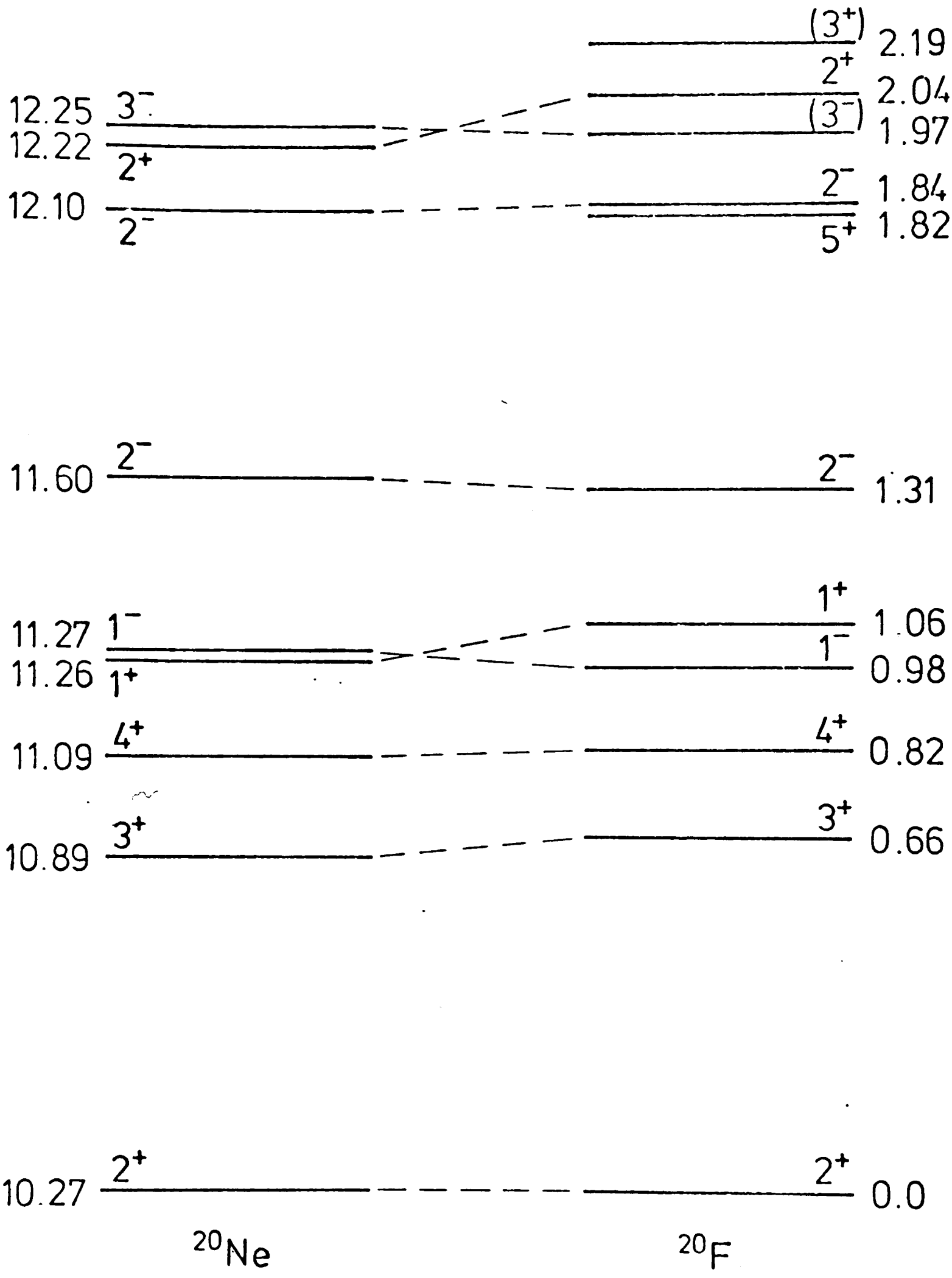

Fig.4.1.1 Comparison of T=1 energy levels in ^{20}Ne with ^{20}F.

observed states are discussed in detail below.

4.2 The 10.27 MeV (2^+; 1) State

In their survey of the reaction $^{16}O(\alpha,\gamma)^{20}Ne$ Pearson and Spear[Pe64b] saw a strong resonance corresponding to a state in ^{20}Ne with excitation 10270±9 keV and with a total width less than 2 keV. They claimed evidence for a weak (3%) ground state branch but the main γ-decay observed was to the 1.63 MeV(2^+) state with $\omega\gamma$=22±3eV. They measured the angular distribution of this branch and obtained a good fit for a $J^\pi=2^+$ hypothesis with a mixing ratio of δ=-0.02 (the sign has been changed in order to follow the convention of Rose and Brink[Ro67]). This decay was therefore shown to be M1 with a strength of 0.33 Weisskopf units allowing a definite T=1 assignment to be made. As has been shown above, the first T=1 state in ^{20}Ne was expected at about this energy. Further alpha capture work has been performed by Ingalls[In76a], who has provided an improved value for $\omega\gamma$ of 19.7±1.6eV, and by Alexander et al[Al72b] who measured the excitation energy to be 10271±3keV. More recently Snover et al reported a value for Γ_γ of 4.02±0.21eV [Sn78] from which it can be deduced that the $\omega\gamma$ they obtained was 19.4±1.0eV.

Torgerson et al[To73] studied the β^+ decay of ^{20}Na, which they formed by the charge exchange reaction $^{20}Ne(p,n)^{20}Na$, and gave a value for the ratio of the observed intensity of α-radiation from the $^{20}Ne(E_x$=10.27) state to the total intensity of 1.63 MeV γ-radiation from ^{20}Ne. Ingalls[In76b] in similar work obtained a value for the ratio of 8.64 MeV γ-radiation from the 10.27→1.63 decay to the total 1.63 MeV γ-radiation which, combined with the other ratio, implies a value for

$\Gamma_{8.64}/\Gamma_\alpha$ of 0.035±0.008. Ingalls later used this ratio and his value of $\omega\gamma$ [In76a] together with the ground state γ-branching ratio from Pearson and Spear[Pe64b] to deduce values for Γ_α and $\Gamma_{8.64}$ of 116±20eV and 4.08±0.33eV respectively. On the assumption that the isospin forbidden α-decay is entirely due to T=0 impurity he calculated the intensity of such an impurity to be ~1%.

This state has been seen in the two particle transfer reaction $^{18}O(^3He,n)^{20}Ne$ by Gul et al[Gu70] and weakly in the one particle transfer reactions $^{19}F(^3He,d)^{20}Ne$ [Be75, Se76] and $^{19}F(d,n)^{20}Ne$ [La68]. It has also been populated by Millington et al[Mi74] in the reaction $^{21}Ne(d,t)^{20}Ne$, the strength being consistent with the analogue reaction to the ground state of ^{20}F.

The work on this state was performed in advance of the rest of the work described in this thesis and has been described by Fifield et al[Fi77]; a brief description will be included here for completeness. For this state only, the MkII version of the gas target was used instead of the MkIII version. It had a longer target chamber (19cm) with shorter nozzles and was usually used with lower gas pressures. It has been described by Allen et al[Al76]. The interest in studying this state arose from the simple relationship between the isovector M1 matrix element for the γ-decay of the T=1 state in ^{20}Ne to a given state and the analogous weak magnetism contribution to the β-decay of ^{20}F and ^{20}Na to the same state. This follows from the conserved vector current theory, the effect of weak magnetism being to affect the shape of the β-spectrum and also the β-γ correlation.

Spectra were accumulated on and off resonance (fig.4.2.1) and evidence was seen for the following decays:- R→0.00(0^+); R→1.63(2^+); R→4.97(2^-); R→5.62(3^-); R→7.42(2^+) and R→7.83(2^+). The transition strengths were measured relative to the decay of the 8.78 MeV (6^+) state, which has been measured absolutely by Rogers et al[Ro71f], and the apparent strength of the ground state branch had to be corrected for summing in the detector of the R→1.63 and 1.63→0.00 decays. The value of 19.7±2.1eV for the $\omega\gamma$ of the R→1.63 transition is in excellent agreement with the value obtained by Ingalls[In76a]. However, it can be seen from table 4.2.1 that the branching ratio for the decay to the first excited state is only 88.9% instead of the value of 96.6% implied by the work of Pearson and Spear, and this has a slight effect on the widths deduced by Ingalls[In76a]. The total width of the state is 121.6±23eV and comprises an alpha width of 117±22eV and a total gamma width of 4.6eV. Our observed weak ground state branch (0.65%) is clearly much weaker than could have been observed by Pearson and Spear so the 10.27 MeV radiation they detected must have been due to summing in their detector despite their attempt to correct for this effect. The other weak branches all give rise to γ-rays lying in a region of the spectrum where they would easily be obscured by the usual contaminant reactions occurring in solid targets at this energy, so it is not surprising that only the 90% branch has been reported previously. The decay scheme is shown in fig.4.2.2.

In later work, intended primarily to test the MkIII target, the mixing ratio (δ) for the main primary transition was measured to be $-0.038^{+0.035}_{-0.028}$. This is in good agreement with the value -0.020 ± 0.013 obtained by Pearson and Spear.

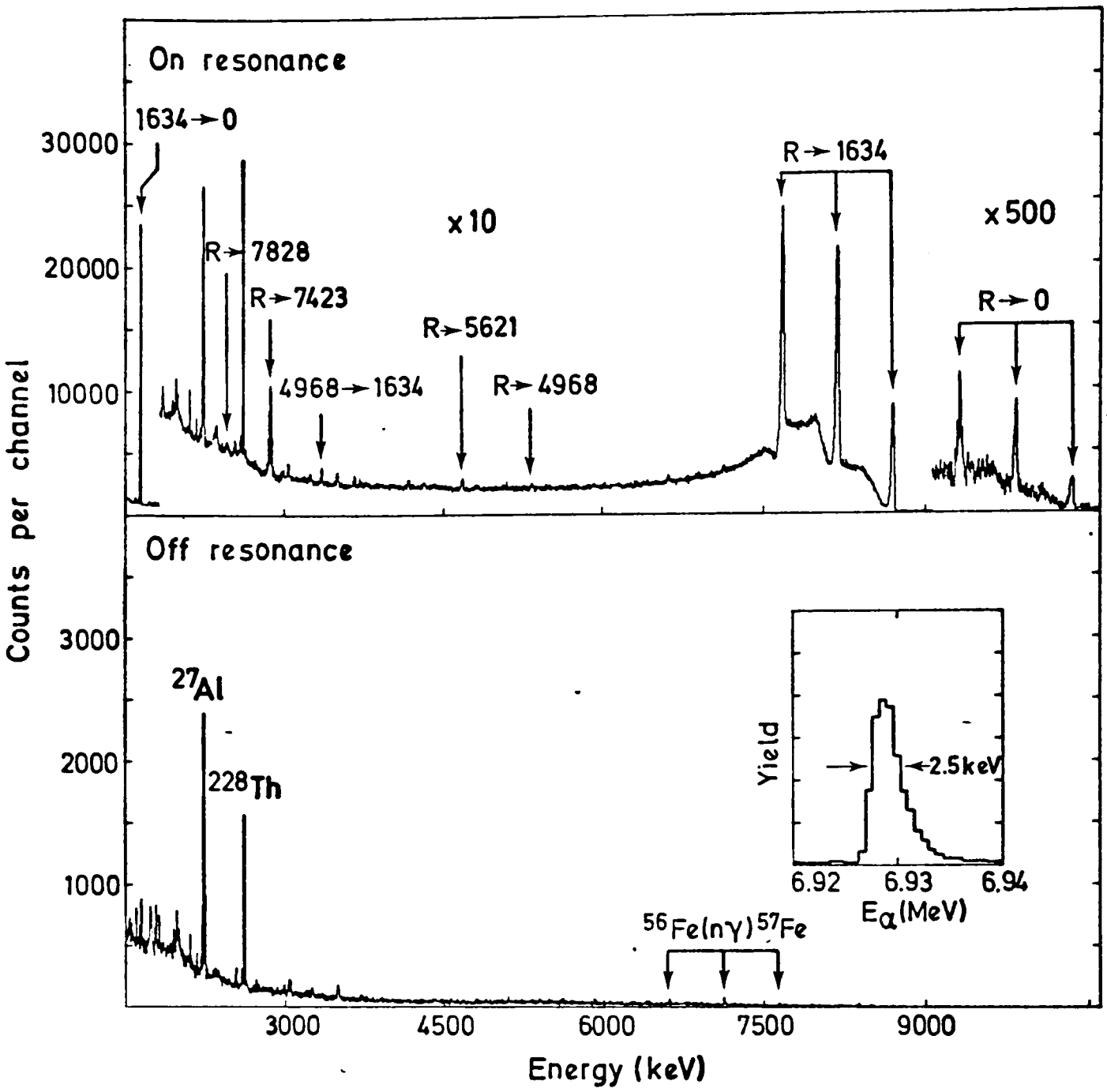

Fig.4.2.1 Spectra of γ-rays taken on and off the 6.93 MeV resonance in the $^{16}O(\alpha,\gamma)^{20}Ne$ reaction using a target pressure of 0.8 torr. The two spectra have been normalised to the same collected charge. Peaks arising from the decay of the 10.27 MeV $2^+;T=1$ level in ^{20}Ne are labelled on the on-resonance spectrum by the corresponding transition. The peaks labelled in the off-resonance spectrum are contaminants discussed in chapter 1. The inset shows a yield curve over the resonance taken with a target pressure of 0.04 torr.

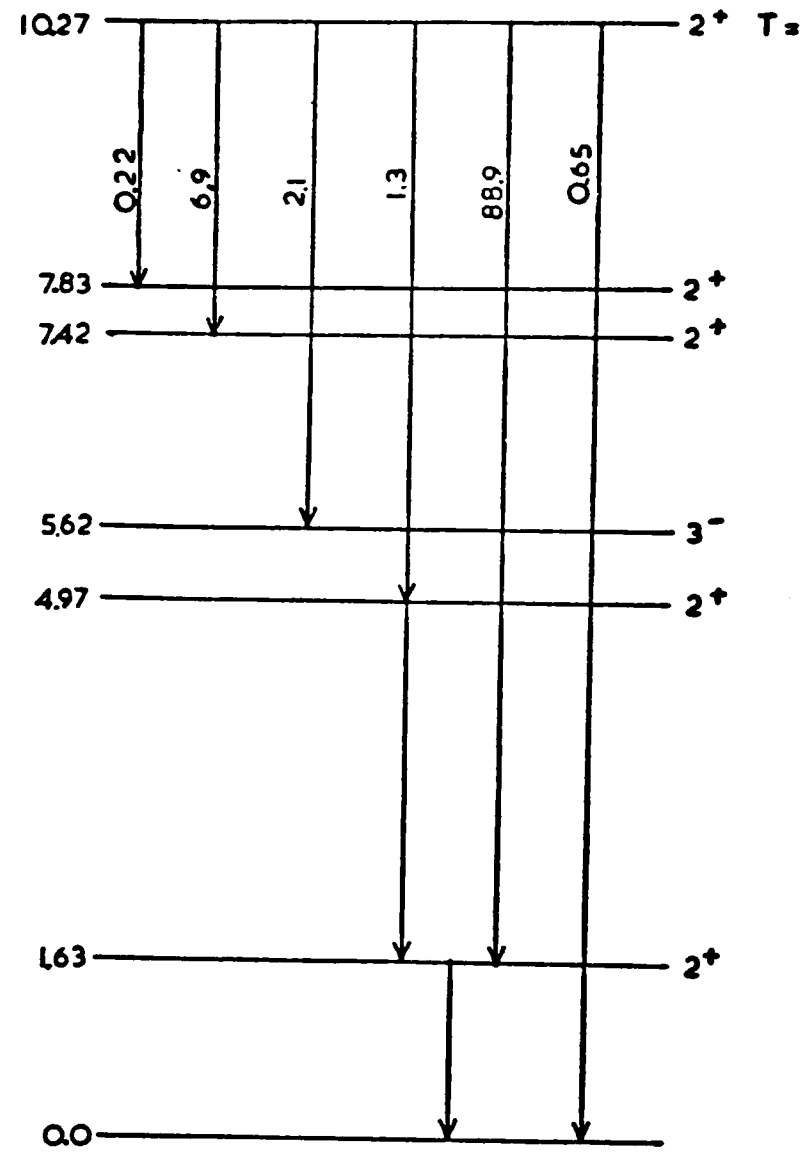

Fig.4.2.2 Decay scheme of the 10.27 MeV 2^+, T=1 state in ^{20}Ne. The numbers shown on each transition are the relative intensities.

Table 4.2.1 10.27 MeV $2^+;1$

	Present work	Previous
E_x	10271.2±2.7	10271[a]
Implied E_α	6926.5±3.4	
Γ	<1; (122±20eV**)	120±20eV[b]
J^π	$2^+;1$	$2^+;1$
Total $\omega\gamma$ (ev)	22.14±2.11	

Detector at 12.5cm 55°*

	$E_\gamma(\theta)$	Branching Ratio %	Γ_γ** (eV)	Mλ	B(Mλ)W.u.	Previous Γ_γ
R→0.00(0^+)	10266.1±5.0	0.65±0.14	0.029±0.008	E2	0.10±0.03	0.14±0.03[c]
R→1.63(2^+)	8636.3±3.2	88.9±0.5	4.10±0.44	M1	0.31±0.03	4.08±0.33[b]
R→4.97(2^-)	5305.2±3.8	1.3±0.1	0.060±0.008	E1	$(8.3\pm1.0)\times10^{-4}$	<0.32[c]
R→5.62(3^-)	4649.6±2.2	2.1±0.2	0.097±0.014	E1	$(2.0\pm0.3)\times10^{-3}$	-
R→7.42(2^+)	2847.9±1.2	6.9±0.4	0.31±0.04	M1	0.65±0.08	-
R→7.83(2^+)	2442.9±2.6	0.22±0.06	0.008±0.002	M1	0.027±0.006	-
4.97→1.63	3332.0±1.9					

a) [Al72b]

b) Ingalls et al [In76a]

c) γ branching ratio from Pearson and Spear[Pe64b] applied to $\Gamma_\gamma(R\to1.63)$ from In76a

* MkII target.

** Γ derived by applying improved γ-ray measurements to the calculation of Ingalls[In76a]; this also gives Γ_α=117±20eV and these two values are used in calculating Γ_γ

In this and other tables all energies and total widths are given in keV unless otherwise stated.

4.3 The 11.09 MeV (4^+) State

This state was seen by Pearson and Spear[Pe64b] at an excitation of 11.08±0.02 MeV with a total width of less than 3keV. Their measurement of $\omega\gamma$ for the decay to the 4^+ state at 4.25 MeV was 37±4eV. They measured the angular distribution of this decay which implied that $J^\pi=4^+$ and that the mixing ratio $\delta=+0.238\pm0.023$; however a 2^+ assignment could not be ruled out. This gives an M1 strength of 0.6 Weisskopf units, implying a $\Delta T=1$ transition. They therefore identified this level as the $T_z=0$ analogue of the 0.82 4^+ T=1 state in ^{20}F.

Litherland et al[Li67] also observed the γ-decay to the 4.25 MeV state, and more recently Steck[St78] studied this resonance and obtained a value of δ similar to that of Pearson and Spear but with a larger error. His value of $\omega\gamma$ was lower (30±3eV) and he placed an upper limit on the possible $R\rightarrow1.63$ transition of $\omega\gamma\leq0.6$eV. Again a 2^+ assignment could not be excluded but 4^+ was favoured.

Apart from alpha-capture reactions, this state may first have been seen by Butler[Bu60] who used the γ-ray threshold technique in the reaction $^{19}F(d,n\gamma)^{20}Ne$. He saw evidence for a level at 11.11±0.02 MeV which did not decay to the ground state. It has also been seen in $^{19}F(^3He,d)^{20}Ne$ by Sen Gupta et al[Se76] and by Betts et al[Be75] who found that it was weakly populated and that the angular distribution was not characteristic of a direct stripping reaction. This was consistent with the results of the $^{19}F(d,p)^{20}F$ reaction populating the analogue state in ^{20}F [Fo72b, Fo74]. The pickup reaction $^{21}Ne(d,t)^{20}Ne$ has been used by Millington et al[Mi74], who measured the excitation energy to be 11.086±0.010 MeV and found $\ell_n=2$. The strength ($C^2S=0.18$) was in

agreement with their measurement for the reaction $^{21}Ne(d,^{3}He)^{20}F$ populating the analogue state ($C^2S=0.26$), since the spectroscopic factor should be the same in each case and the values of C^2 come from isospin Clebsch-Gordan coefficients and have the ratio 1:2.

In the present work a strong resonance was observed at a beam energy of 7.95 MeV in a yield curve measured with a target thickness of 9.7keV (800μ gas pressure). The peak to background ratio was 50:1 in the gate covering the range 6.3 MeV < E_γ < 6.9 MeV and the total width was deduced to be less than 1keV, improving the limit set previously by Pearson and Spear and by Steck[St78]. The yield curve is shown inset in fig.4.3.1. A spectrum (fig.4.3.1) was accumulated on resonance for an integrated beam charge of 5.3×10^{-2}C of He^{++} and with a target gas pressure of 800μ as for the yield curve. It can be seen from the spectrum that the oxygen gas had been contaminated with air at some stage and this has led to the large peak corresponding to the reaction $^{14}N(\alpha,p\gamma)^{17}O$. It is thought this may have been due to a leak in the gas recovery network. The measured value of $\omega\gamma$ for the R→4.25 transition is in good agreement with the values reported by Steck[St78] and by Pearson and Spear. The observed energy of the γ-ray from this transition enables an accurate determination of the excitation giving a value of 11087±3keV after allowing for recoil. This is in good agreement with the value of Pearson and Spear and of Millington et al[Mi74] but just above the upper bound of the error quoted by Steck.

In addition to the dominant R→4.25 decay mode a very weak branch to the 1.63 MeV(2^+) state was observed which has not been reported previously. The peak in the spectrum includes a contribution from summing in the detector of the primary and secondary decays in the

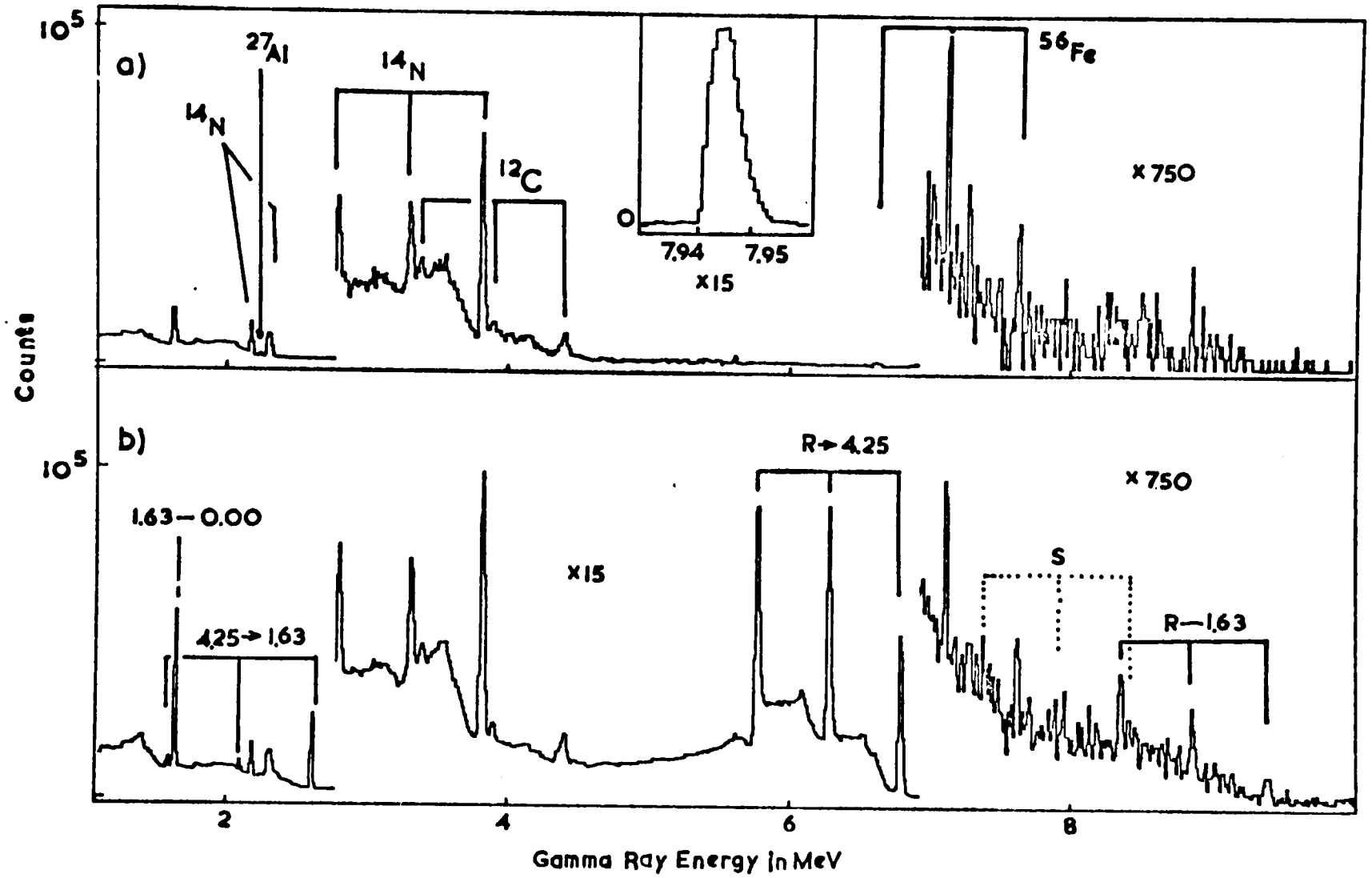

Fig.4.3.1 Spectra of γ-rays taken (a) off and (b) on the 7.95 MeV resonance in the $^{16}O(\alpha,\gamma)^{20}Ne$ reaction, using a target pressure of 0.8 torr. The two spectra have been normalised to the same collected charge. Peaks arising from the decay of the 11.09 MeV 4^+;T=1 level in ^{20}Ne are labelled on the on-resonance spectrum by the corresponding transition. The position of the peak due to the summing of the transitions R → 4.25 and 1.63 → 0.00 is marked 's'. The peaks labelled ^{14}N on the off-resonance spectrum are discussed in the text; the other peaks are discussed in chapter 1. The inset shows a yield curve over the resonance, taken with a target pressure of 0.8 torr.

cascade R→4.25→1.63→0.00. The magnitude of this effect can be estimated from the summing of the primary and tertiary decays which is barely observable but for which a limit can be obtained. This permits a lower limit on the R→1.63 transition strength to be derived and shows that at least half of the observed peak in the spectrum is due to the R→1.63 decay γ-ray. The information extracted from this spectrum is presented in table 4.3.1.

The measurement by Pearson and Spear of the mixing ratio (δ) for the primary transition leads to a large E2 component which exceeds the recommended upper limit for transitions of this type [En74]. The more recent measurement by Steck[St78] adds little additional information as the large error bar includes both zero and the Pearson and Spear value. It was therefore decided to measure the angular distribution for this resonance with the gas target.

The resonance was located approximately centrally in the target chamber by measuring a yield curve with a gas pressure of 800μ. Spectra were then accumulated with the 16.6% Ge(Li) detector held fixed at 135° to the beam direction and the intrinsic germanium detector at angles of 25°, 40°, 50°, 65° and 90°. Both detectors were at a distance (target to can) of 12cm and the integrated beam charge at each angle was about 0.02C. The correction procedure showed the resonance to be central for four of the angles but not for the 90° case so the intensity at this angle was not used. A plot of the corrected intensity at the other angles against $\cos^2\theta$ is shown in fig.4.3.2b together with the best fit for a $J^{\pi}=4^+$ assumption. A χ^2 plot as a function of $\tan^{-1}\delta$ is shown in fig.4.3.2a and this shows that the best value of δ is 0.01 ± 0.06 which is consistent with zero and inconsistent with the value of Pearson and

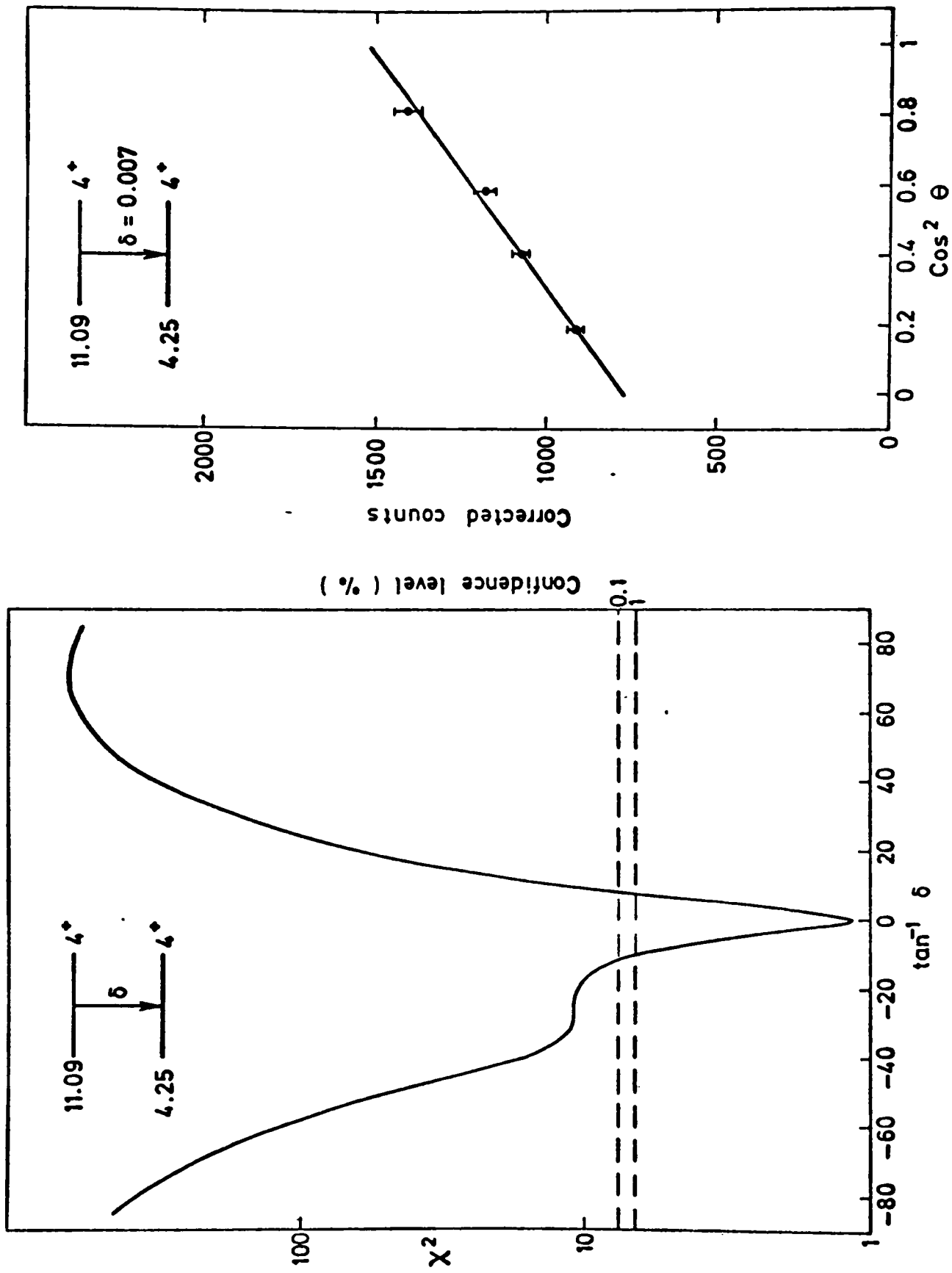

Fig.4.3.2 (a) χ^2 plot from the fit to the γ-ray angular distribution of the 11.09 → 4.25 MeV transition for a spin hypothesis of 4^+ for the 11.09 MeV level.
(b) The measured angular distribution after correction. The solid line is the best fit, obtained for δ=0.007.

Spear. This disagreement can be explained by the use of NaI detectors in close geometry by Pearson and Spear together with the strong 6.92 and 7.12 MeV background radiation from the $^{13}C(\alpha,n\gamma)^{16}O$ reaction which they observed. In contrast the spectrum in fig.4.3.1 can be seen to be very clean in the region of the R→4.25 transition and the angular resolution of the germanium detector at 13cm (front face) is much better.

Having cast doubt on the quality of the angular distribution measurement of Pearson and Spear, the evidence for the spin of this resonance must be reviewed. From fits to the distribution shown in fig.4.3.2b, spin-parity assignments of 3^- and 5^- can be rejected since they require unacceptably large M2 strengths of >350 and >150 Weisskopf units respectively, while a 2^+ assignment would require an M3 strength in excess of 10^5W.u. and so can be rejected. The fit for a 6^+ assignment is acceptable for a mixing ratio of zero and so this spin cannot be rejected on angular distribution grounds. However, the observed decay to the 2^+ state at 1.63 MeV rules out this possibility. In addition the work of Millington et al, described above, populatd a level at this excitation with the $\ell=2$ transfer of a proton in the reaction $^{21}Ne(d,t)^{20}Ne$, which is not consistent with a 6^+ assignment. The observed primary decay to the 4.25 MeV (4^+) states is therefore a pure M1 transition with a strength of 0.5 W.u. which indicates that the 11.09 MeV state has T=1 and is therefore the analogue of the 0.82 MeV state in ^{20}F.

Table 4.3.1 11.09 MeV $4^+;1$

	Present work	Previous
E_x	11087±3	11077±8[St78] and 11086±10[Mi74]
Implied E_α	7948±4	
Γ	<1	≤3[St78]
J^π	4^+, T=1	$4^+;1$
Total $\omega\gamma$ (ev)	30.2±3.5	
Detector at 10cm 125°		

$E_\gamma(\theta)$	Branching Ratio %	$\frac{\Gamma_\alpha\Gamma_\gamma}{\Gamma}$ eV		Mλ	B(Mλ)W.u.	Previous $\frac{\Gamma_\alpha\Gamma_\gamma}{\Gamma}$
R→1.63(2^+)	9394.5±4.7	0.5±0.25*	0.016±0.008	E2	0.08±0.04	≤0.07[St78]
R→4.25(4^+)	6795.3±0.4	99.5±0.25	3.33±0.39	M1	0.50±0.06	3.38±0.33[St78]
R→5.62(3^-)		< 1	< 0.03	E1	$< 4\times10^{-4}$	
R→7.01(4^-)		< 0.5	< 0.02	E1	$< 6\times10^{-4}$	< 10[Pe64b]
4.25→1.63	2597.0±0.3					
1.63→0.00	1623.3±0.3					

* Corrected for summing of cascade via 4.25.

4.4 The 11.27 MeV (1^-;1) State

The next natural parity state in ^{20}F is the 1^- state at 0.98 MeV which lies only 80keV below the unnatural parity 1^+ state. The proximity of the analogues of these two states in ^{20}Ne has in the past led to some confusion and has meant that they have been unresolved in several reactions. Another consequence of the existence of this close doublet will be discussed below.

Pearson and Spear[Pe64b] saw the ground state decay of a natural parity state at an excitation of 11.27±0.03 MeV and witn a total width of less than 4keV. The transition had a strength ($\omega\gamma$) of 0.7eV which implied that the spin and parity were 1^- or 2^+. Since then radiative alpha capture has been used by Steck[St78] and by Davidson and Lowry[Da78] who measured the angular distribution of the ground state radiation and defined the spin as 1^-. Steck limits the total width to less than 0.3keV and gives the transition strength for R→1.63(2^+) as $\omega\gamma$=0.23eV which is just less than the limit set by Pearson and Spear. The ground-state decay strength (B(El)=4.4×10^{-4} Weisskopf units) and the narrow total width ($\leq$0.3keV) both give support to a T=1 assumption for this state, particularly since the excitation is close to that expected of a 1^- T=1 state. However these arguments are not definite and conclusive evidence will be presented below. The values for the excitation of this state and for its ground state decay strength given in the two recent papers [St78 and Da78] differ significantly and it will be shown that the values reported by Davidson et al are more in accord with the results reported here.

Millington et al[Mi74] did not resolve the 1^+-1^- doublet in the reaction $^{21}Ne(d,t)^{20}Ne$ but, in addition to the ℓ_n=0+2 components expected for the 1^+ state, they included in their fit to the distribution an ℓ_n=1 component which would arise from the analogue of the 0.98 MeV 1^- level in ^{20}F which they had populated in the analogue reaction $^{21}Ne(d,^3He)^{20}F$. The ratio of C^2S for the two 1^- states is in fair agreement with the theoretical value for analogue states as explained earlier. Betts et al[Be75] did not resolve the doublet either, but also included an ℓ=1 component in their fit for the $^{19}F(^3He,d)^{20}Ne$ reaction and obtained a spectroscopic strength consistent with a previous $^{19}F(d,p)^{20}F$ experiment [Fo74]. It thus seems that the particle reactions also lend support to a T=1 assignment for this state.

In the present work, a strong (30:1) resonance was seen in gate 2 (6 MeV < E_γ < 8.2 MeV) of a yield curve measured using a gas pressure of 200μ. The beam energy was 8.18 MeV and the total width was deduced to be less than 1keV. A spectrum (fig.4.4.1) was accumulated on resonance for an integrated beam charge (He^{++}) of 0.15C using a gas pressure of 800μ which corresponds to a target thickness of 9.5keV. In addition to the previously reported decays to the ground state and to the 1.63 MeV (2^+) state, we observed peaks in the spectrum corresponding to decays to states at 4.97 (2^-), 5.78 (1^-), 8.85 (1^-) and 9.32 (?) MeV. The decay scheme is shown in fig.4.4.2.

The ground state decay strength ($\omega\gamma$=1.14±0.14eV) is consistent with the value of Davidson and Lowry[Da78] but in conflict with the value of Steck which is only half this value and has a small quoted error (0.58±0.05eV). The 2.5% branch to the 1.63 MeV (2^+) state is very weak and the full energy peak in the spectrum is too weak to give an accurate

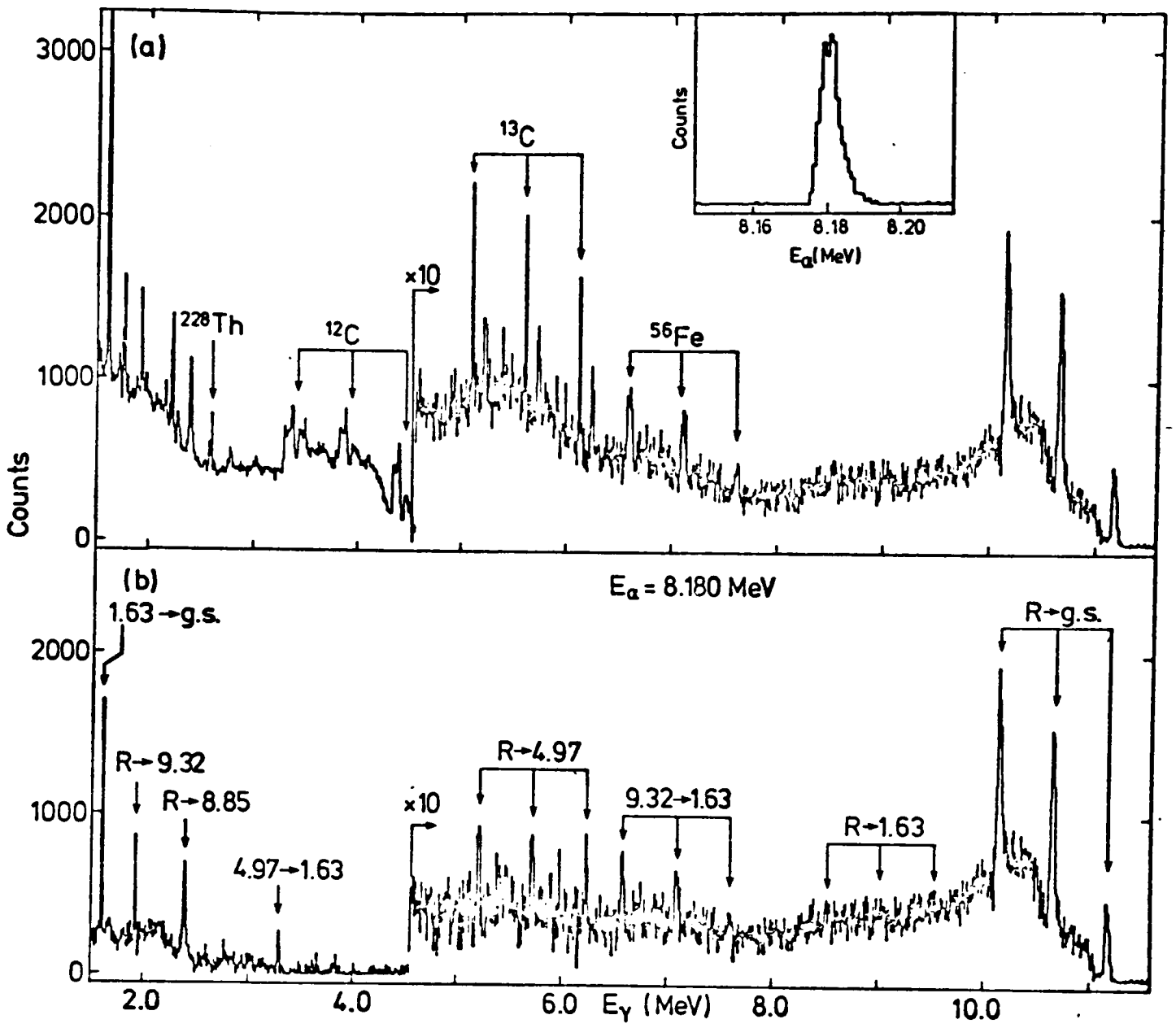

Fig.4.4.1 (a) Spectrum of γ-rays taken on the 8.18 MeV resonance in the $^{16}O(\alpha,\gamma)^{20}Ne$ reaction and (b) the same spectrum after subtraction of a normalised off-resonance spectrum, both with a target pressure of 0.8 torr. Peaks arising from the decay of the 11.27 MeV $1^-;T=1$ level in ^{20}Ne are labelled in (b) and contaminants are labelled in (a). The inset shows a yield curve over the resonance with a target pressure of 0.8 torr.

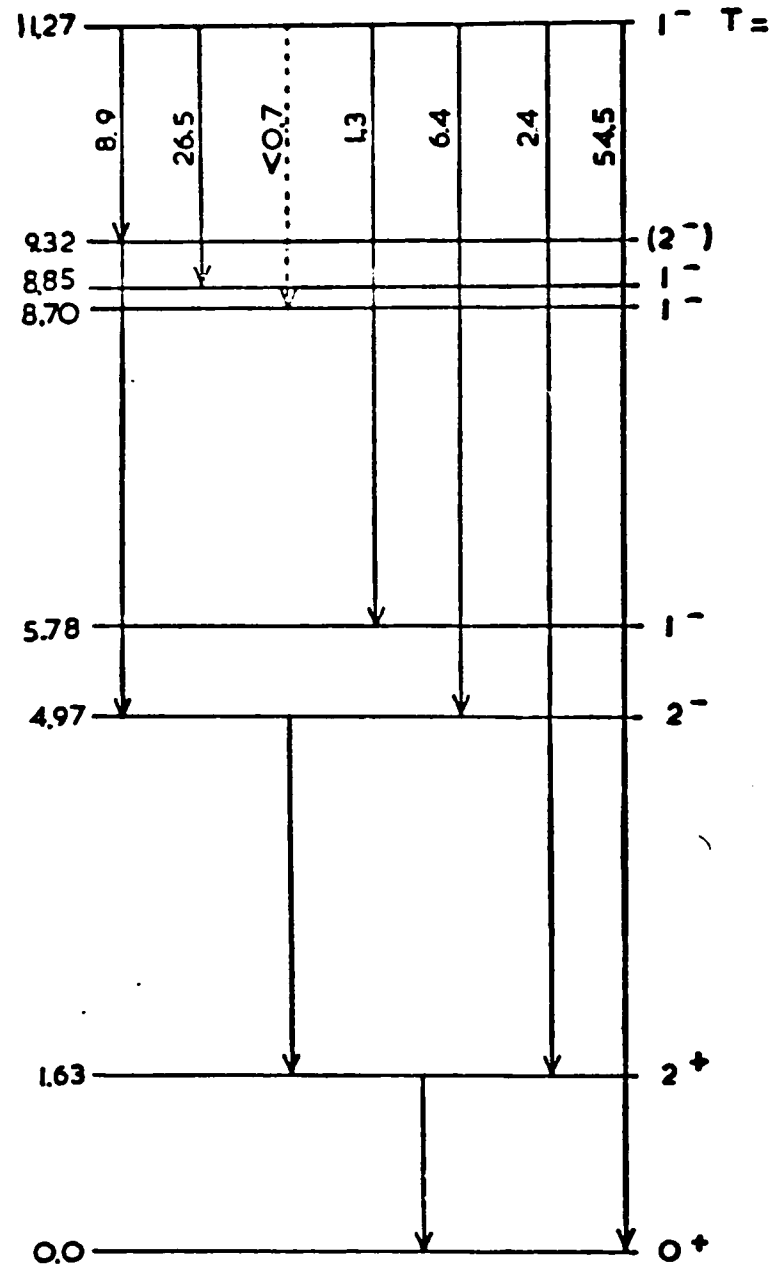

Fig.4.4.2 Decay scheme of the 11.27 MeV 1^-;T=1 state in ^{20}Ne. The numbers shown on each transition are the relative intensities.

strength estimate so the double escape peak was used. The reduced transition strength ($B(E1)=(3.0\pm1.5)\times10^{-5}$W.u.) is very weak for a $\Delta T=1$ transition and is weaker than the value reported by Steck by a factor of 5. It is difficult to see how his value can be correct given the clean nature of our spectrum (fig.4.4.1) at this γ-ray energy. The M1 decay to the 4.97 MeV (2^-) state has a reduced transition strength of $(8.4\pm1.6)\times10^{-3}$ which again is weak for an isospin favoured transition, and the strength of $(2.6\pm1.4)\times10^{-3}$ W.u. to the 5.78 MeV (1^-) state is even weaker.

The most significant decay mode of this resonance is the 27% branch to the 1^- state at 8.85 MeV. The M1 reduced transition strength, B(M1), is 0.64 ± 0.08 Weisskopf units which is unambiguously of $\Delta T=1$ nature, confirming the T=1 assignment to this resonance. An interesting point to note in the spectrum (fig.4.4.1) is that the peak for this transition is noticeably broader than others of this γ-ray energy due to the natural width ($\Gamma=19$keV) of the 8.85 MeV state. No secondary decay is seen because the 8.85 MeV state decays by α-emission.

Another interesting branch is to a state at 9.32 MeV. The strength of this decay confines it to be M1 or a rather strong E1 ($B(E1)=1.6\times10^{-2}$W.u.), limiting the spin of the 9.32 MeV state to $0^\pm$, $1^\pm$ or $2^\pm$. A surprising fact is that the decay of the 9.32 MeV state to the 1.63 MeV (2^+) state is seen, despite the fact that this state has 4.59 MeV available for alpha decay and is clearly not high spin or T=1. This strongly implies unnatural parity and the observed γ-decay rules out J=0 leaving $J^\pi=1^+$ or 2^-. The latter is preferred because of the large E1 strength implied by 1^+ and also because no ground state decay is observed. A problem arises in this spectrum because the observed

9.32→1.63 strength is only half that of the R→9.32 strength. If the 9.32 has unnatural parity there can be no α-branch, so a gamma branch may have been missed. A likely candidate is 9.32→4.97 (2^-) as this would occur just below the 4.4 MeV peak from $^{12}C(\alpha,\alpha'\gamma)$, but a tentative upper limit on this decay is too low.

The γ-ray energies for the primary and secondary decays via the 9.32 MeV state imply an excitation for this state of 9318.2±2 keV. This value is in good agreement with the value of 9318±6 given by Medsker et al[Me75] who populated a state in this region in the reaction $^{12}C(^{12}C,\alpha)^{20}Ne$ but saw some evidence for natural parity. They postulate the existence of a doublet to account for the wide variations in excitation for states reported in this region. Millington et al saw a state at 9357±17keV with ℓ_n=1 angular distribution in the reaction $^{21}Ne(d,t)^{20}Ne$ [Mi74] but they point out that the shape of the triton peak in the spectrum implies the possible presence of a contaminant peak arising from ^{22}Ne in the target. Since the excitation energy obtained here for the possible 2^- is inconsistent with that obtained in the pickup reaction, it seems likely that the latter does not represent a state in ^{20}Ne but a contaminant.

However, Millington et al. tentatively suggest that this state may be the 2^- member of the $K^\pi=1^-$ band based on the 1^- state they see at 8839±8 keV and formed by coupling a $1/2^-[101]$ hole to a $3/2^+[202]$ particle. They see the 1^- state with a strength (C^2S=0.33) in good agreement with that predicted (C^2S=0.34) by the Nilsson model for the head of this band. The fact that the capture results presented here show strong M1 transitions of similar strength to the 8.85 (1^-) and 9.32 (2^-?) MeV states lends strong support to the idea that they are members

of the same band. Another possible candidate for the band head is the 8.70 MeV (1^-) state, but the limit on the transition strength to this state (table 4.4.1) is twenty times weaker than to the 8.85 MeV state, so the latter is favoured by strength considerations. This matter is further discussed in the section on the 8.70 MeV state (Chapter 5).

Keen interest has recently been shown in the 11.27 MeV state due to the possibility that the doublet consisting of this state and the neighbouring 1^+ T=1 state, together with the broad (Γ=170keV) 1^- T=0 state at 11.23 MeV, might be a suitable nuclear system for studying a possible parity non-conserving nucleon-nucleon force. This has been discussed in detail by Davidson and Lowry[Da78]. The magnitude of any effect depends roughly on the separation and widths of the states involved and at present the excitations of the T=1 doublet seem to be the subject of some confusion. Recent values for the excitation of the 1^+ T=1 state are 11261±5keV[In76b] and possibly 11249±3keV from a private communication reported by Davidson and Lowry[Da78]. Similarly, for the 1^- T=1 state, Steck gives E_x=11259±8 whereas Davidson and Lowry give 11278±4 keV. The mean of these conflicting values is 11274.2±3.6keV which is in good agreement with the value of 11273±4keV derived in the present work from the energies of the various γ-decays.

The separation of the 1^+ and 1^- T=1 states in ^{20}Ne has recently been measured directly by Fifield et al[Fi79] using a magnetic spectrometer to study deuterons from the reaction $^{19}F(^3He,d)^{20}Ne$. A value of 12±1keV for the separation was obtained which means that any parity non-conserving α-decay of the 1^+ state will be due to mixing with the broad 1^- T=0 state and not with the T=1 state.

Table 4.4.1 11.27 MeV $1^-;1$

	Present Work	Previous
E_x	11273±4	11278±4 [Da78] and 11259±8 [St78]
Implied E_α	8180±5	
Γ	< 1	< 0.3 [St78]
J^π	T=1	$1^-;1$
Total $\omega\gamma$ (eV)	2.09±0.25	
Detector at 8cm 135°		

	$E_\gamma(\theta)$	Branching Ratio %	$\frac{\Gamma_\alpha\Gamma_\gamma}{\Gamma}$ eV	Mλ	B(Mλ) W.u.	Previous $\frac{\Gamma_\alpha\Gamma_\gamma}{\Gamma}$
R→0.00(0^+)	11177.2±3.5	54.5±2	0.38±0.05	E1	$(5.3\pm0.7)\times10^{-4}$	0.33±0.10 [ua78]
R→1.63(2^+)	8543.0±5.2	2.4±1	0.017±0.007	E1	$(3.0\pm1.5)\times10^{-5}$	0.08±0.02 [St78]
R→4.97(2^-)	6249.5±1.6	6.4±1	0.045±0.009	M1	$(8.4\pm1.6)\times10^{-3}$	—
R→5.78(1^-)	5438±5	1.3±0.7	0.009±0.005	M1	$(2.6\pm1.4)\times10^{-3}$	—
R→8.85(1^-)	2407.2±1.0	26.5±1.5	0.185±0.025	M1	0.64±0.08	—
R→9.32(2^-?)	1939.3±0.6	8.9±1	0.062±0.010	(M1)	0.41±0.07	—
R→8.70(1^-)	5.438±5		<0.005	M1	<0.02	
9.32→4.97	7617.1±3.1					
4.97→1.63	3303.2±1.7					
1.63→0.00	1619.45±0.4					

4.5 The 12.22 MeV (2^+;1) State

Evidence for a 2^+ T=1 level in this region of excitation came from Kuan et al[Ku72]. They were studying the second T=2 level in ^{20}Ne, which they populated as a resonance in the $^{19}F(p,\gamma)^{20}Ne$ reaction, and observed a 10.6 MeV γ-ray which they identified as the second member of the cascade 18.43 $(2^+;2) \rightarrow 12.25(1^+,2^+,3^+;1) \rightarrow 1.63(2^+;0) \rightarrow 0.00(0^+;0)$. This gamma decay had been seen previously by Butler[Bu60] who used the gamma ray threshold technique in the reaction $^{19}F(d,n\gamma)^{20}Ne$. Kuan et al identify this state with that observed by Lawergren et al[La68] who used the reaction $^{19}F(d,n)^{20}Ne$ and measured an angular distribution characteristic of $\ell=2$, relating their results to previous work on the analogue reaction $^{19}F(d,p)^{20}F$ [Ro63] in order to assign T=1. In calculating the decay strength of the 18.43 MeV $(2^+;2)$ level, Kuan et al assume that $\Gamma_\alpha << \Gamma_\gamma$ for the 12.25 MeV $(2^+;1)$ state which implies remarkably inhibited α-decay. With this assumption the decay strength of the T=2 level is 0.06W.u. which is rather weak compared to all known isovector transitions from 0^+ T=2 states.

Marrs et al[Ma77] set out to resolve the contradiction between the exceedingly narrow state implied by Kuan et al and a resonance seen in alpha capture by Pearson and Spear with a width of 40 keV and $\omega\gamma$=6eV. They used coincidence measurements in the reaction $^{19}F(^3He,d\gamma)^{20}Ne$ and showed that $\Gamma_\gamma/\Gamma > 0.25$ for a state at 12.22±0.03 MeV in ^{20}Ne. They also repeated the work of Pearson and Spear, using smaller beam energy steps over the region of interest, and found evidence for the existence of a doublet consisting of states at 12.216±0.005 and 12.254±0.005 MeV; the latter will be discussed later. For the 12.22 MeV level they obtained a value for $\Gamma_\alpha\Gamma_\gamma/\Gamma$ of 0.292±0.044eV which, when combined with

the limit on Γ_γ/Γ, assumed to apply to this state, gives $0.29 \leq \Gamma_{\alpha_o} \leq 1.17$eV and $\Gamma_\gamma \geq 0.39$eV. This very narrow width for alpha decay is strong support for a T=1 assignment. They also measured the angular distribution of the gamma ray and obtained a good fit for a $J^\pi=2^+$ hypothesis with small mixing ratio.

It will be shown in the next section that the upper member of the doublet has $J^\pi=3^-$ and T=1, being the analogue of the 1.97(3^-?) state in ^{20}F, and also that it cannot be the state seen by Kuan et al, so the 12.22 MeV (2^+;1) state can be confidently identified as the level seen in the cascade from the 18.43 MeV (2^+;2) level. It should be noted that the spectroscopic strength for the reaction $^{19}F(^3He,d)^{20}Ne$ populating the 2^+ state is in good agreement with the value for the $^{19}F(d,p)^{20}F$ reaction to the analogue state[Be75] and further that the strengths to the 2^+ and possible 3^- states in ^{20}F are in the ratio 50:1[Fo74]. This strongly implies that the $^{19}F(^3He,d\gamma)^{20}Ne$ work of Marrs et al was only populating the lower member of the doublet as they assumed when applying the value of Γ_γ/Γ, obtained from this reaction, to the 2^+ level.

In the present work a yield curve was measured with a gas pressure of 100μ corresponding to a target thickness of 0.8keV, and is shown in fig.4.5.1. Two sharp states are visible in the gate corresponding to capture γ-rays, in marked contrast to the solid target work. The width of each was deduced to be ≤1keV and their separation in beam energy is 44±2keV. In the gate containing 6.13 MeV γ-rays from $^{16}O(\alpha,\alpha'\gamma)^{16}O$ the lower state is absent as might be expected from its small α_o width. A spectrum (fig.4.6.1) was accumulated at the lower resonance for a beam charge of 4.0×10^{-2}C and at a gas pressure of 1 torr. The decay to the 1.63 MeV (2^+) state was seen and a value for $\omega\gamma$ of 1.41±0.23eV was

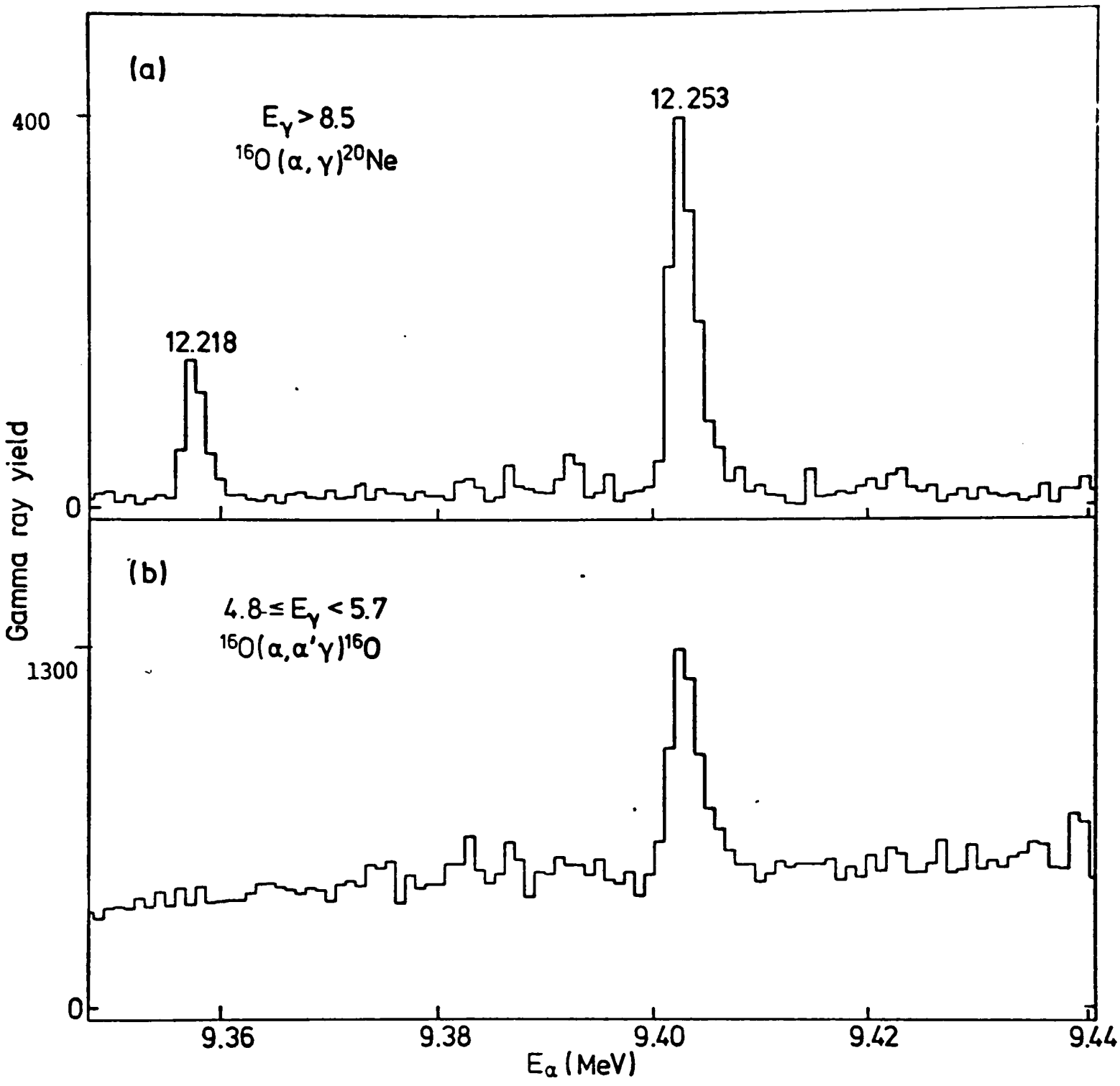

Fig.4.5.1 Yield of γ-rays as a function of beam energy in the vicinity of the 12.22/12.25 MeV doublet in ^{20}Ne. The selected regions of the γ-ray spectrum are indicated and correspond to the $^{16}O(\alpha,\gamma)^{20}Ne$ and $^{16}O(\alpha,\alpha_2\gamma)^{16}O$ reactions for (a) and (b) respectively. This yield curve was accumulated in about 20 minutes, the total charge being 4.6×10^{-3} C.

obtained. This is in good agreement with Marrs et al. No ground state decay was observed and a limit of $\omega\gamma < 0.08$eV can be placed on it, so the source of the ground state radiation seen by Steck ($\omega\gamma$=2.7eV) is not clear since the other member of the doublet will be shown to have $J^{\pi}=3^{-}$, making a ground state decay of the required strength impossible.

Poor subtraction of a background spectrum and limited statistics prevented proper determination of the size and energy of the 1.63→gs peak. Similar problems affected the upper member of the doublet and will be discussed more fully in the next section. This prevented a proper correction procedure from being performed so no excitation energy can be reliably deduced from the spectrum. However, an energy was deduced for the upper member of the doublet (E_x=12253±3keV), and the measured separation leads to an excitation for this state of 12218±4keV which is in good agreement with the value of Marrs et al. The energy of the primary γ-ray was used in the correction procedure for obtaining the value of $\omega\gamma$.

Table 4.5.1 12.22 MeV $2^+;1$

	Present Work	Previous
E_x	12218 ±4	12216 ±5 a)
Implied E_α	9362 ±5	
Γ	<1	<0.1 a)
J^π		$2^+;1$
Total $\omega\gamma$ (eV)	1.41 ±0.23	
Detector at 10cm 135°		

	$E_\gamma(\theta)$	Branching Ratio %	$\frac{\Gamma_\alpha\Gamma_\gamma}{\Gamma}$	Mλ	B(Mλ)W.u.	Previous $\frac{\Gamma_\alpha\Gamma_\gamma}{\Gamma}$
R→1.63(2^+)	10477.3 ±1.65	~100	0.28 ±0.05	M1	>0.013**	0.29 ±0.04 a)
R→0.00(0^+)		<5	<0.014	E2		<0.004 a)
R→4.25(4^+)		<20	<0.056	E2		<0.009 a)
R→4.97(2^-)		<20	<0.056	E1		<0.01 a)
R→5.62(3^-)		<20	<0.056	E1		
1.63→0.00 *						

a) [Ma77]

* obscured; see text

** assumes $\Gamma_\alpha/\Gamma \leq 0.25$ [Ma77], so $\Gamma_\gamma \geq 0.37$eV

4.6.1 The 12.25 MeV (3^-;1) State

As discussed above, the first real information about this state comes from Marrs et al who measured its excitation to be E_x=12254±5 keV and width as 5keV. They also measured the decay strength to the 1.63 MeV (2^+) state ($\omega\gamma$=3.9±0.8eV) and the angular distribution of this decay which implied $J^\pi=2^+$ or 3^-. This state presumably formed the bulk of the R→1.63 strength seen by Pearson and Spear and by Steck who obtained $\omega\gamma$=5.8±0.5eV.

From the yield curve shown in fig.4.5.1, for which the target thickness was 0.8keV, a total width of less than 1keV can be deduced. This is in marked contrast to the value of Marrs. The discrepancy arises from incorrect unfolding of the two resonances by Marrs et al due to their use of the wrong target thickness. They measured their target thickness as 85keV for the 6.93 MeV 2^+ T=1 resonance and then used a value of 80keV for the 9.4 MeV resonance instead of 70keV as deduced from Northcliffe and Schilling [No70] for a Ta_2O_5 target. Steck studied this region of excitation using elastic alpha scattering and found no trace of a 5keV wide state but saw some slight structure in the excitation function, implying the existence of a narrow (<2keV) state which may simply be the 2^+ level. No evidence for this state has been seen in other particle reactions which, though interesting, is not surprising as Millington et al, who saw many of the low lying states in ^{20}F together with their analogues in ^{20}Ne, did not see the 1.97 MeV state in ^{20}F in their study of the pickup reactions $^{21}Ne(d,^3He)^{20}F$ and $^{21}Ne(d,t)^{20}Ne$. The ^{20}F state was, however, seen weakly by Fortune et al[Fo74] in $^{19}F(d,p)^{20}F$ and by Rollefson et al[Ro70] in the two particle transfer reaction $^{18}O(^3He,p)^{20}F$, but not in $^{19}F(d,p)^{20}F$. The two

particle reaction $^{18}O(^{3}He,n)^{20}Ne$ was studied by Gul et al[Gu70] but they report no evidence for this state and would probably not have resolved it from the 12.22 MeV (2^+;1) and 12.24 MeV (4^+;0) states.

A spectrum was accumulated on the upper resonance of fig.4.5.1 with a target thickness of 10.8keV (1000μ) for an integrated beam charge (He^{++}) of 3.3×10^{-2}C; the 16.6% Ge(Li) detector was positioned at 135° and the intrinsic detector was at 30°. Further spectra were then accumulated with the detector at 135° (the monitior) kept fixed and the intrinsic detector (the movable) at 90°, 60°, 45° and 25°, enabling a five point angular distribution to be measured. The five monitor spectra were added together giving a spectrum corresponding to a total integrated beam charge of 11.207×10^{-2}C (fig.4.6.1). Peaks corresponding to decays to the 1.63(2^+) and to the 5.62(3^-) MeV states were observed together with a broader peak corresponding to the inelastic scattering reaction populating the 6.13 MeV (3^-) state in ^{16}O. Only the decay to the 1.63 MeV (2^+) state has been reported previously.

At this beam energy (9.40 MeV) contaminant reactions are a problem even with a windowless gas target. This was exacerbated by the presence of ^{14}N in the gas as already mentioned. In this case however, the most troublesome contaminant γ-ray comes from the reaction $^{17}O(\alpha,n)^{20}Ne^*$ populating the 1.63 MeV state in ^{20}Ne. Although the gas used was depleted in ^{17}O, the differential cross section for this reaction at this beam energy is between 3 and 7 mb/sr[Ha67] which is much greater than typical capture cross sections (~1μb) so the reaction rate is observable. This reaction meant that neither the size nor energy of the resonant 1.63 MeV γ-ray peak could be determined accurately, making the normal correction procedure for a long target impossible. An attempt

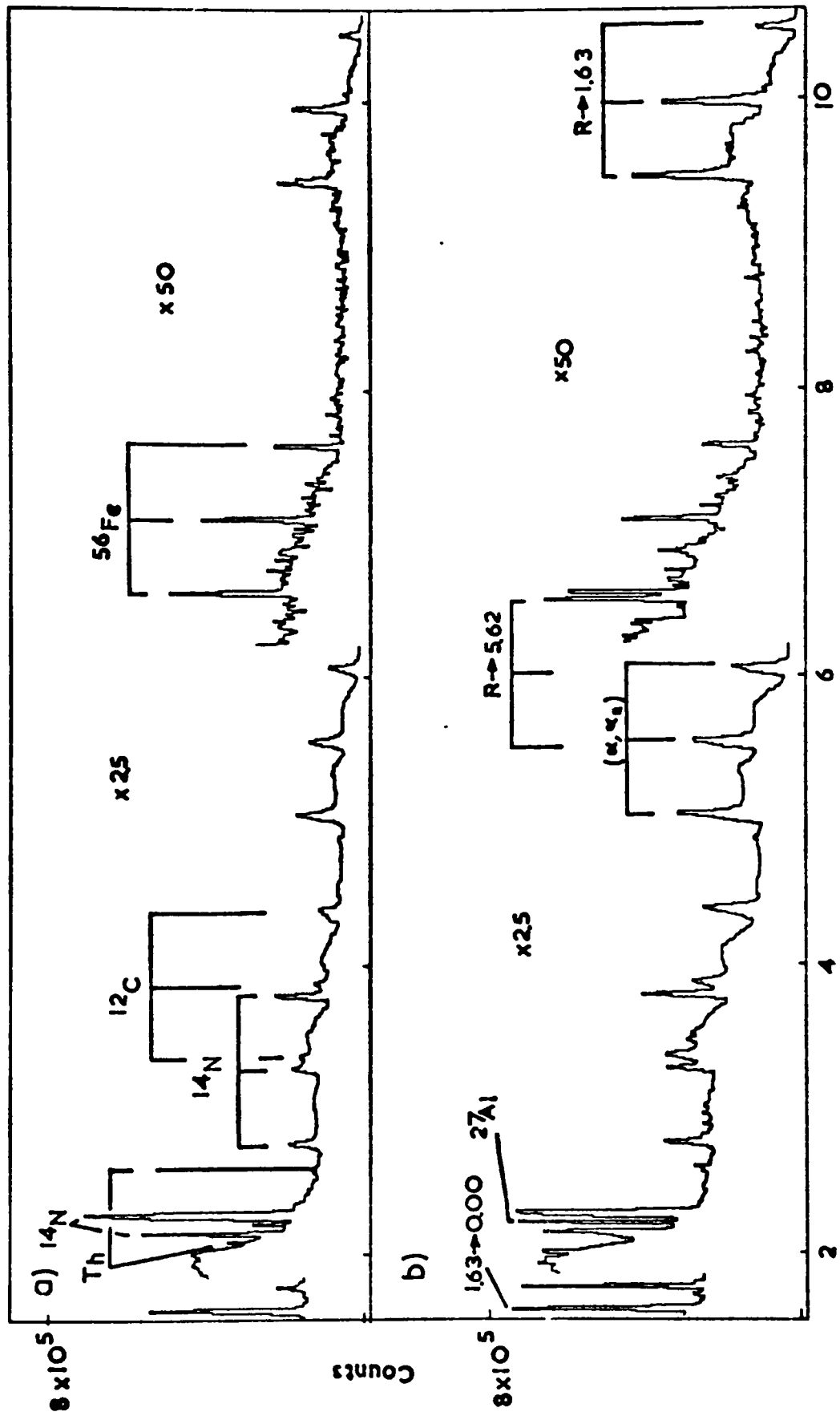

Fig.4.6.1 Spectra (a) on the 9.36 MeV (2^+) resonance and (b) on the 9.41 MeV (3^-) resonance, normalised to the same collected charge. Contaminant peaks are marked in (a) and peaks arising from the decay of the 12.25 MeV 3^-;T=1 level are marked in (b). The peaks marked (α,α_2) come from the inelastic reaction $^{16}O(\alpha,\alpha_2\gamma)^{16}O$ and are resonant in (b); the peaks in (a) are due to the background. The R → 1.63 decay is resonant in both spectra. The Al contaminant peak is marked in (b) as it is more prominent there.

was made to alleviate the problem by repeating the experiment using a thin target, as the non-resonant background would be proportional to target thickness, but this did not achieve much improvement and a thin target increases the problems caused by resonance profile movement due to beam energy changes. The solution which was adopted was to use the doppler shift of the R→1.63 decay, seen in the monitor detector, in order to fix the resonance profile position in the target. Unlike the 1.63→0.00 decay the energy of this transition is not known accurately - Marrs et al quote an error of 5keV[Ma77]. However, the effect of this uncertainty is reduced by the larger Doppler shift of a high energy γ-ray and also it does not significantly affect the estimate of the relative positions of the resonance profile at the five angles but only their mean position.

Fig.4.6.2 shows the angular distribution of the sum of the number of counts in the full energy, single escape and double escape peaks for the R→1.63 transition together with the best fit for an assumption of $J^{\pi}=3^{-}$ for this state. The values shown have been corrected for the effect of a long target on the assumption that the excitation of this state is exactly 12253keV. Also shown is the corrected distribution of the counts in the full energy peak of the R→5.62 transition, the escape peaks being obscured by the inelastic peaks. Again a fit is shown for the assumption of 3^{-}.

Fig.4.6.2 also shows plots of χ^2 versus arctan(δ) for different spin assumptions for the two transitions. It can be seen that only in the case of the hypothetical $4^{+}\rightarrow 2^{+}$ transition does the value of χ^2 not descend to a feasible value for any value of δ, so a 4^{+} hypothesis can be rejected, leaving 1^{-}, 2^{+} and 3^{-} all giving reasonable fits.

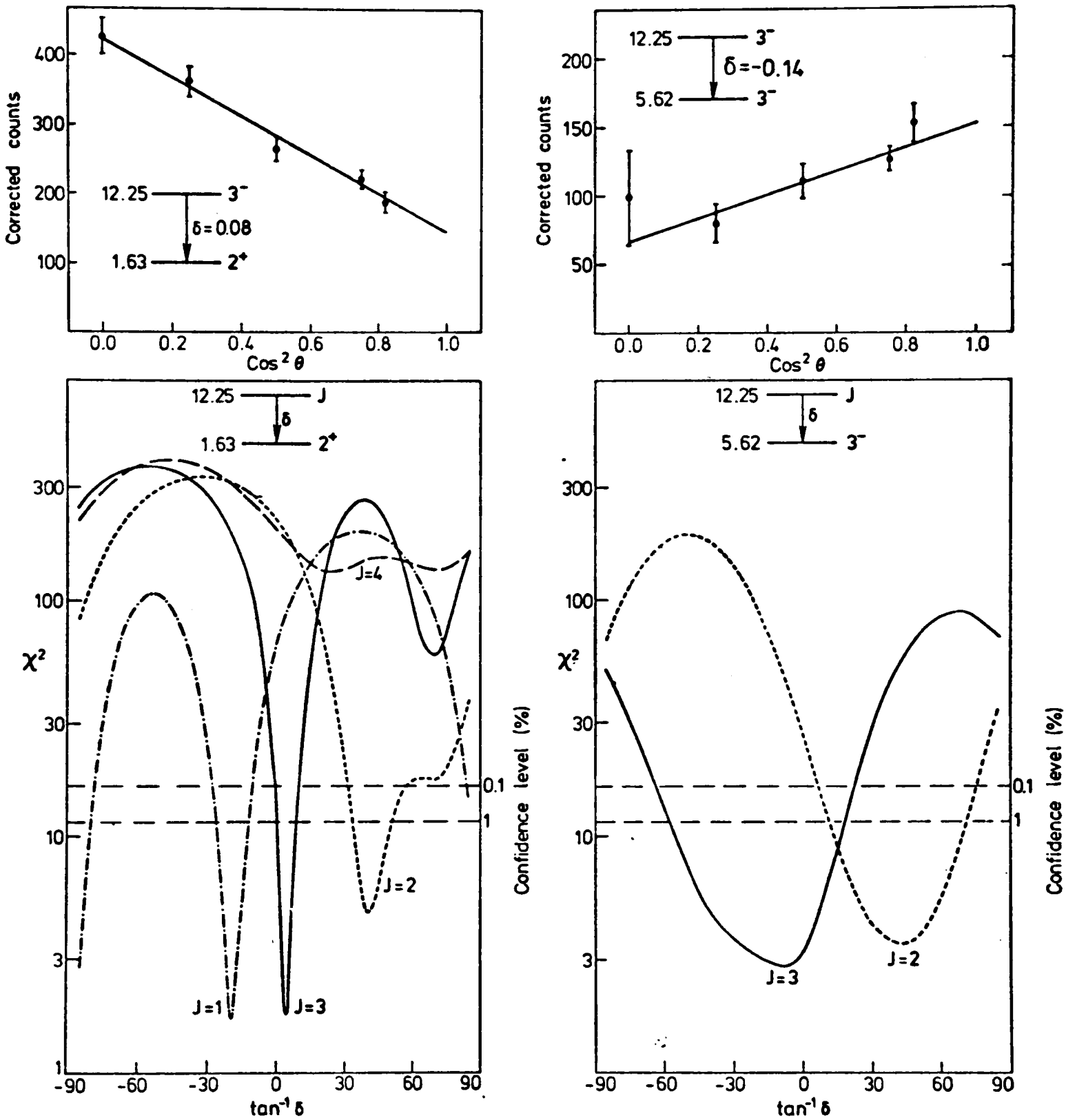

Fig.4.6.2 χ^2 plots from the fits to the γ-ray angular distributions of the 12.25 → 1.63 and 12.25 → 5.62 MeV transitions for various spin hypotheses for the 12.25 MeV level. The angular distributions are shown with the best fits for $J^{\pi}=3^{-}$.

The fit for the possible $2^+ \rightarrow 3^-$ transition gives a best value for δ of 0.93 which implies a strength for the M2 component of 163 Weisskopf units. Indeed at the 0.1% confidence level one can say that $\delta > 0.123$ so that $|M(M2)|^2 > 5.2$. This rules out the hypothesis $J^\pi = 2^+$ using the recommended upper limit for M2 T-allowed transitions of 3 Weisskopf units due to Endt et al[En74].

If the resonance has $J^\pi = 1^-$ then the decay to the 3^- would be E2 with M3 admixture so that virtually any finite δ would imply an unrealistic M3 strength. The best value of δ from the fit is 0.47 and to 1% confidence $\delta > 0.0087$ so that $|M(M3)|^2 > 293$. This would rule out 1^- at the 1% confidence level but the decay to the 2^+ state gives additional evidence. The best value of δ for this E1/M2 transition is -0.35 ± 0.04 giving $|M(M2)|^2 = 10.3 \pm 2.0$ Weisskopf units which is unrealistically high.

The hypothesis that $J^\pi = 3^-$ gives a good fit for both transitions. For $R \rightarrow 3^-$ the mixing ratio (δ) is -0.15 ± 0.36, giving $|M(E2)|^2 = 0.23$ with an error bar ranging from zero to 2.2 Weisskopf units. The $R \rightarrow 2^+$ transition has a best fit for δ equal to 0.080 ± 0.023, giving $|M(M2)|^2 = 0.26$ with an error range of 0.13 to 0.43 Weisskopf units.

The angular distribution measurements therefore rule out spin hypotheses of 1^-, 2^+ and 4^+ and show that 3^- is consistent with all the available data so the assignment $J^\pi = 3^-$ is adopted.

This discussion has all assumed an excitation of 12253keV for the correction procedure. The correction was also performed for the 2^+ and 3^- hypotheses (the alternatives given by Marrs et al) for excitations of 12251, 12256 and 12261 keV in order to examine the sensitivity of the

spin assignment to excitation energy. The effect of increasing the excitation from 12251 to 12256 was to change the implied beam energy by less than 1keV as compared to an energy spread between the runs at different angles of 1.5keV. The higher excitations improve the fit for both $3^- \rightarrow 3^-$ and $2^+ \rightarrow 3^-$ and raise the error on the mixing ratio in the latter case so that with E_x=12256 the confidence in rejecting 2^+ is reduced, a 1% confidence level requiring $|M(M2)|^2 > 8.0$ Weisskopf units but a 0.1% confidence level only requiring $|M(M2)|^2 > 2.3$W.u. However, the quality of the fit for $3^- \rightarrow 2^+$ and $2^+ \rightarrow 2^+$ gets worse for higher excitations, χ^2 rising from 4.8 to 8.9 for the case of $2^+ \rightarrow 2^+$ with Ex=12256. The value of δ remains feasible. For a lower excitation energy the fit for $3^- \rightarrow 3^-$ and $2^+ \rightarrow 3^-$ deteriorates and the required M2 strength for $J^\pi = 2^+$ increases, improving the confidence in rejecting 2^+. The fits for $3^- \rightarrow 2^+$ and $2^+ \rightarrow 2^+$ improve.

In summary, the effect of the uncertainty in energy is to reduce the confidence with which a $J^\pi = 2^+$ assumption can be rejected if the excitation is higher than our deduced value of 12253±3 keV. If the excitation is higher by nearly three standard deviations (Ex=12261keV) then the hypothesis can still be rejected at the 1% confidence level. A definite 3^- assignment can therefore be made.

The best estimate of the excitation of this resonance comes from applying the observed doppler shift of the 1.63→g.s. decay to the two observed primary decays in the monitor spectrum. The statistics in this spectrum are good enough to obtain a sufficiently accurate background subtraction for the 1.63 MeV peak because it is the sum of the five runs required for the angular distribution. These two values for the excitation are consistent and when combined with each other, and with

the error in the doppler shift which is common to both, the value of Ex=12253±3keV is obtained after allowing for the recoil shift.

The transition strengths for the γ-decays are shown in table 4.6.1. The previously unobserved R→5.62(3^-) decay branch is rather weak for an isospin allowed M1, but the R→1.63(2^+) branch is typical of a strong isospin allowed E1 and is in good agreement with the value of Marrs et al. As has already been discussed, it is clear from the yield curve (fig.4.5.1) that the inelastic reaction is far stronger for this resonance than for the 12.22 MeV (2^+) level, so the spectrum for the latter was used for off resonance background subtraction in calculating the inelastic strength for the 12.25 MeV state. In addition an estimate of the size of the single escape peak of the R→5.62 decay had to be made using the known detector efficiency calibration in order to subtract its contribution from the full energy inelastic peak. The value obtained for $\Gamma_{\alpha_2}\Gamma_{\alpha_0}/\Gamma$ is 2.0±0.3eV. In conjunction with the two γ-ray strengths this implies that Γ>6.8eV and Γ_{γ_1}/Γ<0.20. The Wigner limit width for α_o decay is 1000 times the α_2 width so the γ-branch is likely to be smaller than the above limit, becoming inconsistent with the limit $\Gamma_{\gamma_1}/\Gamma\geq 0.25$ measured by Marrs et al for the state seen in the $^{19}F(^3He,d\gamma)^{20}Ne$ reaction. Similarly the fact that the γ-branch is not large means that this state is unlikely to be the state seen in the cascade from the T=2 resonance. It is also safe to assume that the values for $\Gamma_\gamma\Gamma_\alpha/\Gamma$ in table 4.6.1 are equivalennt to Γ_γ.

Table 4.6.1 12.25 MeV $3^-;1$

	Present Work	Previous
E_x	12253±3	12254±5 [Ma77]
Implied E_α	9406±4	
Γ	<1	~5
J^π	$3^-;1$	2^+ or 3^-
Total $\omega\gamma$ (ev)	6.6±0.8	
Detector at 10cm 135°		

	$E_\gamma(\theta)$	Branching Ratio %	$\frac{\Gamma_\alpha\Gamma_\gamma}{\Gamma}$	Mλ	B(Mλ)W.u.	Previous $\frac{\Gamma_\alpha\Gamma_\gamma}{\Gamma}$
R→1.63(2^+)	10514.6±1.0	63±2	0.60±0.07	E1	$(1.0\pm0.1)\times10^{-3}$	0.56±0.10 [Ma77]
				M2	0.26±0.15	
R→5.62(3^-)	6566.5±0.8	37±2	0.35±0.04	M1	$0.057^{+0.007}_{-0.013}$	—
				E2	$0.23^{+1.94}_{-0.23}$	
R→4.97(2^-)			<0.04	M1	$<5\times10^{-3}$	
1.63→0.00(2^+)	1618±0.4					
$(\alpha,\alpha'\gamma)$	6074	$\frac{\Gamma_{\alpha_2}\Gamma_{\alpha_0}}{\Gamma} = 2.03\pm0.26$				

4.7 Comparison with Calculations

McGrory and Wildenthal[Mc73] have pointed out that all the states in ^{20}F below 3 MeV can be assigned to four bands predicted by the Nilsson model, with $K^{\pi} = 1^+, 2^+, 1^-$ and 2^-, but that the observed energy spacing differs appreciably from the J(J+1) rule.

Shell model calculations using the effective interaction of Preedom and Wildenthal[Pr72] and Chung and Wildenthal[Ch76], in a full $(2s1d)^4$ basis, predict the first five known T=1 positive parity states in ^{20}Ne in the correct order but with generally increased spacing. The predicted and measured decay strengths are shown in table 4.7.1 where it can be seen that the agreement between calculation and experiment is very good. As a result of this good agreement it is tempting to postulate that the calculation is also correct in the case of the 12.22 MeV $(2^+;1)$ state, enabling a value for Γ_α/Γ to be deduced from the ratio of the calculated transition strength to the observed strength. This leads to an alpha width Γ_α of 0.29eV and $\Gamma_\gamma/\Gamma \approx 0.95$. Such a tiny alpha width, which is only 1/400 of the α width of the lowest 2^+ T=1 level, implies either a very high degree of isospin purity in the 12.22 MeV level or a fortuitous cancellation of the α-particle amplitudes of the 2^+ T=0 levels mixed into it by the Coulomb interaction.

The deduced value for Γ_γ/Γ of 0.95 for the 12.22 MeV (2^+ T=1) level supports the assumption made by Kuan et al[Ku72] in deriving the strength of the decay of the lowest 2^+ T=2 level at 18.43 MeV. For this case the agreement between calculation and experiment is nowhere near as good, the measured strength being a factor of 5 weaker. This is surprising given the simple nature of the two states connected by this

transition and the successful predictions of the calculations for the T=1 levels. A better measurement of the ratio Γ_γ/Γ for the 12.22 MeV (2^+ T=1) level would obviously be interesting.*

Millener (private communication) has performed SU(3) shell model calculations for the two negative parity T=1 levels that we see. His basis consists of all states from the (82), (90), (71), (63) and (44) representations of SU(3), and includes both $p^{-1}sd^5$ and sd^3pf configurations, thus enabling spurious centre-of-mass motion states to be eliminated. The calculated transition strengths to negative parity T=0 states are shown in table 4.7.2, together with the measured values.

It can be seen that for the 11.27 MeV (1^- T=1) level the agreement between experiment and theory is generally quite good, with the two strong M1 decays (to the 1^-_3 and 2^-_2 states) predicted, provided the 9.32 MeV (2^-?) state is identified with the 2^-_2 state in the calculation. However, the decay to the 8.72 MeV (1^-) level is not observed although it is predicted to be a factor of 15 times stronger than could have been observed. Similarly the predicted strength for the decay of the 12.25 MeV (3^- T=1) level to the 5.62 MeV (3^-) level is 4 times stronger than observed.

In general the shell model seems to account quite well for the observed γ-decay of the low lying T=1 states in ^{20}Ne.

* A recent measurement of this ratio has been reported by Catford et al. (Institute of Physics Conference on Nuclear Structure and Elementary Particle Physics, Birmingham 1979), who obtained 0.91 ± 0.04.

Table 4.7.1

Comparison of measured and calculated radiative transition rates for positive parity T=1 and T=2 level in ^{20}Ne

E_i (MeV)	J_i^π, T_i	E_f (MeV)	J_f^π, T_f	$M\lambda$	B(Mλ) (W.u.) experiment	PW a)	CW a)
10.27	$2^+,1$	0.0	$0^+,0$	E2	0.10 ± 0.03 b)	0.10	0.11
		1.63	$2^+,0$	M1	0.31 ± 0.03 b)	0.20	0.27
		7.42	$2^+,0$	M1	0.65 ± 0.08 b)	0.62	0.54
10.89	$3^+,1$	1.63	$2^+,0$	M1	$> 1\times10^{-3}$ c)	0.13	0.14
		4.25	$4^+,0$	M1	$> 8\times10^{-4}$ c)	0.08	0.12
11.09	$4^+,1$	1.63	$2^+,0$	E2	0.09 ± 0.04	0.05	0.05
		4.25	$4^+,0$	M1	0.50 ± 0.06	0.48	0.53
				E2	< 0.4	0.004	0.002
11.26	$1^+,1$	0.0	$0^+,0$	M1	0.38 ± 0.06 d)	0.36	0.34
12.22	$2^+,1$	1.63	$2^+,0$	M1	> 0.013	0.29	0.25
18.42	$2^+,2$	12.22	$2^+,1$	M1	0.06 e)	0.32	0.40

a) Shell-model calculations employing the Preedom-Wildenthal and Chung-Wildenthal effective interactions, effective charges $e_n=0.5e$, $e_p=1.5e$, and bare nucleon g-factors.

b) [Fi77] (also Chapter 4)

c) Limit on lifetime from Ajzenberg-Selove [Aj78]. Branching ratio from Marrs et al [Ma77].

d) Bendel et al [Be71].

e) [Ku72]; assumes $\Gamma_\gamma/\Gamma\sim1$ for 12.22 MeV level.

Table 4.7.2

Comparison of calculated and measured M1 transition rates for negative parity T=1 levels in ^{20}Ne

E_i (MeV)		J_i^π, T_i	E_f (MeV)		J_f^π, T_f	B(M1) (W.u.)	
expt	theory[a]		expt	theory		expt	theory[b]
11.27	10.67	$1^-,1$	5.78	6.70	$1_1^-,0$	$< 5\times10^{-3}$	3.7×10^{-3}
			8.72	8.75	$1_2^-,0$	< 0.02	0.29
			8.85	9.56	$1_3^-,0$	0.63 ± 0.08	1.00
			4.97	(4.97)	$2_1^-,0$	0.009 ± 0.002	0.020
			(9.32)	9.12	$2_2^-,0$	0.40 ± 0.07	0.49
12.25	10.99	$3^-,1$	4.97	(4.97)	$2_1^-,0$	$< 5\times10^{-3}$	1×10^{-3}
			5.62	5.30	$3_1^-,0$	0.06 ± 0.01	0.26

a) Calculated excitation energies normalised to the 4.97 MeV 2^- level.

b) Calculations of Millener. See text.

CHAPTER 5

States in ^{20}Ne with T=0

5.1 Introduction

This chapter describes the five T=0 states in ^{20}Ne whose γ-decay spectra were studied using the gas target. As discussed in chapter 3, the majority of the natural parity T=0 alpha-decaying states in ^{20}Ne have significant natural width ($\geq$5keV) and so are not worth studying with a gas target whose thickness would not generally exceed the resonance width in the laboratory reference frame, and would in many cases be much less. The 8.70 MeV (1^-), 9.11 MeV (3^-), and 11.92 MeV (4^+) states are the only narrow T=0 states in the excitation range 7.0 MeV to 12.45 MeV whose γ-decay has not been reported in detail. Attention was therefore focussed on these states, which are discussed below.

The 11.56 MeV (0^+, 2^+) level had only been studied once when the work described here commenced, but further γ-decay measurements have since been reported. This state is included below, and doubt is cast on a previously reported decay branch.

The γ-decay of the 11.95 MeV (8^+) member of the ground state rotational band has only been measured once. That measurement suffered from severe background problems and had a large error, so in view of the importance of this state, a re-measurement was performed and a more accurate value was obtained.

5.2 The 8.70 MeV (1^-) State

This level was first reported as a resonance by McDermott et al[Mc60] who studied the elastic scattering reaction $^{16}O(\alpha,\alpha)^{16}O$ using a differentially pumped gas target chamber. They measured cross sections at 5 centre of mass angles and saw this resonance at all angles except 90°, which implied $J^\pi=1^-$. They deduced a total width of 2.5keV, but their estimate of the energy of this state, in common with the others they studied, was higher than more recent measurements by 60keV. The reaction $^{12}C(^{12}C,\alpha)^{20}Ne$ has been studied by a number of groups [Pe64, Sc71] but most recently by Medsker et al[Me75] who obtained a value for the excitation of this state of 8694±6keV.

The fact that this 1^- state at 8.70 MeV is seen strongly in the stripping reaction $^{19}F(^3He,d)^{20}Ne$ [Se76] whereas it is not seen in the pickup reaction $^{21}Ne(d,t)^{20}Ne$ [Mi74] implies that it is a $(2s1d)^3(2p1f)$ state. This would mean that it cannot be the head of the $K^\pi=1^-$ band which is expected to have a configuration of $(1p)^{-1}(2s1d)^5$, and this is in agreement with the implications of the γ-decay of the 11.27 MeV (1^- T=1) state discussed in the previous chapter. Conversely, the likely candidate for the band head (the 8.85 MeV level) is seen less strongly in the stripping reaction but is seen in the pickup reaction, which implies that it is a $(1p)^{-1}(2s1d)^5$ hole state as is necessary for it to be a member of the $K^\pi=1^-$ band predicted by the Nilsson model.

In their study of β-delayed alpha emission from ^{20}Na, Polichar et al[Po67] found that a state at 8.74 MeV (presumed to be the 1^- state under consideration) was populated with a strength 0.3% that of the 7.43 MeV state. However, in more recent work, Torgerson et al[To73] failed

to see any evidence for this branch, but found an equivalent strength to the very broad 2^+ state at 8.8 MeV (Γ=800keV). Ingalls[In76b] studied the β-delayed γ-decay and saw no direct evidence for the decay of the 8.70 MeV level, as would be expected if $\Gamma_\gamma << \Gamma_\alpha$. However, from the fact that the single escape peak from the 9.87 MeV → 1.63 MeV decay was too large he inferred the possibility of an underlying peak corresponding to the 8.74 MeV → ground state transition with ^{20}Na branching ratio less than 2×10^{-4}. Ingalls states that if the decay exists it has log Ft > 6.5 which is consistent with a first forbidden decay. No other information on the γ-decay properties of this state has been published.

Using the gas target at a pressure of 200μ, we located a clear resonance at a beam energy of 4.96 MeV. The target gas pressure was then reduced to 43μ, in order to give a very thin target (0.71keV), and a yield curve was measured enabling a width estimate of 2.1±0.8keV (C of M) to be made. This agrees well with the value of 2.5keV obtained by McDermott et al. A yield curve was then measured with a gas pressure of 800μ (13.7keV thickness) in order to position the resonance profile in the centre of the target. The detectors were positioned at angles of 30° (intrinsic Ge) and 135° (Ge(Li)), both at a distance of 10cm. Spectra were then accumulated for an integrated beam charge (He^{++}) of 0.07733C. The beam energy was afterwards lowered by 17keV and off-resonance spectra were accumulated for the same beam charge. Peaks were clearly visible in the on-resonance spectrum corresponding to a decay to the ground state and evidence was seen for a weak branch to the 1.63 MeV (2^+) state.

On examination of the spectrum it was apparent that the calculated strength (after off-resonance subtraction) for the 1.63 MeV → ground state decay was much too strong to be consistent with the weak R→1.63 MeV decay. The likely explanation for this is that the 1.63 MeV γ-rays come from the $^{17}O(\alpha,n\gamma)^{20}Ne$ reaction as explained in chapter 3, and that the difference between the yields at the two beam energies is due to a strong $^{17}O(\alpha,n)^{20}Ne$ resonance, reported by Bair and Haas[Ba73] to be at a beam energy of 5.00 MeV and with a width of the order of 60keV. The cross section for $^{17}O(\alpha,n\gamma_{1.63})^{20}Ne$ implied by the observed strength at E_α=4.96 MeV is 50mb assuming 60ppm of ^{17}O (target gas composition quoted by supplier). This should be compared with the 180mb quoted as the peak cross section for the $^{17}O(\alpha,n_o)^{20}Ne$ resonance and with the $^{17}O(\alpha,n_1)^{20}Ne$ cross section of approximately 60mb at the higher beam energy of 10 MeV. The lack of published $^{17}O(\alpha,n_1)^{20}Ne$ cross section data at this energy prevents quantitative explanation but the observed figure is not unreasonable. The effect of this is to prevent the usual correction for long target effects using the 1.63 MeV γ-ray, so the correction procedure was applied on the assumption that the resonance profile was central in the target chamber. This is what would be expected on the basis of the yield curve measurement which immediately preceded the accumulation of the spectra and thus it is safe to assume that the correction procedure is in fact substantially correct.

Another point to note is that a weak non-resonant decay to the ground state was observed, with a cross section of the order of 1μb. A possible source of this radiation is the very broad underlying 2^+ state at an excitation of 8.8 MeV, reported to have a width of the order of 800keV [Mc60]. If these values are assumed for its excitation and

width, then the observed strength would imply a value of $\omega\gamma$ for this state of 2eV which is a 15 Weisskopf unit E2 transition. Considering the limited information available on the broad state this is a reasonable figure and provides a plausible explanation of the observed γ-decay.

The two observed decay modes of this resonance have comparable reduced strengths which are typical of isospin forbidden E1 decays and are given in table 5.2.1. Neither has been reported previously. The γ-ray energy of the main branch was measured in both detectors, enabling an estimate of 8704±7keV to be made for the excitation of this state. In the absence of in-situ $^{56}Fe(n,\gamma)^{57}Fe$ γ-rays, the accuracy of the energy calibration is limited and the uncertainties in the resonance profile affect the mean doppler shift, so the error is larger than for the other excitation energies measured in this work.

Table 5.2.1 8.70 MeV (1^-)

	Present Work	Mean	Previous
E_x	8704±7	8698±5	8694±6 [Me75]
Implied E_α	6969±9	6960	
Γ	2.1±0.8		2.5 [Mc60]
J^π			1^- [Mc60]
Total $\omega\gamma$ (eV)	0.21±0.05		

Detector at 10cm 135°

	$E_\gamma(\theta)$	Branching Ratio %	Γ_γ (eV)	Mλ	B(Mλ) W.u.	Previous Γ_γ
R→0.00 (0^+)	8640±7	87±8	0.061±0.015	E1	$(1.9\pm0.4)\times10^{-4}$	—
R→1.63 (2^+)	7023±7	13±8	0.009±0.006	E1	$(5.1\pm3.4)\times10^{-5}$	—
R→4.97 (2^-)		<8	<0.006	M1	$<6\times10^{-3}$	—
1.63→0.00 (0^+)	*					

* Obscured

5.3 The 9.11 MeV (3^-) State

McDermott et al[Mc60] saw this state as a resonance in the elastic scattering reaction $^{16}O(\alpha,\alpha)^{16}O$ at a beam energy of 5.53 MeV. The disappearance of this resonance at 90° and 140.8° indicated that the resonance had $J^\pi=3^-$, and they deduced its width to be 2keV in the laboratory frame. Later work by John et al[Jo69], using the same reaction, provided a value for the excitation of the state of 9118±5keV and an improved estimate of 3.2keV for the width in the centre of mass frame.

Another value for the excitation comes from the $^{12}C(^{12}C,\alpha)^{20}Ne$ work of Medsker et al[Me75] who quote a value of 9110±6keV. In their paper the authors speculate that this state may be the head of a $K^\pi=3^-$ band, the 4^- member being a state which they observed at 10.69 MeV with possible unnatural parity and which has since been shown [Fi76] to have $J^\pi=3^+$ or 4^-. Like the 8.70 MeV state, the 9.11 MeV state is seen in the reaction $^{19}F(^3He,d)^{20}Ne$ [Se76] but not in $^{21}Ne(d,t)^{20}Ne$ [Mi74], which implies that its configuration is $(2s1d)^3\ (2p1f)^1$. The gamma decay properties of this state have not previously been reported.

This resonance was located using a target gas pressure of 200μ (3.2keV target thickness). A further yield curve was measured with reduced target gas pressure, but poor statistics prevented a good fit of a yield curve function to the observed peak, so the only esimate of the resonance total width that could be made was $\Gamma\leq 3.2$keV (C of M). This is in good agreement with John et al. A target pressure of 800μ (12.8keV thickness) was used to accumulate spectra for an integrated beam charge of 0.1202C with both detectors at 8cm and at angles of 135° and 30°.

The beam energy was then reduced by 16keV and off resonance spectra were accumulated for a charge of 0.1015C.

Resonant decays were seen to the states at 1.63 MeV (2^+), 4.97 MeV (2^-) and 5.62 MeV (3^-). The reduced transition strengths to the last two are very similar as might be expected from their similar structure as members of the $K^\pi=2^-$ band. A limit was placed on the strength of the possible transition to the 4.25 MeV (4^+) state, the reduced strength being less than half the strength to the 1.63 MeV (2^+) member of the same band. This is in fact the weakest resonance studied in this thesis, the strongest branch having a partial width of only 12.5 meV, and this accounts for the poor estimate of the total width from the yield curve. The value of 9111±3keV for the excitation energy was derived from the measured γ-decays in both the monitor detector and the intrinsic detector at 30°, and is in excellent agreement with the value obtained by Medsker et al[Me75]. These results are shown in table 5.3.1.

Table 5.3.1 9.11 MeV (3^-)

	Present work	Previous
E_x	9111±3	9110±6 [Me75]
Implied E_α	5477	
Γ	≤3.2	3.2 [Jo69]
J^π		3^- [Mc60]
Total $\omega\gamma$ (eV)	0.18±0.03	
Detector at 8cm 135°		

	$E_\gamma(\theta)$	Branching Ratio %	Γ_γ(meV)	Mλ	B(Mλ) Wu	Previous Γ_γ
R→1.63(2^+)	7426.2±4.5	50±5	12.5±2.6	E1	$(6.0\pm1.3)\times10^{-5}$	—
R→4.97(2^-)	4110.6±1.6	33±5	8.4±1.6	M1	$(5.7\pm1.1)\times10^{-3}$	—
R→5.62(3^-)	3465±3	17±4	4.4±1.2	M1	$(5.0\pm1.4)\times10^{-3}$	—
R→4.25(4^+)		<6.3	<1.6	E1	$<2.8\times10^{-5}$	—
4.97→1.63	3309.6±1.1					
1.63→0.00	1621.2±1.0					

5.4 The 11.56 MeV (?) State

This state has been the subject of some confusion since it was first reported by Pearson and Spear[Pe64b], who gave rough values for its $\omega\gamma$ and excitation energy of 0.5±0.3eV and 11560±40keV respectively. According to the recent compilation [Aj78], there are three unnatural parity states (one of them with T=1) within a range of ±50keV of this state, and one of these has almost exactly the same energy as the level under discussion (11555±6keV [Me75]). It is therefore not surprising that earlier experiments often did not have sufficiently accurate energy calibration or resolution to be able to distinguish between these four states. In addition, Ajzenberg-Selove[Aj72] and Medsker et al[Me75] incorrectly identified the presumed unnatural parity 11528±6keV level of Häusser et al[Ha71] with the state seen by Pearson and Spear, although the former does not decay to the 1.63 MeV (2^+) state and the latter does. The more recent compilation [Aj78] seems to link the natural parity state seen in the $^{16}O(\alpha,\gamma)^{20}Ne$ and $^{16}O(\alpha,\alpha)^{16}O$ reactions with the state seen by Ritter et al[Ri69] in the $^{19}F(d,n)^{20}Ne$ reaction, by Betts et al[Be75] in the $^{19}F(^3He,d)^{20}Ne$ reaction and by Marrs et al[Ma77] in the $^{19}F(^3He,d\gamma)^{20}Ne$ reaction. However, this last work identified the state as having $J^\pi=3^+$ from its large γ-decay branch (Γ_γ/Γ) which exceeds 70%. In combination with the $\omega\gamma$ value from Pearson and Spear (if the same state) this would imply $\Gamma_{\alpha_o}<0.7$eV which would be extraordinarily narrow for a natural parity resonance at this energy. The states seen in alpha capture and $^{19}F(^3He,d)^{20}Ne$ cannot therefore be the same.

Evers et al[Ev77] studied the $^{18}O(^3He,n)^{20}Ne$ reaction and populated a state in ^{20}Ne at an excitation of 11480±60keV. From the fact that they only observed a peak corresponding to this state at 0° and 5° they

suggested that it has $J^{\pi}=0^{+}$ and that it is the third 0^{+} state predicted at 11.37 MeV in full sd shell model calculations by Chung and Wildenthal. This reaction proceeds mainly by the direct single step transfer of a singlet proton pair, and so can only populate natural parity states; therefore the state they saw is presumably the level under discussion.

Recently work has been reported by Steck[St78] on both elastic α-scattering and α-capture. The scattering experiment gave a distribution typical of $\ell=2$, but a reasonable confidence level could also be ascribed to an $\ell=0$ assumption. The capture results showed a decay branch to the 1.63 MeV (2^{+}) state with $\omega\gamma=0.41\pm0.05$eV and a 30% branch to the 4.25 MeV (4^{+}) state. This latter branch has a large error (80%) on its strength and was presumably rather doubtful as the author states that possible J^{π} values for the resonance are 0^{+}, 1^{-}, 2^{+}, 3^{-} and 4^{+} despite the fact that if it were 0^{+} or 1^{-} the decay to the 4^{+} level would be an E4 or E3 transition of unreasonable strength. Earlier elastic scattering work by Hunt et al[Hu67] found a resonance in this region and they also tentatively assigned $J^{\pi}=2^{+}$.

With the gas target a clear resonance was seen in a yield curve in the γ-ray energy gate which covered the range 8.8 MeV < E_{γ} < 10.8 MeV. The target pressure was 200μ, giving a target thickness of 2.3keV. The deduced resonance width was 1.3±0.8keV (C of M) which is consistent with the value obtained by Steck of 1.0±0.5keV. A target pressure of 800μ (9.2keV) was used to accumulate both on-resonance and off-resonance spectra, the detectors being positioned at angles of 30° and 135° and at a distance of 8cm. Because of the known weak nature of this resonance, the integrated beam charges were 0.201C and 0.155C for the on and off

resonance spectra respectively. The length of time required for these runs (4-5 hrs) meant that the beam focussing conditions tended to drift, and so significant contamination from the $^{13}C(\alpha,n\gamma)^{16}O$ and $^{12}C(\alpha,\alpha'\gamma)^{12}C$ reactions in the nozzles was seen. Also significant non-resonant 4.25 MeV (4^+) → 1.63 MeV (2^+) and 1.63 MeV (2^+) → g.s. decays were seen. These are likely to arise from the $^{17}O(\alpha,n\gamma)^{20}Ne$ reaction.

A clear set of three peaks was seen for the R→1.63 MeV (2^+) decay and a value for $\omega\gamma$ of (0.41 ± 0.06)eV was deduced which is in good agreement with Steck. Good limits were set on the possible decays to the ground state and to the 4.25 MeV (4^+) state. This latter limit ($\omega\gamma<0.02$eV) is in disagreement with the $\omega\gamma$ of (0.2 ± 0.15)eV for the transition which Steck claimed to observe. As mentioned above, the large error and the fact that he does not rule out spins of 0^+ and 1^- imply a low confidence in this branch. The upper limit on the E2 ground state transition of 6×10^{-3}Wu (if $J^\pi=2^+$) is rather weak for nuclei of mass $\leq$20 [Sk66] and for mass >20 [En74], but typical values for E2 transitions are hard to define due to the existence of many collectively enhanced E2 transitions. This fact might favour a $J^\pi=0^+$ assignment as the transition strength to the 1.63 MeV (2^+) state would then be 1.6 Wu (E2), which is a more typical value for an E2 transition, and no ground state decay would be expected because of the 0→0 selection rule. This assignment would agree with the assumption of Evers et al. An angular distribution measurement was not attempted in view of the weak nature of the resonance.

Table 5.4.1 11.56 MeV (?)

	Present Work	Mean	Previous
E_x	11557±6	11555±5	11552±8 [St78]
Implied E_α	8535±8		
Γ	1.3±0.8		1.0±0.5 [St78]
J^π			0^+?[Ev77]; 2^+?[St78]
Total $\omega\gamma$ (eV)	0.41±0.06		0.61±0.17 [St78]

Detector at 8cm 135°

	$E_\gamma(\theta)$	Branching Ratio %	Γ_γ* eV	Mλ*	B(Mλ)Wu*	Previous Γ_γ*
R→1.63(2^+)	9843.5±9	100	0.082±0.012	M1	$(4.1\pm0.6)\times10^{-3}$	0.08±0.01 [St78]
R→0.00(0^+)		<4	$<3\times10^{-3}$	E2	$<6\times10^{-3}$	
R→4.25(4^+)		<5	$<4\times10^{-3}$	E2	$<74\times10^{-3}$	0.04±0.03 [St78]
1.63→0.00	1621.2±0.3					

* These columns assume $J^\pi=2^+$

5.5 The 11.92 MeV (4^+) State

The only previous reports of the properties of this level have both come from Chalk River, where this level was seen as a resonance in elastic alpha scattering [Ha72] and also in the inelastic reaction $^{16}O(\alpha,\alpha_2\gamma)^{16}O$ [Al67, Al72a]. The elastic scattering work established the excitation and width of the ^{20}Ne state to be 11925 ±5keV and 0.44keV respectively. The angular distribution showed the spin to be 4 and of course the resonance has natural parity. The inelastic properties of the resonance were used by Alexander et al[Al72a] to provide a convenient calibration of beam energy in the region of the 11.948 MeV (8^+) level, but they do not report the partial width for the α_2 decay mode. The γ-decay properties of this state have not been reported.

The resonance was located by measuring a yield curve with a target pressure of 200μ (2.2keV). It was found to be very weak, occurring most strongly in the γ-ray energy gate covering the range 7.1→8.2 MeV with a peak to background ratio of 1:2. Spectra were accumulated for an integrated beam charge of 0.0652C with the gas pressure maintained at 800μ (8.9keV). The detectors were at a distance of 8cm and at angles of 30° and 135°. Off-resonance spectra were accumulated for a beam charge of 0.0651C. The quality of the spectra obtained is not as good as for the other resonances studied, as this was the last resonance studied before the contaminated target gas was replaced. The spectra show significant contamination from α-induced reactions on ^{14}N and the yield of non-resonant 1.63 MeV γ-rays from $^{17}O(\alpha,n\gamma)$ is enormous. For this reason the normal correction procedure for a long target was not applied and the errors on the transition strengths have been increased to allow for the uncertainties which result. No sensible estimate of the

excitation could be made from the γ-decay; the estimate shown in table 5.5.1 is derived from the calibration of the beam analysing magnet. The spectra show the resonance to decay to the 1.63 MeV (2^+) state and to the 4.25 MeV (4^+) state, both decays being rather weak. In addition the previously observed α_2 decay was seen and a value for Γ_{α_2} of 0.58 ± 0.10eV was obtained. This is much smaller than the total width of 0.44keV, as was assumed by Häusser et al[Ha72] in their analysis.

Table 5.5.1 11.92 MeV (4^+)

	Present Work	Previous
E_x	11924 ±6 (a)	11925 ±5 [Ha72]
Implied E_α	8994 ±8 (a)	
Γ	<1	0.44 ±0.15 [Ha72]
J^π		4^+ [Ha72]
Total $\omega\gamma$ (eV)	0.23 ±0.06	—

Detector at 8cm 135°

	$E_\gamma(\theta)$	Branching Ratio %	Γ_γ eV	Mλ	B(Mλ)Wu	Previous Γ_γ
R→1.63(2^+)	10201 ±7(c)	21 ±11	$(5.2 \pm 3.3) \times 10^{-3}$	E2	0.017 ±0.011	—
R→4.25(4^+)	7597 ±5	79 ±11	$(20.0 \pm 5.6) \times 10^{-3}$	M1	$(2.1 \pm 0.6) \times 10^{-3}$	—
4.25→1.63	2591 ±2					
1.63→0.00	(b)					
$^{16}O(\alpha,\alpha_2\gamma)^{20}Ne$			Γ_{α_2}=0.58 ±0.10eV			—

(a) E_α and E_x derived from analysing magnet calibration and two separate yield curves.

(b) Impossible to separate non-resonant contribution.

(c) Deduced from single escape peak.

5.6 The 11.95 MeV (8^+) State

Rotational bands in light nuclei have been the subject of interest for a long time ever since Litherland et al[Li58] demonstrated their existence in ^{25}Mg. As discussed in chapter 3, their interest arises from the fact that their energy spacings and transition strengths are easily described in a semi-classical collective model but are also described by shell model calculations, in particular using the SU(3) classification scheme.

The lower members of the ground state band in ^{20}Ne were first identified by Litherland et al[Li61] who showed that the 1.63 MeV (2^+) and 4.25 MeV (4^+) states have large E2 transition strengths which are characteristic of in-band transitions. Litherland et al later identified the 8.78 MeV (6^+) state as belonging to this band [Li67], measuring its E2 strength to be 28 W.u. The strengths of the two lower transitions have been re-measured by Häusser et al[Ha71] and the $6^+ \rightarrow 4^+$ decay was remeasured by Diamond et al[Di71] and by Rogers et al[Ro71f]. These more recent values are shown in table 5.6.1 and fig.5.6.1, where it can be seen that the shell model description is clearly favoured over the simple rotational model by the $6^+ \rightarrow 4^+$ decay. A more severe test is the decay of the 8^+ state since it can be seen that the shell model predicts a substantially weaker transition than does the rotational model since the latter predicts the transition strengths to rise monotonically with increasing spin.

An 8^+ level was first identified by Kuehner and Ollerhead[Ku66], through angular distribution measurements in the $^{12}C(^{12}C,\alpha\alpha)^{16}O$ reaction, at an excitation of 11.99 MeV. Subsequently it was studied in

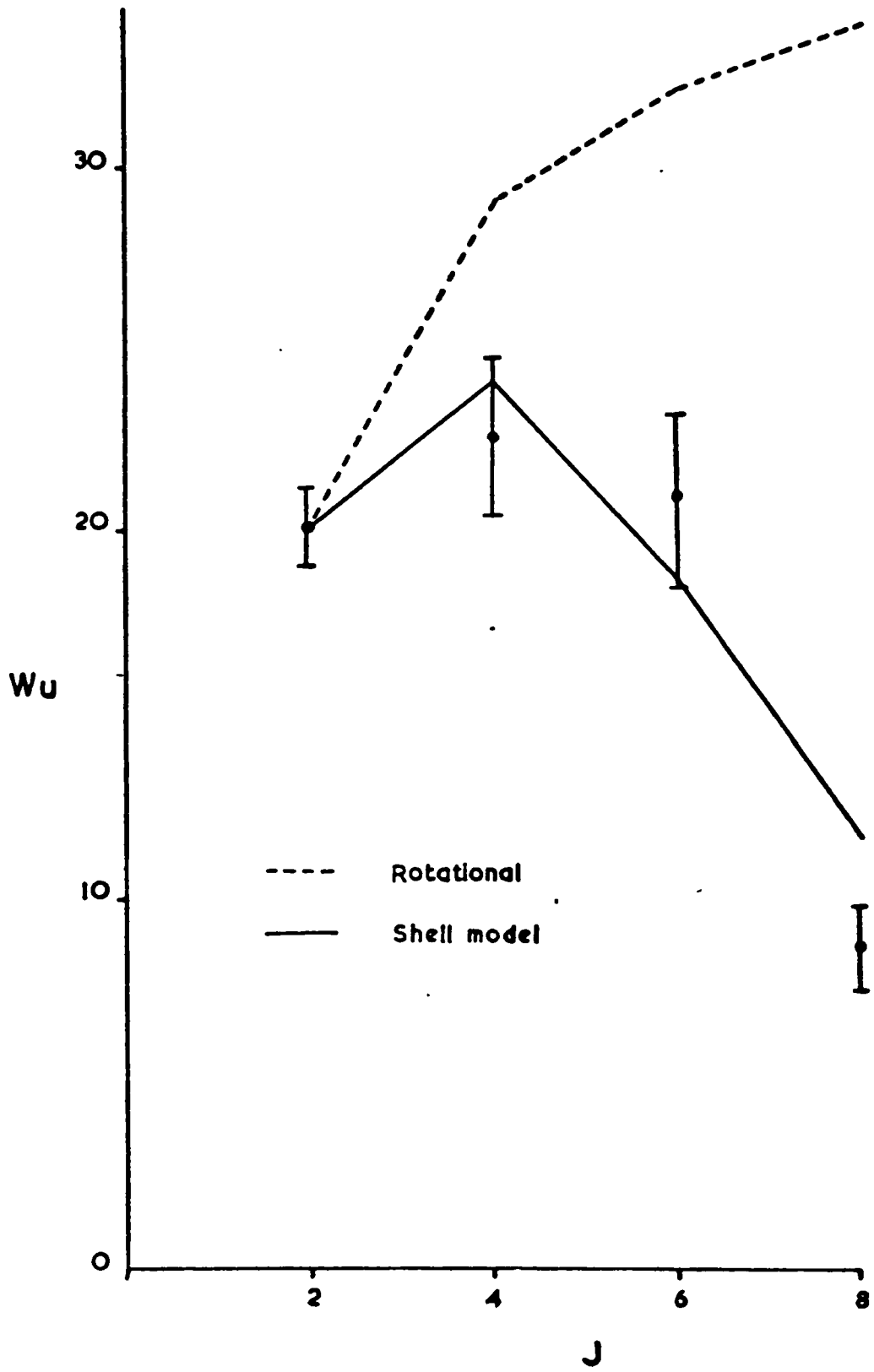

Fig.5.6.1 E2 transition strengths for the ^{20}Ne ground state band compared with rotational and shell model predictions with a complete $(sd)^4$ basis.

the $^{16}O(\alpha,\alpha)^{16}O$ elastic scattering reaction by Häusser et al[Ha72] who obtained a much more precise value for the excitation of 11948±5keV and found its width to be 35±10eV. They calculated that the reduced width was only an eigth of the value for the 6^+ member of the band (θ^2=0.085), which made its membership of the band seem unlikely, but Fortune et al[Fo72a] have shown that the reduced width is only a factor of two smaller than the reduced width of the 6^+ if suitable single particle widths are calculated by using the right well parameters. The elastic scattering work established the energy separation between the 8^+ state and a 4^+ state at 11925±5keV, which was known to have a decay branch to the 6.13 MeV state in ^{16}O resulting in a 6.13 MeV γ-ray [Al67].

Knowledge of this separation allowed Alexander et al to locate the 8^+ resonance in the $^4He(^{16}O,\gamma)^{20}Ne$ reaction by first locating the 4^+ resonance in the inelastic reaction $^4He(^{16}O,\alpha_2\gamma)^{16}O$ [Al72a]. A previous attempt to find the 8^+ had been thwarted by not knowing sufficiently accurately where to look. They obtained a value for the decay strength of 7.5±2.5 W.u. which was in fair agreement with the SU(3) shell model calculations of Harvey[Ha68] but which certainly ruled out the simple rotational model.

They used the inverse capture reaction with an oxygen beam in order to avoid the problems of high energy (9 MeV) alpha capture, but nevertheless they experienced severe background problems, due mainly to the inelastic scattering of the ^{16}O beam, and the 3.17 MeV γ-ray only appears in their spectrum after subtracting an off-resonance spectrum and then smoothing the resultant spectrum. We therefore felt it to be desirable to remeasure this transition strength and accept the challenge of looking for this resonance with the gas target, using the

conventional alpha capture reaction. In fact it would not have been possible for us to use the inverse reaction as the cryopumps cannot pump helium, so there was no choice but to use alpha capture on an oxygen target. Provided that the background can be held sufficiently low, a helium beam has an advantage over an oxygen beam in that a much more intense beam is available from the injector since no stripping or negative ion formation is required.

The use of the cryogenically pumped gas target greatly reduced the background seen in the detectors, eliminating the $^{13}C(\alpha,n\gamma)^{16}O$ reaction, and the main remaining source of unwanted radiation was the $^{12}C(\alpha,\alpha'\gamma)^{12}C$ reaction on carbon contamination in the tantalum pumping nozzles. Unfortunately this reaction has a large broad (70keV) resonance at a beam energy of 8.98 MeV [La64; see also chapter 6 of this thesis] which overlaps the energy of 9.02 MeV [Ha72] where the 8^+ resonance was expected. This radiation was particularly troublesome because the γ-ray energy is 4.4 MeV, giving a double-escape peak in the detectors at 3.4 MeV which is close to the energy of the $8^+ \rightarrow 6^+$ transition in ^{20}Ne (the only possible γ-decay for the 8^+) at 3.2 MeV. The problem was exacerbated by the fact that one pumping nozzle was up-beam from the detector and one down-beam, leading to very pronounced Doppler broadening of the contaminant peaks, as can be seen in fig.5.6.2.

This made it very difficult to find the resonance by our usual yield curve methods, as tiny fluctuations in beam direction or focussing conditions caused a fraction of the beam to strike the pumping nozzles, thus temporarily increasing the count rate in the selected γ-ray energy gate, and giving rise to spurious peaks. For this reason, instead of

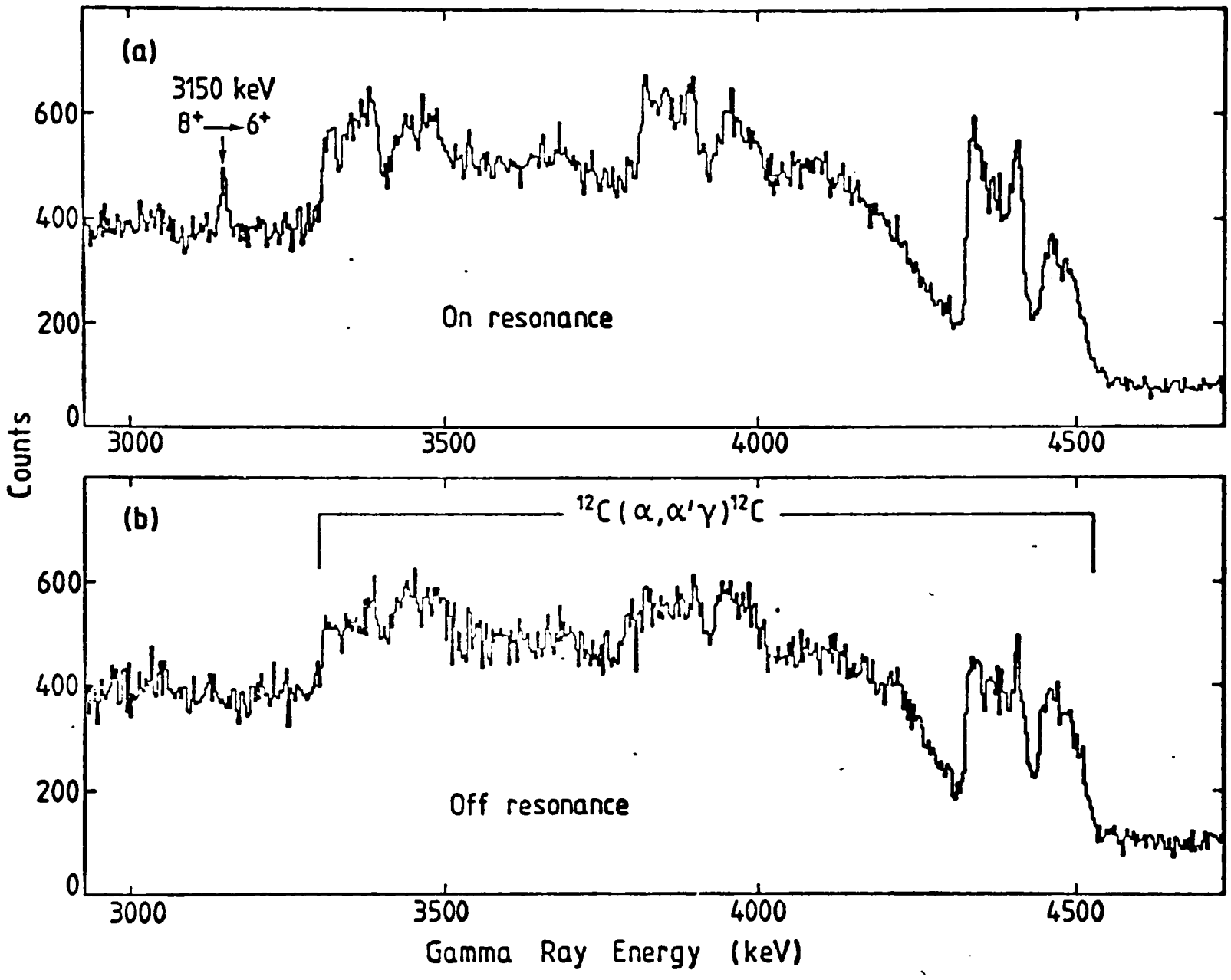

Fig.5.6.2 Spectra of γ-rays taken (a) on and (b) off the 9.02 MeV resonance in the $^{15}O(\alpha,\gamma)^{20}Ne$ reaction, taken with a target pressure of 0.6 torr and using the 25% Ge(Li) detector. The off-resonance spectrum has been normalised to the same collected charge. The resonant 3.150 MeV γ-ray from the decay of the 11.95 MeV (8^+) state is marked in (a) and the Doppler shifted and broadened 4.44 MeV γ-rays from the $^{12}C(\alpha,\alpha'\gamma)^{12}C$ reaction are evident in both spectra.

the usual NaI crystal, a 25% efficient Ge(Li) detector, close to the target and at 90° to the beam direction, was used for the yield curves in order to resolve the desired γ-ray from the contaminant peaks and so set a tighter energy gate. A yield curve over the 4^+ resonance at an excitation of 11.925 MeV was measured in order to establish the beam energy calibration and then after several attempts a small peak was seen in a yield curve covering the beam energy range of interest.

The 25% Ge(Li) was then moved to an angle of 127° at a distance (target to can) of 11.5cm and the usual 16.6% Ge(Li) was positioned at 46° and 10cm. The target pressure was maintained at 600μ (6.7keV) and spectra were accumulated for an integrated beam charge of 0.151C (470×10^{15} incident particles; cf 7.7×10^{15} ^{16}O nuclei in Al72a). The beam energy was then reduced by 12keV and off-resonance spectra were accumulated, with the same detector geometry and gas pressure, for a beam charge of 0.10C. A week later, when beam was again available, a yield curve was again measured over the 4^+ resonance and then the beam energy was raised by the same amount as in the previous run, in order to locate the 8^+ resonance without attempting a yield curve measurement. Spectra were accumulated with the larger detector now at 125° and 9.8cm and the other as before. Three further pairs of spectra were accumulated with minor beam energy adjustments between the runs in an attempt to keep the resonance profile central in the target chamber. The gas pressure for this set of runs was 800μ which corresponds to a target thickness of 8.9keV.

In all ten spectra a γ-ray peak was clearly visible at the expected energy and it was absent from the off-resonance spectra. The first of the five spectra taken with the 25% Ge(Li) detector is shown in

fig.5.6.2, together with the off-resonance spectrum taken with the same detector. The spectra can be seen to be dominated by the large double peaks from inelastic α-scattering in carbon in the two nozzles, but they are flat in the region of interest, with the resonant $8^+ \rightarrow 6^+$ decay showing clearly.

The normal correction procedure, using the 1.63→g.s. decay, or another transition of known energy, was not possible as the only γ-ray from the decay of the 8^+ state is that coming from the $8^+ \rightarrow 6^+$ transition, and its energy is only known to ±5.5keV (0.2%), using the excitation values known for the two states [Ha72]. There is no secondary transition because the 6^+ state is unbound to alpha decay. The procedure which was adopted was to correct the number of counts seen in the $8^+ \rightarrow 6^+$ γ-ray peak in each of the ten spectra for each of a range of possible values for the transition energy, using the implied Doppler shift for that peak. Thus for each detector and each assumed transition energy a mean value of the corrected number of counts per unit beam charge could be calculated by combining the values from the five runs. In fact there were not always five values to be combined for each detector because a further requirement of the correction procedure was that the resonance profiles predicted by the two detectors should be consistent and realistic, and the values from a case for which this was not so were not included.

The second run was at the highest beam energy of the five runs (3keV higher than the fourth run) and for an assumed transition energy of 3175keV or greater the resonance profile was predicted to be mainly out of the target chamber, making the observed strength improbable. Similarly the fourth run was at the lowest beam energy of the four runs

with 800μ gas pressure, and did not give consistent profiles for transition energies below 3170keV. These two facts make it very likely that the transition energy lies in the range $3170 \leq E_t \leq 3174$ which agrees well with the value for E_t of 3172±5.5keV deduced from the excitation energies in the literature [Aj78].

The corrected mean intensity for each energy assumption could then be related to the $\omega\gamma$ of the 10.27 MeV (2^+;T=1) level as usual in the case of the 16.6% detector. For the 25% detector, the relative efficiency curve was measured using a ^{56}Co source, enabling a reliable extrapolation to the γ-ray of interest at 3.17 MeV. A spectrum of the T=1 resonance was measured using this detector, enabling a comparison between the secondary decay of this resonance and the $8^+ \rightarrow 6^+$ decay to be made. In making this comparison, a correction was made for the non-resonant contribution of 1.63 MeV γ-rays from the $^{17}O(\alpha,n\gamma)^{20}Ne$ reaction due to the trace of ^{17}O in the target gas.

The result of the analysis described was to produce two values for $\omega\gamma(8^+ \rightarrow 6^+)$ for each assumption of transition energy, one from each detector. These pairs of values are inconsistent if $E_t < 3170$keV but their agreement improves as E_t rises, since the value deduced from the 16.6% detector at 46° drops, due mainly to angular distribution effects. The transition energy for which exact agreement occurs is sensitive to the difference between the two values and in itself is not significant as the error bars overlap for $E_t \geq 3170$keV. For the expected transition energy of 3172keV the mean value of $\omega\gamma$ is 131±18 meV, which corresponds to 9.2±1.3 W.u., where the errors include the errors in measuring both the strength of the $8^+ \rightarrow 6^+$ decay and the strength of the T=1 resonance and also the quoted error in the value of $\omega\gamma$ for the T=1 state. The

effect of allowing the transition energy to vary over the range 3170keV to 3174keV is to introduce an extra 3% error which has negligible effect on the final error. A larger variation of 6keV would have no additional effect if the transition energy were larger than assumed, but would increase the predicted $\omega\gamma$ by 12% if it were smaller. As shown above, such a large variation seems improbable, so a final value of 9.2 ± 1.3 W.u. is adopted.

The value obtained for $\omega\gamma$ agrees well with the less precise value of 7.5 ± 2.5 W.u. measured by Alexander et al[Al72a], and is closer to the SU(3) shell model prediction of Harvey[Ha68] which is quoted in their paper. In similar calculations Akiyama et al[Ak69] obtained a similar value and they report that the (80) representation of SU(3) accounts for 81% of the intensity of the 8^+ wave function and up to 91% for the other members of the ground state band. Full $(sd)^4$ calculations using matrix elements due to Preedom and Wildenthal[Pr72] and Chung and Wildenthal[Ch76] both predict weaker transitions in the ground state band than are actually observed. When normalised to the experimental $2^+ \rightarrow 0^+$ transition strength (as shown in fig.5.6.1 and table 5.6.1) the agreement between calculation and experiment is good for the $4^+ \rightarrow 2^+$ transition and reasonable for the $8^+ \rightarrow 6^+$ transition; the prediction for the $6^+ \rightarrow 4^+$ transition is too low by 20%. As can be seen from the figure, however, the general relationship between the transition strengths in the band is predicted quite well.

The effective charges needed for the shell model calculations to reproduce exactly the experimental transition rates are shown in table 5.6.1. In calculating these a nuclear size parameter of $1.072A^{1/6}$fm was used, following the work of Schwalm et al[Sc77]. The first three

effective charge values, with a mean of 0.53 ± 0.02, differ significantly from the value 0.35 ± 0.02 obtained by Schwalm et al from a fit to 26 B(E2) values distributed throughout the sd shell, implying extra core polarisation in ^{20}Ne for this band. The effective charge for the $8^+ \rightarrow 6^+$ transition is, however, less than for the other transitions in the band, suggesting that less core polarisation is involved and hence that the intrinsic structure of the 8^+ state is not quite the same as for the other band members.

Table 5.6.1 B(E2) values within the ^{20}Ne ground-state band

Transition	$B_{exp}(E2)$ (e^2fm^4)	$B(E2)_{J\to J-2}/B(E2)_{2\to 0}$ Expt.	SM[a]	SU(3)[b]	Additional effective charge[g] ε
$2^+ \to 0^+$	65.7±3.4[c]				0.53±0.03
$4^+ \to 2^+$	73.3±7.0[d]	1.12±0.13	1.19	1.27	0.49±0.05
$6^+ \to 4^+$	68.0±7.6[e]	1.04±0.13	0.93	1.07	0.58±0.06
$8^+ \to 6^+$	28.6±3.7[f]	0.44±0.06	0.58	0.64	0.39±0.05

a Shell model calculations within a complete $(sd)^4$ basis, using the effective interaction of Preedom and Wildenthal [Pr72].

b SU(3) calculations [Ha68] assuming the states to be described by the (80) representation.

c Weighted average of the values given by Olsen et al [Ol74] and Schwalen et al [Sc77].

d Häusser et al [Ha71].

e Weighted average of the results of Diamond et al [Di71] and Rogers et al [Ro71f].

f Weighted average of present work and result of Alexander et al [Al72a].

g See text.

Table 5.6.2 11.95 MeV (8^+)

	Present Work	Previous
E_x	11949 ±4	11948 ±5 [Ha72]
Implied E_α	9024 ±5	
Γ	<1	0.035 [Ha72]
J^π		8^+ [Ha72]
Total $\omega\gamma$ (eV)	0.131 ±0.018	0.104 ±0.035 [Al72a]

Detectors at 9.8cm (125°) and 10cm (46°)

	$E_\gamma(\theta)$ (a)	Branching Ratio %	Γ_γ eV	Mλ	B(Mλ)Wu	Previous Γ_γ
→8.78(6^+)	3150.2 ±1.7	100	$(7.71 \pm 1.06) \times 10^{-3}$	E2	9.2 ±1.3	$(6.12 \pm 2.06) \times 10^{-3}$ [Al72a]

a) Detector at 127° and 11.5cm as for spectrum shown in fig.5.6.2.

5.7 The 12.14 MeV (6^+) State

Pearson and Spear [Pe64b] saw this resonance in the inelastic alpha scattering reaction $^{16}O(\alpha,\alpha_2\gamma)^{16}O$. From measurements of the resultant γ-ray intensity they deduced a value for $\omega\Gamma_{\alpha_2}\Gamma_{\alpha_0}/\Gamma$ of 100 ± 50eV in the laboratory frame of reference. Kuehner and Almqvist [Ku67g] measured the α-α correlation in the reaction $^{12}C(^{12}C,\alpha)^{20}Ne^* \rightarrow ^{16}O+\alpha$ and showed that $J^\pi=6^+$. Balamuth et al [Ba72] observed coincidence events between the 6.13 MeV ^{16}O γ-rays and the alpha particles from the reaction $^{12}C(^{12}C,\alpha)^{20}Ne^*$ and deduced a value for the branching ratio Γ_{α_2}/Γ of 0.060 ± 0.015. They used this value and the value of $\omega\Gamma_{\alpha_2}\Gamma_{\alpha_0}/\Gamma$ from Pearson and Spear [Pe64b] to deduce a value of 128 ± 72eV for the total width of the 12.14 MeV state. However this is in fact the value for the laboratory frame as Pearson and Spear did not apply the kinematic factor of 16/20 to their widths.

The narrow α_0 width for this state led Balamuth et al to identify it as the 6^+ member of the $K^\pi=0^+$ band with lower members at 7.20 (0^+), 7.83 (2^+) and 9.04 MeV (4^+) as these all have small reduced widths ($\sim 10^{-2}$). In fact the 6^+ member has a reduced α_0 width of 10^{-3}. The small overlap with the ^{16}O ground state plus alpha particle, which is implied by this inhibited decay, supports the suggestion [Mi71] that the band is based on two alpha particles in the sd shell outside a ^{12}C core. This hypothesis is strengthened by comparing the cross sections for the 12.14 MeV and 12.59 MeV 6^+ states in the reaction $^{12}C(^{12}C,\alpha)^{20}Ne$ and $^{16}O(^6Li,d)^{20}Ne$ [Fo72a]. As would be expected for a $(p^{-4}sd^8)$ state, the 12.14 MeV state is the weaker in the alpha transfer reaction but is the stronger in the eight particle transfer case.

The $^{16}O(\alpha,\alpha_2\gamma)^{16}O$ resonance was seen clearly in a yield curve and spectra were accumulated with a target pressure of 1000μ (10.9keV). The 16.6% Ge(Li) was positioned at 9cm and 125° while the smaller intrinsic detector was at 10cm and 30°. The integrated beam charge on resonance was 0.1124C and for the off resonance spectra it was 0.0854C. The 6.14 MeV γ-rays were very clear and allowed a good estimate of $\Gamma_{\alpha_2}\Gamma_{\alpha_0}/\Gamma$ to be made, permitting an improved estimate of Γ using the value of Γ_{α_2}/Γ from Balamuth et al[Ba72]. No capture γ-rays were observed, the limits on the $\omega\gamma$ of possible E2 decays to the 4^+ states at 4.25 MeV and 9.03 MeV being 0.1 and 0.2eV respectively. The corresponding reduced widths would be 0.13 Wu and 24 Wu. The large limit for the in-band transition arises in part from the ^{14}N contamination of the target gas, as the expected γ-ray peak would occur on the Compton peak arising from the reaction $^{14}N(\alpha,p\gamma)^{17}O$.

In the absence of capture γ-rays, the only estimate of excitation energy that could be made was from the beam energy as measured relative to the 9.404 MeV resonance (Ex=12.25 MeV) with the NMR probe in the beam energy analysing magnet. The deduced excitation of 12137±5keV is in good agreement with the excitation reported by Medsker et al[Me75].

Table 5.7.1 12.14 MeV (6^+)

	Present Work	Previous
E_x	12137±5 (a)	12134±6 [Me75]
Implied E_α	9261±6	
Γ	<1; (0.103±0.030 (b))	0.128±0.072 [Ba72]
J^π		6^+ [Ku67g]
Total $\omega\gamma$ (eV)	<0.2	
Detector at 9cm 125°		
$^{16}O(\alpha,\alpha_2\gamma)^{16}O$	Γ_{α_2} = 6.2±0.9eV	Prev Γ_{α_2} = 6.2±3.1eV [Pe64b]

(a) Measured relative to 12.25 MeV level.

(b) Uses value for Γ_{α_2}/Γ of 0.06±0.015 from Ba72, together with present value for $\Gamma_{\alpha_2}\Gamma_\alpha/\Gamma$

CHAPTER 6

Gas Target Study of the Reaction $^{12}C(\alpha,\gamma)^{16}O$

6.1 Introduction to ^{16}O

The tightly bound doubly magic nucleus ^{16}O is of great interest in the study of the structure of light nuclei. Its closed shell nature means that all its intrinsic excited states are necessarily of a particle-hole nature, and because the ground state is spherically symmetric, no rotational bands can be built on it. The first excited state lies at an energy of 6.05 MeV and has J^{π} equal to 0^+ instead of the usual 2^+ for the first excited states of most even-even nuclei. This state is believed to be of 4-particle 4-hole nature [Zu68] and is sufficiently deformed to be the intrinsic state for a rotational band comprising states at 6.92 MeV (2^+), 10.35 MeV (4^+) and 16.29 MeV (6^+). The 8^+ member has not yet been identified but predictions for its energy are 20.1 MeV [Ce66] and 17.5 MeV [Ke65]; both calculations systematically give predictions for the other members of this band which are too low. The second excited state lies at an energy of 6.13 MeV and has a J^{π} value of 3^-. It is a well known example of an octupole vibrational state, its E3 decay probability being 14 single particle units.

The binding energy of an α-particle in ^{16}O is 7.162 MeV [Wa77] and the threshold for the reaction $^{12}C(\alpha,\alpha_1\gamma)^{12}C$ through the first excited state of ^{12}C at 4.44 MeV is 5.92 MeV. Above a bombarding energy of 6.7 MeV the very large background of 4.44 MeV γ-rays obscures weak capture resonances (fig.6.2.1b). The main aim of these experiments was therefore to search for narrow capture resonances in the region E_α=5.22

to 6.9 MeV (E_x=11.08 to 12.3 MeV).

Inspection of the compilation by Ajzenberg-Selove [Aj77] shows many broad levels but very few narrow states with natural parity. In fact, applying the criteria used in chapter 3 for ^{20}Ne, there are only three natural parity levels with widths less than 15 keV known in the excitation range available to us of 9.8 MeV (E_α=3.5 MeV) to 14.3 MeV (E_α=9.5 MeV). These are the 2^+ state at 9.85 MeV, the 4^+ state at 11.10 MeV and the 0^+ state at 12.05 MeV. In view of the advantages offered by a thin gas target when locating narrow resonances, it was considered that an α-capture survey using the cryogenically pumped target might detect as yet undiscovered sharp resonances, as had been found when studying ^{19}F [Sy76]. Although a previous survey had been reported by Larson and Spear [La64], a repeat was felt to be justified since the earlier work used a thick target (~30 keV), and, because of serious background problems, was only looking for ground-state radiation.

6.2 Alpha Capture using Methane

The normal problems associated with radiative capture work and described in chapters 1 and 2 clearly apply here, but in addition the fact that the target itself consists of carbon greatly increases the magnitude of the $^{13}C(\alpha,n\gamma)^{16}O$ background. The cryogenically pumped gas target provides a clean system, and a suitable gaseous compound of carbon could be isotopically depleted in ^{13}C and hopably kept free from subsequent contamination.

Methane (CH_4) was chosen as a suitable gas since it does not introduce extraneous nuclei and is a very suitable gas for use in a thermal diffusion plant, which was the method chosen to reduce the ^{13}C content.

We learnt (Dr G.C.Cowan, private communication) of a large stock of carbon monoxide depleted in ^{13}C which remained at the Los Alamos Laboratory after a major ^{13}C enrichment programme. A large quantity of this material was transferred to the Monsanto Chemical Company's Laboratory at Miamisberg Ohio, converted to CH_4 and run through the Company's gaseous diffusion columns. In this way the ^{13}C content was further reduced to a calculated level of less than 2ppm, and twenty litres of gas were supplied in two batches.

On receipt of the methane it was decided to check the ^{13}C content by passing a beam through it and searching for 6.13 MeV γ-rays from the $^{13}C(\alpha,n\gamma)^{16}O$ reaction. This was done with a beam energy of 6.107 MeV (as calculated from the magnetic field of the analysing magnet) which corresponds to resonance #5 in the study of this reaction by Spear et al[Sp63]. This resonance is stated in their paper to have a width of 45 keV, so errors in beam energy (~10 keV) would not significantly affect the anticipated yield. A spectrum was accumulated for an integrated beam current (doubly charged) of 0.186C, using a target gas pressure of 600μ, which at this beam energy corresponds to a target thickness of 8 keV. The intrinsic germanium detector was used at a distance (target to front of can) of 10cm and at a forward angle of 25° to the beam direction in order to reduce the Doppler broadening of γ-rays emanating from the gas, so making them more visible above background. The spectrum obtained showed clear peaks from the neutron capture reaction

$^{56}Fe(n,\gamma)^{57}Fe$ and also small clear 6.13 MeV peaks, but as these were sharp and not Doppler shifted they had to be coming from reactions in the pumping nozzles and collimators. No broadened, Doppler shifted 6.13 MeV peaks were observed, implying a limit on the ^{13}C abundance of less than 6ppm. The absence of these γ-rays demonstrated that the gas was sufficiently pure and that the α-capture survey was worth performing.

Initially the two resonances at beam energies of 3.58 MeV and 4.25 MeV were studied briefly, in order to confirm that we could see states in ^{16}O which were already known. At these beam energies, where the reaction $^{13}C(\alpha,n\gamma)^{16}O$ is no problem, the gas target confers little advantage. The first of these resonances corresponds to the 9.85 MeV (2^+) state studied by Larson and Spear [La64] and by Brochard et al[Br70]. This is a weak resonance, its main γ-decay branch, to the ground state, having an $\omega\gamma$ of only 30 meV. It was found in a yield curve and a spectrum was accumulated which showed the principal decay, but it was not considered worth while to run for long enough to improve on the already published data.

The second of these resonances corresponds to the 10.35 MeV 4^+ member of the 4p-4h rotational band based on the 6.05 MeV (0^+) state, and has been studied by Chew and Lowe [Ch75]. This broad resonance was located in a yield curve using a target pressure of 1 torr, and a spectrum was accumulated in which the decay to the 6.92 MeV (2^+) state was clearly seen. A useful estimate of the strength could not be made because the target thickness (~18 keV lab.) was less than the resonance's natural width (35 keV lab.), making the yield strongly dependent on the unknown gas pressure profile and on the exact position of the peak of the resonance within the target chamber. These effects

are only minor for thick target yields.

A continuous yield curve was then measured in 1 keV beam energy steps, covering the beam energy range 5.22→9.53 MeV which corresponds to an energy range in ^{16}O of 11.08→14.31 MeV. The gas pressure used was 200μ, so the target thickness varied from 3 keV to 1.5 keV. The detected γ-rays were sorted into seven 'gates' in order to distinguish between ground state, cascade and inelastic γ-rays.

Figure 6.2.1b shows the yield in the energy gate accepting γ-rays in the range 3.4→5.0 MeV, which arise primarily from the inelastic scattering of α-particles, exciting the ^{12}C target nucleus to a state at 4.44 MeV. The resonances observed are those observed by Larson and Spear [La64] with the addition of the peak at 7.04 MeV which corresponds to the 12.44 MeV(1^-) state in ^{16}O. The shape of the 3^- T=1 resonance peak (E_x=13.26 MeV) shows a strong interference effect, presumably due to mixing with the 3^- T=0 state at 13.13 MeV. Taking values from the compilation [Aj77], the resonance strengths $(2J+1)\Gamma_{\alpha_0}\Gamma_{\alpha_1}/\Gamma$ for these two states are 115 keV (T=0) and 22.5 keV (T=1). The heights of the peaks in fig.6.2.1b are not in this ratio but are nearly equal because the total widths of the two states are in a similar ratio, and hence the two ratios cancel since the yield from a thin target is reduced by the ratio of target thickness to resonance total width. The even stronger 4^+ resonance at a bombarding energy of 8.96 MeV (E_x=13.88 MeV) has a strength of 141 keV (again deduced from [Aj77]) and is the cause of the background problems experienced when studying the 8^+ state in ^{20}Ne [Chapter 5].

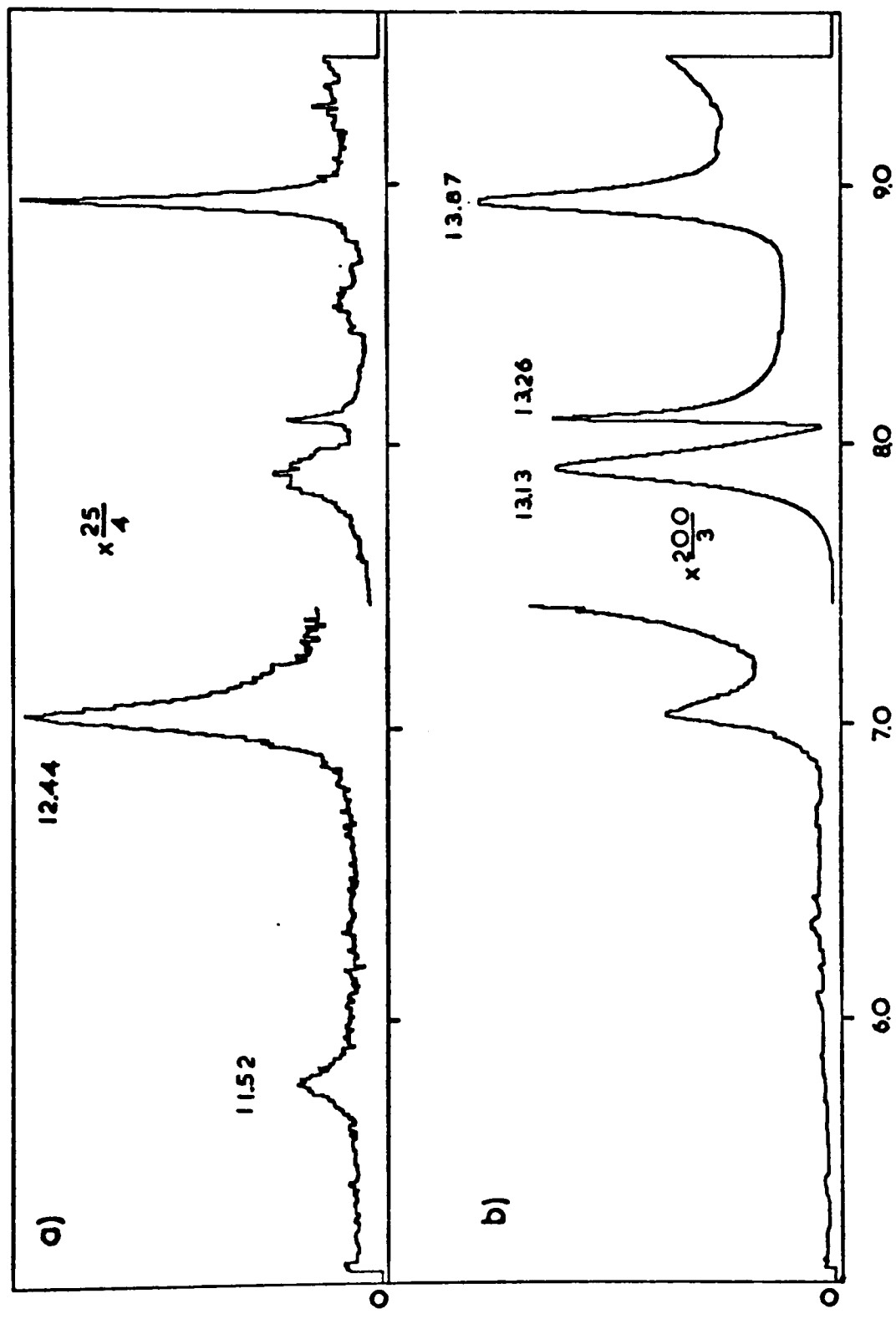

Fig.6.2.1 Yield of γ-rays as a function of beam energy for the $^{12}C(\alpha,\gamma)^{16}O$ reaction where (a) $E_\gamma > 8$ MeV and (b) $3.4 < E_\gamma < 5.0$. The latter includes the 4.44 MeV γ-rays from the $^{12}C(\alpha,\alpha'\gamma)^{12}C$ reaction. Peaks are labelled by the corresponding states in ^{16}O. The high energy half of (a) is affected by pile-up.

Despite pile-up rejection electronics, the enormous yield of 4.4 MeV γ-rays from $^{12}C(\alpha,\alpha_1\gamma)^{12}C$ above a bombarding energy of 6.9 MeV reduces sensitivity to weak capture resonances, and the same reaction in the pumping nozzles makes beam conditions far more critical. For this reason, spurious bumps occurred towards the high energy end of the other gates, but they could be identified because the up-sweep and down-sweep curves were accumulated separately, and a spurious bump was unlikely to arise in the same position in both scans.

The lower half of the yield curve corresponding to ground state decay (E_γ>8 MeV) is shown in fig.6.2.1a. Two resonances are evident: the 2^+ state at 11.52 MeV and the 1^- state at 12.44 MeV. These were both seen with similar relative intensities by Larson and Spear. Both decay to the ground state, and the better peak to background ratio of the earlier work was due to the use of a thicker target, since both states have large natural width.

The two gates covering the γ-ray energies 5.0→6.3 MeV and 6.3→7.0 MeV, intended to show resonances decaying via the 6.13 MeV (3^-) and 6.92 MeV (2^+) states, reveal the 4^+ resonance at a beam energy of 5.25 MeV (E_x=11.10 MeV) and nothing else below the inelastic threshold.

Thus, apart from the 0^+ state at 12.05 MeV, the known capture resonances were observed but no new resonances were found, confirming the lack of narrow natural parity states in ^{16}O, in marked contrast to ^{19}F and also to ^{20}Ne. This was a somewhat surprising and unexpected result.

6.3 The 11.10 MeV (4^+) state

The only resonance studied in detail was the 4^+ 11.10 MeV state. Spectra were accumulated for an integrated beam charge of 0.197C (He^{++}) on resonance and for 0.116C below the resonance. The target pressure was maintained at 1 torr, so that the beam energy loss through the target was 15 keV. The 16% Ge(Li) detector was positioned at an angle to the beam of 135°, with its can at a distance of 8cm from the centre of the target. The spectrum (fig.6.3.1) shows both primary and secondary γ-rays in the cascade 11.10→6.92→0.00 and also in the weaker branch 11.10→6.13→0.00. The stronger secondary transition (6.92→0.00) was used for fixing the resonance profile in the long target correction procedure.

The strength obtained for the stronger branch (via the 6.92 MeV level) is somewhat larger than the value obtained by Brochard et al.[Br75], but our value for the weaker branch is significantly less than theirs (table 6.3.1). By inspection of fig.6.3.1 it is difficult to see how the branch via the 3^- state could be the stronger of the two. An indication of the source of the discrepancy lies in the spectrum of γ-rays coincident with 6.92 MeV γ-rays presented by Brochard et al. In their spectrum, there is a noticeable peak showing 6.13 MeV γ-rays in random coincidence, implying severe contamination problems. This must cast doubt on their estimate of the branch via the 6.13 MeV state. The strengths obtained in this work are shown in table 6.3.1.

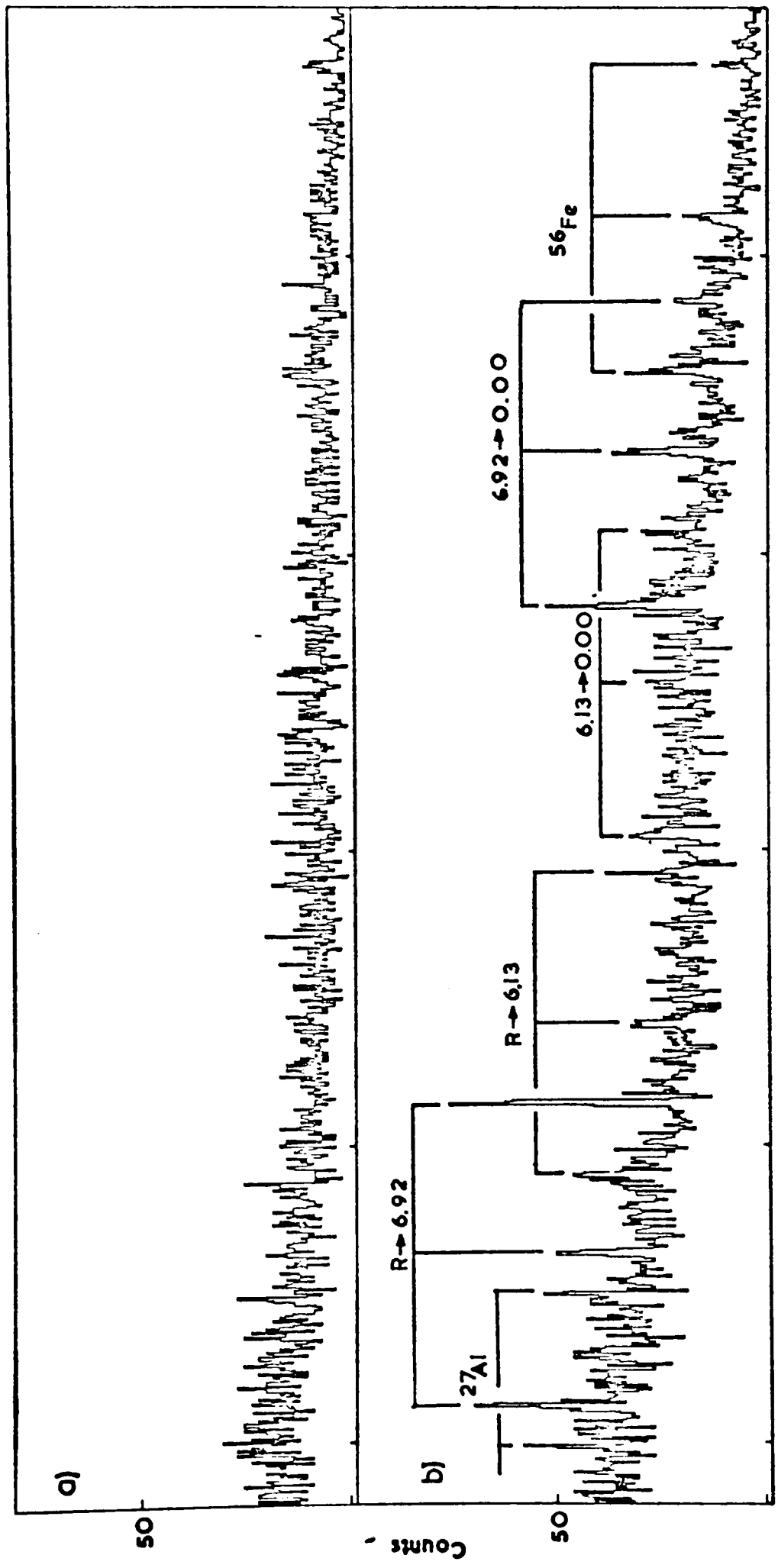

Fig.6.3.1 Spectra (a) off and (b) on the 5.25 MeV resonance in the $^{12}C(\alpha,\gamma)^{16}O$ reaction. Resonant γ-rays from the decay of the 11.10 MeV 4^+ state in ^{16}O are marked in (b) as are peaks due to Al and Fe which are not visible in (a). The spectra are normalised to the same collected charge and were taken with a target pressure of 1 torr.

Table 6.3.1 11.10 MeV (4^+)

	Present Work	Previous
E_x	11098±4	11095±2 [Aj77]
Implied E_α	5249±5	
Γ		0.28±0.05 [Aj77]
J^π		4^+ [La66]
Total $\omega\gamma$ (ev)	$(44\pm8)\times10^{-3}$	
Detector at 8cm 135°		

$E_\gamma(\theta)$	Branching Ratio %	Γ_γ(meV)	Mλ	B(Mλ)Wu	Previous Γ_γ meV
R→6.13(3^-)	4916.5±3.7	29	1.4±0.6	E1	$(2.7\pm1.1)\times10^{-5}$	3.1±1.3*
R→6.92(2^+)	4144.0±0.9	71	3.5±0.6	E2	1.42±0.24	2.5±0.6
6.13→0.00	5050.6±4.4					
6.92→0.00	6855.5±3.0					

* [Br75]; see text.

6.4 The 12.05 MeV (0^+) State

The 0^+ state at 12.05 MeV was not seen in the yield curves, despite several attempts to locate it. The fluctuations in our yield curves are not simply due to counting statistics, and therefore the setting of limits on unobserved resonances is rather subjective. However, the fact that the background at the bombarding energy where this state is expected is only a factor of two greater than for the 4^+ resonance makes an estimate possible. The total $\omega\gamma$ for the 4^+ level is 44 meV and much of this strength would be expected to appear in the 5.0→6.3 MeV gate since this gate includes Compton scattered 6.92 MeV γ-rays as well. Certainly the resonance appears most strongly in this gate. A peak of a third of this size should have been visible above the increased background, implying that as the 0^+ state was not seen, its $\omega\gamma$ value must be less than 15 meV, since, like the 4^+ state, the main decay branch would be expected to be via the 6.92 MeV (2^+) level. One Weisskopf unit for this E2 transition is 7 meV, so a 2 W.u. strength would be required for this state to have been observed as a resonance. The relevant sections of the yield curve are shown in figs.6.4.1a and 6.4.1b.

The only information about the electromagnetic properties of this state which has so far been published is the monopole matrix element for electro-excitation of this state. This quantity was measured by Bergstrom and Auer [Be73] who studied the inelastic scattering of electrons on ^{16}O. They obtained a value of $4fm^2$ which is a factor of 4 greater than the prediction of Erikson [Er71] who used the wavefunctions of Brown and Green [Br66]. They point out that this large discrepancy does not in fact have much significance because the calculation of

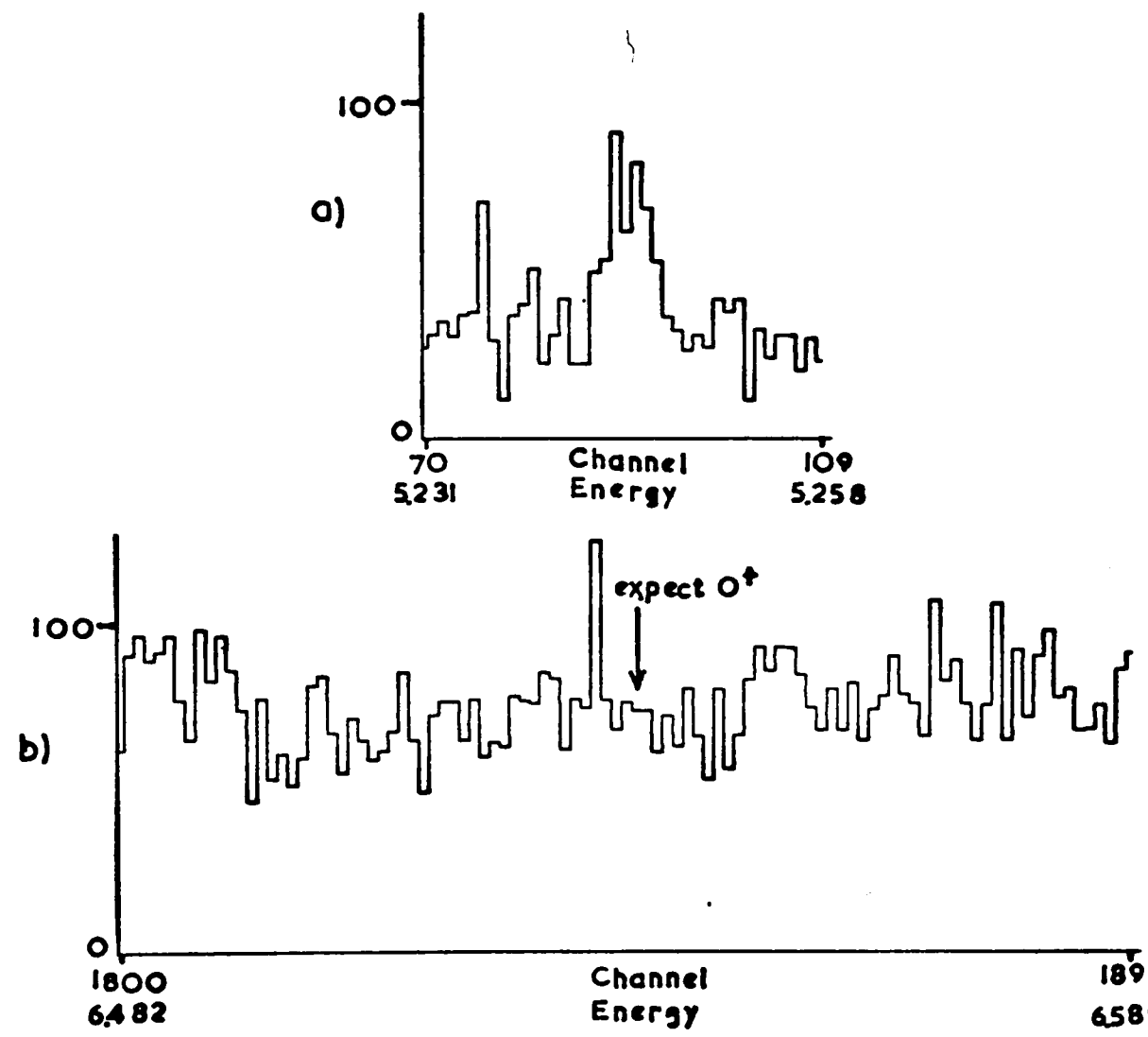

Fig.6.4.1 Yield of γ-rays where $5.0 < E_\gamma < 6.3$ MeV as a function of beam energy in the region of (a) the 11.10 MeV 4^+ state and (b) the 12.05 MeV 0^+ state for which the expected position is marked. The vertical scale in both is the same and the target pressure was 0.2 torr.

monopole matrix elements is difficult due to large cancellations.

6.5 Discussion

Larson and Tombrello studied the 11.10 MeV (4^+) and 12.05 MeV (0^+) states by elastic α-scattering [La66] and derived values for their spins, parities and widths. These states were also observed by Meier-Ewert et al [Me68] in the reaction $^{12}C(^6Li,d)^{16}O$, the low strength of the 0^+ state suggesting a 2-particle 2-hole nature. However, Weibezahn et al [We71] populated both states in the reaction $^{14}N(^3He,p)^{16}O$ and reported that neither was predominantly of 2p-2h nature.

Weak coupling model calculations by Arima et al.[Ar67] predict five closely spaced positive parity states with spins 0→4 at an energy of 12 MeV, formed by coupling the first 2^+ states in ^{12}C and ^{20}Ne. They identify four of these five states with the known states in ^{16}O at 11.08(3^+), 11.10(4^+), 11.26(0^+) and 11.52 MeV (2^+). From consideration of the widths of the 2^+ and 4^+ states (74 keV and 0.3 keV), the 12.05 MeV state (Γ=1.5 keV) seems a more likely candidate for the predicted 0^+ level than the 11.26 MeV state (Γ=2500 keV), which has only been reported once [Bi54] and whose existence has been questioned by Marvin and Singh [Ma72] who failed to observe any evidence for it in their repeat of the earlier elastic scattering work.

Calculations have recently been performed by Dr.B.A.Brown (private communication) using the two sets of matrix elements used by McGrory and Wildenthal [Mc73] in a $1p_{1/2}$-$1d_{5/2}$-$2s_{1/2}$ basis. The effective interactions are an empirical interaction due to Reehal [Re73] and a

primarily realistic interaction due to Zucker [Zu69]. A harmonic oscillator potential with $\hbar\omega$=13.5 MeV was used, with effective charges for the neutron and proton of 1.0 and 2.0 electron charges respectively, chosen by fitting the large B(E2) values for the decay of the first 2^+ state. These large effective charges arise from the truncation of the model space and allow for polarisation of the ^{12}C core. The two effective interactions make similar general predictions for ^{16}O but give different strength predictions for some of the weaker E2 transitions. Confidence in the results is to within a factor of two or three.

For the second 4^+ state (11.10 MeV), the predicted B(E2) strengths to the lowest 2^+ state (6.92 MeV) are 14 and 15 e^2fm^4 for the Reehal and Zucker interactions respectively. The measurement reported above, in section 3 of this chapter, gave a value of 3.4 e^2fm^4, over a factor of 4 lower.

As stated previously, it is not clear whether the state at 12.05 MeV is the third or fourth 0^+ state, because of doubts about the existence of the reported broad state at 11.26 MeV. The predictions for the strength of the decay of the third 0^+ state to the first 2^+ state are 23 and 7.5 e^2fm^4 whereas they are 6.0 and 10.0 e^2fm^4 for the fourth 0^+ state. These should be compared with the value of 5 e^2fm^4 derived above as an upper limit for the strength of the 12.05 MeV state, consistent with our observations. This limit is less than a factor of 2 below the weaker prediction for the third 0^+ state and so, although the fact that we did not observe this state is surprising, no particular significance can be inferred. A further attempt to locate this state as a resonance in α-capture would seem worth while, particularly if good beam conditions were available.

REFERENCES

Aj72 F.Ajzenberg-Selove, Nucl.Phys. A190 (1972) p1

Aj77 F.Ajzenberg-Selove, Nucl.Phys. A281 (1977) p1

Aj78 F.Ajzenberg-Selove, Nucl.Pnys. A300 (1978) p1

Ak69 Y.Akiyama, A.Arima and T.Sebe, Nucl.Phys. A138 (1969) p273

Al67 T.K.Alexander, W.T.Diamond, A.J.Ferguson, R.W.Ollerhead, J.A.Kuehner and A.E.Litherland, CRNL Report AECL-3009 (1967); AECL-3108 (1968)

Al72a T.K.Alexander, O.Häusser, A.B.McDonald and A.J.Ferguson, Nucl.Phys. A179 (1972) p477

Al72b T.K.Alexander, B.Y.Underwood, N.Anyas-Weiss, N.A.Jelley, J.Szücs, S.P.Dolan, M.R.Wormald and K.W.Allen, Nucl.Phys A197 (1972) p1

Al76 K.W.Allen, S.P.Dolan, A.R.Holmes, T.J.M.Symons, F.Watt, C.H.Zimmerman, A.E.Litherland and A.M.J.Sandorfi, Nucl.Instr. & Meth. 134 (1976) p1

Ar67 A.Arima, H.Horiuchi and T.Sebe, Phys.Lett. 24B (1967) p129

Ba72 D.P.Balamuth, J.W.Noé, H.T.Fortune and R.W.Zurmühle, Phys.Rev. C6 (1972) p1694

Ba73 J.K.Bair and F.X.Haas, Phys.Rev. C7 (1973) p1356

Be71 W.L.Bendel, L.W.Fagg, S.K.Numrich, E.C.Jones and H.F.Kaiser, Phys.Rev. C3 (1971) p1821

Be73 J.C.Bergstrom and I.P.Auer, Nucl.Phys. A215 (1973) p232

Be75 R.R.Betts, H.T.Fortune and R.Middleton, Phys.Rev. C11 (1975) p19

Bi54 J.W.Bittner and R.D.Moffat, Phys.Rev. 96 (1954) p374

Br66 G.E.Brown and A.M.Green, Nucl.Phys. 75 (1966) p401

Br70 F.Brochard, P.Chevallier, D.Disdier, V.Rauch and F.Scheibling, J.Phys.(France) 31 (1970) p255

Br75 F.Brochard, P.Chevallier, D.Disdier, V.Rauch and F.Scheibling, J.Phys.(France) 36 (1975) p113

Bu60 J.W.Butler, Phys.Rev. 118 (1960) p222

Bu71 J.Bussiere and J.M.Robson, Nucl.Instr. & Meth. 91 (1971) p103

Ca53 J.R.Cameron, Phys.Rev. 90 (1953) p839

Ce66 L.S.Celenza, R.M.Dreizler, A.Klein and G.J.Dreiss, Phys.Lett. 23 (1966) p241

Ch75 S.H.Chew and J.Lowe, Nucl.Phys. A252 (1975) p8

Ch76 W.Chung, PhD Thesis, Michigan State University (1976)

Co76 J.H.Cobb, W.W.M.Allison and J.N.Bunch, Nucl.Instr. & Meth. 133 (1976) p315

Da78 J.M.Davidson and M.M.Lowry, Phys.Rev. C18 (1978) p2776

De71 W.Del Bianco and E.Boridy, Nucl.Instr. & Meth. 92 (1971) p111

Di71 W.T.Diamond, T.K.Alexander and O.Häusser, Can.J.Phys. 49 (1971) p1589

Do75 S.P.Dolan, Oxford D.Phil. Thesis (1975)

Dw71 M.R.Dwarakanath and H.Winkler, Phys.Rev. C4 (1971) p1532

El58 J.P.Elliott, Proc.Roy.Soc. A245 (1958) p128 and p562

En74 P.M.Endt and C.Van der Leun, Nucl.Data 13 (1974) p67

Er71 T.Erikson, Nucl.Phys. A170 (1971) p513

Ev77 D.Evers, C.Ley, E.Spindler, W.Assmann, K.Rudolph and P.Konrad, Nucl.Phys. A275 (1977) p363

Fi76 L.K.Fifield, R.W.Zurmühle and D.P.Balamuth, Phys.Rev. C14 (1976) p1010

Fi77 L.K.Fifield, F.P.Calaprice, C.H.Zimmerman, M.J.Hurst, A.Pakkanen, T.J.M.Symons, F.Watt and K.W.Allen, Nucl.Phys. A288 (1977) p57

Fi79 L.K.Fifield, University of Oxford Report on Nuclear Structure Research 1978-1979

Fi80 L.K.Fifield, M.J.Hurst, E.F.Garman, T.J.M.Symons, F.Watt, and K.W.Allen Nucl.Phys. A334(1980) p109

Fo72a H.T.Fortune in Proc. of Heavy Ion Summer Study, Oak Ridge National Laboratory (1972) p353
also H.T.Fortune, R.R.Betts, J.D.Garrett and R.Middleton Phys.Lett. 44B (1973) p65

Fo72b H.T.Fortune, G.C.Morrison, R.C.Bearse, J.L.Yntema and B.H.Wildenthal, Phys.Rev. C6 (1972) p21

Fo74 H.T.Fortune and R.R.Betts, Phys.Rev. C10 (1974) p1292

Ga80 E.F.Garman, Oxford D.Phil. Thesis (1980)

Go66 G.Gobert, G.S.Mami and A.Sadeghi, Nucl.Instr. & Meth. 42 (1966) p250

Gu70 K.Gul, B.H.Armitage and B.W.Hooton, Nucl.Phys. A153 (1970) p390

Ha67 L.F.Hansen, J.D.Anderson, J.W.McClure, B.A.Pohl, M.L.Stelts, J.L.Wesolowski and C.Wong, Nucl.Phys. A98 (1967) p25

Ha68 M.Harvey, In Advances in Nucl.Phys. Ed. M.Baranger and E.Vogt Vol. 1 (1968) p67

Ha71 O.Häusser, T.K.Alexander, A.B.McDonald, G.T.Ewan, and A.E.Litherland Nucl.Phys. A168 (1971) p17

Ha72 O.Häusser, A.J.Ferguson, A.B.McDonald, I.M.Szöghy, T.K.Alexander and D.L.Disdier, Nucl.Phys. A179 (1972) p465

Hu67 W.E.Hunt, M.K.Mehta and R.H.Davis, Phys.Rev. 160 (1967) p782

Hu80 M.J.Hurst, L.K.Fifield, E.F.Garman, T.J.M.Symons, F.Watt, and K.W.Allen, J.Phys.G:Nucl.Phys 6 (1980) p891

In76a P.D.Ingalls, Nucl.Phys. A265 (1976) p93

In76b P.D.Ingalls, Phys.Rev. C14 (1976) p254

Jo69 J.John, J.P.Aldridge and R.H.Davis, Phys.Rev. 181 (1969) p1455

Ke65 I.Kelson, Phys.Lett. 16 (1965) p143

Ku66 J.A.Kuehner and R.W.Ollerhead, Phys.Lett. 20 (1966) p301

Ku67 J.A.Kuehner and E.Almqvist, Can.J.Phys. 45 p1605

Ku72 H.M.Kuan, G.L.Latshaw, W.J.O'Connell, D.W.Heikkinen, E.G.Adelberger, A.V.Nero and S.S.Hanna, Nucl.Phys. A193 (1972) p497

La64 J.D.Larson and R.H.Spear, Nucl.Phys. 56 (1964) p497

La66 J.D.Larson and T.A.Tombrello, Phys.Rev. 147 (1966) p760

La68 B.T.Lawergren, A.T.G.Ferguson and G.C.Morrison, Nucl.Phys. 108 (1968) p325

Li58 A.E.Litherland, H.McManus, E.B.Paul, D.A.Bromley and H.E.Gove, Can.J.Phys. 36 (1958) p378

Li61 A.E.Litherland, J.A.Kuehner, H.E.Gove, M.A.Clark and E.Almqvist, Phys.Rev.Lett. 7 (1961) p98

Li67 A.E.Litherland, R.W.Ollerhead, P.J.M.Smulders, T.K.Alexander, C.Broude, A.J.Ferguson and J.A.Kuehner, Can.J.Phys. 45 (1967) p1901

Lo73 D.S.Longo, J.C.Lawson, L.A.Alexander, B.P.Hichwa and P.R.Chagnon, Phys.Rev. C8 (1973) p1347

Ma72 T.P.Marvin and P.P.Singh, Nucl.Phys. A180 (1972) p282

Ma77 R.E.Marrs, E.G.Adelberger and K.A.Snover, Nucl.Phys. A277 (1977) p429

Mc60 L.C.McDermott, K.W.Jones, H.Smotrich and R.E.Benenson, Phys. Rev. 118 (1960) p175

Mc73 J.B.McGrory and B.H.Wildenthal, Phys.Rev. C7 (1973) p974

Me68 K.Meier-Ewert, K.Bethge and K.O.Pfeiffer, Nucl.Phys. A110 (1968) p142

Me75 L.R.Medsker, H.T.Fortune, R.R.Betts and R.Middleton, Phys.Rev. C11 (1975) p1880

Mi71 R.Middleton, J.Phys.(France) 32 (1971) p39

Mi74 G.F.Millington, J.R.Leslie, W.McLatchie, G.C.Ball, W.G.Davies and J.S.Forster, Nucl.Phys. A228 (1974) p382

No70 L.C.Northcliffe and R.F.Schilling, Nucl.Data A7 (1970) p233

Ol74 D.K.Olsen, A.R.Barnett, S.F.Biagi, N.H.Merril and W.R.Phillips, Nucl.Phys. A220 (1974) p541

Pa64 P.B.Parks, P.M.Beard, E.G.Bilpuch and H.W.Newson, Rev.Sci.Instr. 35 (1964) p549

Pe64 J.D.Pearson, E.Almqvist and J.A.Kuehner, Can.J.Phys. 42 (1964) p489

Pe64b J.D.Pearson and R.H.Spear, Nucl.Phys. 54 (1964) p434

(N.B. References to decay widths in this paper have been corrected to the centre of mass by the kinematic factor 16/20)

Po67 R.M.Polichar, J.E.Steigerwalt, J.W.Sunier and J.R.Richardson, Phys.Rev. 163 (1967) p1084

Pr72 B.M.Preedom and B.H.Wildenthal, Phys.Rev. C6 (1972) p1633

Re73 B.S.Reehal, B.H.Wildenthal, Particles & Nuclei 6 (1973) p137

Ri69 R.C.Ritter, J.T.Parson and D.L.Bernard, Phys.Lett. 28B (1969) p588

Ro63 V.M.Rout, W.M.Jones and D.G.Walters, Nucl.Phys. 45 (1963) p369

Ro67 H.J.Rose and D.M.Brink, Rev.Mod.Phys. 39 (1967) p306

Ro70 A.A.Rollefson, P.F.Jones and R.J.Shea, Phys.Rev. C1 (1970) p1761

Ro71f D.W.O.Rogers, J.H.Aitken, A.E.Litherland, W.R.Dixon and R.S.Storey, Can.J.Phys. 49 (1971) p1397

Ro71o D.W.O.Rogers, K.W.Allen, H.C.Evans, N.A.Jelley, A.E.Litherland and B.Y.Underwood, Phys.Lett. 37B (1971) p65

Ro78 C.Rolfs, J.Görres, K.U.Kettner, H.Lorenz-Wirzba, P.Schmalbrock, H.P.Trautvetter and W.Verhoeven, Nucl.Instr. & Meth. 157 (1978) p19

Sc71 D.Schwalm, K.Traxel, H.Weiss, M.Morando and B.Povh, Phys.Rev. C4 (1971) p10

Sc77 D.Schwalm, E.K.Warburton and J.W.Olness, Nucl.Phys A293 (1977) p425

Se76 H.M.Sen Gupta, T.A.Belote and D.Roaf, Nucl.Phys. A267 (1976) p205

Sk66 S.J.Skorka, J.Hertel and T.W.Retz-Schmidt, Nucl.Data 2A (1966) p347

Sn78 K.A.Snover, K.Kim and P.A.Dickey, Bull.Am.Phys.Soc. 23 (1978) p501

Sp63 R.H.Spear, J.D.Larson and J.D.Pearson, Nucl.Phys. 41 (1963) p353

St78 D.J.Steck, Phys.Rev. C17 (1978) p1034

Sy76 T.J.M.Symons, Oxford D.Phil. Thesis (1976)

To73 D.F.Torgerson, K.Wien, Y.Fares, N.S.Oakey, R.D.Macfarlane and W.A.Lanford Phys.Rev. C8 (1973) p161

Wa77 A.H.Wapstra and K.Bos, Atom. & Nucl. Data Tables 19 (1977) p175

Wa78 F.Watt, L.K.Fifield, M.J.Hurst, T.J.M.Symons, C.H.Zimmerman and K.W.Allen Nucl.Instr. & Meth. 151 (1978) p163

We71 R.Weibezahn, H.Freiesleben, F.Pühlhofer and R.Bock, Nucl.Phys. A176 (1971) p645

Wo74 M.R.Wormald and J.Takacs, Nucl.Instr. & Meth. 114 (1974) p263

Zi77 C.H.Zimmerman, Oxford D.Phil. Thesis (1977)

Zu68 A.P.Zucker and B.Buck, Phys.Rev.Lett. 21 (1968) p39

Zu69 A.P.Zucker, Phys.Rev.Lett. 23 (1969) p983